UNIVERSITAT DE BARCELONA

Dynamical and Mechanical Characterisation of Bi- and Tri-dimensional Neuronal Cultures: from Health to Disease

Clara Fernández López

.

UNIVERSITAT DE BARCELONA

DOCTORAL THESIS

Dynamical and Mechanical Characterisation of Bi- and Tri-dimensional Neuronal Cultures: from Health to Disease

---

Author:
Clara Fernández López

Director:
Dr. Jordi Soriano & Dr. Ramon Planet

November 13, 2023

UNIVERSITAT DE BARCELONA

Dynamical and Mechanical Characterisation of Bi- and Tri-dimensional Neuronal Cultures: from Health to Disease

Memoria presentada para optar al grado de doctor por la
Universitat de Barcelona
Programa de doctorado en Física

Autor: Clara Fernández López

Director: Dr. Jordi Soriano & Dr. Ramon Planet

Tutor: Giancarlo Franzese

UNIVERSITAT DE BARCELONA

"*No need to hurry. No need to sparkle. No need to be anybody but oneself.*"

Virginia Woolf

Abstract

In this PhD thesis, we leverage the well–established foundations of physics of complex systems and integrate insights from medicine and materials engineering to advance our understanding of neuroscience. Our primary focus revolves around neuronal cultures, serving as the central protagonists in our exploration. We aspire to establish a robust connection between neurons, the underlying physics dictating their interactions, and the materials shaping their *in vitro* environment.

Within the scope of this research, we push the boundaries of primary neuronal cultures to model neurodegenerative diseases (ND), with a specific focus on tauopathies—an array of devastating disorders characterized by abnormal forms of the microtubule-associated protein *tau*. Alzheimer's disease, a prominent member of this group, was first described in 1906 and is anticipated to afflict 139 million people worldwide by 2050. Despite ongoing clinical trials, no effective treatment exists to prevent or cure tauopathies.

This doctoral thesis delves into various facets of this group of NDs, employing experimental approaches to emulate sporadic tauopathies *in vitro*. Conducted as part of the 'La Caixa Health Research 2019' initiative, an anti–aggregation inhibitor for these abnormal forms of tau was developed. Our initial work was to test the neurotoxicity of the inhibitor by checking whether its presence affected the optimal development of neurons in culture. To do this, we applied calcium fluorescence imaging techniques to record neuronal activity, as well as tools based on dynamical systems, data science, and complex networks, to examine dynamic and functional features of neuronal networks treated with this inhibitor. The results revealed that the anti–tau agent had no adverse effects on the healthy development of cultured neurons. The subsequent phase involved probing the impact of extracellular 'pathological' tau on the neuronal activity of primary cortical cultures derived from wild–type mice. Employing a carefully designed experimental setup, extracellular tau from various sources was introduced into primary neuronal cultures. Just as for the previous step, we compared dynamic and functional features of neuronal networks untreated and treated with tau. Surprisingly, the results demonstrated that there were no discernible changes in the cultured neurons after treatment with pathological extracellular tau. This outcome suggests that either the *in vitro* model is not suitable for detecting anomalies associated with tau, or the disease is much more complex than initially assumed, and tau protein is just one ingredient of a much more intricate molecular puzzle.

One of the limitations of our study was the challenge of replicating the tauopathy disease scenario within a standard bi–dimensional (2D) neuronal culture. The absence of three–dimensional (3D) network organisation raised concerns about potential alterations in the susceptibility of primary neurons to the effects of extracellular

seed–competent tau. This challenge extends beyond our specific investigation and contributes to the broader debate surrounding the faithfulness of 2D *in vitro* environments in replicating real conditions akin to the brain. In response to this limitation, the last decade has witnessed the introduction of 3D neuronal cultures, aiming to establish more representative *in vitro* models. In our endeavor to contribute to this evolving field, we merged insights from neuroscience and materials science to explore the use of *PEGylated fibrin*, a semi–synthetic hydrogel, as a 3D scaffold for neuronal cultures. PEGylated fibrin hydrogel is composed by polyethylene glycol (PEG) and a fibrin gel, which results from the reaction between two components of the fibrinogen–thrombin coagulation cascade. The selection of this material was not arbitrary, being motivated to fulfill several crucial requirements for the healthy development of neurons within its structure. These prerequisites included biocompatibility, a suitable porous structure, and a stiffness mimicking that of the brain.

While PEGylated fibrin hydrogels have found applications in tissue engineering, their mechanical properties remain relatively unexplored. This information is pivotal for understanding the neuron–matrix relationship and determining the lifespan of cultures. To address this gap, we conducted a comprehensive mechanical characterization of PEGylated fibrin hydrogels using a rheometer. Our meticulous protocol allowed for a systematic investigation of the evolution of the hydrogels' mechanical properties over a three–week period, shedding light on the degradation of the hydrogel structure over time. This investigation encompassed hydrogels seeded with neurons, providing valuable insights into the impact of neuronal network development within the hydrogel structure. Our findings reaffirmed the suitability of the selected hydrogel for preparing 3D neuronal cultures. The hydrogel's stiffness closely mimicked that of the actual brain, and it demonstrated an optimal lifespan for studying the development of neuronal cultures.

In an effort to bridge the two central lines of research, namely neuronal culture functional traits (in health and disease) and neuronal environment (2D or 3D), we delved into examining the intricate relationship between the mechanical properties of the scaffold and the functional organisation of neuronal networks cultured within these structures. The microstructure of PEGylated fibrin hydrogels can be finely tuned by adjusting certain aspects of the polymerization process, such as the concentration of thrombin, a key reagent influencing the stiffness of the final structure. By employing our established protocol, we characterized the mechanical properties of three PEGylated fibrin hydrogel variants depending on their concentration of thrombin. Simultaneously, through calcium imaging, we recorded the spontaneous activity of neuronal networks developed within these diverse structures and conducted a comprehensive functional analysis. While our preliminary results indicated an interesting correlation between the initial neuronal development and the stiffness of the hydrogel, deciphering this effect proved challenging due to the myriad factors at play and the limitations of

available microscopy techniques in this study. Our investigations served as a pioneering step, laying the groundwork for future research in an exciting multidisciplinary field in which neuronal cultures are central actors.

Resumen

Esta tesis doctoral se enmarca en la física de los sistemas complejos, a la que se suman conceptos de medicina y ciencia de materiales, para profundizar en nuestro conocimiento en el ámbito de la neurociencia. Los protagonistas de esta investigación son los cultivos neuronales primarios en los que nos basamos para establecer una relación sólida entre las neuronas en cultivo, la física subyacente que guía sus interacciones y los materiales que dan forma a su entorno *in vitro*.

En el trabajo llevado a cabo durante estos años hemos intentado ampliar los límites de los cultivos neuronales primarios para modelar enfermedades neurodegenerativas (ND), en particular para modelar tauopatías— un conjunto de enfermedades caracterizado por el depósito de formas anormales de la proteína *tau*, la cual está asociada a la estabilidad de los microtúbulos de las neuronas. Un miembro destacado de este grupo de NDs es la enfermedad de Alzheimer, que fue descrita por primera vez en 1906 y que se prevé que afectará a más de 139 millones de personas en todo el mundo en 2050. A pesar de estos alarmantes números, no existe aún un tratamiento efectivo para prevenir o curar esta enfermedad u otras tauopatías, ya que las terapias desarrolladas hasta la fecha han sido incapaces de generar resultados positivos en los ensayos clínicos. Esto se debe en gran medida a la dificultad de encontrar modelos *in vitro* o *in vivo* que realmente reproduzcan el complejo escenario de estas patologías en el cerebro.

Esta tesis doctoral explora diversas facetas de las tauopatías utilizando un enfoque experimental que simula el aspecto esporádico de estas enfermedades. Como parte de la iniciativa 'La Caixa Health Research 2019', un proyecto colaborativo entre cuatro grupos de investigación y guiado por el Dr. José Antonio Del Rio (Institut de Bioenginyeria de Catalunya, IBEC), se desarrolló un agente inhibidor de agregación de estas formas anómalas de tau. Nuestro trabajo inicial fue probar la neurotoxicidad del inhibidor comprobando si su presencia en cultivos neuronales primarios afectaba de alguna forma al desarrollo óptimo de las neuronas en cultivo. Para ello aplicamos técnicas de imagen de fluorescencia de calcio para registrar actividad neuronal, así como herramientas basadas en sistemas dinámicos, ciencia de datos y redes complejas para examinar características dinámicas y funcionales de las redes neuronales tratadas con dicho inhibidor. Los resultados revelaron que el agente anti–tau no tenía efectos adversos en el desarrollo saludable de las neuronas cultivadas.

La siguiente fase de este proyecto incluía la evaluación del daño causado por formas anómalas de tau en cultivos neuronales primarios provenientes de ratones tipo '*wild-type*'. Utilizando una configuración experimental cuidadosamente diseñada, introdujimos tau extracelular patológica de diversas fuentes en cultivos neuronales y, al igual que para el caso del inhibidor, comparamos características dinámicas y funcionales de las redes neuronales sin tratar y tratadas con tau. Sorprendentemente, los resultados demostraron que no había cambios discernibles en las neuronas cultivadas

después del tratamiento con tau extracelular patológica. Este resultado indica que, o bien el modelo *in vitro* no es adecuado para detectar anomalías asociadas a tau, o bien la enfermedad es mucho más compleja de lo inicialmente supuesto y la proteína tau es un ingrediente más de un puzle molecular mucho más complejo.

En este contexto de autocrítica sobre el uso de cultivos neuronales, una limitación de nuestro estudio fue el desafío de replicar el escenario de una tauopatía en un cultivo neuronal bidimensional estándar (2D). La falta de una organización tridimensional (3D) de la red neuronal puede disminuir la susceptibilidad de las neuronas a los efectos de las formas anormales de tau. Este desafío va más allá de nuestra investigación particular, formando parte de un debate más amplio en la comunidad neurocientífica sobre la conveniencia de los entornos *in vitro* 2D para replicar condiciones similares a las del cerebro de forma verídica. Por lo tanto, en nuestro esfuerzo por contribuir a este campo en evolución, fusionamos conocimientos de neurociencia e ingeniería de materiales para explorar el uso de un hidrogel semisintético como matriz 3D para cultivos neuronales. El hidrogel de fibrina PEGilada está compuesto por polietilenglicol (PEG) y un gel de fibrina, resultado de la reacción entre dos componentes de la cascada de coagulación, fibrinógeno y trombina. La selección de este material no fue arbitraria; debía cumplir con varios requisitos cruciales para el desarrollo saludable de las neuronas dentro de su estructura. Estos requisitos incluyeron biocompatibilidad, una estructura porosa adecuada y una rigidez que imitara la del cerebro.

Aunque estos hidrogeles se han aplicado con éxito en ingeniería de tejidos, sus propiedades mecánicas permanecen relativamente inexploradas. Esta información es fundamental para comprender la relación entre las neuronas y la matriz y determinar la vida útil de los cultivos. Para abordar esta cuestión, realizamos una caracterización mecánica exhaustiva de los hidrogeles de fibrina PEGilada utilizando un reómetro. Nuestro protocolo nos permitió realizar un seguimiento sistemático de la evolución de las propiedades mecánicas de los hidrogeles durante un período de tres semanas, obteniendo información sobre la degradación de la estructura del hidrogel con el tiempo. Esta investigación abarcó hidrogeles sembrados con neuronas, proporcionando valiosa información sobre el impacto del desarrollo de la red neuronal dentro de la estructura 3D del hidrogel. Nuestros hallazgos reafirmaron la idoneidad del hidrogel, demostrando que tiene una rigidez que se asemeja a la del cerebro real y que tiene una vida útil óptima para estudiar el desarrollo de los cultivos neuronales.

En un esfuerzo por vincular las dos líneas de investigación mencionadas anteriormente, nos sumergimos en examinar la compleja relación entre las propiedades mecánicas de la matriz 3D y la organización funcional de las redes neuronales cultivadas dentro de estas estructuras. La microestructura de los hidrogeles de fibrina PEGilada puede ajustarse finamente mediante la modificación de ciertos aspectos del proceso de polimerización, como la concentración de trombina, un reactivo clave que influye en la rigidez de la estructura final. Creamos entonces tres variantes de este hidrogel con diferentes concentraciones de trombina. Utilizando el protocolo diseñado

anteriormente, pudimos caracterizar las propiedades mecánicas de las tres variantes de fibrina PEGilada. Simultáneamente, registramos la actividad espontánea de las neuronas en cultivo dentro de estas estructuras y realizamos un análisis funcional integral de las redes neuronales resultantes. Aunque nuestros resultados son preliminares, indicaron una correlación interesante entre el desarrollo neuronal inicial y la rigidez del hidrogel. Descifrar este efecto resultó desafiante debido a la multitud de factores en juego y las limitaciones de las técnicas de microscopía disponibles en este estudio. Aun así, esta investigación sirve para asentar las bases para futuras investigaciones en este apasionante campo multidisciplinar.

Acknowledgements

Mi interés por la investigación empezó en la Universidad de Sevilla, en unas jornadas de puertas abiertas para alumnos de bachillerato. Desde ese día me imaginé en un laboratorio, jugando a investigar, pero nunca pensé que esa investigación fuese a ser real. El síndrome de la impostora me persigue desde que acabé el máster, ¿Qué puedo aportar yo que no aporte nadie más? Desde entonces me he disfrazado con una falsa seguridad. En estos años de tesis doctoral he aprendido mucho sobre mi investigación, pero también sobre mí misma. Me he descubierto resolviendo problemas, respondiendo preguntas y aportando ideas dentro de una comunidad de gente maravillosa y eso me ha llenado de orgullo. Así que, aunque parezca egoísta, quiero agradecer este trabajo, en primer lugar, a mí misma, por toda la lucha mental, por no rendirme y por el esfuerzo.

Los guías imprescindibles en este viaje, emprendido hace años, han sido mis directores de tesis, Jordi y Ramon, a los que les debo la ilusión con la que me han transmitido su pasión por la investigación. Me han sabido apoyar en cada etapa de mi Tesis, no solo profesionalmente si no también personalmente. Soy muy afortunada de haber contado con vosotros de tener tan buenos ejemplos de personas y de profesionales en el mundo de la ciencia. Muchas gracias de corazón.

Por el laboratorio de Jordi han pasado muchas personas maravillosas con el poder de trasmitir su pasión por la ciencia y de formar una comunidad multidisciplinar donde enriquecerme y aprender todos los días. Quiero darles las gracias a todas ellas. En primer lugar, muchas gracias a Estefanía y a Marc, que me acogieron y me guiaron en los primeros pasos en el laboratorio. Supisteis transmitirme vuestra ilusión por lo que hacíais, y eso es innato. Los dos me habéis acompañado a lo largo de los cinco años de trabajo y espero que siga siendo así en el futuro.

En mi primer congreso conocí a Sergio. Ademas de compartir director de tesis, hemos compartido cenas, eventos de jardinería, tardes de juego en casa de Jordi... has sido un compañero chulísimo durante estos años y espero que nuestra amistad sea duradera. Quiero agradecer también a Jaime Aspas todos los cafés de risas y quejas (no sé cuál de las dos une más), has sido una válvula de escape muchos días en los que el trabajo era un 'rollo'. Por supuesto, quiero mencionar a Rucsanda y agradecerle su compañía, sus consejos y todas las veces que ha rezado por nosotros a su virgen de los cultivos. También han pasado por el laboratorio muchos estudiantes, a los que he tenido el placer de guiar y acompañar, de la misma manera que mis compañeron lo como hicieron conmigo. He aprendido mucho de vosotros y hemos pasado muy buenos ratos, así que agradezco a Sàlem, a Imanol, a Mireia y a Sarah por sus esfuerzos, sus ganas de aprender y, sobre todo, los buenos momentos vividos.

Al poco tiempo de empezar oficialmente el trabajo de mi tesis conocí a Júlia, convirtiendose en mucho más que una compañera de proyecto. Estos años hubieran sido muy diferentes sin ti, sin tu energía y sin tu inagotable amor por la ciencia. Nos unió la ciencia y desde entonces has sido amiga, cuidadora y compañera de viajes. Muchas gracias amiga mia por todo. Un beso enorme para ti y para Jorge.

Muchas gracias a la ciencia por poner también en mi camino a Akke y a Anna. The international team of the lab. I could not be more proud of the team you form, of your generosity and kindness. It has been a pleasure to share all this time with you. Special mention to Anna, who besides being a friend inside the lab has been, is, and will be, a friend outside it. In a city to which none of us belong, we have become a family and we have shared many moments together. Thank you very much for everything.

Thanks also to Marta Picco, not only for all the singing moments in the lab, but for being my fairy godmother the three weeks I spent in Genova. Thank you so much for taking care of me and welcoming me with open arms. See you soon around Barcelona, I wish you all the best in this new chapter of your live.

I would also like to take a moment to thank Michela for her hospitality in Genova, for hosting me and showing me all the fascinating work she does in her research group. You are a great example of a PI and a human being who cares about the people around you. It has been a pleasure to be part of your team, even if it was for a short time.

En este orden de cosas necesito encontrar un hueco para mi amiga María Casado. La vida nos ha vuelto a unir lejos de Sevilla para que nos acompañemos y nos demos energía y ánimos durante nuestra etapa pre–doctoral. Me encanta que nos hayamos vuelto a encontrar, muchas gracias por haberme cuidado.

Dejando a un lado mi trabajo en el laboratorio, esta etapa ha conllevado pasar cinco años y medio en una ciudad diferente a mi ciudad natal. Barcelona puede ser difícil para alguien de fuera, pero yo he tenido la suerte de encontrar a personas que han sabido arroparme como si fueran mi familia, en una ciudad en la que la mía propia (la de sangre) estaba lejos. Gracias a mi familia del máster, gracias a Laura, a Nerea, a Marc, a Pere, a Jiahui, a Pepe... gracias por toda la compañía. Sé que nuestra amistad durará mucho tiempo porque es fácil llevaros en el corazón. Quiero hacer una mención especial a Laura, por toda su fuerza, y porque mientras escribo esto tú estás trayendo vida y Nico está llegando al mundo.

Muchas gracias a mis queridos amigos sevillanos en Barcelona, a Fran y Asun por su interminable energía y ganas de acoger. A Belén por ser ella, ¡qué divertido ha sido pasar todo ese tiempo contigo! Me alegro mucho de haber podido compartir esta etapa contigo. Barcelona no hubiera sido la misma sin ti, ni sin Héctor, por supuesto.

Siempre nos quedarán las tardes del Xampanyet.

Muchas gracias a Julia por ser amiga, hermana, y madre, todo a la vez. Por todas las horas que nos hemos hecho compañía en casa, todas las horas de paseo, por los ataques de risa en el suelo del pasillo y por sostenerme cuando yo no podía (corazones rotos y chinches incluidas) y también por traer a mi vida a Gonzalo, que ya se queda para siempre (espero). Muchas gracias a Carmen, mi amiga tesoro que siempre está. Para ti es tan fácil que es imposible no responderte con el mismo amor que tú me das. Sé que estás tan orgullosa de mi como yo de ti. Siempre.

Qué guay ha sido que Jaime me siguiera a Barcelona y se trajera a Irene con él. Habéis sido un apoyo fundamental para mí estos años. Siempre me acordaré de todos los mojitos que nos hemos bebido en vuestra terraza mientras arreglábamos (nada más lejos de la realidad) el mundo. Habéis sido un equipo divertidísimo e imprescindible en mi vida en Barcelona. Muchos besos también a Gaia y a Giorgio por todo el amor (y todo el tiramisú).

En Barcelona he tenido también familia (de la de sangre) y quiero darle las gracias a mi tía Encarna y a mi tío Aurelio por todo el cariño que me han dado.

Lejos de Barcelona, en Madrid, también tengo una pequeña familia a la que agradecer su amistad, cariño y todo el apoyo, durante estos años de trabajo en mi tesis. Gracias a Adri, a Alicia, a Estefi, a Mar, a María Cañete, a Marta Vacas, a Marta Santos, a Nora y a Sergio. Os quiero mucho.

Llegamos a Sevilla y no hay nada más bonito que llegar a casa. En Sevilla tengo amigos del alma que me cuidan en la distancia, vienen a verme, me hacen hueco cuando paso por allí y me apoyan siempre. Espero haber estado a la altura de todo lo que me aportáis. Gracias a Claudia por guiarme siempre, desde que tengo uso de razón me coges de la mano y me sostienes. Gracias a Pedro por su energía, por ser uno de mis mayores fans y a la vez unos de mis ídolos. Muchas gracias a Uri por ser como es, por ser un amigo tan genial. Gracias a Malena por estar siempre, te quiero muchísimo.

No puedo olvidarme de Pilar, mi profesora de inglés y, más importante, amiga. Muchas gracias por todo.

Muchas gracias a Jose. Has estado siempre apoyándome, como amigo y como pareja. Rebosas un amor tan bonito, que es imposible no contagiarse. No sé como agradecerte que cada día estés conmigo. Este trabajo también es para ti, para tu madre y para tu padre, con mi deseo de ayudaros y que estas contribuciones a la ciencia sirvan

para que un futuro tengamos mas información y recursos para combatir enfermedades como el Alzheimer.

Quiero finalizar dándole las gracias a mi familia. A mis padres que me han hecho estar orgullosa de mí misma en cada paso que he dado. No sé cómo daros las gracias por vuestro apoyo incondicional, por todo el amor que desbordáis y por vuestra sabiduría. Gracias a mi hermana Elena, eres tan especial que no sé qué puedo decirte, espero que sigas luchando por todo lo que quieres. Gracias a mi abuelo Manolo por estar siempre orgulloso de mí y muchísimas gracias a mi abuela Esperanza, te amo. Muchas gracias a mis titos, a mis primos y a toda mi familia de San Fernando. A mi tía Sagrario y a mis abuelos, Ignacio y Sara. Mención especial a Benito por ser mi apoyo emocional y mi fiel acompañante durante muchas horas de trabajo frente al ordenador.

Nunca me imaginé haciendo un doctorado, pero cuando se presentó la oportunidad de ayudar a Jordi en el proyecto de La Caixa no dudé ni un momento. Es muy importante la labor de la ciencia para entender enfermedades tan complejas como el Alzheimer. Una enfermedad que desgraciadamente vivimos de cerca en nuestra familia, así que no dudé en querer entenderla mejor y poder aportar mi granito de arena en investigar la enfermedad que sufrió mi abuela Sara. Muchas gracias Jordi por dejarme participar en este proyecto. Abuela, esta va por ti.

Contents

List of Figures

List of Tables

List of Abbreviations

2D	Two-dimensional
3D	Three-dimensional
AD	Alzheimer's Disease
AVVs	Adeno–Asociated viruses
BBB	Blood–Brain–Barrier
CFP	Cyan Fluorescence Protein
CNS	Central Nervous System
DIV	Day *in vitro*
DMSO	Dimethyl Sulfoxide
ECM	Extracellular matrix
ES	Embryonic Stem cells
FENS	Federation of European Neuroscience Societies
fps	frames per second
FUDR	(5-fluoro-deoxy-uridine)
$GABA_A$	Gamma-Aminobutyric Acid type A
GECIs	Genetically Encoded Calcium Indicators
GFP	Green Fluorescent Protein
GTE	General Transfer Entropy
hiPSC	human induced Pluripotent Stem Cells
IBEC	Institute of Bioengineering of Catalonia
IBI	Inter Burst Interval
LVR	Linear Viscoelastic Region
MEAs	Microelectrode arrays
MEM	Modified Eagle Medium
MI	Mutual Information
MT	Microtubule
MTBD	Microtubule's binding domain
NDs	Neurodegenerative Diseases
NFTs	Neurofibrillary Tangles
PBS	Phosphate-buffered saline
PDL	Poly-D-lysine
PDMS	Polydimethylsiloxane
PEG	Polyethylene glycol
PEG-NHS	Mono-Methyl polyethylene glycol succinate N-succinimidyl ester

PLL	Poly–L–Lysine
PrP	Prion Protein
PrDs	Prion Diseases
pTau	Hyperphosphorylated tau
RD	Repeat domain
ROIs	Regions Of Interest
RPM	Revolutions per minute
SAOS	Small Amplitude Oscillatory Shearing
SEM	Scanning Electron Microscopy
SENC	Sociedad Española de Neurociencia
TE	Transfer Entropy
TIF	Triton X-100 insoluble fraction
tPA	tissue plasminogen activator
uPA	urokinase plasminogen activator
YFP	Yellow Fluorescence Protein

List of Symbols

A	Population activity
E	Young's modulus
G'	Storage modulus
G''	Loss modulus
G^*	Complex shear modulus
G_E	Global Efficiency
Q	Modularity index
τ	Shear stress
ω	Oscillation frequency
γ	Shear deformation
δ	Phase shift
ν	Poisson's ratio

A mi abuela Sara

1 General Introduction

The brain is widely acknowledged as the most intricate system in nature. During development *in vivo*, a single cell exhibits the remarkable ability to give rise to an entire human body. Among this inspiring phenomenon, one that truly stands out is the formation of the brain itself, which is achieved by the most complex choreography and orchestration of cells, creating the elaborate organ that governs our thoughts, emotions, and actions. Throughout the annals of scientific exploration, the quest to understanding this enigmatic powerhouse has driven humanity's pursuit of knowledge and innovation.

Neurons are the main players in the well–functioning of the brain; they bear the responsibility of processing information gleaned from sensory organs, translate it into rhythmic activity, and process it to make sense of the environment and interact with it. Indeed, among the primary functions performed by neuronal activity are the storage, retrieval, and continuous updating of encoded information. This dynamic process enables us to comprehend the world around us, tap into our memories, and initiate purposeful actions. Nevertheless, the precise rules governing these operations and the underlying intricacies of their organisational dynamics remain a subject of ongoing exploration and discovery. These inquiries sowed the seeds of what would later evolve into a complex and multidisciplinary field, *neuroscience*, which seeks to unravel the intricacies of the brain and cognition.

The birth of modern neuroscience can be ascribed to a man who hunched over a microscope in Spain at the beginning of the 20th century. Santiago Ramón y Cajal, often referred to as the 'father of modern neuroscience', was a neuroanatomist that in 1891 formulated the *neuron doctrine*, which proposed that the nervous system was composed of individual cells called *neurons* that were discrete and did not physically merge into one another, as was previously believed (Cajal, 1954; Guillery, 2005). Ramón y Cajal began his work out of an interest in visual arts and photography, and dedicated himself to pioneer in the refinement of innovative techniques for staining and visualizing nerve cells and their sophisticated processes under the microscope. His meticulous and artistically impressive drawings of neurons have been acclaimed for their remarkable accuracy and aesthetic appeal, as exemplified in Figure 1.1. In recognition of his groundbreaking work, Ramón y Cajal was jointly honored with the Nobel Prize in Physiology and Medicine in 1906, alongside Camillo Golgi, who laid the foundations of silver staining techniques (Pannese, 1999)

The neuron doctrine reflects, in its roots, the predominant view and methodologies of the early 20th century, which claimed that single neurons could explain everything,

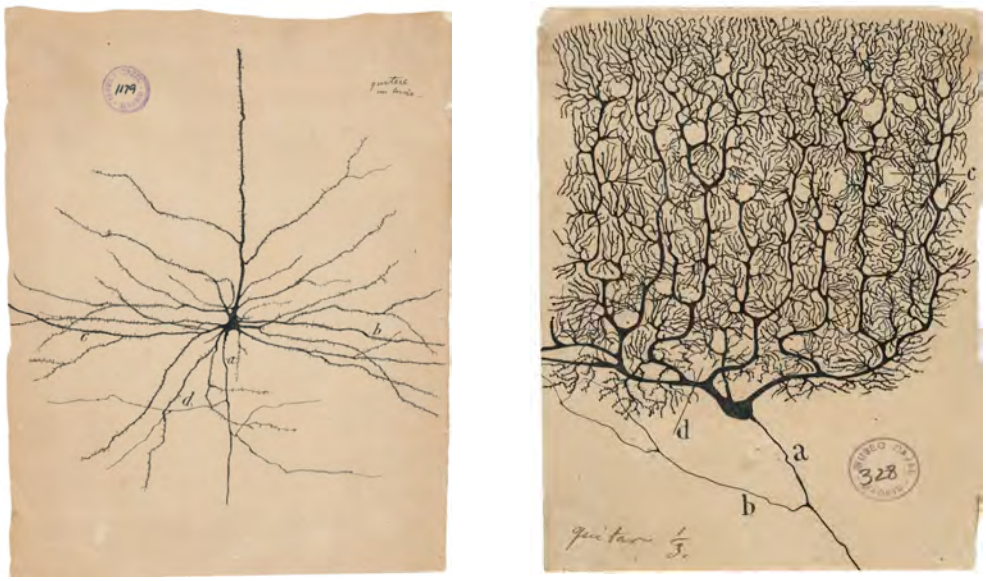

Figure 1.1. Ramón y Cajal's most iconic images. **Left**: a Purkinje neuron; Ramón y Cajal studied them with fervour and illustrated their tree–like structure in great detail, as in this particular neuron of the cerebellum. **Right**: a Pyramidal neuron in the cerebral cortex, the outer part of the brain that processes our senses, controls motor activity and helps us perform higher brain functions, such as decision-making. In both drawings, axons are indicated with the letter '*a*'.

thus fostering the use of single–neuron anatomical and physiological techniques. However, the landscape of neuroscience has evolved significantly since then, with advancements in multineuronal recording techniques revealing that assemblies of neurons, in contrast to individual cells, can form physiological entities and give rise to emergent *functional states* or *complex collective behaviour*. This change in paradigm from 'a collection of individual cells' to a 'networked system' marked the beginning of a new era in neuroscience, characterised by *neural network models*, which postulate that neuronal circuit functions emerge through the coordinated activation of groups or ensembles of interconnected neurons (Churchland and Sejnowski, 1992) (see Figure 1.2). These neuronal assemblies produce functional states that cannot be identified by just studying individual neurons at a time, thus requiring a *mesoscopic*, integrated view at the level of the neuronal circuit. The impressive advancements in optical, electrophysiological, and computational tools since the 1980s have opened the door to the study of communities of neurons, enabling a deeper understanding of the emerging complex states and collective behaviour that the circuits are able to produce.

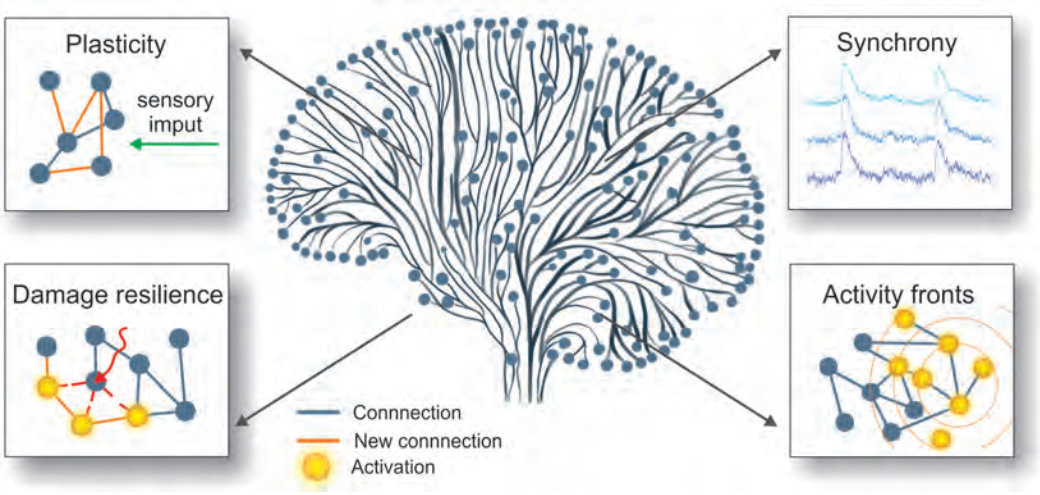

Figure 1.2. The connection of neurons to form a neural network transcends the mere aggregation of single neurons. Within the brain, emergent phenomena, including synchrony, neuronal activity fronts, plasticity, and resilience to damage, come into play. These collective aspects underscore the complexity and interconnected nature of neuronal networks. This figure provides a visual representation of the intricate dynamics that shape neuronal network behaviour, in which yellow auras represent neuronal activations and orange connections are new connections.

1.1 The mammalian brain

During embryogenesis, neuroblasts, the precursor cells for neurons, undergo a process of division and differentiation that gives rise to the cellular components of both the peripheral and central nervous systems (CNS). Neuroblasts are destined to differentiate either into neurons, responsible for the transmission and processing of information, or into glial cells, which play diverse and complementary roles within the nervous system (e.g., regulation of the biochemical environment or assistance in neuronal communication). In addition to neurons and glial cells, the nervous tissue encompasses the extracellular matrix (ECM), blood vessels, as well as cerebrospinal fluid–filled spaces, such as ventricles and the spinal canal. Nascent neurons extend multiple protrusions that can develop into intricate structures, with many tree–like branches or processes. In immature neurons and in many *in vitro* experiments, these structures are referred to as *neurites*. As neurons mature, one of these neurites differentiates into an *axon*, a specialized neuronal extension designed for transmitting signals to other cells, enabling downstream communication with neurons, organs, muscles, and the skin. The remaining neurites evolve into *dendrites*, which are shorter and highly branched processes responsible for receiving information. Axon terminals connect to dendrites or neuronal bodies to establish specialized connections called *synapses* and that are the true computational building blocks of a neuronal network. As the brain develops, neurons form increasingly complex networks in which communication between neurons primarily relies on synaptic specialization, chemical or electrical signals transmitted

among different elements within the neuronal circuits. The growth of these circuits is guided by growth cones, which are found at the leading tips of neuronal processes. Once the neuronal network is established, axons continue to grow passively through stretching mechanisms (Weiss, 1941; Essen, 1997). Interestingly, the genetic information stored in the initial cell shapes a coarse human brain with the minimal instruction set to crudely operate. Once the human is born, sensory input and environmental interaction refines brain's connectivity to achieve precise functionalities, a process that actually never ends.

The cerebral cortex constitutes the outermost layer enveloping the cerebrum. It is characterised by its folded and wrinkled appearance, measuring approximately 2 to 4 millimeters in thickness and housing billions of neurons that conduct high–level executive functions. In almost all mammals, including humans, the cortex is divided into two hemispheres by the longitudinal fissure, further divided into four distinct lobes with specialized functions: frontal, parietal, occipital, and temporal, as detailed in Figure 1.3a (Shipp, 2007). The cortex hosts about $10-20$ billion neurons (Von Bartheld, Bahney, and Herculano-Houzel, 2016) that are organised into six horizontal layers defined as supragranular (Layer II and III), granular (Layer IV) and infragranular (Layer V and VI) (Mountcastle, 1997). Within this intricate neuronal architecture, neurons establish horizontal connections both within and across cortical areas. Additionally, they form radial connections within functional columns that encompass neurons from various layers (Amorim Da Costa and Martin, 2010). Throughout evolution, neuronal circuitry within the neocortex has significantly expanded in both size and complexity, leading to the emergence of a diverse array of neuronal types that can be broadly categorized into two main groups: excitatory pyramidal neurons, which constitute the vast majority, and inhibitory cortical interneurons that establish local connections within the neocortex (Rash and Grove, 2006; Greig et al., 2013; Lodato and Arlotta, 2015).

The brain ultimately sets a network of connections governed by complex dynamic patterns that ensure its proper functioning. Minimal deterioration of these connections can lead to the onset of neurological disorders (Öngür et al., 2010; Yao et al., 2010; Gan et al., 2018). Interestingly, many diseases are strongly linked to abnormalities in the cerebral cortex, resulting in cognitive or motor impairments. Hence, gaining insights into the role of cortical neuronal circuits in maintaining healthy functionality, understanding the mechanisms governing their activity, and, most crucially, unraveling how a cascade of damage can culminate in system failure are imperative steps for advancing the development of innovative treatment approaches.

Due to ethical issues and the limited accessibility to human tissue for study, animal models have played a fundamental role in the study of neuronal dynamics during development, maturation and disease. In particular, the use of rodents (including mice and rats), which are the primary subjects of scrutiny in the field of neuroscience research, has significantly advanced the understanding of numerous biological processes (Semple et al., 2013; Dawson, Golde, and Lagier-Tourenne, 2018). Rodents exhibit certain

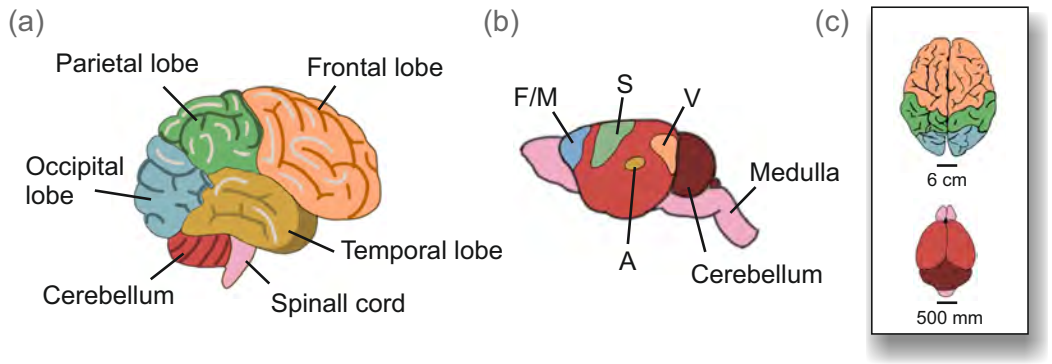

Figure 1.3. Human vs. mouse schematic brains **(a)** A schematic diagram of the human brain cortex reveals four distinct lobes, each performing specific functions. The frontal lobe, situated anteriorly to the central sulcus, houses the motor cortex. The parietal lobe lies behind the central sulcus, separated from the occipital lobe by the parieto–occipital sulcus, receives sensory and proprioceptive input from across the body. The occipital lobe houses the visual cortex, where information from the retina is received and processed to interpret and recognize visual stimuli. Lastly, the temporal lobe is responsible for processing auditory stimuli through the auditory cortex. **(b)** Schematic illustration depicting the primary neocortical areas in mice, specialized in processing different sensory modalities and overseeing precise motor control: the frontal/motor cortex (F/M), the somatosensory cortex (S), the auditory cortex (A), and the visual cortex (V). **(c)** The mouse brain (bottom) is much smaller than the human's (top). In addition, there are some differences regarding the cortical folding: the mouse cortex is smooth while human cortex is wrinkled, enabling higher cognitive functions.

genetic and physiological resemblances to humans, making them valuable models for mimicking neuronal diseases, both *in vivo* and *in vitro* settings. In contrast with the human cortex, four different areas can be defined in the mouse neocortex (see Figure 1.3b) (Rash and Grove, 2006).

It is worthy to mention that the mouse brain is smaller than human's, and presents some differences regarding the external appearance, as the mouse brain is relatively smooth. In contrast, human brain is highly folded, which increases the surface area of the cortex enabling higher cognitive functions (Figure 1.3c). In addition, in spite of being organised in columns, the thickness of the layers and the number of neurons varies considerably between species (DeFelipe, 2011). On the other hand, while certain key events during corticogenesis appear to follow a consistent pattern in both humans and rodents, it is important to note that there are substantial disparities in the timing of cell expansion and neuronal maturation across species. For instance, the generation of induced cortical neurons *in vitro* takes at least forty times longer in humans as compared to rodents (Espuny-Camacho et al., 2013; Semple et al., 2013). Moreover, human pyramidal cells exhibit distinct anatomical characteristics when compared to their rodent counterparts, including unique membrane properties and a higher number of dendritic spines—-synapses per cell (Eyal et al., 2016; Deitcher et al., 2017). Despite the utility of rodent model in research, these marked differences underscore the caution required when extrapolating results directly from animal models to humans.

1.2 Neuronal connectivity

Neuronal circuits, especially within the mammalian brain, exhibit a distributed connectivity pattern characterised by a matrix in which a given neuron receives input signals from several other neurons, while it simultaneously sends output signals to an extensive population of downstream neurons (Greig et al., 2013; Yuste, 2015). This rich connectivity leads to spatiotemporal activity patterns that involve different types of neuronal populations and timescales, which can be either localized neuronal discharges in response to external stimuli or spontaneous activations that span the entire brain (Deco et al., 2008; Blankenship and Feller, 2010). This spontaneous brain activity is not random but displays specific features underpinning brain function. This phenomenon is often referred to as the brain's *resting state* (Deco, Jirsa, and McIntosh, 2011; Deco and Jirsa, 2012). Remarkably, it plays a crucial role in facilitating rapid communication between different brain regions, sustaining alertness, enabling swift responses to external stimuli, and continuously fine–tuning and maintaining neuronal circuits (Deco, Jirsa, and McIntosh, 2011; Cohen and D'Esposito, 2016).

At early developmental stages of the vertebrate brain, neurons in the cerebral cortex show spontaneous network activity (Khazipov and Luhmann, 2006). In this context, as said above, traditional models of development include an early stage in which rough wiring of the nervous system is established. In this stage, cells show a non–correlated cell–by–cell activity that determines events as neuronal migration or neuronal differentiation (Spitzer, 2006; Gonzalez-Islas and Wenner, 2006; Luhmann et al., 2016). Later on, during a second developmental stage, a refinement of established connections occurs driven by sensory experience that is governed by interactions between a functionally–oriented nervous system and external stimuli (Riccomagno and Kolodkin, 2015). The importance of spontaneous activity becomes evident when considering that disturbances in its spatiotemporal patterns lead to extensive motor and cognitive impairments, as seen in conditions like Parkinson's, Alzheimer's, and other neurodegenerative diseases (Seeley et al., 2009; Fox and Greicius, 2010; Fornito, Zalesky, and Breakspear, 2015).

The fact that spontaneous activity exhibits non–random attributes raises the question of their origin and functional significance. The concept that the structure of neurons and neuronal circuitry is shaped by the conservation of resources, such as space and material, has long been recognized as crucial, as articulated by Ramón y Cajal in 1891. A wide spectrum of factors influences the cost of neuronal communication including wiring length, the timing of signal propagation, or the metabolic cost of neuronal activity (Laughlin and Sejnowski, 2003; Lennie, 2003). In most of the cases, the cost of communication is proportional to the spatial distance between neuronal elements (Chklovskii, 2004). Therefore, dynamic neuronal patterns need meticulous optimization to achieve an equilibrium between energy usage and functionality. This optimization involves moving away from random network distributions, which are highly

costly, given that their topology lacks any correlation with physical space (Sporns, 2011; Bullmore and Sporns, 2012). Instead, brain connectivity drawn a complex topological network including the existence of the, so called, *networks communities* or modules, groups of densely interconnected neurons that enable the formation of functional communities and specialization.

Hence, communities play a vital role in preserving the costs associated with neuronal communication and wiring while enhancing local efficiency. Nonetheless, establishing a communication between different communities requires the addition of high–cost long–distance axonal projections, which give rise to connector hubs (Meunier, Lambiotte, and Bullmore, 2010; Bullmore and Sporns, 2012). This structural aspect of brain organisation endows it with the capacity to function either as a cohesive whole (integration) or as a network of specialized, localized communities (segregation) (Sporns, 2013a). This equilibrium between segregation and integration, often referred to as the *segregation–integration balance* (Deco et al., 2015), operates at various scales within the brain. Swift transitions between these modes of operation are thought to be crucial for optimal brain performance.

1.2.1 Classification of neuronal connectivity

The anatomical or *structural connectivity* of the brain describes the physical arrangement of connections between circuit elements, encompassing synapses, neurons, and different brain regions (Figure 1.4a). However, brain connectivity transcends beyond the mere anatomical connections; it also encompasses the dynamic interaction patterns that accompany neuronal activity (Horwitz, 2003). Thus, *functional connectivity* appears as an additional yet important description that characterises the level of dynamic interactions across neurons or neuronal circuits. Conceptually, the functional connectivity reflects patterns of *statistical correlations* between neuronal elements, typically assessed through techniques like cross–correlation, covariance, or mutual information (Figure 1.4b). Therefore, functional connectivity is defined as the statistical interrelationship among remote neurophysiological events, and often based on patterns of synchronised neuronal activity or temporal correlations (Friston, 2011).

However, identifying statistical relationships between stimuli and responses accounts for only a portion of neuronal dynamics. To gain a more comprehensive understanding of the actual connectivity within a neuronal circuit, the concept of *effective connectivity* has been also introduced. Effective connectivity is centered on unraveling the causal influence and, in turn, directed flow of information between different elements (Figure 1.4c). Effective connectivity aims to determine not only whether neurons or brain regions are correlated but also the direction and strength of the information flow between them (Vicente et al., 2011). It is calculated using information–theoretic approaches such as transfer entropy (Vicente et al., 2011; Orlandi et al.,

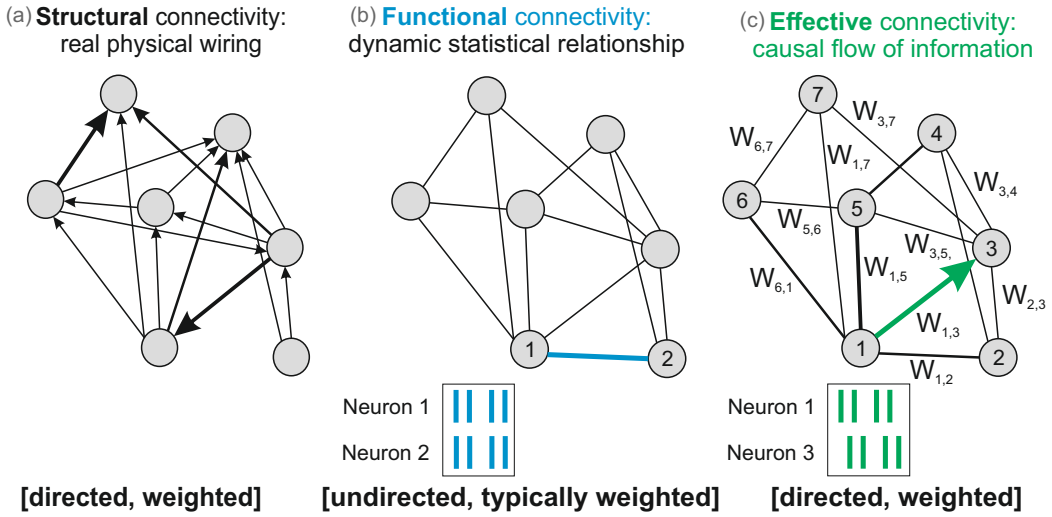

Figure 1.4. Classification of neuronal connectivity. **(a)** The structural connectivity of a neuronal network is defined by the real physical wiring, the synaptic connections. Structural connections are directed and weighted. **(b)** Functional connectivity is defined as the statistical relationships between firing neurons. It depends on the analysis method. In the example, neurons 1 and 2 activate together (blue lines) meaning that they are statistically related. Therefore, they are functionally connected. **(c)** Effective connectivity is based on the causal flow of information between neurons. It is difficult to assess and depends on the chosen analysis method. In the example, the green arrow signifies that the activity of neuron 1 causally affects the activity of neuron 3, i.e., neuron 1 activates neuron 3.

2014). In summary, functional connectivity focuses on identifying statistical associations between the activities of neuronal elements, while effective connectivity takes a further step by seeking to establish causal relationships and the direction of information flow. Both concepts offer valuable insights into how the brain functions and communicates, addressing different aspects of neuronal interactions.

The growing wealth of empirical data related to brain networks, ranging from studies that employ tract–tracing methods in mammalian brains (Felleman and Van Essen, 1991; Scannell et al., 1999) to those utilizing non–invasive neuroimaging techniques (Achard et al., 2006; Hagmann et al., 2008), has inspired collaborative efforts focused on creating comprehensive maps of connectivity, known as *connectomes*, for a variety of organisms including humans (Sporns, Tononi, and Kötter, 2005). The connectome seeks to map all the neuronal connections or pathways between individual neurons in the brain and can be structural or functional depending on the type of connections that it refers to (Bullmore and Bassett, 2011). Nevertheless, the relationship between structural connectivity and effective–functional connectivity is interesting and needs to be treated with due care. Researches frequently complete their investigations by incorporating structural connectivity alongside functional and effective connectivity measures (Damoiseaux and Greicius, 2009; Kim et al., 2011). While effective connectivity is often viewed as a proxy for structural connectivity (Messé et al., 2014),

it is essential to recognize that effective connectivity alone does not provide a comprehensive or fully adequate description of neuronal connections. Indeed, making the assumption that functional or effective connectivity uncovers the entirety of the structural network within a neuronal circuit is a perilous oversimplification (Logothetis, 2008; Bijsterbosch et al., 2020).

Indeed, it is crucial to acknowledge that structural and functional–effective connectivity exhibit distinct spatiotemporal characteristics (Betzel et al., 2014). Functional and effective connectivity are inherently dynamic and variable, undergoing rapid changes on the order of milliseconds. These fluctuations often mirror shifting patterns of intrinsic neuronal activity or responses to external stimuli, such as alterations in network organisation in response to varying task demands (Cohen, 2018). In contrast, structural connectivity operates on longer timescales, shaped by processes like growth, connectional maturation, and plasticity. These disparities underscore the multifaceted nature of brain connectivity, with each description providing unique insights into neuronal functioning and adaptability.

1.3 From the brain to neuronal cultures

Extensive examination of neuronal circuitry within the brain has undergone meticulous scrutiny, facilitated by classical anatomical methods and the aforementioned connectome investigations (Sporns, 2013b; Fornito, Zalesky, and Breakspear, 2015). However, a conspicuous knowledge gap persists regarding the essential structural components of circuits responsible for executing specific motor and cognitive tasks within the brain. Unravelling the intricacies of the brain and its information–processing building blocks has long been hindered by the challenge of accessing and regulating the complex microenvironments within the neuronal cytoarchitecture of the brain. These challenges, also hampered by ethical considerations, have underlined the need to develop *in vitro* models of neuronal circuits.

In 1910, Ross Granville Harrison at Yale University developed a method that demonstrated for the first time that living tissues from vertebrates could be cultivated and studied outside the body. He not only demonstrated that the neuron doctrine hypothesis was correct, but gave birth to the concept of *neuronal culture*, in which neurons and the networks they form can be explored in exquisite detail using a wide spectrum of techniques (Harrison, 1910). Since then, protocols for primary neuronal cultures have improved significantly, as reviewed in Millet and Gillette, 2012; Chiappalone, Pasquale, and Frega, 2019.

Primary neuronal cultures are typically derived from embryonic rodents, often rats or mice, or invertebrates such as locusts. Neurons are typically isolated from cortical or hippocampal tissue, dissociated mechanically, and then placed onto sterile surfaces along with a nutrient–rich medium, where they can be sustained for weeks when provided with the appropriate conditions (Banker and Cowan, 1977). Isolated primary

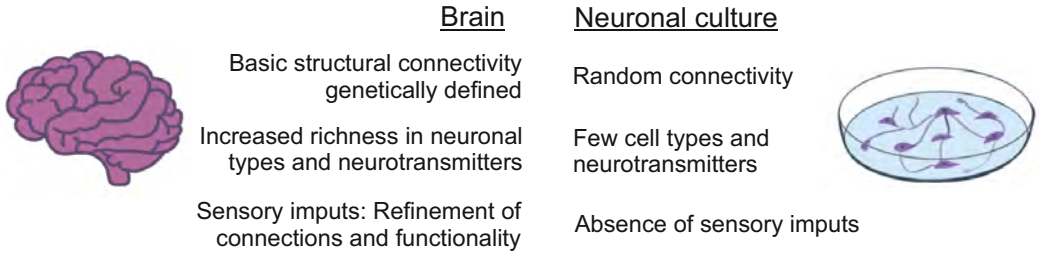

Figure 1.5. Neuronal cultures have been optimized as models of the brain, yet notable differences persist. In the brain, the foundational structural connectivity is genetically pre–defined, encompassing a diverse array of neuronal types and neurotransmitters to ensure optimal functioning. This intricate network is further honed by sensory inputs from the environment, shaping the brain's ultimate functionality. In contrast, neuronal cultures exhibit a purely random structural connectedness, refined primarily for energy efficiency aspects due to the absence of environmental input. Moreover, the neuronal population in cultures is confined to the initially seeded neurons, limiting the diversity seen in the brain.

rodent neurons undergo a development process in culture that results in the acquisition of morphologies and characteristics resembling neurons in their natural *in vivo* environment. However, as illustrated in Figure 1.5, there are some discernible differences when comparing neurons in culture with their natural brain environment, such as a smaller range of neuronal types and neurotransmitters, or a randomly driven connectivity due to the absence of genetic guidance or sensory input.

Within a few days under cultured conditions, neurons mature *in vitro*, establish synapses and generate action potentials (Bacci et al., 1999; Tibau et al., 2018). This maturation process give rise to spontaneous activity, which can be viewed as a relatively straightforward yet crucial network function (Saberi-Moghadam et al., 2018; Cohen et al., 2008). This spontaneous activity is believed to arise from the intrinsic neuronal dynamics coupled with neuronal noise and connectivity correlations. Random activity events are further amplified through specific mechanisms in which each spike from a presynaptic neuron heightens the likelihood of activating several neighbouring neurons, ultimately giving rise to propagating waves of activity (Mazzoni et al., 2007; Wu, Huang, and Zhang, 2008; Orlandi et al., 2013). *In vitro*, neuronal spontaneous activity patterns are characterised by discrete time series of action potentials separated by extended quiescent intervals, conforming spike trains. The accumulative effect of individual spikes ultimately leads to coordinated neuronal activations, manifested as either avalanches (Beggs and Plenz, 2003; Pasquale et al., 2008) or highly synchronised events known as *network bursts* (Rolston, Wagenaar, and Potter, 2007; Orlandi et al., 2013).

After decades of extensive utilization, protocols for primary neuronal cultures have become firmly established and highly reliable, encompassing well–defined media formulations and specific growth factors (Brewer et al., 1993; Brewer, 1995). One notable advantage stems from the similarity between human and rodent neurons, which enables researchers to regard rodent's–derived cultures as valuable models for investigating the

intricacies of the human brain and its associated pathologies. This positioning has elevated rodents to a prominent status as leading experimental models in the field of neuroscience.

An alternative approach involves the use of stem cells to establish neuronal cultures, but the ethical considerations surrounding embryonic stem (ES) cells have restricted their widespread usage. However, the landscape changed dramatically with the groundbreaking invention of human induced pluripotent stem cells (hiPSCs), which involve the reprogramming of somatic cells to acquire pluripotency (Takahashi and Yamanaka, 2006; Takahashi et al., 2007), to later induce the differentiation onto neurons (Nishikawa, Goldstein, and Nierras, 2008; Shi et al., 2017). This technological breakthrough revolutionized the study of human neurons, as hiPSC–derived neuronal cultures maintain their intrinsic human characteristics while eliminating the need for animal models. Consequently, hiPSC–derived neuronal cultures offer the advantage of retaining human traits and obviating the use of animals, making them a valuable resource for neuroscience research.

HiPSCs represent a relatively recent technology pioneered by Yamanaka and his colleagues in 2006, for which they were awarded the Nobel Prize in Medicine in 2012 (Takahashi and Yamanaka, 2006). However, the protocols for hiPSC culture and differentiation are currently characterised by their slow, challenging, and partially unresolved nature. While hiPSCs are undeniably regarded as a promising avenue for neuroscience research, their practical utility has been hindered by the difficulty of establishing rapid and consistent cultures. Furthermore, as neurons in hiPSC–derived cultures mature, they undergo significant alterations in both their individual and collective activity (Koroleva et al., 2021). This dynamic evolution complicates the selection of an optimal time point for data acquisition or network analysis. Consequently, for the purposes of this Thesis, we opted for primary neuronal cultures. These cultures offer the advantage of enabling a swift exploration of experimental concepts and the acquisition of preliminary results in a reasonable time frame of about $1-2$ weeks, which contrasts with the $4-6$ weeks needed for obtaining mature hiPSCs (Koroleva et al., 2021)

1.3.1 Engineered circuits in two–dimensional neuronal cultures

In cultured environments, neurons possess the remarkable capacity to spontaneously extend neurites and establish synaptic connections with neighbouring neurons. When allowed to grow without physical constraints, these neurites tend to randomly extend, eventually covering the entire culture area. In such conditions, synapses are established between neurons that happened to encounter one another, resulting in neuronal cultures devoid of any predefined architectural plan. In this context of a highly isotropic networks, *in vitro* neuronal circuits have been instrumental in demonstrating a wide range of functions, including the investigation of complex oscillatory activities. In

2008, Bruce Wheeler introduced the innovative concept of *brain–on–a–chip* as the *'wild idea that nerve cells grown in culture could have reliable computational functions [...] thanks to applications of both engineering and applied biology'* (Wheeler, 2008). Brain–on–a–chip denotes an artificially designed system in which neurons can thrive, develop, and establish intricate connections, and within a predefined layout that guides neuronal connections. Scientists have since envisioned the potential for achieving more distinctive and advanced functions by constructing *in vitro* neuronal circuits with specific structural organisation (Wheeler and Brewer, 2010; Shein-Idelson, Ben-Jacob, and Hanein, 2011; Brofiga et al., 2021). These organised structures aim to confer the capacity for directed connectivity, modular arrangements, or controlled growth, thereby opening up new possibilities for scientific exploration.

In the pursuit of creating structured neuronal circuits within a 2D culture, precise spatial control over neurons and their processes emerges as one of the most pivotal techniques. One advanced method involves using microfabrication to guide the development of neuronal systems. This process imprints both neuronal components and how they connect onto a surface (Huh et al., 2010; Pan et al., 2015; Yamamoto et al., 2018). This approach provides enhanced control over the resulting network, as illustrated in Figure 1.6a, that shows a specially designed modular network. This ingenious layout was accomplished by applying microstamped adhesive proteins onto a substrate (Yamamoto et al., 2018). These methods are often integrated with recording approaches such as microelectrode arrays (MEAs) (Bisio et al., 2014), or they enable optical investigations through calcium imaging or immunofluorescence techniques (Albers and Offenhäusser, 2016; Yamamoto et al., 2018).

Additionally, microfluidic culture chips have been utilized to control neuronal growth since the introduction of Campenot chamber in 1977 (Campenot, 1977). These devices typically enable the separation of cell bodies from axons by controlling neurite outgrowth based on size, enabling the interrogation of sub–regions and their microenvironments. Furthermore, innovative techniques have been developed to precisely guide the direction of synaptic connections, achieved through the strategic design of microgrooves and compartmentalized chambers (reviewed in Wang et al., 2023).

Another approach involves the development of neuronal networks that harmoniously blend free self–organisation and engineering. They can be crafted through the application of topographical designs, e.g. as in Montalà-Flaquer et al., 2022. In this approach, neurons are cultivated on a two–level substrate with subtle variations in height where the topography itself plays a pivotal role in roughly steering the network's connectivity (Figure 1.6b). In the work of Montalà-Flaquer et al., 2022, this directed connectivity evidenced that the diversity of spontaneous activity patterns within the neuronal networks is governed by the physical connections between neurons and the cell density (as also observed in Messé et al., 2014).

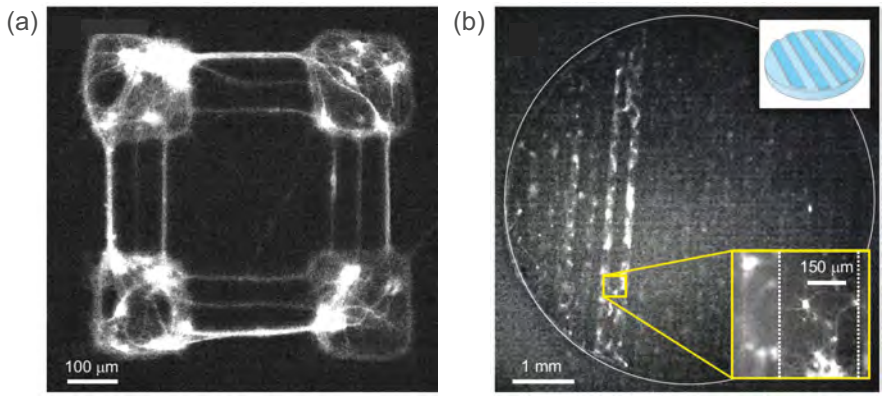

Figure 1.6. Engineering two–dimensional neuronal cultures. **(a)** Fluorescence image of an engineered neuronal culture in which neurons grow in small squared modules of 200 μm lateral size. Modules are interconnected through narrow corridors exclusively permitting the passage of axons. This innovative design was achieved through microstamping adhesive proteins onto a substrate (Yamamoto et al., 2018). **(b)** Fluorescence image showcasing an engineered neuronal culture by using topographical patterns (top-right sketch). Neurons in this culture were cultivated on top of a substrate featuring periodic tracks, each measuring 300 μm in width and rising to a height of 70 μm. These tracks were separated by 300 μm (as indicated by the white dotted lines in the bottom-right inset). This topographical culture exhibits a dynamic behaviour in which neuronal activity can manifest in different areas within the culture or across its entirety (Montalà-Flaquer et al., 2022). In the example provided, two tracks on the left side of the culture exhibit activation, while the rest of the network remains inactive.

1.3.2 Three–dimensional neuronal cultures

One of the primary challenges in studying functional interactions within large neuronal populations is the inherent difficulty of accessing deep neuronal circuits within the brain. For this reason, the 2D neuronal cultures described above were introduced, and taking advantage of their accessibility for observation and ease of manipulation. In recent years, however, tissue engineering has introduced innovative approaches for studying neuronal cultures *in vitro* with higher structural complexity, i.e. beyond a mere bidimensional surface (Chow et al., 2022). Drawing upon principles from biology, engineering, and materials science, efforts have led to the development of an interdisciplinary field that seeks to create functional, durable, and biocompatible substrates to bring to light three–dimensional (3D) neuronal cultures (Ozgun et al., 2022). These advancements provide a unique opportunity to investigate systems comprising thousands of neurons within a native, brain–like organisation and environment, all under precise control.

Figure 1.7 illustrates the differences between cell cultures in 2D and 3D environments. In essence, 3D matrices create an environment where cells can grow and develop while experiencing signals and mechanical forces akin to those found in the brain. Firstly, the secretion of factors by neurons generates concentration gradients, thereby enhancing their reception by adjacent cells. The presence of a surrounding

matrix confers numerous advantages for neuronal development. Notably, cell polarization in 3D is dictated by cell behaviour rather than the influence of the substrate, as seen in 2D cultures. Moreover, the internal matrix structure in 3D settings poses obstacles to cell spreading and migration, emulating the forces encountered in the brain that govern these migration processes. Conversely, on a flat, smooth surface, neurons encounter no hindrances and can move freely across it. Lastly, cell–matrix interactions, which are vital for healthy development, are significantly intensified within 3D environments, creating a more conducive environment for proper development (Tang-Schomer et al., 2014; Bourke et al., 2018). Through its physical structure, 3D matrices shape individual cell destinies, leading to alterations in tissue architecture, circuit development, and network functionality. This is why the mechanical properties of the matrix that hosts the 3D culture are of paramount importance. It is crucial that the matrix can withstand the mechanical stresses imposed by the extracellular matrix of the brain, stresses to which neurons are naturally exposed. Simultaneously, the matrix must possess the ideal combination of rigidity and resilience to effectively support and sustain the neurons throughout the culture period, which can extend up to one month for primary cultures and several months for hiPSCs cultures.

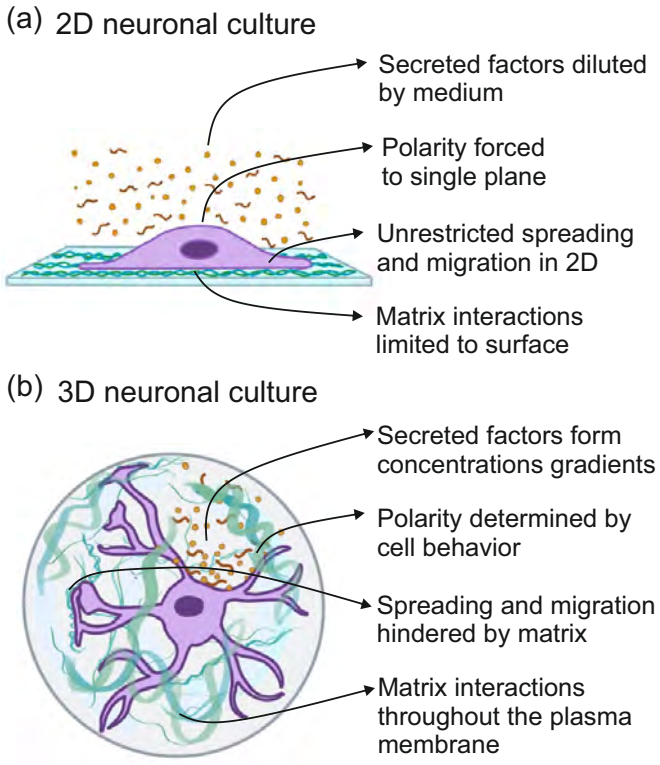

Figure 1.7. Comparison between neuronal cultures on different environments. **(a)** A 2D substrate such as glass. **(b)** A 3D matrix. The comparison outlines some of the important physiological features that affect cellular behaviour and development. Adapted from Ozgun et al., 2022.

3D cultures represent a significant step forward in modeling complex neuronal circuits, enabling the formation of synapses and the development of intricate circuitry with brain–like structures. The presence of the aforementioned 3D environment enables the emergence of a more diverse repertoire of spontaneous neuronal activity patterns, in comparison to conventional 2D preparations (Frega et al., 2014; Ulloa Severino et al., 2016; Brofiga et al., 2020). These 3D cultures exhibit organisational features, such as modularity (Bourke et al., 2018; Dingle et al., 2020; Rabadan et al., 2022) that closely mimic brain activity, which results in more intricate systems for conducting connectivity studies. As a result, 3D cultures offer a promising avenue for more accurately replicating the complexities of neuronal networks and their behaviour.

Stem cell research also propelled 3D tissue culture technologies, leading to *organoids*. Firstly introduced by Dr. Yoshiki Sasai, organoids demonstrated that stem cells can self–organise to produce complex 3D tissues (Eiraku et al., 2008; Lancaster et al., 2013). What sets brain organoids apart from previous human neuron models is the presence of cellular assemblies with spontaneously organised layers, closely resembling the natural developmental process of the human brain. This structural mimicry holds great potential for the creation of intricate neuronal circuit constructs. However, it is worth noting that the connectivity within these assemblies does not faithfully replicate the *in vivo* neuronal connections (Souza, 2017). Several challenges are associated with brain organoids, including uncontrolled development and the variability in cell types, which can lead to poor reproducibility (Silva et al., 2019). Additionally, brain organoids encounter similar imaging limitations as *in vivo* studies, demanding the application of advanced microscopy techniques such as light sheet microscopy (Hillman et al., 2019). Alternatively, researchers may opt to confine the study of activity to a single plane within the organoid to accurately capture and record its functional dynamics (Paşca et al., 2015). Electrophysiology approaches may be employed, although they often provide lower spatial resolution as compared to calcium imaging techniques (Quadrato et al., 2017).

In summary, brain tissue engineering seeks to develop complex *in vitro* 3D neuronal cultures, offering promising opportunities for regenerative medicine. This approach is especially encouraging when utilized alongside hiPSCs, which opens up new horizons for the study of brain connectivity, although it is essential to exercise caution due to its associated limitations.

1.3.3 Neuronal cultures as models for neurological disorders

In recent years, modern network science has opened up exciting avenues for understanding the brain as a complex system of interacting units. Remarkably, within this framework of complex networks, a meticulous exploration of functionally active neuronal networks seeks to bridge gaps in our understanding of the typical organisation of

brain networks, which has paved the way for investigating network alterations in neurological and psychiatric conditions (Schlachetzki, Saliba, and Oliveira, 2013; Stam, 2014; Medaglia and Bassett, 2017).

Brain disorders encompass a diverse range of neurological and psychiatric conditions that affect the structure and function of the brain. These conditions can arise from various factors, including genetics, environmental influences, infections, traumatic injuries, and aging (Brown, Lockwood, and Sonawane, 2005; Dugger and Dickson, 2017; Hou et al., 2019). Disorders broadly include those alterations caused by acute damage, as stroke or traumatic brain injury, neurodevelopmental deficits, as autism or schizophrenia, and neurodegenerative diseases. This last group encompass pathologies such as Alzheimer's, Huntington's, Parkinson's diseases, which may uniquely affect specific cell types or regions of the nervous system but have whole–brain implications, from cognitive decline to acute motor tremors.

Contemporary research aims to establish a connection between disease–induced structural changes and the corresponding functional or cognitive impairments and their evolution over time. This ambitious goal has required the development of experimental and analytical tools capable of effectively comparing structural and functional networks in both healthy and diseased conditions. Consequently, researchers have meticulously crafted various *in vivo*, *ex vivo*, and *in vitro* models to facilitate these investigations. *In vitro* models, despite being far from a naturally–formed brain, offer interesting advantages, including the possibility of studding isolated cells in an environment that resembles the one of the disease. They yield critical insights into disease mechanisms and are widely employed for the investigation of potential pharmacological targets. Moreover, they can be tailored based on collected data to enhance the development of prognosis tools, treatment strategies, or the evaluation of novel therapies.

As examples of the use of *in vitro* models, rodent primary neuronal culture were used to study the impact of a focal lesion in network communication in stroke, where a focalized lesion can cause a cascade of damage (Sala-Jarque et al., 2020; Teller et al., 2020; Ayasreh et al., 2022). These models enable the exploration of the characteristic time–scale required for cultures to recover their pre–damage activity levels. Investigations like this one shed light on the capacity of neuronal circuits to sustain withstand damage, activate response mechanisms, and ultimately restore network activity and communication. In the context of neurodegenerative diseases, primary neuronal cultures have proven invaluable for studying deficits in the coordination of neuronal activity in a Huntington's disease model (Fernández-García et al., 2020). They have also been instrumental in investigating the effects of the aggregation of pathological proteins in Alzheimer's disease models on neuronal activity (Teller et al., 2015; Sala-Jarque et al., 2022). Remarkably, stem cell lines can be obtained from patients affected by genetic neurodegenerative diseases allowing for the investigation of these diseases in detail *in vitro* and to develop human–specific treatments (Ardhanareeswaran et al.,

2017; Engle, Blaha, and Kleiman, 2018; D'Souza et al., 2021). For example, network alterations in genetic Parkinson's disease were investigated using hiPSC–derived cultures (Fernández-Santiago et al., 2015; Carola et al., 2021). Results showed that neuronal cultures affected with Parkinson's disease exhibited an excessive integration in the network, a behaviour that could be minimized by correcting the genetic alteration (a malicious mutation in the LRRK2 gene) with CRISPR–Cas9 technology, restoring cultures' health (Calatayud et al., 2019; Carola et al., 2021).

The availability of systematic platforms capable of replicating the *in vivo* neuronal environment is paramount for gaining a deeper comprehension of brain functions in both healthy and diseased states. Recent advancements in microfluidics and microelectromechanical systems have yielded innovative platforms where, not only the microenvironments, but also the cellular morphology can be meticulously regulated using fluidic and patterning technologies (as reviewed in Van Der Meer and Van Den Berg, 2012; Yi et al., 2015; Osaki et al., 2018). In this direction, 3D neuronal cultures have been introduced with the aim of more accurately replicating the pathological conditions observed in neurological disorders, including potential alterations that may appear in cell–matrix and cell–cell interactions. Within this framework, biomaterials can serve as supportive matrices for cell proliferation, offering a platform for transplantation, as well as carriers for the delivery of various active molecules for the treatment of neurodegenerative disorders (Zhang et al., 2022). Furthermore, brain organoids have emerged as a significant advancement, derived from patient–induced pluripotent stem cells, to model disease phenotypes. This approach gained prominence following Lancaster *et al.*'s groundbreaking work in 2023, which demonstrated the differentiation of cerebral organoids from hiPSC obtained from individuals with microcephaly (Lancaster et al., 2013; Koroleva et al., 2021). Brain organoids are of particular importance due to their diverse cellular composition, which can aid in the understanding of cell–type–specific phenotypes associated with neurological disorders.

1.4 Scientific contribution of this PhD Thesis

In the intersection of neuronal cultures, NDs, and bioengineering, the initiative to develop an *in vitro* model capable of approaching the complexity of taoupathies takes shape. This group of diseases, marked by the accumulation of abnormal forms of tau protein, impacts more than 55 million people worldwide according to *Alzheimer's Disease International* (https://www.alzint.org/), yet little is known about their origin and neuronal-level symptoms. In Dr. Soriano's laboratory, we aimed to illuminate this mystery by investigating how the presence of abnormal forms of extracellular tau influences the development of primary mouse neurons *in vitro*, to have better approaches in order to develop new treatments. This involved characterising the neuronal dynamics and functionality of the treated networks and establishing differences between 'healthy' neuronal networks and tau–treated ones.

Concurrently, our project endeavors to contribute to the advancement of biomaterials suitable for studying 3D neuronal cultures, adding a crucial layer to our understanding. As mentioned in preceding sections, 3D cultures offer enhanced richness to *in vitro* models, mirroring natural neuronal environments more closely, and resulting in dynamic activity patterns that significantly enrich our research. In the realm of scaffolds tailored for hosting neuronal networks, mechanical properties emerge as pivotal factors, crucial for ensuring the robust and coherent development of neuronal networks. Considerations such as the stiffness or porosity of the matrix exert profound influences on axonal growth, the spatial organisation of neurons in a three–dimensional space, and the intricate transport of nutrients and molecules through the matrix (Balgude et al., 2001; Flanagan et al., 2002). To deepen our comprehension of mechanical properties and their impact on neuronal development, Dr. Planet guided me into the conduction of experiments involving neuronal cultures in 3D semi–synthetic hydrogels. Our investigation delved into the mechanical characteristics of gels populated with neurons. Additionally, we examined the functional dynamics and organisation of networks grown within these hydrogels, aiming to present a robust platform for the establishment of 3D neuronal cultures. Through these efforts, we sought to forge a meaningful connection between the mechanical properties of the hydrogel and the behaviour of neuronal networks.

In our pursuit, we considered primary neuronal cultures derived from mouse embryos as the core experimental toolbox, and incorporated new elements, namely biochemical action and dimensionality, to contribute our share in advanced platforms for 3D cultures, both in health and disease. In the next chapters we will delineate our objectives to next introduce the general methods use and, finally, detail our results in the different lines of research.

2 Objectives of the present thesis

Over the past few decades, the field of physics of complex systems has evolved into a formidable workshop of 'know–how', providing the means to model and predict phenomena in both the natural world and human–made technologies. Within this framework, one such model of a complex system is a neuronal culture. Their study allows us to examine the formation and development of *do novo* neuronal networks, monitor their spontaneous activity, and act on them via mechanical or biochemical means. The present PhD Thesis represents an interesting fusion of physics of complex systems, materials engineering, neuroscience, and medicine. Its overarching aim is to delve into the intricate characteristics of cortical neuronal cultures through two well–defined lines of research, namely biomedicine and rheology, which blend together to form a third line of research that encompasses bioengineering applications.

Objective 1: effective connectivity in affected neuronal cultures

This objective involves the investigation of neuronal connectivity *in vitro*, with a particular focus on aspects like effective connectivity and network analyses within the context of a group of neurodegenerative diseases generally known as *tauopathies* (Figure 2.1a). In humans, these diseases are characterised by the presence of abnormal aggregations of the microtubule–associated protein tau (pTau) within the brain. This condition is often accompanied by neuronal loss and cognitive decline and encompasses highly relevant diseases such as Alzheimer's disease and Pick's disease, among others. This research initiative was part of a 'La Caixa Health Research Program 2019', titled 'Modulation of Tau Seeding and Pathology in Tauopathies by BBB-nanocarriers, Epitope-Selective Vaccination, and EctoPrP Tau Receptor Bodies' (HR19-00452). This collaborative project united the efforts of four research groups, under the leadership of Dr. José Antonio Del Río (IBEC). Its ultimate objectives included analyzing the progression of tau–related damage both *in vivo* and *in vitro*, investigating the efficacy and possible toxicity of anti–tau agents, and examining the drug delivery capabilities of carriers engineered to transport these anti–tau agents.

In Dr. Soriano's lab, our specific role was to analyze the damage caused by pTau and its progression *in vitro*, and to design new analytical tools for evaluating damage. Within this project we delineated three primary goals: i) demonstrate the non–toxicity of pTau inhibitors (synthesized by Dra. Macarena Sanchez at University of Barcelona)

on cultured cells, ii) provide evidence of network damage *in vitro* due to the action of pTau, and iii) investigate the action of pTau inhibitors in network recovery.

To achieve these goals, we utilized primary neuronal cultures, a model with long–established protocols widely employed in Soriano's lab. In an attempt to replicate the tauopathy scenario, we introduced pTau extracted from various sources into the culture medium, provided by Dr. del Río's group at IBEC. We recorded and analyzed spontaneous neuronal activity, using fluorescence calcium imaging as main experimental tool, to detect differences between pTau–affected cultures and control ones.

Many of the necessary resources to fulfill these goals had to be designed from scratch. While the challenge of undertaking such an ambitious project was exhilarating, time constraints due to the three–year duration of the thesis put immense pressure on the project, forcing the search for innovative and efficient solutions to address complex issues. My immersion in this research topic was comprehensive, investigating every possible parameter that could be altered in the cultures, but with the necessary caution to avoid false positives. Consequently, certain initial project objectives could not be fully realized due to insufficient information at earlier stages. In other words, we extensively explored various aspects of the potential damage induced by the presence of pTau in primary cultures, but we were unable to establish the fundamental mechanisms responsible for tau–related changes, including dynamics and functional connectivity. This affected the third goal of this objective, i.e., the evaluation of network recovery by pTau–inhibitors, which could not be executed.

The main results from this investigation are under preparation for publication in the journal *Biomedicines*, but some key results will be published soon in C. F. López-León *et al.*, *Emergent complex dynamics in neuronal cultures and its relation to neuroengineering and medicine*, book chapter in *Nonlinear Dynamics in Biological Systems*, American Institute of Physics & Springer (2024).

Objective 2: rheological properties of PEGylated fibrin hydrogels

This objective involves the application of materials science in combination with physics of complex systems to investigate the matrix–neuron relationship in 3D neuronal cultures. Under the guidance of Dr. Ramon Planet and Dr. Jordi Soriano, we developed and characterised a 3D scaffold for culturing neurons *in vitro* based on PEGylated fibrin hydrogels. To demonstrate that the 3D matrix exhibited suitable mechanical characteristics for neuronal development, we employed rheological techniques to measure the scaffold's mechanical properties and their evolution over time, establishing a robust platform for constructing 3D neuronal models (Figure 2.1b). This project received financial support from the Generalitat de Catalunya under project 2021-SGR-00450, and from the Spanish Ministerio de Ciencia e Innovación, projects PID2019-108842GB-C21 and PID2021-122369NB-I00.

This line of research was started from the ground up. We formulated the relevant questions and designed the appropriate measurement protocol to characterise the hydrogels used to grow the 3D neuronal networks. Over time, the protocol has been continuously refined and adapted to assess both cell–bound and free–cell matrices, as well as to monitor their changes as they aged.

The main results from this investigation were published in the journal *Gels* in September 2023 (López-León, Soriano, and Planet, 2023).

Objective 3: impact of hydrogels' structure on network dynamics

The aforementioned objectives converged toward the final aim of this PhD Thesis, which entails establishing a cohesive relationship between the mechanical properties of the scaffold containing a 3D neuronal culture and the eventual functional organisation of the resulting network, both in health and disease. To achieve this objective, we conducted a comprehensive characterisation of the mechanical properties of three PEGylated fibrin hydrogels with gradually higher stiffness, concurrently exploring differences in their functional organisation through fluorescence calcium imaging and employing complex system tools for subsequent analysis (Figure 2.1c).

The results from this exploration will be published in *Gels* by January–February 2024.

2.1 The thesis at a glance

The objectives of the present thesis can be summarized as follows:

i) Design an *in vitro* model of tauopathies and investigate the potential conditions induced by the presence of pTau in mouse primary cortical cultures. Develop the essential tools to conduct comprehensive analyses, including assessments of neuronal connectivity and the toxicity of pTau–inhibitors.

ii) Establish and refine a rheological protocol necessary for characterising the evolution of the mechanical properties of 3D hydrogel matrices, and demonstrate their suitability as models for hosting neuronal cultures.

iii) Investigate the potential relationship between the mechanical properties of the scaffolds and the functional characteristics of the neural network that develops within them.

The work carried out to accomplish these objectives is presented in the next chapters of this Thesis, organised as follows. Chapter 3 provides an overview of the general

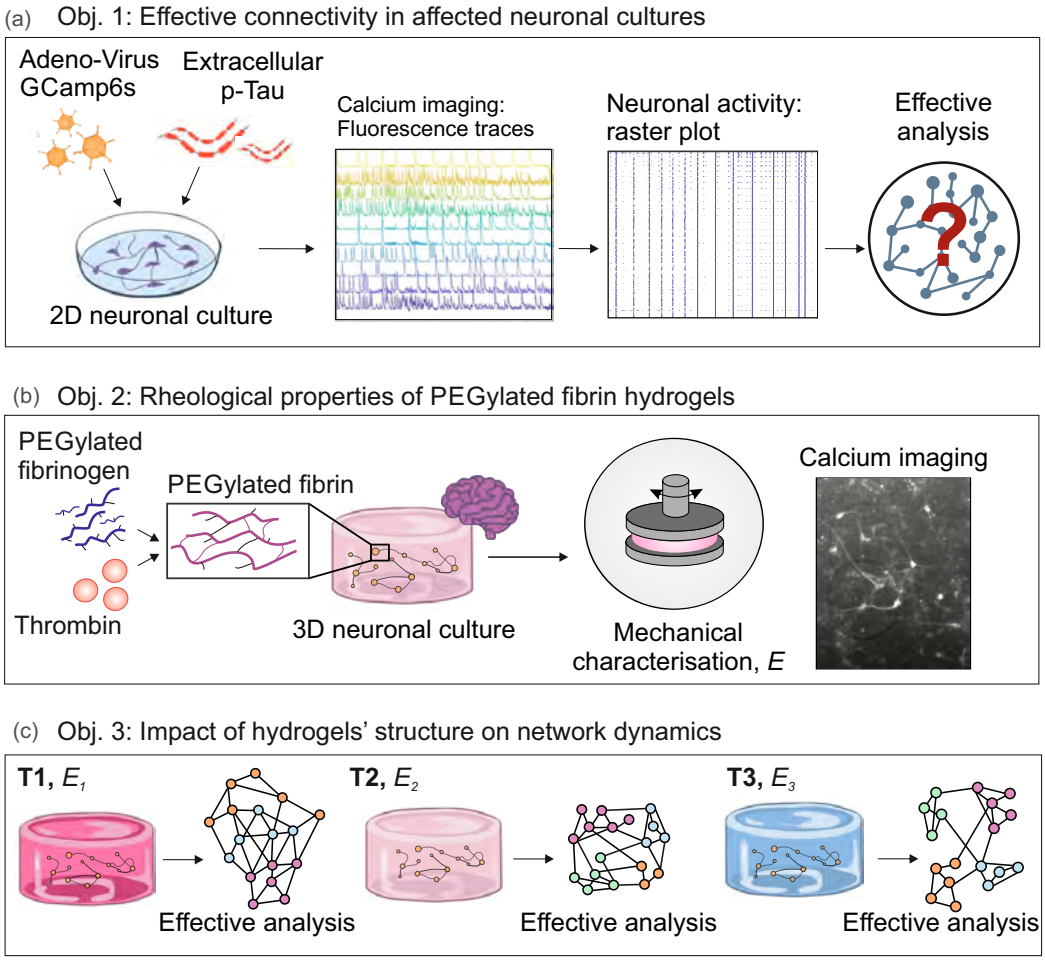

Figure 2.1. Illustration of the PhD objectives. **(a)** Objective 1: effective connectivity in affected neuronal cultures. Primary neuronal cultures were prepared from mouse embryos. To recreate tauopathie's scenario *in vitro* we included abnormal forms of tau in the extracellular medium and recorded neuronal activity by applying calcium imaging techniques. From the activity data we computed the effective connectivity of the affected neuronal cultures. **(b)** Objective 2: rheological properties of PEGylated fibrin hydrogels. PEGylated fibrin hydrogels were prepared and mechanically characterised by using a rheometer. We tracked the evolution of the Young's Modulus E for a three–week period for hydrogels with and without neurons. Calcium imaging test were conducted to verify the culture's viability. **(c)** Objective 3: impact of hydrogels' structure on network dynamics. Three variants of PEGylated fibrin hydrogels were prepared, T1, T2 and T3. We tracked the mechanical behaviour and the effective connectivity of the neuronal networks grown within the structure.

methods used for preparing primary neuronal cultures in both 2D and 3D environments. It also covers the numerical protocols used for data analysis and neuronal network characterisation. Chapter 4 delves into the experiments conducted as part of the 'La Caixa Health' project, which focused on the development of an *in vitro* tauopathies model. This chapter includes an introduction to tauopathies diseases, the preparation

of neuronal cultures affected by the presence of abnormal tau protein, data analysis, results, and a detailed discussion. Chapter 5 outlines the formulation of an hydrogel where neuronal cultures can grow in 3D and the design of a protocol to measure their mechanical properties. We characterised the evolution in time of the rheological properties of this hydrogels and how these properties are altered by the presence of neuronal cultures within the hydrogel. Finally, Chapter 6 presents preliminary results from the investigation of the effects of the mechanical properties of the matrix on the functional organisation of neuronal networks. As complementary aspects, Chapter 7 introduces my contributions to other projects during my three years of work at the University of Barcelona. Then, the Thesis closes with a general discussion of the results in Chapter 8 followed by final conclusions of the three–year work in Chapter 9. All published articles in which I participated are listed at the end of the thesis in Chapter 10.

3 General methods

Primary neuronal cultures represent a remarkable experimental model, offering a controlled, scaled–down, and reproducible platform for exploring the intricacies of complex brain functions. Such a neuronal culture model shapes a tool that have revolutionized our ability to dissect the impact of different physical designs and/or biochemical environments in the physiological development and connectivity of neurons within an *in vitro* framework. This tool finds applications across an array of research domains, including Physics of Complex Systems and Medicine, where it contributes to the investigation of CNS disorders from an *in vitro* perspective. Additionally, the field of Pharmacology benefits from its use by conducting toxicological assessments and drug screening initiatives.

The primary goal of this Chapter is to provide a detailed description of the neuronal cultures' methodologies and resources used in this Thesis. Firstly, a comprehensive overview of neuronal primary cultures is provided. This preamble sets the basis to present the experimental approaches, followed by the preparation of standard 2D neuronal cultures, topographically–patterned cultures, and 3D ones. Secondly, the application of calcium fluorescence imaging techniques is described, a tool that allows the acquisition of spontaneous neuronal activity serving as the source for all experimental data. And, thirdly, concepts from physics of complex systems are introduced to create a data analysis toolkit to study the collective behaviour of neuronal cultures.

3.1 Primary neuronal cultures

Standard primary neuronal cultures are prepared by planting individual cell bodies (somas) onto a 2D flat surface, usually a transparent glass–cover or a silicone elastomer such as polydimethylsiloxane (PDMS). Cells are obtained from the cortex of embryonic rodents, rats or mice (Figure 3.1a). Initially, isolated neurons self–organise to establish connections and evoke spontaneous activity events. Homogeneous neuronal cultures (Figure 3.1b) are those in which single cells are uniformly distributed along the culture surface. Neuron's membrane is covered by glycoproteins and glycolipids that play an important role in cell–to–cell interaction, but also contribute to the negatively charged surface of the membrane. Since glass coverslips and PDMS surfaces posses a negative charge,the cell membrane tends to avoid such surfaces. To promote attachment, adhesive proteins such as poly-L-lisine (PLL) can be used to generate an electrically charged layer suitable for neuronal adhesion.

Homogeneous neuronal cultures (Figure 3.1b) are an accessible approach for investigating the emergence of spontaneous activity (Chiappalone et al., 2006; Orlandi et al., 2013; Hernández-Navarro et al., 2021), the detection of possible alterations when exposed to different perturbations (Jacobi, Soriano, and Moses, 2010; Teller et al., 2015), the development of connectivity (Chiappalone et al., 2007; Soriano et al., 2008), and the resilience to damage (Ayasreh et al., 2022). However, it is important to remark that homogeneous neuronal cultures represent a highly simplified model of brain connectivity, since neurons essentially connect with their neighbours in a highly isotropic way that is very different from the organised structure of the native tissue. Thus, these cultures exhibit a highly coherent bursting behaviour (Orlandi et al., 2013), with neurons collectively activating within a short time window (*network bursts*) while remaining silent in–between bursts. Hence, the functional organisation of the culture is in general highly limited, with very weak brain–like organisational features such as modularity, hubs, smallworldness, or integration–segregation balance. These features are crucial to guarantee robustness and flexibility of neuronal networks, both during development and in mature stages (Meunier, Lambiotte, and Bullmore, 2010; Sporns, 2013a; Finc et al., 2020). Consequently, standard homogeneous neuronal cultures offer limited possibilities when one aspires to shape brain–like *in vitro* systems.

An alternative approach to enrich connectivity are aggregated neuronal cultures, in which neurons are organised in islands of about 100 μm in diameter connected between them by bundles of axons (Figure 3.1c). Aggregation is achieved either by plating neurons in pre–coated drops of PLL or by directly plating them on a bare glass surface. For the latter case, neurons exhibit a preference for avoiding contact with the non–coated surface, attaching to one another by a combination of migration mechanisms and axonal tensile forces (Shein-Idelson, Ben-Jacob, and Hanein, 2011; Santos-Sierra et al., 2014). Aggregated cultures display a richer repertoire of activity patterns as compared to homogeneous ones, in which aggregates are strongly inter–connected, showing a higher modularity with aggregates that coactivate in groups of different sizes. These characteristics offer scientists a more complex tool to study the behaviour of self–organised modular networks (Shein-Idelson, Ben-Jacob, and Hanein, 2011; Santos-Sierra et al., 2014; Teller et al., 2014) and resilience to damage (Teller et al., 2020), while keeping the simplicity of a 2D primary neuronal culture. Despite their advantages, aggregated cultures display some drawbacks. For example, as neurons are organised in small islands, the units under study are substantially larger (aggregate–sized) than for homogeneous cultures (neuron–sized) in the same area. In addition, reproducibility is hindered by the random process of aggregate formation, evidenced by the differences in strength and number of connections between aggregated pairs, as well as in the final layout of the network, which may differ from one preparation to another (Teller et al., 2014).

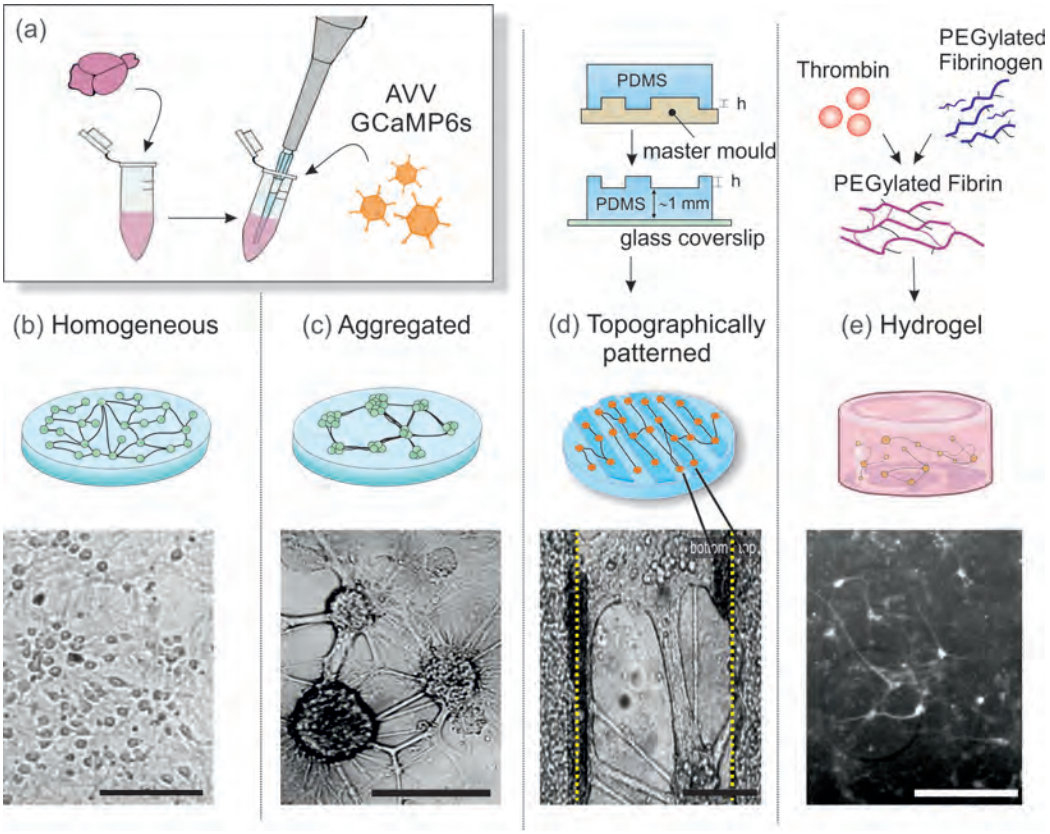

Figure 3.1. Neuronal cultures in Soriano's Lab. **(a)** Mechanical dissociation of cortical tissue from rodents' embryos generates single–neurons that can be culture *in vitro*. **(b)** Homogeneous cultures are obtained by pre–coating the glass surface with an adhesive protein. Neurons then arrange uniformly throughout the culture. **(c)** Aggregated cultures are characterised by the presence of groups of strongly packed neurons that built connection between each other. **(d)** Topographically–patterned cultures, in which neurons grow following topographic patterns made casted on a PDMS mould. For the example, PDMS describes two–level lines that cross the surface. PDMS moulds are obtained by pouring non–cured PDMS over a copper master mould (top sketch). **(e)** PEGylated fibrin hydrogels used as scaffolds to prepared 3D primary neuronal cultures, where neurons build a 3D network throughout the entire volume. Black and white scale bars are 100 μm.

To better control the relationship between activity and connectivity *in vitro*, topographical cultures were developed in Soriano's laboratory, a strategy that combines characteristics of homogeneous and aggregated organisation (Figure 3.1d). Neurons are grown in a PDMS mould with topographical reliefs, shaping different spatial constraints that guide neuronal connectivity (Montalà-Flaquer et al., 2022). The use of these engineered configurations allows to tune the dynamical patterns and functionality of the generated neuronal cultures (Forró et al., 2018; Park et al., 2021), effectually breaking the isotropy in connectivity found in homogeneous neuronal cultures.

Finally, three–dimensional (3D) neuronal cultures are introduced to shape models in which connectivity is not restricted to a single plane, but across a volume that allows

a better approach to the real connectivity of the brain (e.g., cortical columns), enabling connections across all three dimensions of the volume. In a conventional 3D culture, cells are embedded in rigid scaffolds, jelly matrices, or a combination of both. This 3D environment facilitates the emergence of features such as rich spatiotemporal neuronal dynamics, segregated local–global network activities and a hierarchical modular organisation reminiscent of the brain (Bourke et al., 2018; Dingle et al., 2020; Rabadan et al., 2022). In Soriano's Lab we chose a semi–synthetic hydrogel as scaffold to host primary cortical neurons (Figure 3.1e), whose characteristics and preparation protocol will be explained throughout this document.

3.1.1 PDMS patterns

PDMS is a silicone elastomer used in neuroscience and microfluidics to create different types of motifs to tailor or guide the development of neuronal cultures. It presents a low viscosity when uncured allowing it to flow into patterned moulds or different shapes; it can be then easily cured with temperature and detached from the mould. In addition, PDMS is biologically inert and optically transparent, which makes it a suitable candidate for study neuronal activity *in vitro* when combined with microscopy techniques.

In Soriano's Lab, PDMS was employed to break neuronal culture's isotropy, either by restricting available space or by introducing topographical barriers that guide axonal growth. Experimental procedures regarding the preparation of PDMS motifs are explained hereafter.

PDMS topographical motifs

A specially designed printed circuit board (2CI Circuitos Impresos, Spain) was used as a negative mould for the topographical PDMS substrates. The circuit board is formed by a uniform fiberglass bottom layer of 2 mm thick and a top copper layer deposits 70 μm high that shaped different designs of constant height (Figure 3.2a). Two different pattern designs were explored, namely parallel tracks and randomly positioned squares. A zoomed–in view of such patterns is provided in Figure 3.2b. The 'tracks' configuration included parallel rectangular bands 200 μm wide and 20 mm long and separated by 200 μm, while the 'squares' configuration consisted of square blocks of 300 μm lateral size occupying the 15% of a 20×20 mm^2 area. Blocks were placed following a grid of 300 μm spacing, so that there was no overlap between blocks, and the spatial dimensions of the resulting designs were all multiple of the basic square dimensions.

For preparation, a mixture of 90% base and 10% curing agent of PDMS (Sylgard 184, Dow, Corning, Midland, Michigan, USA) was poured on the printed circuit board and cured in an oven for 2h at 90°C. PDMS was then softly removed from the mould,

shaping a topographical relief where the depressions and crevices on the PDMS corresponded to, respectively, the copper imprints and the fiberglass board (Figure 3.2c).

PDMS patterned discs were then pierced using stainless steel punchers (Bahco 400.003.020) to shape a 6 mm diameter discs of typically 1 mm in thickness. PDMS discs were washed in an 90% ethanol solution, dried and attached to 100 μm–thick cover glasses (Marienfeld–Superior) through autoclaving (Selecta 4002515), which in turn strongly bond the PDMS to the glass surface (Figure 3.2d). A coverslip accommodated two PDMS discs in order to optimize resources by facilitating the recordings of two independent discs. Figure 3.2e shows bright–field images of the topographical patterns ready for cell culturing.

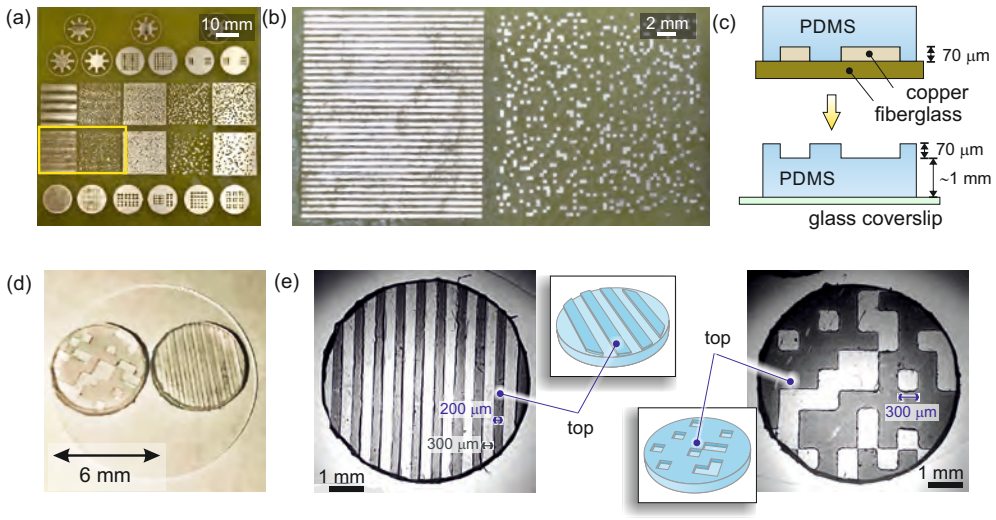

Figure 3.2. PDMS topographical patterns. Figure adapted from Montalà-Flaquer et al., 2022. **(a)** Printed circuit board containing different designs. Copper (bright goldish color) elevates over the fiberglass (dark yellow) by 70 μm. The yellow rectangle highlights the two main designs. **(b)** Detail of 'tracks' (left) and 'squares' (right) designs. For tracks, copper elevations are 200 μm thick and are separated by 200 μm. For squares, copper imprints are 300×300 μm^2 unit size and randomly positioned without overlap and occupying 15% of the available area. **(c)** Sketch of PDMS casting from the printed circuit board. **(d)** A couple of topographical cultures 6 mm in diameter attached to a glass coverslip. **(e)** Detailed bright–field images of the topographical patterns. Transparent and dark areas correspond to PDMS in contact during curing with copper or fiberglass, respectively, and shape the bottom and top regions of the topographical relief.

PDMS moulds to confine wells

For the studies oriented toward the modeling of tauopathies (Chapter 4), we used a PDMS mould to confine two 4 mm cavities onto one glass coverslip surface. PDMS was mixed and cured as described in the previous section. The cavities limited the area in which neurons could grow (Figure 3.3a), providing two independent cavities that fitted in the field of view of the imaging system installed in Soriano's Lab. This

arrangement also facilitated the recordings of two independent ‘wells’, doubling data acquisition.

Since both 4 mm cavities were in the same petri dish, culture medium was also the same for both wells, and thus the same experimental conditions applied in the two studied neuronal cultures. Figure 3.3a shows a schematic illustration of the PDMS moulds together with a fluorescence image of neurons in culture confined within the two 4 mm cavities. Another version of PDMS moulds was used to confine hydrogels for subsequent rheological characterisation (as described in Chapter 5). A PDMS mould with an 8 mm cavity was employed to restrict the hydrogel volume, ensuring that it fitted within the geometry of the rheometer (Figure 3.3b).

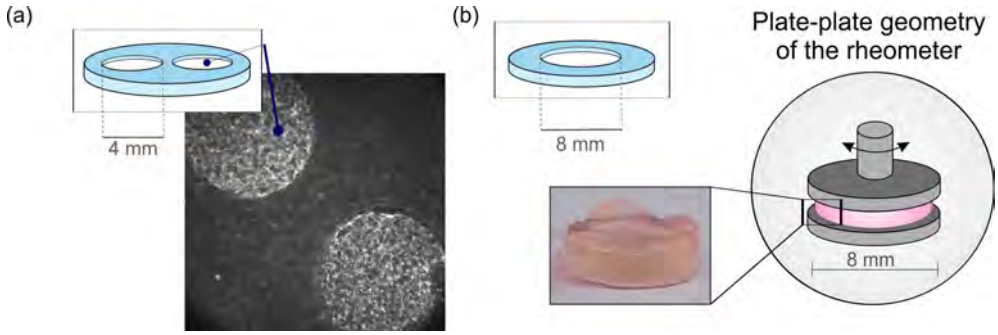

Figure 3.3. PDMS Preparation to confine space. **(a)** PDMS mould confining two different 4 mm cavities and its fluorescence image once seeded with cells. **(b)** PDMS mould designed for preparing hydrogels for future rheological characterisation, for which hydrogels must fit perfectly into the geometry of the rheometer, 8 mm in this case (see Chapter 5 for further details).

3.1.2 Preparation of primary neuronal cultures

All experiments in this thesis were carried out in accordance with the regulations of the Ethical Committee for Animal Experimentation of the University of Barcelona (approved ethical order DMAH-5461) and the laws for animal experimentation of the Generalitat de Catalunya (Catalonia, Spain). Mice were provided by Charles Rivers (Saint Germain Nuelles, France) and dissections were carried out at Soriano’s Lab in the Faculty of Physics of the University of Barcelona.

Before culturing cells, 13 mm glass coverslips were cleaned first in a 70% nitric acid solution for 90 minutes, rinsed twice in double–distilled water and then sonicated in an 90% ethanol solution for 20 min. Coverslips were dried and, if needed, autoclaved in order to attach a PDMS pattern. Glass, or glass–PDMS sets, were placed in a 4–well plate and submerged overnight in a 10 mg/mL PLL solution (Sigma-Aldrich) in Borate Buffer (1 M, pH 8.4) in order to obtain a homogeneous distributions of cells. When preparing aggregated cultures, the coating step was not performed.

Cortical tissue from CD1 mouse embryos at day 16 of development (E16) was extracted. In mice, gestation lasts approximately 20 days, and neurogenesis begins

around E12, peaking around E15 (Bayer and Altman, 1991). Therefore, at E16, the neurons are fully developed but have not yet formed the complete network of connections found in the mature mouse brain. This characteristic allows them to undergo a process of dissociation and culture without being destroyed. Dissections were conducted in L-15 medium (Gibco, ThermoFisher Scientific, Waltham, MA, USA) previously enriched with 4% glucose 1 M, 1% glutamax (Sigma-Aldrich, St. Louis, MO, USA) and 0.4% gentamicin (Sigma-Aldrich, St. Louis, MO, USA). Extracted cortical tissue was then transferred to Plaiting medium (see Table 3.1) where a mechanical dissociation was conducted by repeated pipetting (see illustrative sketch in Figure 3.1a). Pipetting was first carried out with a 1000 μL micro–pipette. The second step involved the use of a glass flame–polished Pasteur pipette tailored to have a $\approx$ 50 μm diameter at tip to ensure a perfect dissociation. The resulting single neurons were diluted in Plaiting medium to have a final concentration of 10^6 cells/mL and seeded in culture plates.

From that moment onwards, adequate culture conditions facilitated the development of neurites (axons and dendrites) that shaped a *de novo* neuronal network with rich spontaneous activity. With the final aim of follow the spontaneous activity of the resulting neuronal network, at day *in vitro* (DIV) 1 cultures were infected with adeno–associated viruses (AAVs) bearing the GCaMP6s Calcium sensor under synapsin-I promoter (AAV9.Syn.GCaMP6s.WPRE.SV40, Addgene) in a 1:1000 ratio. Further information regarding its functionality will be provided in following sections. Although the resulting cultures contained neurons and glial cells, only neuronal activity was recorded as only neurons express the calcium sensor under the synapsin-I promoter. All cultures contained a proportion of 80% excitatory and 20% inhibitory neurons (Soriano et al., 2008).

At DIV 5, medium was changed to Changing medium (composition in Table 3.1) to stop the proliferation of glial cells. From DIV 7 onwards, medium was changed to Final medium (see Table 3.1) and refreshed every two days. Cultures were incubated at 37°C, 5% CO_2 and 95% humidity.

Medium	**Composition**
MEM+3G	Eagle's MEM-enriched with 0.6% glucose, 1% 100X glutamax, and 20 μg/mL gentamicin
Plaiting Medium	90% MEM + 3G, 20 μg/mL gentamicin, 5% horse serum, 5% fetal calf serum and 1 μL/mL B27
Changing Medium	90% MEM, 10% horse serum and 0.5% FUDR
Final Medium	90% MEM and 10% horse serum

Table 3.1. Media composition for preparing primary neuronal cultures

3.1.3 3D Neuronal cultures

The final aim of building 3D cultures was to obtain a more physiologically relevant model that enables the study of neuronal connectivity and functional organisation in a controlled environment. The details of 3D cultures relevance and investigation within this Thesis are exposed in Chapters 5 and 6.

Essentially, we chose a semi–synthetic hydrogel to conduct 3D neuronal cultures. This hydrogel, named PEGylated fibrin, was made of a *synthetic* part, polyethylene glycol (PEG), a polymer widely used in biomedical applications (Pasut and Veronese, 2006), together with a *natural* part known as fibrin, composed of fibrinogen and thrombin, two key players in blood coagulation (Ozgun et al., 2022). Thrombin functions as a serine protease that triggers a polymerization reaction where soluble fibrinogen is converted into insoluble strands of fibrin that polymerize into a 3D organised clot (Blombäck and Bark, 2004). Through a chemical process known as *PEGylation* (Damodaran and Fee, 2010), the natural and synthetic constituents are unified, effectually fixing their individual shortcomings and culminating in an enhanced end product.

PEGylated fibrin preparation

Stock solutions of the main reagent were prepared in advance under sterile conditions. A 25 mg/mL fibrinogen solution (F8630-1G Sigma-Aldrich, St. Louis, MO, USA) was prepared in warm PBS. To prevent the formation of bubbles, we gently deposited small amounts of fibrinogen fibers onto the warm PBS surface until complete dissolution. This process was repeated as needed until the desired fibrinogen concentration was achieved. Thrombin solution (T4648-IKU Sigma-Aldrich, St. Louis, MO, USA) was prepared with a base concentration of 5 U/mL by diluting with warm PBS.

PEGylated fibrinogen solution was then prepared by mixing 121 μL of a 6 mg/mL PEG–NHS solution (713783 Sigma) in PBS with 1 mL of fibrinogen solution to obtain a 5:1 molar ratio. The resulting mixture was incubated at 37°C for 2h to promote crosslinking between fibrinogen and PEG strains. During the incubation process, the PEG monomers polymerized through a process known as radical polymerization, in which the characteristic polymer chain length is determined by the number of free monomers and the time elapsed for polymerization to occur. Although this process can be governed externally, the control of the final length of the PEG chains was not considered in our studies.

PEGylated fibrinogen solution was combined with the neuronal cell suspension, prepared as described in Section 3.1.2, to have a final concentration of $\sim$ 200,000 cells/mL. The final step included the addition of thrombin solution. The role of thrombin was to cleave specific bonds in fibrinogen, resulting in the production of fibrin monomers. These monomers then polymerized through covalent bonds, forming a 3D network. This whole process occurred in just 1 minute, so the mixture had to be carried out all at once to ensure a homogeneous distribution of neurons within the hydrogel.

The final hydrogel had a concentration of 6.5 mg/mL fibrinogen and 0.25 U/mL thrombin. Two different volumes of hydrogel were prepared, 100 μL hydrogel for rheological characterisation (Chapter 5) and 800 μL hydrogels for investigating the functional organisation of neurons in a 3D structure (Chapter 6). For functional connectivity analysis, hydrogels were prepared by mixing 400 μL of cell media, 200 μL of PEGylated fibrinogen solution and 200 μL of thrombin solution and placed on 4–well plates that incorporated clean glass–coverslips. For recording spontaneous activity, the GCaMP6s calcium marker was included in the cell solution before jellification, facilitating the infection process.

Hydrogels were treated as described for 2D cultures. They were incubated at 37°C, 5% CO_2, and 95% humidity. At DIV 5, Plating medium was replaced to Changing Medium to limit glial growth, and thereafter at DIV 7 to Final Medium. From here onward, Final Medium was refreshed every two days.

3.2 Data acquisition: Spontaneous neuronal activity

Although we used cultures derived from dissociated brain tissue, the mechanisms that lead to the emergence of spontaneous activity, i.e., the emission of action potentials throughout the network without any external drive, could be considered similar to those that occur in *in vivo* systems at early times. As highlighted in the introduction, during the early developmental stages of the vertebrate brain, neurons within the cerebral cortex exhibit spontaneous network activity, a pivotal trait in the formation of neuronal circuits (Khazipov and Luhmann, 2006). Initially, this activity manifests as non–correlated, cell–by–cell spontaneous firings (Spitzer, 2006). As neurons progress in their maturation, this spontaneous activity begins to synchronise across groups of cells, marking the onset of functional connectivity. Consequently, throughout development, both *in vivo* and *in vitro*, neurons employ diverse mechanisms to sustain this spontaneous activity. This adaptability allows the developing networks to respond to changes in temporal and spatial correlations among neurons (homeostasis). These networks maintain activity patterns despite experiencing significant depolarizations triggered by excitatory synaptic inputs, followed by prolonged periods of quiescence (Blankenship and Feller, 2010).

In particular for this Thesis, dissociated and isolated cortical neurons exhibit spontaneous neuronal activity after a few days *in vitro*. Neurons in culture form a random network of connections that exhibit collective rhythmic activity that change in time as the network evolves. Changes in *in vitro* activity patterns have been described by monitoring electrical activity (Chiappalone et al., 2006), as well as by inspecting the (Ca^{2+}) transients along time in the neuronal culture of interest (Opitz, De Lima, and Voigt, 2002; Sun, Kilb, and Luhmann, 2010).

To effectively employ different techniques for studying spontaneous activity, it is crucial to have a clear understanding of how neuronal synapses work. Synapses are

specialized cell junctions between neurons that allow the exchange of electrochemical signals in the nervous system. There are two types of synapses in the brain, electrical synapses, in which adjacent neurons are connected by gap junctions allowing the direct flow of ions between cells, and chemical synapses, being these the most abundant in vertebrate brains. In chemical synapses, transmission is mediated by neurotransmitters that are released from the axon of the presynaptic neuron and diffuses to bind receptors on the dendrite of the postsynaptic neuron, leading to the generation of excitatory or inhibitory postsynaptic potentials (Li and Sheng, 2003) (see Figure 3.4).

Neurotransmitter release is mediated by the neuronal action potential. The membrane potential of a neuron is the voltage difference between the extracellular environment and the cytoplasm of the cell. In the resting state, neurons present a negative concentration gradient of typically -70 mV, caused by an imbalance of ions concentration gradient (mainly Na^+, K^+ and Cl^-) across the membrane. Neurons under this condition are considered polarized. The binding of neurotransmitters from a neighbouring neuron initiates an augmented influx of ions, primarily Na^+, through specific ion channels. This results in a swift surge of the membrane potential, known as depolarization. Once the membrane potential reaches a certain threshold, voltage–gated ion channels initiate the propagation of the action potential along the axon. Eventually, the action potential reaches the axonal terminal, stimulating the release of neurotransmitters and inducing depolarization in the following neuron (Li and Sheng, 2003).

Ca^{2+} ions play a crucial role in neurotransmitters release in the synapse. Indeed, in presynaptic terminals, the action potential activate voltage–dependent calcium channels producing an influx of Ca^{2+}, that trigger the release of neurotransmitters (Neher and Sakaba, 2008). Thus, taking advantage of the characteristic events involved in the process of neuronal synapses (either electrical signals or ionic concentrations change), some experimental techniques have been developed to monitor, in real time, the activity of neurons *in vitro*. Some of these techniques will be explained below.

Microelectrode arrays

Firstly introduced by Thomas *et al.* in 1972 (Thomas Jr et al., 1972) for the study of cardiac myocytes in culture, microelectrode arrays (MEAs) are made of an array of micron–sized electrodes that are embedded in a substrate, such as silicon or glass. Since the pioneer work of Pine and Gross, who successfully used MEA on cultured cervical cells (Gross, 1979; Pine, 1980), this technology has been used as a widespread experimental platform for investigating neuronal activity *in vitro*, from dissociated cell culture to brain slices. The importance of MEAs and their applicability can be reviewed in (Kim et al., 2014; Brofiga et al., 2021; Xu et al., 2021).

For cultured neurons, recordings of activity are described by an electrical circuit model (Fromherz et al., 1991; Buitenweg, Rutten, and Marani, 2002). Electrodes are capable of detecting changes in extracellular voltages, which arise from the ionic current flow generated by neurons when they elicit action potentials as a result of synaptic

processes. The ionic flow is subsequently transduced into electronic currents carried by electrons. This bidirectional process allows for the delivery of electrical pulses to stimulate neurons or the conversion of neuronal activity into electronic signals. Electrodes present a micrometer–sized tip that is placed in close proximity to neuronal cell bodies. To record activity of a reasonable number of interconnected neurons, the number of electrodes and their density play a crucial role, varying from one device to another, and ranging from about 64 up to 4,096 in what is known as high–density MEAs.

The detected signal in MEAs, which come from the movement of electrodes around cells, is extremely weak, and therefore amplification and signal processing are required. MEA systems include, in addition to amplifiers and filters, analog–to–digital converters that process the signal and convert it to digital data that can be further analyzed. In this context, some interfaces have been created in a attempt to automate signal analysis. As an example, the named Spycode (Bologna et al., 2010) allows the user to filter the extracted raw data and perform a spike detection analysis that can be applied to study firing patterns of individual neurons and examine network connectivity.

By controlling the culture conditions, neurons grown on MEA devices can maintain the electrical activity for weeks, allowing researches to observe and analyze the complex dynamics of neuronal networks and their evolution with time. MEA technology can also be combined with PDMS patterns to build microfluidic devices (Park et al., 2013), with micropatterning techniques to design specif neuronal networks (Nam,

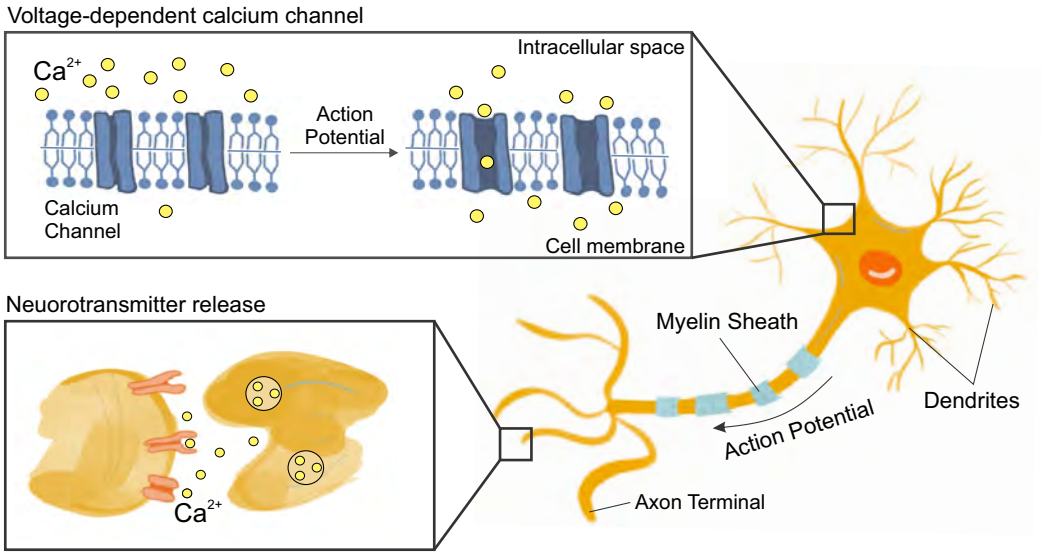

Figure 3.4. Sketch of a chemical synapse. When an action potential occurs, it triggers the opening of calcium channels in the cell membrane. The incoming intracellular calcium ions push the synaptic vesicles (which store neurotransmitters) toward the cell membrane, releasing them into the synaptic cleft. Once this point is reached, the neurotransmitters are bound to the corresponding receptors in post–synaptic neurons.

Branch, and Wheeler, 2006; Jun et al., 2007) or with electrodes of different heights to record the activity of 3D populations (Tedesco et al., 2017; Shin et al., 2021; Muzzi et al., 2023). In this context, MEA technology has revolutionized the study of neuronal circuits and brain function, allowing to investigate neuronal networks in real–time with a high temporal resolution. MEAs are used in various research areas, including neurophysiology (Martinoia et al., 2004; Ahtiainen et al., 2021), neuropharmacology (Vassallo et al., 2017), neurodevelopment (Martens et al., 2016) and the study of neurological disorders (Klein Gunnewiek et al., 2019; Frega et al., 2019).

Fluorescence calcium imaging techniques

Neuronal activity can be effectively monitored through calcium fluorescence imaging, a technique based on the indirect detection of neuronal activity (action potentials) as a result of the rapid increase in intracellular Ca^{2+} concentration upon neurotramsmitter release at the pressynpatic terminals (Grienberger and Konnerth, 2012).

Fluorescence calcium sensors are essentially markers that signal the transmission of the electrical signal from the presynaptic to the postysnaptic neuron. Since the increase of intracellular calcium is considerable (by two orders of magnitude), calcium sensors allow to a neat detection of neuronal activity. The sensors are by themselves small organic compounds that exhibit fluorescent properties when they bind to calcium ions. One of the pioneering calcium indicators used for monitoring neuronal activity is the bioluminescent calcium–binding protoprotein called *aequorin*, which was introduced by the Nobel Prize laureate Shimomura in 1972 (Shimomura, Johnson, and Saiga, 1962). Originally isolated from the luminescent jellyfish *Aequorea victoria*, *aequorin* comprises a noncovalently bound chromophore that undergoes a conformational change after binding with calcium, leading to the emission of a photon (Ohmiya and Hirano, 1996) when stimulated with light of adequate wavelength. Most fluorescence calcium sensors use blue as excitation wavelength, with the emitted light in green.

Over the years, significant advances have been made in the development of calcium indicators, leading to a wide range of excitation/emission spectra and improved calcium affinity. Among these indicators, genetically encoded calcium indicators (GECIs) (Looger and Griesbeck, 2012) have become widely used tools in neuroscience for tracking neuronal activity. GECIs are derived from the green fluorescent protein (GFP) (Miyawaki et al., 1997), which is extracted from the *aequorin* gene. They can be categorized into two groups based on their fluorescence release mechanisms: Förster resonance energy transfer and single–fluorophore indicators.

To express GECIs in neurons, viral transduction techniques are applied, involving the use of AAVs to transduce GECIs into the desired cells. This method allows for high expression levels over extended periods, enabling the tracking of neuronal development over time. However, it is worth noting that long–term expression of calcium

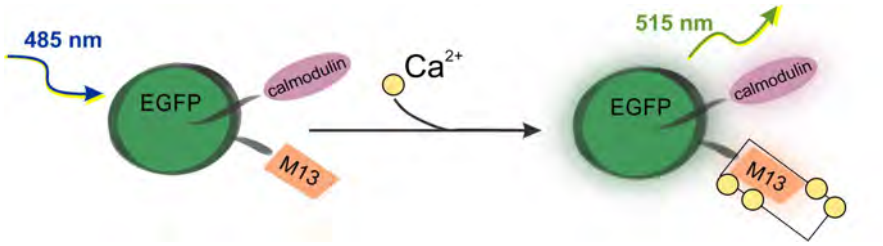

Figure 3.5. GECI GCaMPs are engineered fluorescent proteins composed of an green fluorescent protein (GFP) that has been circularly permuted. This GFP is surrounded on one side by the calcium binding protein calmodulin and on the other side by the calmodulin–binding peptide M13. When calcium is present, interactions between calmodulin and M13 induce conformational changes in the fluorophore environment, resulting in an augmented emission of fluorescence. This property makes GCaMPs valuable tools for detecting calcium fluctuations within biological samples.

markers through AAV–GECIs transduction can induce cytotoxicity in the cells. Thus, optimal AAVs concentration should be carefully evaluated.

In Soriano's Lab, a prominent representative of single–fluorophore GECI indicator was used to track neuronal activity in culture. This indicator belongs to the *GCaMP* family, comprising a circularly permuted GFP attached to a calcium–binding protein. In the presence of free calcium ions, the structural conformation of the protein changes, leading to the emission of fluorescence (Nakai, Ohkura, and Imoto, 2001) (Figure 3.5). The continuous improvement of fluorescent dyes (Chen et al., 2013; Yang et al., 2018) has resulted in GCaMP6s, a vector driven by synapsin promoter (Syn–I) that is only expressed in mature neurons. GCaMP6s present high expression levels and a good signal–to–noise ratio and allows researchers to monitor the behaviour of a large population of neurons with a temporal resolution in the range of $10-50$ ms.

Neuronal activity in this Thesis was visualized through wide–field fluorescence microscopy, an imaging technique (Figure 3.6) to acquire the light emitted by a fluorophore that has been excited by the adequate wavelength (Homma et al., 2009). Particularly, GFP—like proteins emit green light ($\lambda = 515$ nm) when excited by blue light ($\lambda = 485$ nm). For that, a mercury lamp combined with adequate filters and a series of mirrors were attached to the microscope. Recordings were conducted on a Zeiss Axiovert inverted microscope equipped with a high–speed camera (Hamamtsu Orca Flash 4.0). A typical calcium imaging experiment in our laboratory consisted in the recording of spontaneous activity for about 15 min at typically 33 images/s (30 ms between consecutive frames). Images were acquired with the camera software Hokawo 2.10 with an image size of 1024×1024 pixels and a spatial resolution of 5.76 μm/pixel when using a $\times 2.5$ objective. With assistance of an optical zoom, it was possible to cover the entire area of the 2D culture under study. However, for investigating neuronal activity in 3D cultures, our set–up only allowed us to perform recordings on a single focused plane.

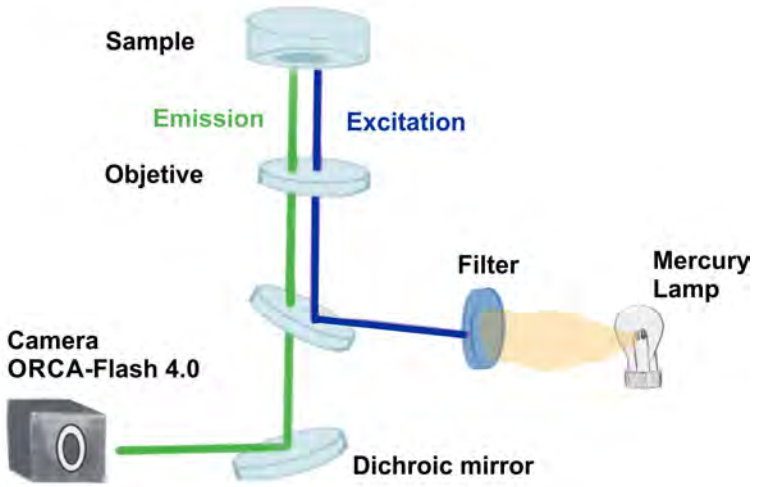

Figure 3.6. Diagram of the Wide-Field fluorescence microscopy set-up in Soriano's Lab. A mercury lamp serves as the source of the fluorescence light. To modify the wavelength of the incoming white light, a blue filter is used. The light then passes through dichroic mirrors, which direct the beam toward the objective lens, focusing on the sample. Simultaneously, the light is guided backwards toward the camera sensor. The camera is connected to a computer equipped with the Hokawo software, allowing for efficient image capture and analysis. This setup enables the visualization of fluorescently labeled calcium ions within the sample, providing valuable insights into neuronal network processes.

3.3 Data analysis tools

3.3.1 From fluorescence recordings to spikes

The recorded fluorescence data were analyzed with our custom–made Matlab code NETCAL (Orlandi et al., 2017), in combination with a number of packages developed in Soriano's Lab along 15 years of expertise. Briefly, the main goal of data analysis was to convert fluorescence recording onto time series of neuronal activations, easily manageable for future analysis (e.g., the study of dynamical and functional features of the neuronal network). All procedures described here were similarly applied for the different types of 2D neuronal cultures, and adapted to the analysis of single–focused plane within the 3D hydrogel.

For data processing, two different aspects were crucial, namely the identification of neuronal somas and the detection of neuronal spikes from the fluorescence traces. Thus, for each experiment, a high–contrast fluorescence image was obtained as the pixel–to–pixel average matrix of all frames in the recording. In this image, Regions of Interest (ROIs) were identified, either manually or automatically by applying a built–in NETCAL option which process the image to detect objects and boundaries, as exemplified in Figure 3.7 (steps #1 and #2).

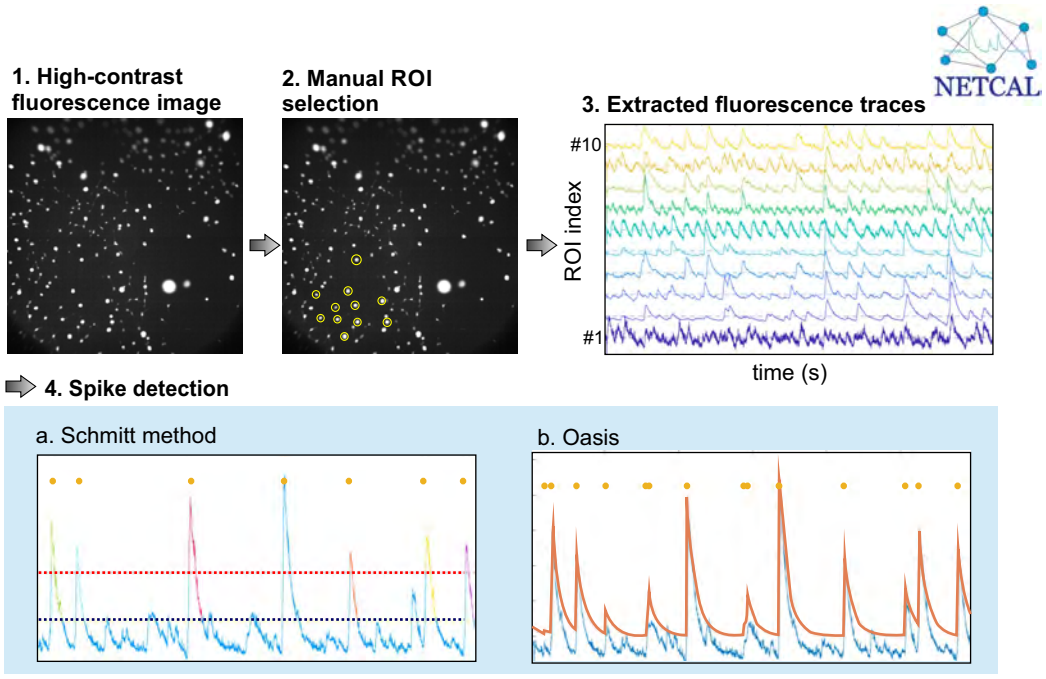

Figure 3.7. Pipeline for the processing of fluorescence recording to obtain time series of neuronal activations. NETCAL provides a high–contrast fluorescence image obtained from the pixel–to–pixel average matrix of all frames in the recording. In this figure, the fluorescence image corresponds to a 3D neuronal culture grown on a PEGylated fibrin hydrogel at DIV 12. The first step involves selecting the ROIs of the culture, in this case a manual detection was performed with colored dots representing the ROIs detected by the NETCAL algorithm. Fluorescence traces from each ROI are then extracted and smoothed. The last step corresponds to the detection of spikes from the fluorescence traces. Two methods are shown: a) Schmitt method, in which a upper (red) and a lower (blue) threshold are established; fluorescence intensity needs to remain within these limits at least 100 ms to be considered a spike (orange dots). b) Oasis method, which uses biophysical models for the dynamics of fluorescence traces to predict the activity events.

An alternative approach, frequently employed in our work, was to apply a grid to define ROIs within the cultured area. This method enables the users to construct a customized network of squares across the culture surface, with dimensions that can be adjusted to accommodate neuron sizes. Usually, one ROI corresponds to one neuron, but a compromise between the appropriate ROI size and a manageable number of ROIs is required to avoid imposing an excessively high computational burden. Typically, aggregated cultures where analyzed by using the automatic ROIs detection tool by taking advantage that they are relatively large objects (Figure 3.8a). On the other hand, for 2D homogeneous neuronal cultures a circular grid covering the culture area was used to establish a total number of 1,300 ROIs (see Figure 3.8b). In 3D neuronal cultures, for those displaying an homogeneous 3D distribution of neurons, a squared grid of 900 ROIs was applied covering the whole visual area. For those cases in which neurons were not homogeneously distributed, automatic detection of ROIs was applied.

Once ROIs were mapped, the average fluorescence intensity (gray scale level) of the pixels within each ROI was extracted to obtain the set of *raw fluorescence traces* $F_i(t)$ for each ROI i (Figure 3.7, step #3). Each trace was corrected from drifts and normalized as $\Delta F F_i(t) = (F_i(t) - F_{i,0})/F_{i,0}$ where $F_{i,0}$ is the basal fluorescence level of neuron i, i.e., its background signal when non–active. This step was crucial since the biophysically relevant quantity is the relative change in fluorescence (and not its absolute value), which is proportional to the number of action potentials elicited by the neurons (Koester and Sakmann, 2000; Grienberger and Konnerth, 2012).

The identification of spike trains from fluorescence traces requires the introduction of a model able to capture the fast increase ($10-50$ ms) and slow decay ($1-4$ s) in fluorescence intensity, characteristic from spontaneous neuronal activity (Smetters, Majewska, and Yuste, 1999). In the absence of a universal model for detecting neuronal spikes and activity events, we adopted the *Schmitt Trigger Method* to establish an automatic analysis that yields reliable results under various culturing conditions.

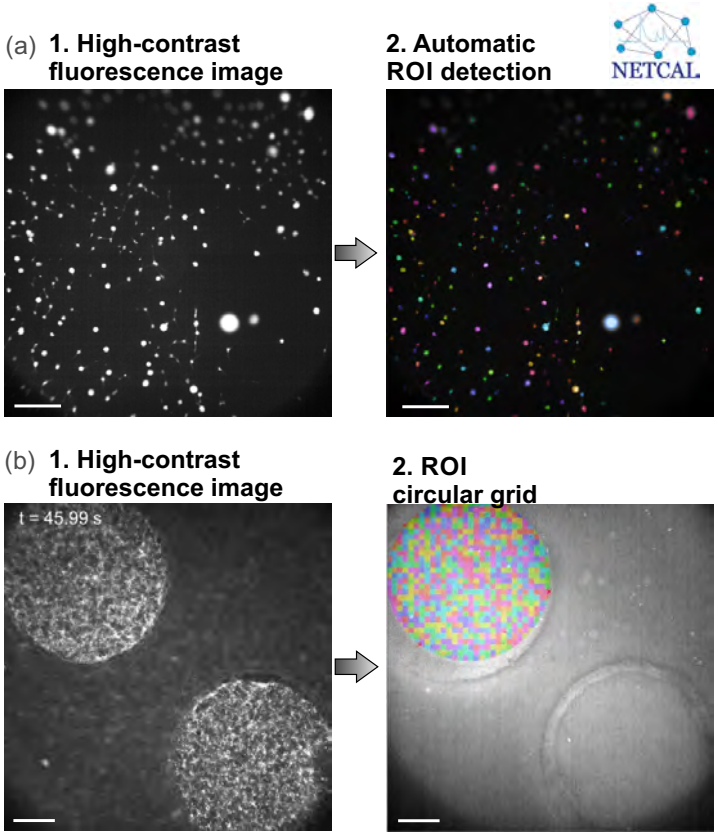

Figure 3.8. Examples of ROIs selection. **(a)** Automanic ROI detection, performed by processing the image to detect round objects and boundaries thanks to a built–in NETCAL option. **(b)** Grid selecction. In this example, a circular grid of 1,300 ROIs was applied to cover the area of 2D homogeneous culture grown in 4 mm PDMS cavities. Scale bar is 1 mm.

This method identifies a spike, signifying neuronal activity, when the fluorescence intensity remains above a higher threshold for at least 100 ms and subsequently drops below a lower threshold, indicating the end of the spike and complete neuron depolarization (Grewe et al., 2010). The selection of these two–threshold values aims to eliminate camera noise while capturing the first activity event of each fluorescence peak (Figure 3.7, step #4a). Other methods rely on biophysical information to predict spikes trains, such as the *Oasis* method (Friedrich, Zhou, and Paninski, 2017), which uses the kinetics of the fluorescence indicator to predict an activity event (Figure 3.7, step #4b). While the Oasis method offers greater details on neurons' dynamics, particularly the emission of concatenated action potentials, we concluded that the Schmitt method better suited our experimental purposes, revealing the moment of a neuronal activation regardless the number of subsequent repetitions. This fact was crucial to study dynamical features such as the richness in spatiotemporal activity patterns or their velocity of propagation, as well as connectivity traits, which will be explained in detail in the next section. As can be observed in Figure 3.7, step #4, when comparing the two mentioned methods on the same fluorescence trace, the Oasis method detected more spikes than those of the Schmitt method.

Finally, the resulting train of detected spikes for each ROI was presented as a *raster plot*, which serve as the fundamental dataset for subsequent dynamical and functional analyses of the network in each culture. Raster plots represent the ROI index versus time, with a dot indicating a neuronal activation. In this kind of representations, network bursts of coherent collective activity are easily spotted as the quasi–synchronous activation of a large number of neurons in a small time window. Representative examples of raster plots for the different culture designs described before are provided in Figure 3.9a.

3.3.2 Network dynamics

A *de novo* neuronal culture establishes a pattern of connections on the substrate that shapes, together with intrinsic neuronal dynamics and noise, the activity of the emerging network. Neuronal network dynamics refers to the activity patterns and interactions among the neurons within the network. Understanding this dynamics is crucial for unraveling the mechanisms behind the complex networks of connections that underlie network behaviour and, in the context of the brain, its complex functions. Within this subsection, we introduce dynamical parameters of the network in an effort to provide objective metrics for describing the behaviour of our neuronal networks *in vitro*. We thus delve into explanations for *population activity*, *velocity of propagating fronts*, and *inter–burst interval*. For clarity in the description of the different metrics, we provide representative examples of their meaning and usefulness for each culture type.

Population activity.— Also known as 'global network activity' (GNA) and denoted by A, it quantified the fraction of neurons in the network that coactivated in a short time window, with values ranging from 0 (indicating no collective activity) to 1 (representing full network activation). This measure provided valuable insights into synchronised neuronal activity within the network. An average population activity close to 1 indicated that the network exhibited a strongly synchronised bursting activity, i.e., it was locked in an on–off state of activity. On the other hand, an average value around 0.5 evinced a more segregated, dynamically rich network, able to exhibit collective events with a different number of participating neurons. In summary, A offered a concise characterisation of the network's coherence and capacity for coordinated activity.

To calculate A, a sliding window was used on the raster plot, with a width of 1 s and a step of 0.1 s. As said above, high peaks in A were indicative of strong coordinated activity and were referred as *network bursts*. These bursts were considered significant if their amplitude, denoted as A_b, satisfied the condition $A_b > \mu_{bgnd} + 3 \cdot SD_{bgnd}$, where μ_{bgnd} and SD_{bgnd} represented the mean and standard deviation of the background activity, respectively. Typically, significant bursts were defined as those with $A > 0.1$, corresponding to 10% of the network being active. All significant burst amplitudes A_b, across repetitions and under a specific experimental condition, were pooled to create the distribution of amplitudes.

Figure 3.9a compares the characteristics of collective activity among the four different experimental configurations presented before: standard 2D neuronal cultures with either a homogeneous distribution or aggregated, 2D neuronal cultures grown on PDMS topographical patterns, and 3D neuronal cultures utilizing PEGylated fibrin as a scaffold for neuronal growth. Representative raster plots for cultures at DIV 12 are shown, where the spontaneous activity of all cultures was recorded for 10 min. For clarity in the figure, only the first 5 min of the recordings were plotted. Population activity was displayed below the raster plots to provide a better overview of the dynamical behaviour of the different neuronal configurations.

Homogeneous 2D neuronal cultures showed few activity events, but they encompassed $A_b \simeq 1$, i.e., this cultures were strongly bursting. Aggregated and topographically patterned cultures presented a broad range of collective events in which A_b varied between 0.1 and 1, indicating that the network was not always fully synchronised. This type of behaviour suggests a rich repertoire of activity patterns. Hence, these configurations can be viewed as richer experimental models as compared to standard 2D cultures. Finally, the raster plot for 3D neuronal culture exhibited a state of intense activity, in which A_b was large, in the range $0.6 - 1$. However, collective events encompassed neurons across the volume, i.e., not only those in focus, but also neurons out of focus. This is because our recordings were confined to a single reference plane and, thus, our analysis incorporated neurons firing on different planes.

Propagating fronts and their velocities.— The structure of propagating fronts was

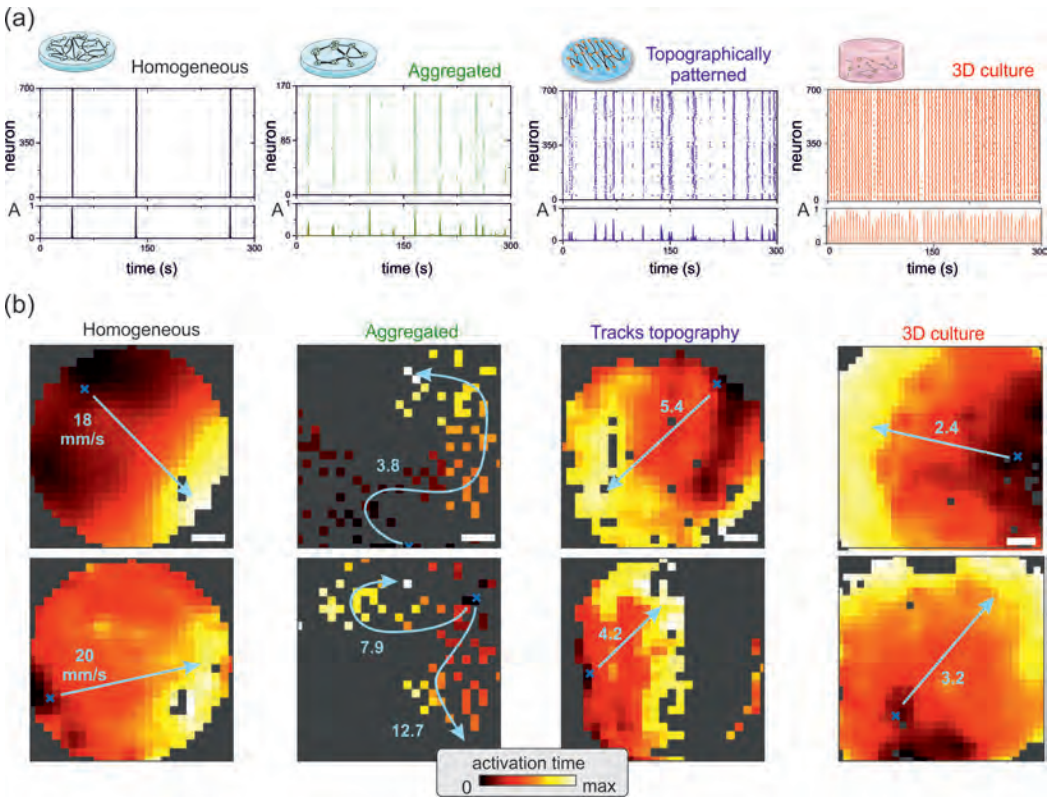

Figure 3.9. Representative dynamical features in different neuronal culture designs at DIV 12. **(a)** Raster plots (top) and global network activity ('GNA', bottom) of neuronal cultures grown on a flat surface with a homogeneous distribution of neurons (black, left), a flat surface with neuronal aggregates (green, center–left), a PDMS topographical surface shaped as parallel tracks that guide neuronal connections along them (blue, center–right), and PEGylated fibrin hydrogel (red, right). 2D cultures were 6 mm diameter and 3D culture was 13 mm diameter and $\approx$ 1.5 mm high. **(b)** Illustrative spatiotemporal fronts of activity propagation for the four network designs. Velocities are much lower for the non–homogeneous and 3D configurations. Black–yellow maps show the relative activation time of each ROI. Blue crosses mark the origin of activity. Scale bar is 1 mm.

obtained by combining the information of the neurons participating in each bursting event with the spatial location of the neurons as ROIs. Figure 3.9b illustrates such spatiotemporal propagation of spontaneous activity as heat maps. The representations were constructed by, first, identifying in the population activity profile the significant network bursts (those with $A > 0.1$) and retrieving afterwards the activation times and spatial coordinates of the neurons that participated in them. As shown in the figure, propagation was represented as a black–red–yellow pattern that was proportional to the time of activation of each ROI, with dark colors corresponding to earlier activations. In some cases, such as the top example for 3D cultures, a neat quasi–circular front could be observed.

Each pattern also shows a blue cross that denotes the *burst initiation point*, i.e.,

where activity most likely initiated. The identifcation of this point involved selecting a group of 10 ROIs with the shortest activation times and analyzing all possible combinations of 4 ROIs within the group. For each combination, the average inter–ROI Euclidean distance, denoted as d_0, and the average activation time, denoted as t_0, were calculated. The combination yielding the lowest d_0 and shortest t_0 (referred to as t_0^{min}) was chosen as the initiator, and the centroid of the ROIs (x_0, y_0) (the blue cross on the images) was evaluated.

The characteristic *velocity of propagation* for each detected burst was computed as follows. First, the Euclidean distance d_i between each ROI i and the origin of activity (x_0, y_0) was calculated. Subsequently, d_i was plotted as a function of t_i', which represents the activation times relative to the origin of activity. The global propagation velocity was estimated by determining the slope of the linear fit $d_i(t_i')$, with the intercept fixed at $(0,0)$. Only fits with Pearson's regression coefficients $r \geq 0.75$ were considered valid, with the best fits corresponding to bursts that propagated as neat circular fronts (Orlandi et al., 2013), which were typically observed in dense homogeneous cultures, either 2D or 3D.

The velocity of the propagating front has been related in the literature with connectivity properties of the network (Feinerman, Segal, and Moses, 2005; Jacobi and Moses, 2007; Jacobi, Soriano, and Moses, 2010), being the velocity higher for a stronger connectivity. For instance, as depicted in Figure 3.9b, the homogeneous cultures displayed a propagation pattern compatible with a circular front, suggesting an isotropic connectivity in which neurons connect to one another within a characteristic length–scale of easily 1 mm (Montalà-Flaquer et al., 2022). Homogeneous cultures exhibited velocities around 20 mm/s. On the other hand, propagation of activity in aggregate cultures was characterised by chained activations, often resulting in serpent–like excursions across the culture, and typical velocities in the range of $4-15$ mm/s. These velocities were considerably smaller than in the homogeneous case, indicating a dominant short–range connectivity of about 100 μm (average inter–aggregate distance). Conceptually, since connectivity and velocity are related, changes in neuronal connectivity due to development or damage could in principle be indirectly detected by analyzing the velocities of activity fronts.

Patterned cultures exhibited a diverse range of activity propagation profiles, often constrained by topographical obstacles, such as tracks. This fact evidenced that inter–track connectivity shaped in great manner the structure of the front. The typical propagation velocities for patterned cultures were approximately 5 mm/s. Notably, during these experiments, we were able to measure the velocity along tracks in some fronts, yielding velocities of about 20 mm/s (Montalà-Flaquer et al., 2022), indicating that the connectivity along tracks was approximately 8 times stronger than across tracks. Interestingly, the study of propagation fronts in 3D cultures revealed circular fronts, similar to those observed in homogeneous 2D cultures, but with substantially lower velocities of about 3 mm/s. Additionally, the 3D fronts displayed a more diverse

range of propagation profiles.

Overall, as a summary, Figure 3.10a shows the distribution of population activity values for different configurations of neuronal cultures. The data reveals that homogeneous 2D neuronal cultures tended to exhibit a tightly synchronised bursting behaviour. In such cases, all neurons activated collectively ($A \simeq 1$). Conversely, configurations that deviate from homogeneity displayed an increased dynamic variability, enabling the system to showcase more intricate patterns of activity. On the other hand, Figure 3.10b compares the characteristic velocities in the four configurations. We can observe that the velocity of the propagation front decrease as the culture experiences higher spatial restrictions, i.e., from homogeneous to aggregates and topographical tracks, and finally to 3D structures. Altogether, these results evidence that overall network dynamics is effectually enriched when the connectivity goes beyond the isotropy of standard 2D cultures, either by introducing physical constraints or by introducing a new spatial dimension for neurons to connect to.

Inter–burst interval.— Denoted as IBI, it provided the typical timing between consecutive bursts. The rate of bursting was calculated as the number of bursts produced per unit time, often expressed in bursts per second or Hertz (Hz), and the IBI was obtained as IBI $= \langle t_{i+1} - t_i \rangle_n$ being t_i the activation time of a specific bursting event i, t_{i+1} the time of the preceding event, and n all the observed events. IBI is inversely proportional to the firing frequency, with IBI being lower when a neural network is more active (less time elapsed between events).

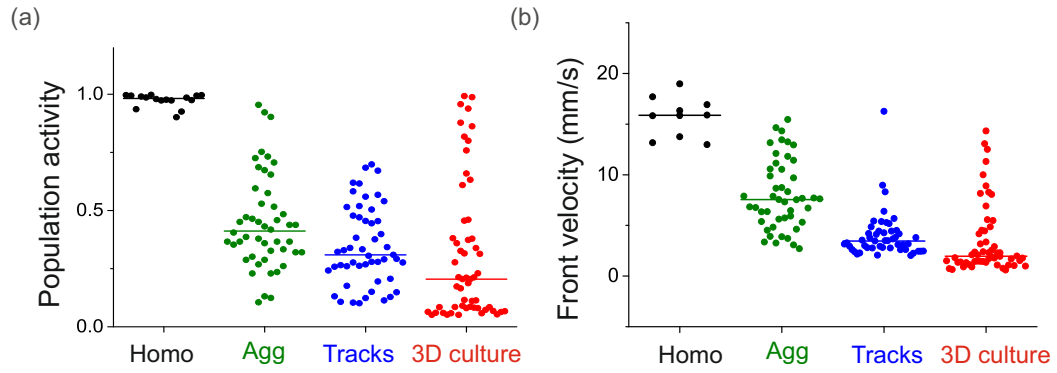

Figure 3.10. Dynamics in different neuronal cultures at day *in vitro* 12. **(a)** Distribution of population activity, which is significantly more spread for those cases deviating from a 2D homogeneous distribution, indicating a rich variability in collective activity. **(b)** Distribution of measured characteristic velocities for the four configurations. The distributions are substantially shifted toward lower values as more spatial constraints are imposed on the connectivity.

3.3.3 Functional analysis

An overview of Transfer Entropy

Information theory, introduced by Claude Shannon in 1948 (Shannon, 1948), has found extensive applications in neuroscience, particularly in the study of non–linear interactions among neurons. In essence, Shannon entropy quantifies the average amount of information that can be extracted from a discrete variable X, given its underlying probability distribution $p(x)$, by applying:

$$H_X = -\sum_{i \in X} p(x_i)\ \log_2 p(x_i). \tag{3.1}$$

A higher entropy indicates a higher uncertainty, or variability, in the information contained in X. Mutual information (MI) quantifies the amount of information shared between two random variables, i.e the reduction of uncertainty about one variable by observing another. When considering two processes (X,Y) with joint probability $p(x,y)$, the error of assuming independence between them is given by $p(x,y)/p(x)p(y)$, leading to

$$\mathrm{MI}_{XY} = \sum_{i \in X, j \in Y} p(x_i,y_i)\ \log\left(\frac{p(x_i,y_i)}{p(x_i)\ p(y_i)}\right). \tag{3.2}$$

This expression is a specific case of the Kullback–Leibler divergence, also known as relative entropy (Kullback and Leibler, 1951). A high mutual information value indicates a strong statistical dependency between the two variables, providing insights into their relationship and interactions.

MI is symmetric, meaning that it measures the amount of shared information of two variables without considering the direction of the information flow. However, in neuroscience, modifications need to be introduced to capture the asymmetric nature of information exchange, i.e directionality.

One such modified measure is *Transfer Entropy* (TE) (Schreiber, 2000) which takes into account the directional flow of information between two variables. To do so, TE introduces a time lag to one of the processes, allowing researchers to account for the temporal dependencies between the variables. The Markov property establishes that the conditional probability of a memoryless system depends only on the present state as:

$$p(x_{n+1}|x_n^k) = p(x_{n+1}|x_n^k, y_n^k), \tag{3.3}$$

where n is the discrete time index and x_n^k a vector whose entries are the samples of X at the different time steps $n, n-1, \ldots, n-k$ for Markov order k. Conceptually, k means the dependence on the history. For instance, first order Markov property says that the future state depends only on the current. Second order Markov property says that the future depends on current state and the previous state.

Overall, any deviation from the Markov condition reflects the degree of causality between the two systems. Therefore, TE serves as an asymmetric measure of uncertainty between two time–series processes X and Y, making it particularly useful in capturing the causality or directed information flow between elements of a complex system, such as neurons in the brain.

The mathematical expression of TE from X to Y is given by

$$TE_{X\to Y} = \sum_{x_{n+1},x_n,y_n} p(x_{n+1},x_n^k,y_n^k)\log\frac{x_{n+1},x_n^k,y_n^k}{p(x_{n+1}|x_n^k)}. \tag{3.4}$$

Based on our experience in data analysis in neuronal cultures, we set $k = 2$ for all the analyses, with aligns with the extensive studies and simulations on TE conducted by Soriano's research group and collaborators (Stetter et al., 2012; Orlandi et al., 2014).

In essence, TE is a powerful tool in neuroscience that goes beyond simple correlation analysis to examine the directional flow of information between elements of a complex system, a concept known as *effective connectivity*. Since its development, TE has enabled researchers to unveil causal relationships and investigate the flow of communication as well as direct interactions among various brain regions during diverse cognitive processes (Wibral et al., 2011; Shovon et al., 2017).

Generalized Transfer Entropy

Generalized Transfer Entropy (GTE) is an extension of the concept of TE that was specially introduced for neuronal cultures in order to reach a balance between neuron–to–neuron contributions (spikes) and whole–network synchronous events (network bursts). Within the framework described by TE, network bursts would shape an all–to–all connectivity since all neurons interact identically to one another. GTE procured a new scenario in which the details of neuronal interactions could be uncovered underneath this synchronised events, rendering much richer effective networks.

For GTE to reveal information beneath synchronous events, in the original work described in (Stetter et al., 2012; Orlandi et al., 2014) a threshold condition was imposed on the calcium fluorescence signal of the neurons, minimizing the impact of network bursts in the detection of causal relationships between single neurons. In later works (Tibau et al., 2020; Ludl and Soriano, 2020; Montalà-Flaquer et al., 2022) such a threshold was imposed on during significance analysis (see later), so that effective connectivity could be computed directly on the raster plots and then GTE scores filtered out to consider only those that reflected the interactions of interest, either whole–network communication or neuron–to–neuron communication. The whole GTE analysis was included as a self–customized Matlab code developed in Soriano's Lab.

Thus, raster plot in a typical experiment, containing series of 1s and 0s (presence or absence of activity, respectively) were analyzed to compute the TE score $TE_{I\to J}$

between spike trains of every pair of neurons I and J. Conceptually, an effective connection from I to J would be established whenever the information contained in I significantly increased the capacity to predict future states of J. Data was then normalized by using the z–score construction, and by comparing the transfer entropy estimate $TE_{I\to J}$ with the joint distribution of all input X to J and output I to Y (for any X and Y), as

$$z_{I\to J} = \frac{TE_{I\to J} - TE_{\text{joint}}}{\sigma_{\text{joint}}}, \tag{3.5}$$

where TE_{joint} and σ_{joint} are the average value of the joint distribution and its standard deviation, respectively.

Finally, A *significance* threshold z–score, z_{th}, was established to decide which effective interactions were accepted, setting $z_{I\to J} = 1 \;\forall\; z_{I\to J} \geq z_{\text{th}}$ and 0 otherwise.

We note that the chosen threshold for the z–score, z_{th}, plays precisely the role of the threshold condition for the fluorescence signal in the original GTE formulation. Low z_{th} values (typically in the range $[0.5-1]$) would render networks that highlight global interactions, middle values (typically $z_{\text{th}} = 2$) would reflect a balance between effective communication at both global and local scales, while high values ($z_{\text{th}} \gtrsim 4$) would reflect strong neuron–to–neuron interactions.

Based on different analyses of data under diverse conditions (Ludl and Soriano, 2020; Fernández-García et al., 2020; Montalà-Flaquer et al., 2022) we found that a threshold $z_{\text{th}} = 2$ reflected well the effective connectivity of neuronal cultures and its change during development or perturbations. Thus, in this Thesis, we considered that those links that verified $z_{I,J} \geq 2$ were deemed as significant and set to '1'; the rest set to '0'. The resulting network (and connectivity matrix) was therefore directed but unweighted.

A clarification of the terms 'functional' and 'effective'

As mentioned in the Introduction, the concept of 'connectivity' in neuroscience may refer to structural (repertoire of physical synaptic connections), functional (statistical relationships between active neurons) or effective (causal, direct influences between active neurons). Since our GTE tool provide networks that reflect causal interactions, all our networks depict *effective connectivity* and will be referred as such.

However, when referring to overall network characteristics we will use the term 'functional organisation' or 'functional traits', despite being derived from effective networks. The reason for this apparent confusion in terminology is the lack of a standardized convention in the literature combined with the abuse of the word 'functional', which may refer to the organisational state of a neuronal network, its capacity to convey task–oriented information, or a characteristic response upon stimuli. Also, the

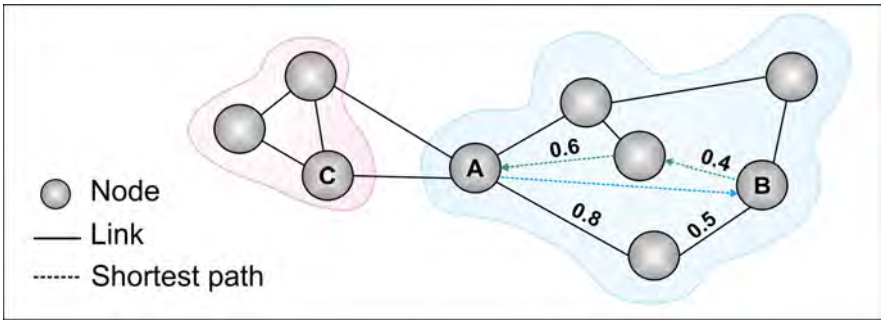

Figure 3.11. Scheme of basic graph theory features. Representation of a small neuronal network represented as a weighted and directed network, in which most of the weights and the arrows are omitted for simplicity. Nodes represent neurons and links neuronal connections. Color shadings in the back differentiate two functional modules. The dashed blue line corresponds to the shortest path from A to B, while the dashed green line represents the shortest path from B to A, reflecting the network's directed nature, i.e. asymmetric. Despite other available routes from B to A with equal lengths, in weighted networks, the shortest path also guarantees the lowest cost.

wording 'effective organisation' or 'effective traits' can lead to confusion since, in the English language, 'effective' is a synonym for 'adequate' or 'competent'.

Network analyses

In the past decade, *network science* has found its way into a diverse array of applications, including neuroscience (Bassett and Sporns, 2017). The brain's neural elements form a complex system of interconnected components that can be effectually represented using *graph theory* (Bassett and Bullmore, 2006; Bullmore and Sporns, 2009; Farahani, Karwowski, and Lighthall, 2019; Bessadok, Mahjoub, and Rekik, 2022). Graph theoretical approaches offer a mathematical framework to model communication between elements of a network by defining a finite set of *nodes* connected by links, or *edges*. As sketched in Figure 3.11, these elements are chosen based on the system under study. For neuronal cultures, a node represents a neuron or a neuronal aggregate, and edges denote connections between neurons. Connections here can be either of structural nature, e.g. experimentally extracted synaptic links or the ground–truth layout in numerical simulations, or from statistical nature, e.g., GTE–inferred effective links.

In our case, since we could not access the structural blueprint of our cultures, all the network analyses considered here were derived from effective interactions. Additionally, generally speaking, a graph could be classified as either directed or undirected, depending on whether the connections between vertices carry directional information, i.e, causal relationships. Another characteristic of the network is whether it is weighted or unweighted, which is determined by the capacity of the edges to have different values.

GTE analysis led to effective connectivity and therefore all our network studies were based on directed networks, which can be represented as an adjacency matrices (Figure 3.12). In these representations, the $N \times N$ nodes are disposed along the x and y axes, with a dot indicating that an effective connection exits between nodes. We note that our matrices were binarized, i.e., unweighted.

Some topological features of the network were extracted from the *connectivity matrices* by using resources from the Brain Connectivity Toolbox programmed and run in Matlab (Rubinov and Sporns, 2010). These features essentially included modularity and global efficiency, and are described in the following paragraphs.

Communities and modularity.— Broadly speaking, the functional or effective connectivity in a network reflects the dynamics of the underlying neuronal system. In the brain, neurons shape a information flow that promotes a functional segregation of the neuronal network by forming strongly coupled local communities. In addition, functional integration is promoted by the existence of a global communication between these communities. The balance between segregation (at a community level) and integration (whole network) plays a vital role in the functioning of distributed networks that underlie cognitive processes (Sporns, 2013a). Thus, the identification of communities is very important to understand the degree of segregation or integration in a neuronal network Additionally, in general, the presence of communities reflect the existence of non–random features in a neuronal network and therefore it is worth analyzing them in the context of neuronal cultures.

Thus, network segregation attributes were computed to objectively detect the presence of neuronal communities within a neuronal network. The *modularity index* Q gives information about the tendency of neurons in the network to form such functional groups, communities of neurons that are more connected within the group than with the rest of the network. Optimal community structure was computed using the Louvain algorithm (Blondel et al., 2008). This algorithm consisted in two phases that were repeated until a maximum in modularity was obtained.

In the first phase, each node of the network was randomly assigned to a module, or community. From each node i the neighbours j were considered, the algorithm evaluated whether there was a gain in modularity if i was placed in the j community. The node i was then placed in the community for which the gain was maximum and positive, or i stayed in its original community if the gain was negative. This process was repeated for all nodes until a local maxima of modularity was reached. Modularity, Q, could be defined as:

$$Q = \frac{1}{2m} \sum_{0 \leq i,j \leq N} \left(A_{i,j} - \frac{k_i k_j}{2m} \right) \delta(c_i, c_j), \tag{3.6}$$

where N is the number of nodes, $A_{i,j}$ represents the weight of the connection between i

and j, $k_i = \sum_{j=1}^{N} A_{i,j}$ is the sum of the weights of the connections attached to neuron i, c_i is the community to which neuron i belongs to, $m = (1/2)\sum i, j = 1^N A_{i,j}$, and $\delta(u,v)$ is the Kronecker Delta with $\delta(u,v) = 1$ for $u = v$ and 0 otherwise. We note that, in our case, the networks are binary and therefore $A_{i,j}$ is non–weighted.

In the second phase of the algorithm a new network was built, in which nodes were defined as the communities found in the previous phase. The weight of the new links were computed by summing the weight of the links between nodes in the corresponding pairs of communities (Arenas et al., 2007). Conceptually, this second phase analyzed the connectivity between the detected communities and investigated whether the arrangement provided the maximum modularity. If that was not the case, the first and second phases were repeated.

Louvain algorithm allows not only to detect different functional communities but also to know their composition as well as their interconnections and dependencies. The final value of Q is constrained between 0 and 1, where a value close to 0 indicates that the entire network functions as a unique community, and a value close to 1 indicates that each neuron (or ROI) operates as an independent community. A value of $Q \simeq 0.3$ suggests the presence of well–defined yet interconnected communities.

Global efficiency and integration.— Integrative processes of the network were computed based in the evaluation of the efficiency of global communication. When considering a weighted matrix $A_{i,j}$ ($N \times N$ nodes), the concept of the *shortest path* $d_{i,j}$ is described as the route between nodes *(i,j)* that minimizes the sum of the weighted links crossed. The *shortest path* average value considering every possible pair of nodes in $A_{i,j}$ is known as the *characteristic path length*, L (Barabási, 2009) and can be calculated as:

$$L = \frac{1}{N(N-1)} \sum_{i \neq j \in A} d_{i,j}. \tag{3.7}$$

Latora and Marchiori defined the efficiency of a path between two nodes as the inverse of the shortest path that link them (Latora and Marchiori, 2001; Latora and Marchiori, 2003). When considering a path that does not exist, $d_{i,j}$ is considered infinite and, therefore, the efficiency is zero. The *global efficiency*, G_E, can be calculated as the average efficiency over all pair of nodes. Hence, G_E rates the efficiency of the network to exchange information as a whole, and is defined as:

$$G_E = \frac{1}{N(N-1)} \sum_{0 \leq i,j \leq N} \frac{1}{d_{(i,j)}}, \tag{3.8}$$

where N is the number of nodes in the network and $d_{i,j}$ the length of the shortest topological path connecting nodes i and j, with non–connected nodes procuring $d_{i,j} \to \infty$. G_E ranges between 0 and 1. A value of $G_E \simeq 0$ indicates that nodes in the network

are effectually disconnected. Conversely, for $G_E \simeq 1$, all neurons are interconnected and the network is capable of exchanging information at a whole network scale.

Figure 3.12a depicts an example of a connectivity matrix obtained from an homogeneous neuronal culture grown on the top of a 6 mm PDMS disc, pre–coated with PLL to ensure neuronal adhesion. Along the diagonal we can distinguish 5 different neuronal communities, the off–diagonal connections refer to the connections between the functional communities. This network demonstrates a substantial global efficiency $G_E = 0.47$, indicating a thoroughly integrated network structure. Despite the presence of discernible modules, the network exhibits strong interconnectivity among them as evidenced by a low modularity value ($Q = 0.26$). The Gephi graph of the matrix can be found below it, representing the spatial distribution of the functional communities within the culture surface.

By contrast, figure 3.12b, represents a connectivity matrix from an homogeneous culture grown on the top of a 6 mm PDMS topographically patterned mould. As for the previous case, the PDMS was pre–coated with PLL. In this culture, the connectivity matrix exposed a segregated neuronal network with 4 communities strongly differentiated ($Q = 0.49$). As it can be observed in the Gephi graph below, the four communities were distributed along the patterned tracks of the PDMS mould, evidencing that topographical patterns could, indeed, guide the functional connectivity of the network (Montalà-Flaquer et al., 2022).

3.3.4 Statistics and significance tests

The results presented throughout the thesis were expressed as mean $\pm$ standard error of the mean, defined as $\mathrm{SD}_{\mathrm{error}} = \sigma/\sqrt{n}$, with σ the standard deviation and n the number of independent samples, in our case neuronal cultures. In all cases, systematic error has been determined to be negligible.

Statistical significance analyses were performed using the unpaired Student's t–test or two-way ANOVA. Either Matlab or Origin 9.1 were used for the plotting of distributions and corresponding statistics. The p–value for significance p was indicated as * for $p < 0.1$, ** for $p < 0.01$, *** for $p < 0.001$, and 'n.s.' when no significant differences were found, i.e. for $p \geq 0.1$.

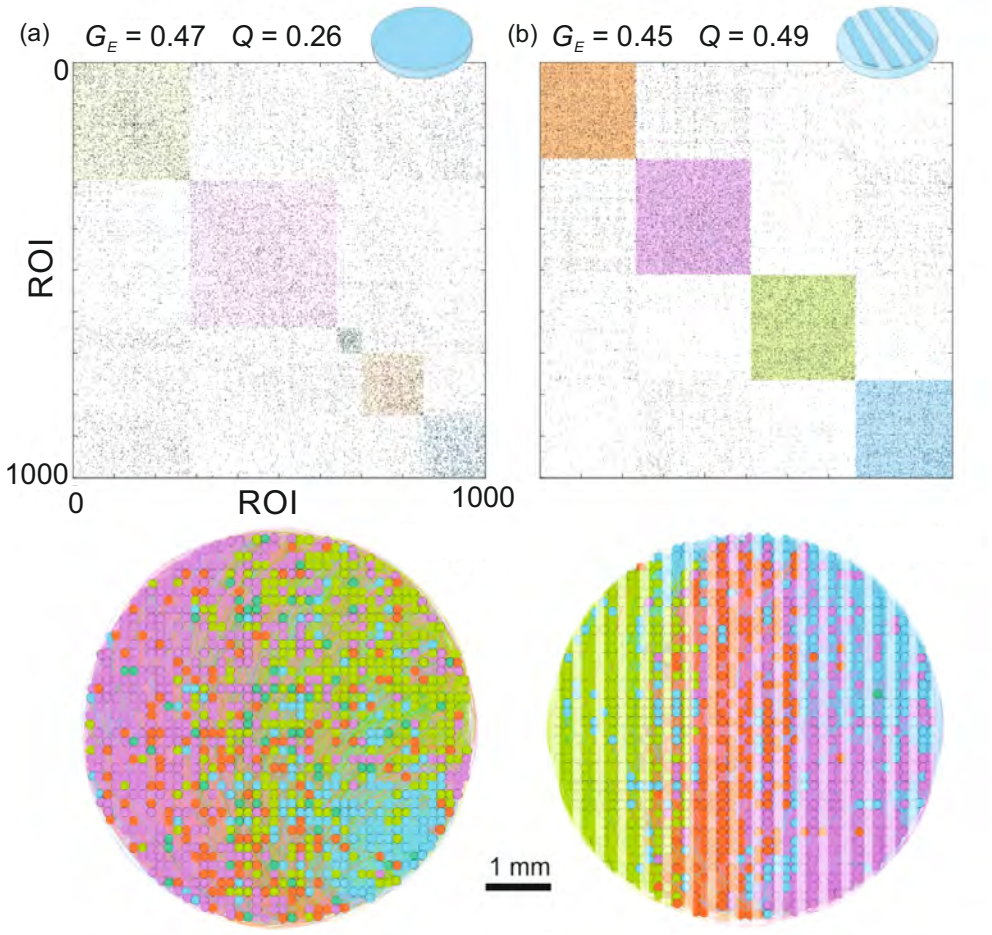

Figure 3.12. Example of connectivity matrices and Gephi graphs. **(a)** A homogeneous culture grown on the top of a 6 mm PDMS disc. The matrix represents an integrated neuronal culture with $G = 0.47$ and $Q = 0.26$. At the bottom, the Gephi graph shows the spatial distribution of the 5 functional modules indicated in the diagonal of the connectivity matrix. **(b)** Connectivity matrix of a topographical–guided neuronal cultures grown on the top of a 6 mm PDMS disc with parallel rectangular tracks of 300 μm wide and 20 mm long and separated by 300 μm. Results exhibit a high modularity with $Q = 0.49$ that evince a segregated connectivity with four strongly differentiated communities guided along the parallel tracks of the PDMS pattern. Plots adapted from (Montalà-Flaquer et al., 2022).

4 2D primary neuronal cultures as models for tauopathies

4.1 Introduction

Neurodegenerative diseases (NDs) are highly intricate and multifaceted chronic medical conditions which, nowadays, require a deep collaborative effort of various scientific disciplines simply to comprehend fundamental aspects of their nature. Among NDs, tauopathies stand out as clinically, biochemically, and heterogeneously diverse diseases characterised by the abnormal misfolding and aggregation of hyperphosphorilated forms of the microtubules (MTs)–associated protein *tau* in specific brain regions (hereinafter referred to as *pTau*).

There are more than 25 NDs classified as tauopathies, including Alzheimer's disease (AD), aging–related tau astrogliopathy, argyrophilic grain disease, primary age–related tauopathy, Pick's disease, and globular glial tauopathy, among others (Cleveland, Hwo, and Kirschner, 1977; Ballatore, Lee, and Trojanowski, 2007; Sanders et al., 2014). Over 55 million people worldwide live with dementia, a number that is set to rise to 139 million by 2050 according to *Alzheimer's Disease International* (International, 2023). Despite significant efforts to gain a better understanding of the pathophysiological aspects of tauopathies, little is known about their origins, evolution, and potential treatments.

In this context, the project led by Dr. José Antonio del Río, entitled 'Modulation of Tau Seeding and Pathology in Tauopathies by BBB-nanocarriers, Epitope-Selective Vaccination, and EctoPrP Tau Receptor Bodies' aimed at exploring new ideas under the financial support of a *'La Caixa' Health Research* 2019 program. This ambitious project put together four research groups under a common goal: to elucidate disease–specific variations for the internalization, propagation, and spread of pTau species. The objective was to develop region selective peptide blood–brain barrier (BBB) shuttles equipped with pTau aggregation inhibitors, with the aim of blocking pTau seeding and spreading.

In Soriano's lab we were tasked with the analysis of pTau damage progression *in vitro*. To do so, we explored changes in the behaviour of cortical primary neuronal cultures by applying two major strategies: i) the study and quantification of changes in cell dynamics, and ii) the application of detailed graph analysis of the data by using information–theoretic algorithms among all pairs of recorded neurons in combination

with graph–theoretical analyses. Our initial hypothesis was that graph analysis would show evident functional deficits, such as a decrease in overall connectivity, the loss of neuronal hubs, or a failure in the communication and integrability of the pTau–affected cultures. However, regrettably, as we will elaborate next, such a hypothesis could not be proved, and we could not see significant and conclusive differences.

Throughout this Chapter, we will provide essential insights into tauopathies, which will enhance our understanding of the methodologies used in conducting experiments and their subsequent analysis. Following this introduction, we will present the results obtained and engage in a comprehensive discussion within the context of tauopathies and their impact on neural networks.

4.1.1 Tau protein in a healthy brain

Tau is a MTs–associated protein initially described by Weingarten et al., 1975. It plays a pivotal role in the CNS by participating in the assembly and stabilization of MTs. Tau is a hydrophilic protein that can be divided into four main domains based on their biochemical properties (see Figure 4.1). These domains include the N-terminal domain, which is involved in regulating mucrotubules dynamics, the proline–rich domain, the MTs binding domain (MTBD), which plays a crucial role in tau's ability to bind and stabilize microtubules, and the C–terminal tail, a consistent feature across different tau isoforms. Biophysical studies have revealed that tau is a natively unfolded protein, characterised by a highly flexible conformation and an overall low content of secondary structure (Chen et al., 1992; Jeganathan et al., 2008; Mukrasch et al., 2009).

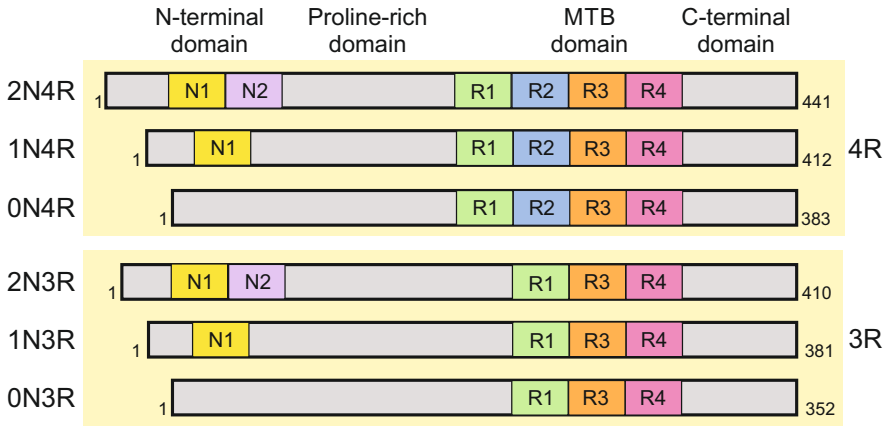

Figure 4.1. Representation of tau protein domains and alternative splicing in the human CNS. Six distinct tau isoforms emerge through alternative splicing of the *MAPT* gene, distinguished by the presence of zero, one, or two N-terminal inserts (0N, 1N, or 2N) and by the presence of either three (3R) or four (4R) MTBDs in the proline–rich domain. The C–terminal region remains consistent across all six human CNS tau isoforms. In the provided diagram, the tau isoforms are presented separately based on whether they are 3R or 4R, with their amino acid sequence extending from the first (left) to the final (right) amino acid, which varies depending on the specific isoform's length

Human tau is encoded by the *MAPT* gene, located on chromosome 17 (Andreadis, 2006). Alternative splicing of this gene gives rise to six tau isoforms, each representing a slightly different version or variant of the same protein. These isoforms result from the exclusion of the N–terminal (0N) segment or the inclusion of one (1N) or two (2N) N–terminal segments. The central portion of tau is characterised by proline–rich domains, while the microtubule binding domain (MTBD) can consist of either 3 (3R) or 4 (4R) repeated domains (see Figure 4.1) (Guo, Noble, and Hanger, 2017). The expression of tau is subject to regulation based on developmental stages: fetal brains predominantly express the shortest tau isoform, 0N3R, whereas in the adult human brain all six isoforms are expressed. In the cerebral cortex of healthy adults, the levels of 3R and 4R tau isoforms are approximately equal (Goedert et al., 1989).

In the brain, tau is primarily found in neurons, also present in oligodendrocytes and astrocytes although at lower levels (LoPresti et al., 1995; Müller et al., 1997). Tau performs various functions within different subcellular compartments. In mature neurons, tau is mainly distributed in axons, where it interacts with microtubules through its MTBD. Its functions include MT stabilization, promotion of MT assembly, and the regulation of dynamic instability in MTs, facilitating cytoskeletal reorganisation (Feinstein and Wilson, 2005; Mandelkow and Mandelkow, 2012). Consequently, tau plays a crucial role in axonal elongation and maturation. Additionally, tau may impact axonal transport through various mechanisms (Stamer et al., 2002; Vershinin et al., 2007; Dixit et al., 2008). Smaller amounts of tau can be found in dendrites and dendritic spines (Ittner et al., 2010; Kimura et al., 2014), where it has been reported to be involved in the regulation of synaptic plasticity (Chen et al., 2012; Frandemiche et al., 2014).

Beyond axons and dendrites, tau has also been detected in neuronal nuclei and non–neuronal cells, where it appears to play a role in maintaining the integrity of genomic DNA, cytoplasmic RNA, and nuclear RNA (Violet et al., 2014; Qi et al., 2015). While tau is primarily an intracellular protein, emerging evidence suggests that tau is physiologically released onto the extracellular space by cultured cells *in vitro* and by neurons in mouse brains *in vivo*. The mechanisms underlying tau release remain unclear, but it has been reported that neuronal activity may regulate this release (Pooler et al., 2013; Yamada et al., 2014). Figure 4.2 illustrates the roles of tau in a healthy brain.

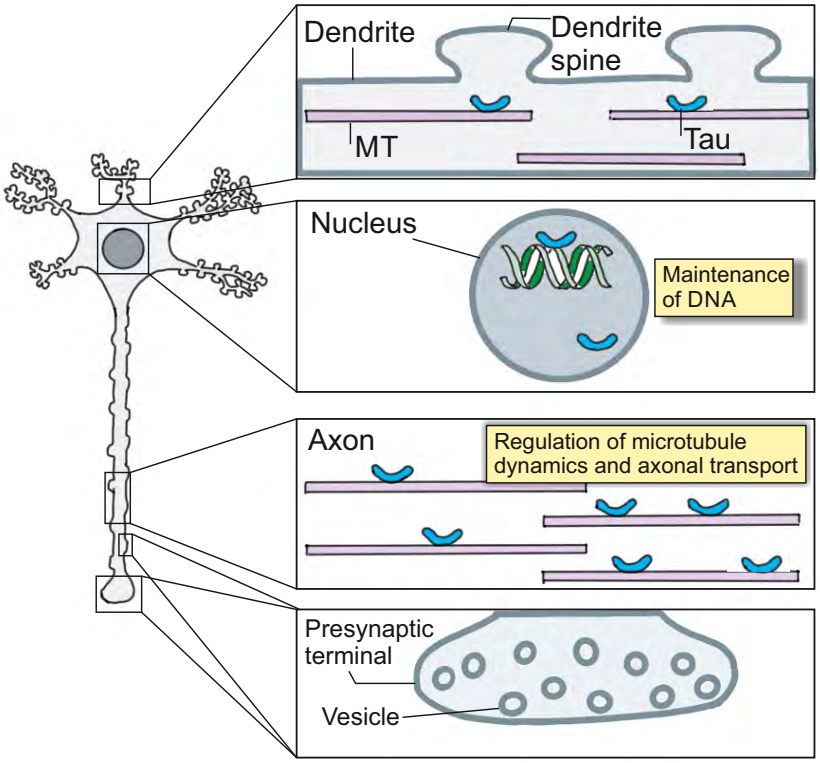

Figure 4.2. Functions of tau in a healthy brain, adapted from Wang and Mandelkow, 2016. Tau serves multiple physiological functions within the nervous system. In healthy neurons, it predominantly localizes within axons and plays a crucial role in MT stabilization. Beyond its role in regulating MT dynamics, tau is also implicated in modulating axonal transport through various mechanisms. Although a minor fraction of tau is found within dendrites, its precise function in this context remains uncertain. Additionally, a portion of tau is situated within the nucleus, where it potentially contributes to the preservation of genomic DNA integrity.

Phosphorilation of tau

The physiological functions of tau are subjected to a wide range of post–transalational modifications, covalent processing events that change the properties of a protein (Gong et al., 2005; Martin, Latypova, and Terro, 2011). Phosphorylation is the most commonly described post–translational tau modification, which is tightly regulated by multiple kinases and phosphatases under physiological conditions. They play a crucial role since phosphorylation negatively modulates tau affinity to MTs (Biernat et al., 1993; Martin et al., 2013).

However, *hyperphosphorylated tau* (pTau) is the major component of neuronal and glial inclusions in human tauopathies (Grundke-Iqbal et al., 1986). Tau phosphorylation increases under pathological conditions, which reduces its affinity for MTs (Meyer

et al., 1995) and effectively leads to the detachment of tau. This results in MT disassembly in axons and, therefore, in cytoskeleton's destabilisation (Ksiezak-Reding et al., 2003). Detached tau may also mislocalize into presynaptic terminals, inducing synaptic dysfunction and, eventually, synapse loss (Decker et al., 2015). Although 'pathological' tau cannot enter the nucleus, DNA damage is possible due to the loss of the DNA–protective function of tau (Sultan et al., 2011). In addition, phosphorylation in proline–rich domain induces a subtle increase in the propensity of tau to self–aggregate (Eidenmüller et al., 2001). These abnormal forms of tau may be released onto the extracellular space where they assemble into filaments and neurofibrillary tangles (NFTs) globally known as *tau aggregates*. These tau aggregates gradually overburden neurons, affect fundamental cell functions and ultimately cause neuronal death (Ward et al., 2012). Figure 4.3 summarises the effects that the presence of pathological forms of tau may cause.

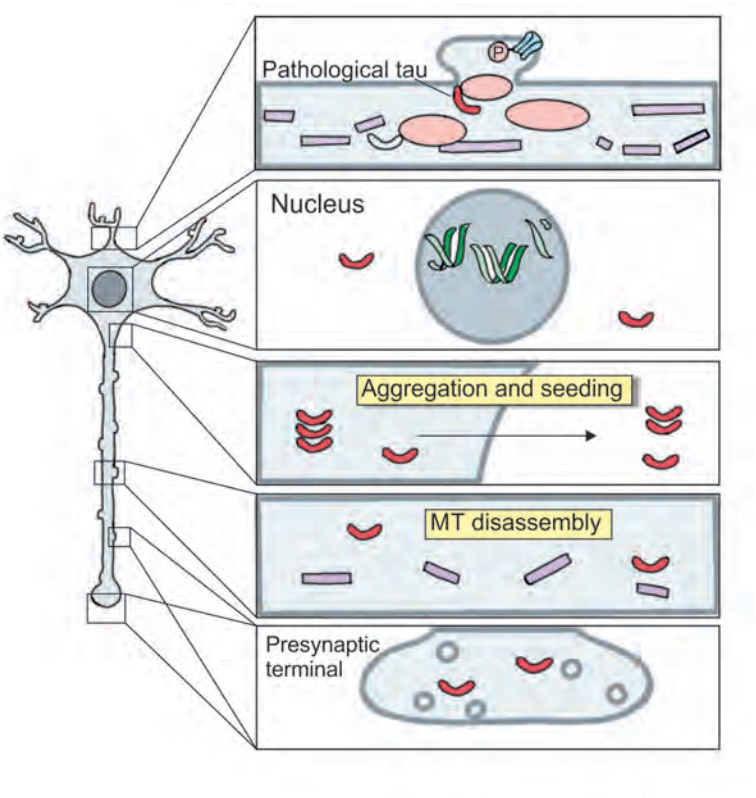

Figure 4.3. Tau in disease, adapted from Wang and Mandelkow, 2016. In conditions of pathology, tau becomes hyperphosphorilated and detaches from MTs, resulting in MTs disassembly. pTau can mislocalize into presynaptic terminals, triggering synaptic dysfunction and loss. Importantly, pTau is unable to access the nucleus, potentially leading to DNA damage. Furthermore, tau may aggregate, contributing to the deterioration of neuronal function. These tau aggregates may be released into the extracellular space and subsequently taken up by other neurons, facilitating the propagation of tau pathology.

4.1.2 Tauopathies and the prion–like hypothesis

As mentioned earlier, the presence of tau aggregates is a common histopathological hallmark among various tauopathies (Lee, Goedert, and Trojanowski, 2001). The differences between this diverse group of disorders lie in the specific cell types primarily affected by pTau, the distribution patterns of tau aggregates in different regions of the brain, and the distinct characteristics of these aggregates (Götz, Halliday, and Nisbet, 2019). Despite confirming the potential of tau to cause NDs through the identification of tau mutants, the understanding of the mechanisms underlying tau aggregates formation in these conditions and the pathways leading to tau–induced neurodegeneration remains limited.

Some authors hypothesized that tau pathology spreads from cell to cell in a similar way to that described for the prion protein (PrP) (Clavaguera et al., 2009; Sanders et al., 2014). The *prion–like* hypothesis considers that protein tau misfolds and acquires the ability to act as a template, inducing the misfolded form to healthy counterparts, a process known as *seeding* (Frost and Diamond, 2010). Recent publications reported that tau filaments, extracted from the sarkosyl–insoluble fraction of human brain tissues affected by AD, have the ability to induce seeding in cultured cells (Audouard et al., 2016) and in wild–type mice (Lasagna-Reeves et al., 2012; Guo et al., 2016). Subsequently, the prion–like paradigm propagation (*spreading*) of seed–competent tau may occur through a process that includes a donor neuron, which releases tau seeds via exocytosis. Extracellular pTau is then internalized by a nearby neuron by endocytosis. This process might also happen trans–synaptically, after the degeneration of presynaptic neurons that release *pathological* tau to the postsynaptic neuron by synaptic vesicles (Clavaguera et al., 2015; Wang and Mandelkow, 2016). In AD, the process of spreading tau pathology is well–documented and occurs in a specific spatiotemporal manner, following the anatomical connections between brain regions (Braak and Braak, 1991). However, in other tauopathies, the patterns of tau pathology propagation can vary, displaying regional variations or even dependence on specific cell types. Although recent studies have carried out experiments regarding the spreading mechanism of abnormal forms of tau, the details of this process remain unclear (De Calignon et al., 2012; Liu et al., 2012; Vogel et al., 2020).

A hallmark of tauopathies is the disruption of processes like neuronal activity and functional organisation in the brain, fundamental aspects for a correct brain functioning, as they are essential for cognition, memory, and behaviour. Insoluble tau filaments have been proven to influence neuronal excitability and synaptic transmission by altering the balance of intracellular calcium ions (Gómez-Ramos et al., 2008; Bouillet et al., 2022), impairing mitochondrial function (David et al., 2005; Esteras and Abramov, 2020), and promoting the hyperactivity of vulnerable neuronal populations (Dickerson et al., 2005). It has been reported that aberrant neuronal activity, such as network hyperactivity, may be the result of a self–defense mechanism of the brain against early signs of disease. However, these mechanisms may exacerbate tau pathology, creating

a detrimental positive feedback loop that further drives disease progression (Palop and Mucke, 2010; Pooler et al., 2013).

To comprehend the complex interplay between tau pathology and these network abnormalities, researchers have applied advanced neuroimaging techniques, including functional magnetic resonance imaging (Mondadori et al., 2006; Steward et al., 2022) and positron emission tomography (Schöll et al., 2016) to unravel the functional organisation of affected brain regions in tauopathies. Experiments have identified disrupted large–scale networks and altered functional connectivity patterns in individuals with tauopathies. These conditions involve a loss of balance between different brain regions, leading to functional disintegration and cognitive impairment.

Modeling tauopathies

Neuronal cultures play a critical role as experimental models in interdisciplinary neuroscience, providing a controlled environment to investigate the emergence of complex behaviour from interconnected neurons. Primary neuronal cultures have been previously used to study the process of seeding and spreading of pTau, mostly using microfluidics designs, in which researchers independently treated, tuned, and monitored the different chambers, separating neuronal somas from axons (Wu et al., 2013; Calafate et al., 2015). Previous *in vitro* research on the relationship between tauopathies and primary neuronal dysfunction has generally focused on studying changes in neuronal activity at a single time point, typically after the introduction of tau treatment. However, there are no studies investigating the possible effects of pTau in the neuronal activity of *in vitro* neuronal cultures through time–course experiments, neither evaluating changes in the dynamics of the activity or in the functional organisation of the resulting network.

Therefore, we investigated spontaneous neuronal activity in primary neuronal cultures that were pre–treated with extracellular wild–type and seed–competent tau proteins, with a focus on exploring the prion–like hypothesis of pTau propagation. Over a period of 16 days, we closely monitored the cultures to examine potential alterations in neuronal activity and the functional organisation of the *in vitro* neuronal network. With that purpose, we applied specific analysis tools grounded on physics of complex systems. Next, we will discuss the observed changes in the neuronal cultures and evaluate the suitability of using such simplified models to study complex diseases like tauopathies.

4.2 Objectives

The aim of this investigation is to elucidate the effects that pTau exerts on the dynamics of neuronal activity in primary neuronal cultures as well as their functional organisation. To achieve this, we designed an '*in vitro* tauopathy model' by introducing pTau

extracted from various sources into wild–type cortical primary cultures derived from mouse embryos. Subsequently, we recorded neuronal activity from pTau–affected cultures and explored potential effects on neuronal connectivity induced by the presence of pTau.

Additionally, and as a part of the *'La Caixa' Health Research* project, we applied these tools to investigate the toxicity of pTau inhibitors developed within the framework of the program. In this context, we introduced various anti–aggregation inhibitors, developed by the collaborators, into primary neuronal cultures and examined potential differences in connectivity compared to control cultures. After confirming their non–toxicity, the ultimate goal of this investigation was to determine whether pTau inhibitors could reverse the connectivity deficits characterised in the initial phase of this study.

Briefly, the main goals of this research are:

- Test the toxicity of pTau–inhibitors in primary neuronal cultures.
- Build an *in vitro* model of tauopathy and characterise the changes in neuronal dynamics and functional organisation of the network in cortical primary neuronal cultures.
- Explore the effectiveness of inhibitors by proving that the detected changes in connectivity can be reversed when pTau–affected primary cultures are subjected to this treatment.

4.3 Materials and methods

Experiments were carried out in accordance with the regulations of the Ethical Committee for Animal Experimentation of the University of Barcelona (approved ethical order DMAH-5461) and the laws for animal experimentation of the Generalitat de Catalunya (Catalonia, Spain).

Primary neuronal cultures were prepared according to the methods outlined in Chapter 3. In summary, we established cultures using cortical tissue obtained from CD1 mouse embryos, which were mechanically dissociated to isolate individual neurons. To facilitate the imaging of the cultures in the optical system of Soriano's Lab, we affixed a PDMS mould onto a glass cover–slip surface, with the mould containing two circular cavities each measuring 4 mm in diameter (Figure 3.3a in Chapter 3). The cavities effectually shaped wells when bond to the glass surface. The advantage of this arrangement is that it allowed the simultaneous recording of two separate wells under identical conditions, doubling our data acquisition capacity. The PDMS–glass assembly was treated with a PLL coating overnight to ensure a uniform distribution of the neurons in culture.

At DIV 1, we transduced the cells with GCaMP6s, enabling the recording of spontaneous neuronal activity from DIV 7 to DIV 16. All cultures began to degrade beyond this point and recordings were not reliable. Thus, to reliably compare control and affected cultures, we chose to conclude recordings at this stage. This decision ensured that any observed changes in activity could be attributed to the presence of external agents (such as the inhibitor or extracellular tau) and not to the natural degradation of the cultures. Activity data underwent analysis following the procedures outlined in Sec. 3.3 of Chapter 3.

In the following, we will provide a concise overview of the pTau inhibitors used for toxicity testing, along with the protocols employed for preparing the cultures. Additionally, we will outline the various pTau samples utilized to simulate the extracellular environment of an *in vitro* tauopathy and the procedures used for delivering these external agents.

4.3.1 Preparation of an assay for inhibitors of tau aggregation

Within the 'La Caixa' project, Dr. Soriano's group collaborated with Dr. Ernest Giralt and his research team to assess the efficacy of certain pTau–aggregation inhibitors. These inhibitors are peptide shuttles that are highly resistant to proteases, enzymes that break peptide bonds in proteins. Inhibitors were encapsulated within custom–manufactured nanocarriers designed to traverse the BBB. Dr. Giralt's group aimed to investigate various structural configurations of these peptide shuttles to achieve optimal and region–specific delivery to target brain areas. The ultimate goal was to transform the inhibitor–nanocarrier assembly into an effective treatment for various tauopathies. During this study, an engineered compound termed *IN–M4* was identified as the most suitable inhibitor for this purpose, as it had previously been demonstrated its ability to inhibit tau aggregation *in vitro* (Seidler et al., 2019).

Although Dr. Soriano's group tested multiple inhibitors, we focus here on explaining the protocol specifically used for the study of IN–M4 due to its relevance. Briefly, the preparation of the inhibitor stock solution was carried out at IBEC, led by Dr. Júlia Sala, using the raw peptide structure synthesized by Dr. Macarena Sanchez and her research team. To prepare the inhibitor, lyophilized IN–M4 was initially dissolved in dimethyl sulfoxide (DMSO) to achieve a desired stock concentration of 10 mM. Subsequently, the solution underwent filter sterilization using a 0.22 μm sterile syringe filter (Merck Millipore, Germany). The resulting stock solution was then divided into aliquots and stored at -20°C until it was needed for actual *in vitro* tests.

For the experiments, primary neuronal cultures were prepared following the previously described procedure as illustrated in Figure 4.4a. An initial phase was conducted to determine the appropriate concentration of the inhibitor in the culture medium. This concentration was set at 50 μM to explore extreme cases, although such a concentration is substantially higher (by a factor 5) than the typical concentration used for *in*

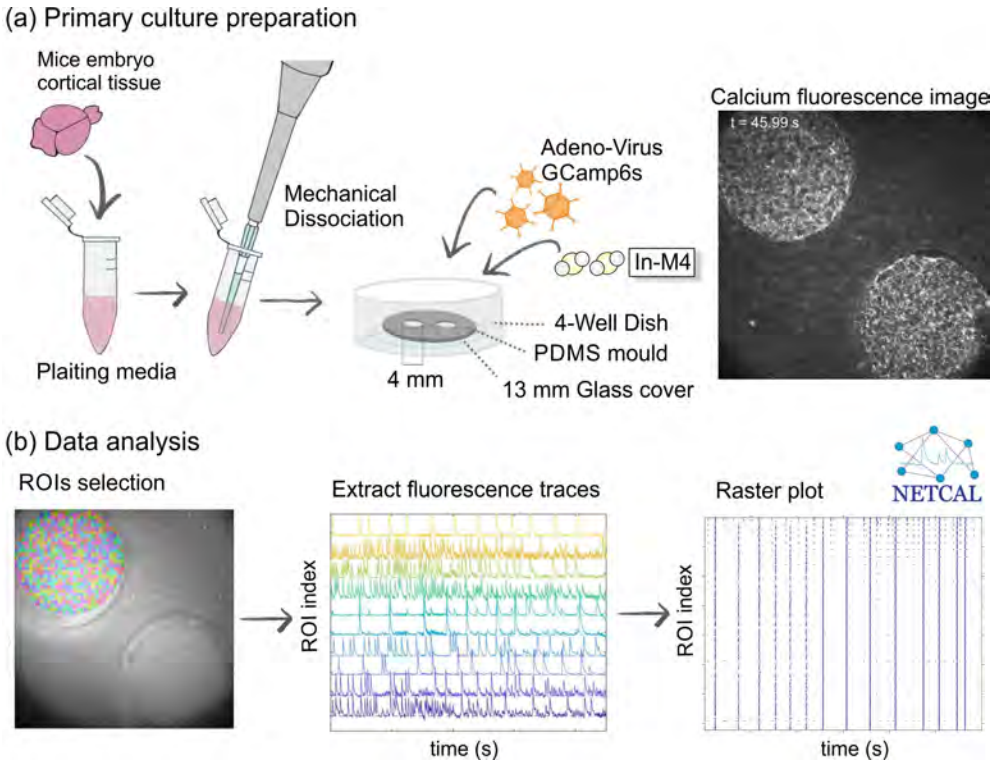

Figure 4.4. Illustrated methods for preparing primary neuronal culture for seeding assay with inhibitors of tau aggregation. **(a)** Experimental setup. Cortical tissue for CD1 mouse embryos were mechanically dissociated and plated in a 4–well plated including a PDMS mould that confined two different 4 mm diameter cavities. At DIV 1 cells were transduced with GCaMP6s. At DIV 5 IN–M4 was included at preset concentration. Activity recordings were then performed from DIV 7 to 16. **(b)** Data analysis of neuronal activity recordings using NETCAL (Orlandi et al., 2017). A circular grid of 30×30 ROIs were established in each cavity. Then, the fluorescence traces were extracted. After applying a spike detection algorithm, spikes were plotted in the form of a raster plot.

vivo treatments. Once the final concentration of the inhibitor in the culture medium was established, we added the required amount of the stock solution to the medium on day DIV 5, during the first medium change. We included control cultures in the recordings to properly evaluate the effect of the inhibitor. Thus, in general, we considered the following preparations:

- Untreated condition: normal culture preparation.
- Control condition: normal cultures loaded with filtered DMSO.
- IN–M4 condition: standard culture that incorporated the IN–M4 inhibitor in its culture medium at DIV 5.

A total number of almost 36 cultures (containing each two 4 mm cavities) from 3 different dissections were prepared in order to achieve reproducibility and sufficient

statistics. From them: 7 were standard cultures, 5 were control condition, and 12 were IN–M4 condition.

We commenced the recording of neuronal activity on DIV 7 and continued monitoring each well until DIV 16. The pipeline for data analysis (detailed in Sec. 3.3) is summarized in Figure 4.4b.

4.3.2 Preparation of an assay for tauopathies *in vitro*

■ Origin and manipulation of extracellular tau samples

To create an *in vitro* environment that simulates a tauopathy, we introduced extracellular tau proteins into the culture medium. Specifically, we considered wild–type tau as a control and pathological tau (pTau) as damaging agent.

Both wild–type and pTau samples were obtained from two distinct sources: (i) tau proteins purified from the insoluble sarkosyl extract harvested from the brains of P301S mice, and (ii) cell–derived tau sourced from a Tau–Biosensor cell line (Holmes et al., 2014). Both samples were meticulously prepared at Dr. Del Río's Laboratory at IBEC, under the responsibility of Dr. Júlia Sala.

(i) Sarkosyl–insoluble fractions from mice brains

The P301S mice are a transgenic model genetically engineered to overexpress the shortest human tau isoform bearing the P301S mutation. This mutation is associated to an inherited form of frontotemporal dementia (Allen et al., 2002). These transgenic mice have been reported to show critical levels of tau filaments aggregates at 9 months of age. For our experiments, brains from 12–month–old P301S (+/-) mice, and their non–transgenic littermates, P301S (-/-), were used for the extraction of the sarkosyl–insoluble tau samples.

Briefly, frozen brains were weighed and homogenized by using a Dounce homogenizer in a 1 : 10 ratio of fresh, ice-cold homogenization buffer [0.8 M NaCl, 1 mM EGTA, 10% sucrose, 0.01 M $Na_2H_2P_2O_7$, 0.1 M NaF, 2 mM Na_3VO_4, 0.025 M β-glycerolphosphate, 0.01 M Tris-HCl, pH 7.4] supplemented with protease inhibitors (Hoffmann-La Roche, Basel, Switzerland). After centrifuging at 16,000 RPM for 22 min at 4°C, the resulting supernatant (SN1) was collected. The pellet was then resuspended in a proportion of 1 : 5 with homogenization buffer and centrifuged again at 14,000 RPM for 22 min at 4°C. The resulting supernatant (SN2) was combined with the SN1, and the mixture (SN1 + SN2) was incubated with 0.1% sarkosyl (Sigma-Aldrich, St. Louis, MO, USA) on a rotating shaker at room temperature for 1 h. The mixture was centrifuged at 35,000 RPM for 63 min at 4°C. The supernatant was discarded, and the remaining pellet (sarkosyl–insoluble fraction), resuspended in 50 mM Tris-HCl, pH 7.4 (200 μL/g starting material), aliquoted and stored at -80°C until use. Protein concentrations were determined using the Pierce™ BCA assay kit (Sigma-Aldrich, St. Louis, MO, USA), and equal amounts of protein were analyzed

by immunoblot.

(ii) Tau sequential extraction from Tau Biosensor cell line

The Tau Biosensor cell line was created to serve as a valuable tool for cell–based assays aimed at investigating specific facets of pathological tau. For our research, we employed the only commercially available cell line designed to detect seed–competent tau in biological samples. Developed by Dr. M. I. Diamond's laboratory (University of Texas, Southwestern Medical Center) and commercialized by the American Type Culture Collection (ATCC), the tau repeat domain (RD) P301S FRET Biosensor, henceforth referred to as Tau Biosensor cell line, was first introduced in 2014 (Holmes et al., 2014). To construct this cell line, researchers genetically modified HEK293 cells to express the tau RD fragment bearing the P301S mutation, coupled with either cyan fluorescent protein (CFP) or yellow fluorescent protein (YFP). Upon the introduction of seed–competent tau, such as brain homogenates from AD patients, the tau RD-CFP and tau RD-YFP fragments undergo aggregation, which can be quantified through flow cytometry or fluorescence imaging.

To perform sequential protein tau extraction from the Tau Biosensor cell line, cells were seeded at a density of $200,000$ cells/well into 60 mm–diameter Petri dishes, which were pre–coated with poly–D–lysine (PDL) at a concentration of 0.1 mg/mL. The cells were maintained in culture medium under controlled conditions at 37°C with 5% CO_2 in a humidified incubator. On DIV 1, cells underwent transduction following the manufacturer's protocol (Holmes et al., 2014), which involved the use of total brain homogenates derived from P301S (+/-) or P301S (-/-) mice, along with empty liposomes serving as a vehicle control condition. Specifically, 1.5 μL of a diluted sample was combined with 8.5 μL of Opti–MEM medium (ThermoFischer Scientific). Subsequently, a mixture comprising 1.5 μL of Lipofectamine-2000 reagent (Invitrogen) and 8.75 μL of Opti-MEM was added to the sample mixture, reaching a final volume of 20 μL. This mixture was incubated for 1 hour at room temperature. Control experiments were conducted with empty liposomes.

After a 24 h of incubation, the transduction solution was removed and the cells washed once with pre–warmed sterile 0.1 M PBS. Fresh maintenance medium was added, and the cells were further cultured. After 48 h, the cells underwent two washes with pre–warmed sterile 0.1 M PBS. Subsequently, cells were harvested by scraping them from the Petri dish surface in Triton X-100 lysis buffer, containing 0.05% Triton X-100 in sterile 0.1 M PBS supplemented with 1X protease inhibitors. The cell suspensions were then centrifuged at $500\times$ g for 5 min at 4°C. The supernatants from this step were further subjected to centrifugation at $1,000\times$ g for 5 min at 4°C. The remaining Triton X-100 soluble fraction was then subjected to high-speed centrifugation at $50,000$ rpm for 30 min at 4°C. Following this, the resulting pellet was washed in 0.1 M PBS and underwent another round of centrifugation at $50,000$ rpm for 30 min at 4°C. The pellet was subsequently resuspended in 50 μL of 50 mM Tris-HCl, pH 7.4,

and designated as the 'Triton X-100 insoluble fraction' (TIF). Notably, each fraction was named based on the sample used during the transduction of Tau Biosensor Cells. Specifically, fractions derived from brain homogenates from P301S (+/-) mice were labeled as 'TIF-P+', those from P301S (-/-) mice as 'TIF-P-', and the vehicle control (empty liposomes) condition as 'TIF-V'. All fractions were aliquoted and stored at $-80°C$ for future use. To determine protein concentrations within these fractions, we utilized the Pierce BCA assay kit (Sigma-Aldrich, Germany), and subsequent immunoblot analysis was performed using equal amounts of protein.

■ Reproducing tauopathy's environment in primary neuronal cultures

In accordance with the procedure outlined at the beginning of this chapter, primary neuronal cultures were established by cultivating individual cortical neurons derived from CD1 mouse embryos. These neurons were cultured on pairs of 4 mm PDMS wells. On DIV 5, cells in culture were subjected to various treatments in order to investigate the impact of pTau.

Our investigation encompassed three distinct experimental scenarios. The scenarios were explored one after another along the three years of the thesis in an attempt to ascertain which one procured the best *in vitro* model for pTau.

- (i) As initial exploration, cells were exposed to either wild–type tau or cell–derived pTau extracted from the Tau Biosensor cell line. This cell–derived approach, relatively easy to obtain, served as a starting point for our study.
- (ii) In the next stage, we sought to directly inoculate the cultured cells with the insoluble sarkosyl fraction extracted from the brains of P301S mice. In this context, the samples might contain not only tau but also other insoluble forms present in the environment, which could contribute to the damaging action of pTau on the cultured cells.
- (iii) Finally, to accelerate the tauopathy scenario, neurons were infected with an adenovirus carrying full–length human tau with the P301L mutation. This infection was combined with the treatment involving the insoluble sarkosyl fraction.

The experimental setups for these scenarios are detailed next.

(i) Neurons in culture treated with Tau Biosensor cell line

Four different conditions were induced in the cultures:

- Untreated: standard cultures were prepared, i.e., following the usual protocols of 2D cultures in the laboratory.
- Vehicle: preparation in which TIF-V was included in the culture medium, i.e. neurons were treated with empty liposomes.

- TIF-P- condition: cells in culture were treated with the TIF extracted from Tau Biosensor cells with the P301S (-/-) insoluble sarkosyl fraction.
- TIF-P+ condition: cells in culture were treated with the TIF extracted from Tau Biosensor cells with the P301S (+/-) insoluble sarkosyl fraction.

Conditions were not refreshed with media changes in an attempt to better replicate the brain scenario. Treatment concentrations were tested and adjusted to 6 and 12 μg/mL of total protein. A total number of almost 40 cultures (containing each two 4 mm cavities) from 4 different dissections were prepared in order to have good reproducibility and statistics. From them: 7 were untreated cultures, 8 were the vehicle condition, 7 were for TIF-P- and 10 were for TIF-P+.

(ii) Neurons in culture treated with insoluble sarkosyl fraction extracted from the brains of P301S mice

Three different conditions were induced in the cultures:

- Untreated: standard culture preparation.
- P301S (-/-) control condition: P301S (-/-) insoluble-sarkosyl fraction was included (*wild–type* tau).
- P301S (+/-) pathological condition: P301S (+/-) insoluble sarkosyl fraction was included (*pathological* tau).

Conditions were not refreshed with media changes in an attempt to better replicate the brain scenario. Treatment concentrations were tested and adjusted to 10 μg/mL of total protein. A total number of almost 60 cultures (containing each two 4 mm cavities) from 9 different dissections were prepared in order to have good reproducibility and statistics. From them: 18 were untreated cultures, 19 were controls and 32 were pathological condition.

(iii) P301L mutation infection–induced by adeno–virus

To accelerate the damage scenario in culture, primary neurons were infected at DIV 1 with 2×10^7 viral particles of AAV2–retro encoding full–length human tau with the P301L mutation (AAV-P301L) under the control of the Syn1 gene promoter (Kindly provided by Dr. José Luís Lanciego, Universidad de Navarra). The incorporation of either P301S (-/-) or P301S (+/-) from insoluble sarkosyl fraction took place at DIV 5, and it was not refreshed in subsequent medium changes. Four conditions were thus considered:

- Untreated: standard culture preparation.
- P301L condition: cells infected with AAV-P301L inducing P301L mutation.
- P301S (-/-) control condition: cells were infected with the adeno-virus at DIV 1. At DIV 5, P301S (-/-) insoluble sarkosyl fraction was included.
- P301S (+/-) pathological condition: cells were infected with the adeno-virus at DIV 1. At DIV 5 pTau were included, i.e. P301S (+/-) insoluble sarkosyl fraction.

Treatment was applied with a concentration of 10 μg/mL to compare them with those prepared in exploration (ii). A total of 37 cultures (containing each two 4 mm cavities) from 4 different dissections were prepared in order to have a good reproducibility and statistics. From them: 9 were standard cultures, 7 were the P301L condition, 7 were controls and 14 were pathological cultures.

Bicuculline assay

Bicuculline, a $GABA_A$ receptor antagonist in inhibitory neurons, was applied to cultured neurons to investigate whether inhibitory action was altered upon pTau treatment. For these tests, activity was recorded for 10 min for cultures at DIV 12. Neuronal cultures were subsequently loaded with 40 μM bicuculline and incubated for 5 min for the drug to take effect. The activity was then recorded for additional 10 min. Following the recordings, the medium was refreshed to remove any traces of bicuculline from the cells. This experimental procedure was repeated three times for each condition using cultures from different dissections.

4.4 Results

4.4.1 IN–M4 neurotoxicity tests

To achieve our primary objective of evaluating the neurotoxicity of the anti–tau aggregation inhibitor IN–M4, we established primary neuronal cultures derived from cortical tissue of CD1 mouse embryos. Within this study, three distinct experimental scenarios were set up. As previously detailed, at DIV 5, the cultured neurons were subjected to one of the following treatments (Figure 4.5): untreated condition, control condition with 50μL DMSO, and treatment with 50μL IN–M4. We recorded spontaneous neuronal activity in these cultures from DIV 7 to 16. In the following, we describe the obtained results for quantifying changes in neuronal activity or functional organisation.

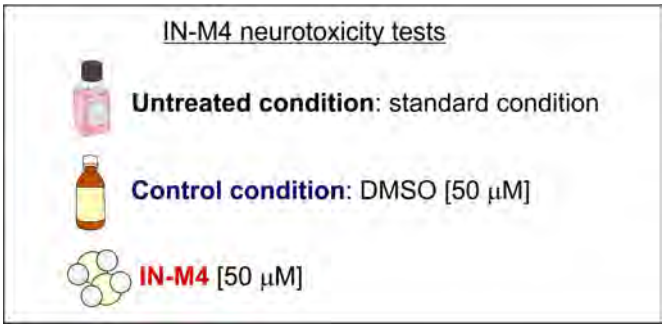

Figure 4.5. Illustrated scheme of conditions for IN–M4 neurotoxicity tests.

Treatment with IN–M4 revealed no dynamical changes in neuronal activity

From the obtained activity data, we extracted several dynamic parameters (see Sec. 3.3.2 of Chapter 3). Specifically, we computed:

- Front velocity: informs about a possible reduction in the propagation of information associated to a decrease in average connectivity.
- Population activity: indicates alterations in whole–network communication and that cause network bursts not to encompass the entire network
- Inter–burst–interval (IBI): indicates alterations in the recruitment process to initiate a burst. 2D cultures show a remarkable periodicity in spontaneous activity that may be altered due to treatment

We note that the velocity is calculated within each burst. Since an experiment may easily contain $10-30$ network bursts, all the measured velocities for a given condition were pooled together in order to calculate the mean values, accompanied by their respective standard errors. The outcome of these analysis is presented in Figure 4.6.

Figure 4.6a shows the progression of front velocity along DIV, showing that the tendency is very similar among conditions. For a more detailed examination, Figure 4.6b displays the distribution of front velocity values for every collective event detected for the untreated ('U', black), control ('C', blue), and inhibitor ('I', red) conditions at DIV 12. The horizontal lines represent the mean, while the colour–coded boxes denote the standard deviation of computed velocity values. As the results show, the conditions exhibited a very similar distribution of data points. However, the computed p–values evinced significant changes for the cultures treated with IN–M4 at DIV 12 ($p_{U-I} = 2.45 \times 10^{-4}$ and $p_{C-I} = 2.15 \times 10^{-4}$), whereas untreated and control were not significantly different ($p_{U-C} = 0.73$). The results indicate that the inhibitor indeed exerts an effect on the propagation velocity of information within the culture.

We must note that the analysis of the results is not straightforward. Indeed, instead of conducting a statistical study pooling together all observations (Figure 4.6b), we

could consider the statistics in which we average the results first within each repetition (Figure 4.6c). In such case, each data point represents the average speed of all collective events within a single culture. Then, when we compare the conditions, the results yield a distinct outcome, in which no significant differences are observed among the various scenarios ($p_{U-I} = 0.50$, $p_{C-I} = 0.61$, $p_{U-C} = 0.84$), thus reaching the conclusion that the presence of IN–M4 does not exert a discernible impact in the development of the neuronal culture.

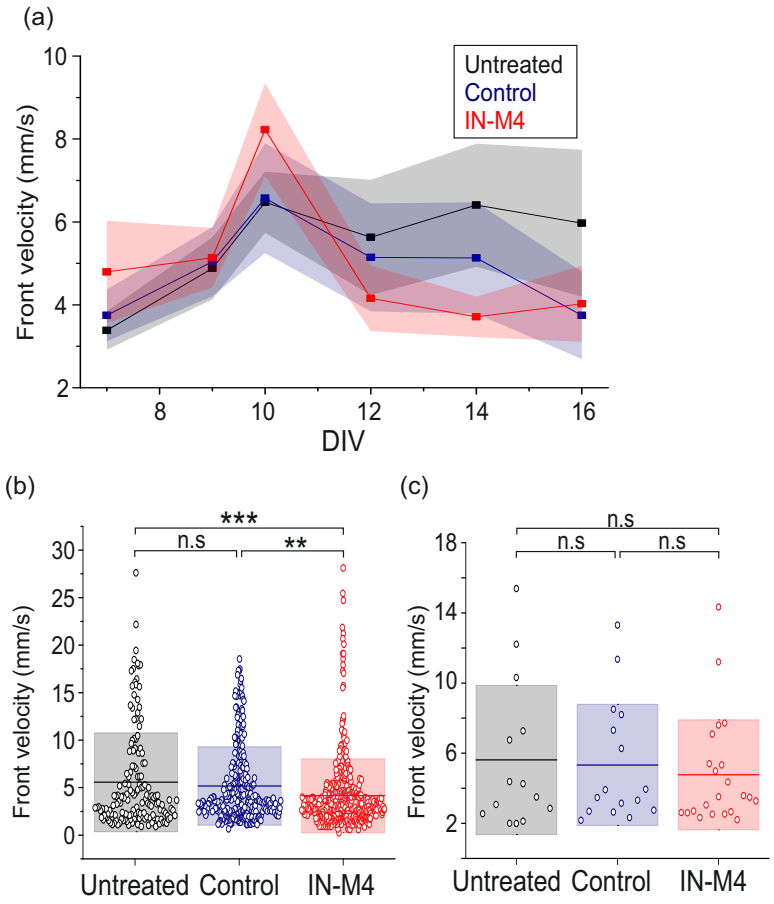

Figure 4.6. Neurotoxicity test of IN–M4: Velocity analysis. **(a)** Evolution of the propagation velocity with DIV, error bars are the standard error. **(b)** Distribution of values for the velocity of the front at DIV 12. Colour boxes represent the standard deviation and the horizontal line is the mean. In this plot every dot is the velocity of one collective event, N= 14 cultures for untreated condition, N= 16 for control and N= 22 for IN–M4 condition. Data was recollected from three different dissections. Significant differences were evidenced for the IN–M4. **(c)** Distribution of values for the velocity of the front at DIV 12, colour boxes represent the standard deviation and the horizontal line is the mean. In this plot every dot is the mean velocity value of all the collective events detected for one culture. * $p <$ 0.05, ** $p < 0.01$, *** $p < 0.001$ (Student's t-test).

With the data at hand, and given the lack of a clear trend in Figure 4.6a, we conclude that IN-M4 had no demonstrable impact in the behaviour of the cultures. The differences in Figure 4.6b could come from statistical artificats grounded on the different number of bursts in each culture, even in those from similar condition.

The examination of population activity (Figure 4.7) provided insights into the synchronised neuronal behaviour within a network, quantified on a scale ranging from 0 (no collective activity) to 1 (nearly every neuron in the network participates in collective events). In Figure 4.7a (left), we observe the temporal evolution of mean population activity along DIV, revealing a similar behaviour across all three conditions. Notably, each condition exhibits a peak at DIV 10, indicating an enhanced level of network synchrony for reasons that are not fully understood that may be related to the cultures reaching a fully mature and well connected system. At DIV 12, discernible differences in the distribution of population activity values seem to appear. This is depicted in Figure 4.7a (center), with population activity distributions providing $p_{U-I} = 3.55 \times 10^{-6}$, $p_{C-I} = 3.57 \times 10^{-6}$, and $p_{U-C} = 0.42$.

In Figure 4.7a (right), we explored the possibility to average results within cultures, computing the mean value of population activity per repetition. In this new scenario, where every culture's potential variability is considered, no significant differences between conditions were found when comparing the p–value ($p_{U-I} = 0.36$, $p_{C-I} = 0.12$, $p_{U-C} = 0.70$).

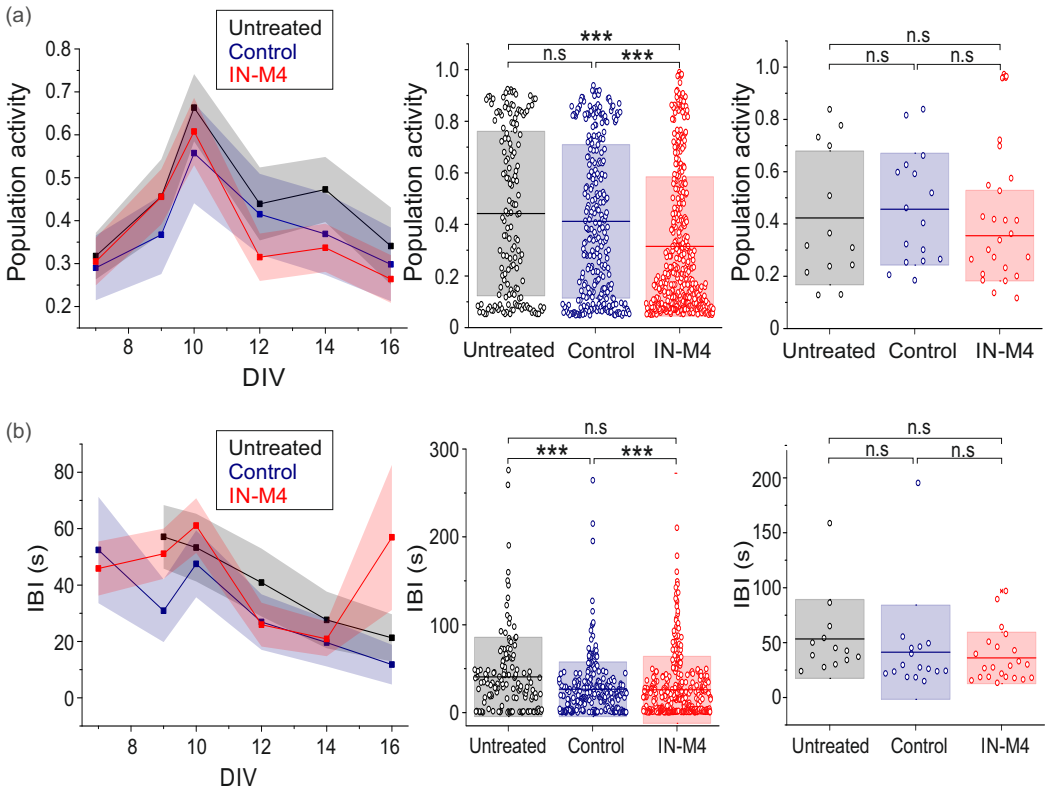

Figure 4.7. Neurotoxicity test of IN–M4: Collective activity analysis. At the left the evolution with DIV of the dynamical parameters is represented, error bars are the standard error. At the center the distribution of values for the different parameters at DIV 12 in which every dot is one spike. At the right, distribution of the mean value per culture. For both cases, colour boxes represent the standard deviation and the horizontal line is the mean. **(a)** Population activity of untreated, control (samples treated with DMSO) and tau–inhibitor IN–M4. **(b)** IBI (s). For this plot $N = 14$ for untreated, $N = 16$ for control and $N = 22$ for IN–M4 condition * $p < 0.05$, ** $p < 0.01$, *** $p < 0.001$ (Student's t-test).

Finally, the IBI characterised the time duration between bursts within the recorded timeframe, measured in seconds. It operates inversely to the frequency of collective events occurring in the neuronal network within a given unit of time. In line with our previous findings, no substantial distinctions emerged among the different experimental scenarios, as shown in Figure 4.7b (left). It is noteworthy that at DIV 16, the inhibitor–treated cultures exhibited an elevated IBI, suggesting a reduction in activity. However, it is important to note that the standard error associated with this measurement overlaps with the other scenarios, rendering this change non–significant.

Figure 4.7b (center), represents the distribution of the population of IBI values at DIV 12 for each pair of network bursts in all cultures. Again, some relevant changes were observed ($p_{C-I} = 2.15 \times 10^{-4}$, $p_{u-C} = 2.14 \times 10^{-4}$, and $p_{u-I} = 0.734$). However, taking into account the IBI mean value of each of the culture for the different conditions, shown in Figure 4.7b (right), no significant changes could be revealed ($p_{u-I} = 0.09$, $p_{C-I} = 0.63$, $p_{u-C} = 0.43$).

No changes in functional organisation were found after treatment with IN–M4

To complete the results, we used GTE to compute the effective connectivity and functional organisation of the investigated cultures, as detailed in Section 3.3.3 of Chapter 3. We then used quantifiers from complex networks to extract key measures that represent the overall behaviour of the cultures. The outcomes of our functional analysis for the three experimental conditions (untreated, control, and IN-M4 tau inhibitor-treated) are presented in Figure 4.8.

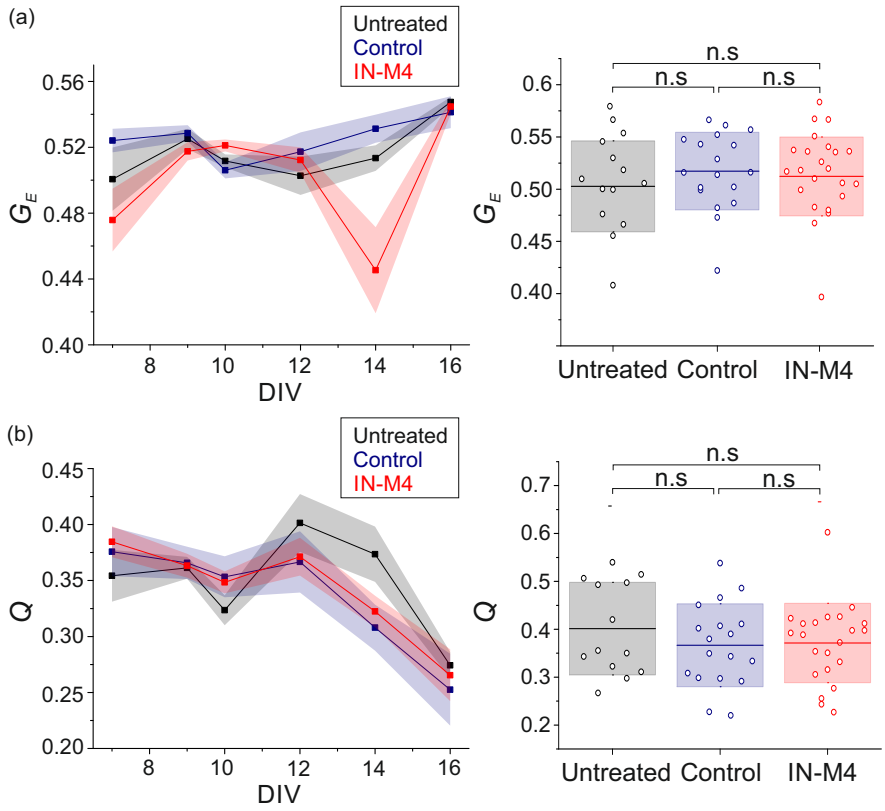

Figure 4.8. Neurotoxicity test of IN–M4: Functional analysis. On the left, evolution along DIV of the functional parameters; error bars are the standard error. On the right, distribution of values for the different parameters at DIV 12; colour boxes represent the standard deviation and the horizontal lines are the mean. **(a)** Global efficiency of untreated, control (samples treated with DMSO) and tau–inhibitor IN–M4. **(b)** Modularity. In all presented data, $N = 14$ for untreated, $N = 16$ for control and $N = 22$ for IN–M4 condition * $p < 0.05$, ** $p < 0.01$, *** $p < 0.001$ (Student's t-test).

The left panels of Figures 4.8a and b summarize the mean values of the global efficiency G_E and modularity Q (with their corresponding standard errors) along DIV. Notably, while the evolution of G_E exhibits variations in the case of IN–M4 treatment, no statistically significant differences were discernible among the three conditions with $p_{U-I} = 0.50$, $p_{C-I} = 0.67$, $p_{U-C} = 0.32$ for G_E and $p_{U-I} = 0.35$, $p_{C-I} = 0.86$,

$p_{U-C} = 0.30$ for Q. This suggests that there is no substantial alteration in the effective connectivity of the neuronal network, irrespective of the presence or absence of treatment. This observation is further corroborated by the distribution of G_E and Q values at DIV 12, as depicted in the right panels of Figures 4.8a and b, where no clear differences appear among the conditions.

We must note that, in the course of the analysis for the functional behaviour, each culture yields a single value for G_E and Q per culture, and therefore there are no possible artifacts associated with a large number of values per culture, as in the dynamic analysis. Consequently, we conclude that there are no statistically significant differences in the functional behaviour between the untreated, control, and IN–M4–treated cultures.

4.4.2 Modeling tauopathies by using tau extracted from the Tau Biosensor cell line

The prion–like hypothesis posits that extracellular seed–competent tau progresses from one affected neuron to a neighbouring healthy one during cell–to–cell transmission. Extracellular tau species have garnered attention as a subject of study following the observation of these *pathological* forms of tau in the cerebrospinal fluid (Kurz et al., 1998).

In an attempt to replicate the prion–like hypothesis and thereby establish a model of tauopathy *in vitro*, we introduced pTau into the extracellular medium of cultured neurons. The aim was to induce anomalies in the cultured cells and quantify degradation in a controlled manner. The samples used were extracted from the Tau Biosensor cell line, as described in Chapter 3, and named TIF-P- (*wild–type* tau) and TIF-P+ (*pathological* tau). As a control, we included the vehicle used for extracting tau from the Biosensor Cells, which, in this particular case, was lipofectamine, at the same concentration as the tau samples (see Figure 4.9).

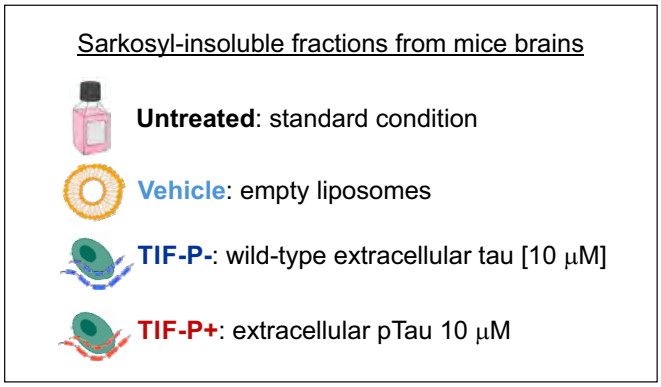

Figure 4.9. Illustrative scheme of conditions for modeling tauopathies by using tau extracted from the Tau Biosensor cell line.

The different conditions were introduced at DIV 5 with the first change of culture medium. Spontaneous activity was recorded from DIV 7 to DIV 16 every two–days, and data analysis was performed as detailed in Chapter 3. The subsequent sections describe the results of the dynamic and functional analysis of the recorded activity data.

Spontaneous activity was assessed to detect changes in the activity patterns exhibited by neurons in culture. Neuronal activity was extracted and presented in the form of raster plots. Figure 4.10 provides a representative raster plot for cultures at DIV 12, accompanied by a population activity diagrams (on top of the rasters) illustrating the fraction of the network that participated in each event of network bursting. As the plots reveal, the four conditions exhibited similar activity, except for a slight decrease in the population activity for the culture treated with TIF-P+, where it appears that fewer neurons participated in collective events. To deepen in this analysis, we computed the mean value of some dynamical parameters, namely the velocity of the propagation front, the population activity and the IBI.

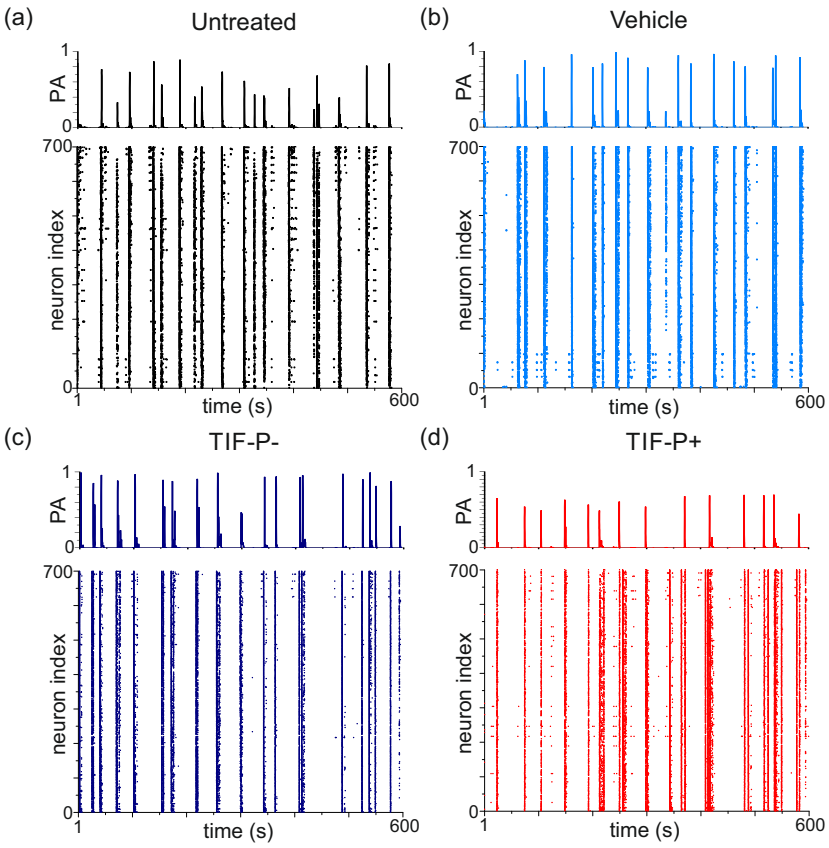

Figure 4.10. Representative raster plots and population activity diagram at DIV 12 for **(a)** untreated culture, **(b)** Vechicle condition, **(c)** TIF-P- (wild–type cell–derived tau) and **(d)** TIF-P+ (pathological cell–derived tau).

Figure 4.11a illustrates the evolution of the front's velocity for untreated ('U', black), vehicle ('V', light blue), TIF-P- ('P-', dark blue), and TIF-P+ ('P+', red) scenarios. It becomes evident that the differences between the trends of the four conditions are more pronounced with DIV. Specifically, at DIV 16, the untreated culture exhibits a significantly lower propagation speed. To confirm the significance of this difference, we plotted the distribution of velocity values at DIV 16 on Figure 4.11b. Indeed, the differences with the TIF-P+ sample are significant when compared to the other conditions ($p_{U-P+} = 1.01 \times 10^{-5}$, $p_{V-P+} = 0.0187$, $p_{P--P+} = 8.89 \times 10^{-8}$).

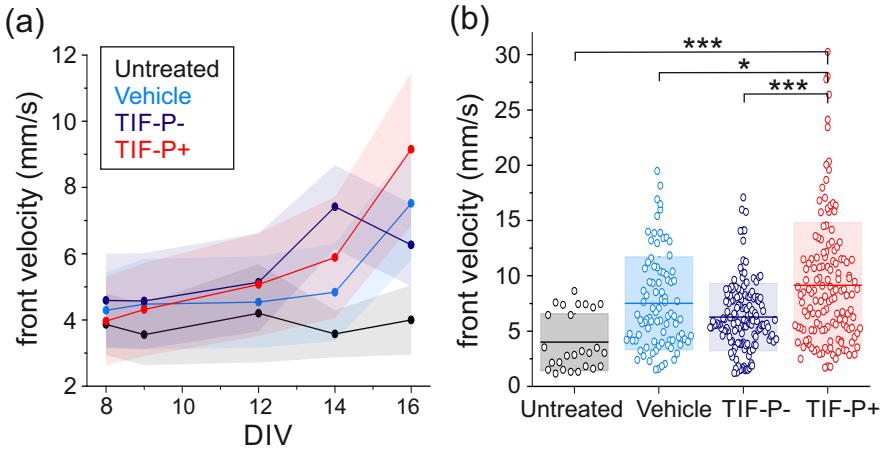

Figure 4.11. Cell derived tau treatment: evolution of front velocity. **(a)** Evolution of the velocity of the propagation front with DIV together with the standard error for untreated, vehicle, TIF-P- and TIF-P+. **(b)** Distribution of the front velocity values pooling together all data at DIV 16. The horizontal liness are the mean value and the colour boxes the standard deviation of the measurements. Each condition has a total $N = 6$ (except untreated condition at DIV 16 for which $N = 4$) for these plots * $p < 0.05$, ** $p < 0.01$, *** $p < 0.001$ (Student's t-test).

It is important to note that the differences between the other conditions compared with the untreated culture were also significant, with values of $p_{U-V} = 9.18 \times 10^{-5}$ and $p_{U-P-} = 4.63 \times 10^{-4}$. Additionally, at DIV 16, there was a substantial difference in the number of collective events (dots in the plot), with all treated cultures procuring much more bursting events than the untreated case.

We recognized the crucial importance of the chosen data treatment method in this analysis. As illustrated in Figure 4.12, results varied depending on whether we pooled together every velocity value, irrespective of its culture of origin (Figure 4.12a) or we considered that every culture could present its own variability and consider only the mean velocity values per culture (Figure 4.12b). For the latter analysis methodology, significant changes were only observable between the pathological treated cultures and the untreated ones ($p_{U-P+} = 0.04$, $p_{V-P+} = 0.21$ and $p_{P--P+} = 0.16$).

This significant difference between untreated and pathological cultures (though weak since the p–value is only 0.04) would suggest that the pathological cultures exhibit an abnormal progatation of information. Since, according to theoretical models (Golomb and Ermentrout, 1999; Bressloff, 2000; Feinerman, Segal, and Moses, 2005), the velocity of propagation is related to the average number of connections per neurons and synaptic strength, the results would suggest that pathological culture evolve forming more connections than expected, which is puzzling since we expected a degradation of connectivity and not an strengthening.

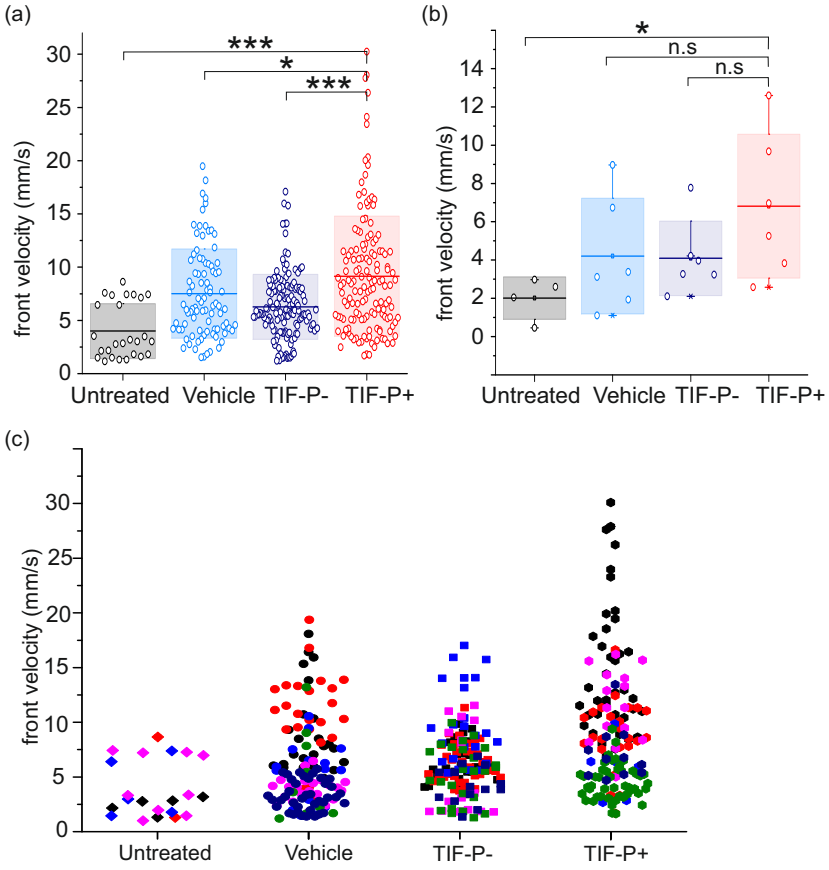

Figure 4.12. Statistical analysis comparison in propagation velocity. **(a)** Distribution of the front velocity values considering every event at DIV 16; the horizontal lines are the mean value and the colour boxes the standard deviation of the measurements. Each condition have a total $N = 6$ (except untreated condition at DIV 16 for which $N = 4$). For these plots, * $p < 0.05$, ** $p < 0.01$, *** $p < 0.001$ (Student's t-test).

The discussion about whether values from the same cultures should be treated independently calls for an exploration of the variability between cultures. In Figure 4.12c, the distribution of front velocity values is presented again, but now they are colour–coded according to the culture they derive from. Notably, clusters of dots with the

same colour tend to gather around similar velocity values, indicating that similar velocities are observed within a culture. However, there are important differences across cultures, since measured velocities in other cultures gather around other values. This variability becomes crucial when conducting significance tests between conditions. In Figure 4.12b, the p–value test was computed taken into account the mean value of each culture. Therefore, moving forward, only this latter analysis, which emphasises the variability *between cultures*, will be presented in future analyses.

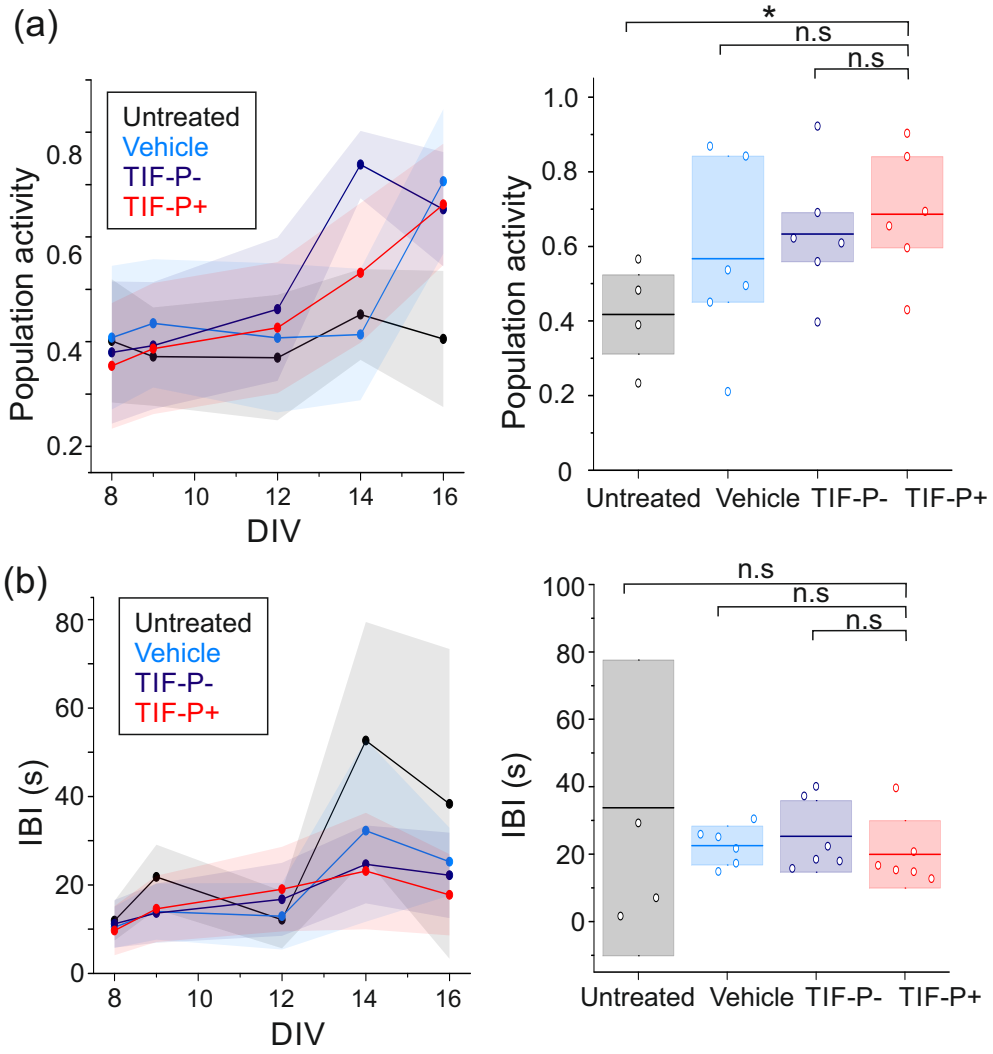

Figure 4.13. Cell derived tau treatment: Dynamical analysis. On the left, evolution of dynamical parameters with DIV together with their standard error for untreated, vehicle, TIF-P- and TIF-P+. On the right, distribution of values at DIV 12. The horizontal lines are the mean value and the colour boxes the standard deviation of the measurements. **(a)** Population activity and **(b)** IBI (s). Each condition has a total of $N = 6$ (except untreated condition at DIV 16 for which $N = 4$). * $p < 0.05$, ** $p < 0.01$, *** $p < 0.001$ (Student's t-test).

When comparing the evolution of population activity with DIV, notable differences emerged between the untreated condition and the treated ones (Figure 4.13a, left panels). Similar to the velocity analysis, we plotted the distribution of mean population activity values at DIV 16 and compared them (Figure 4.13a, right panels). In this case, TIF-P+ only exhibited significant changes when compared to the untreated culture, with $p_{U-P+} = 0.03$, $p_{V-P+} = 0.36$ and $p_{V-P+} = 0.60$.

Likewise, we observed a similar effect when examining the IBI evolution along DIV for the four conditions (Figure 4.13b, left panels), with untreated cultures displaying a higher IBI than the treated ones. Figure 4.13b (right) displays the dispersion of mean values at DIV 16 for the four conditions with $p_{U-P+} = 0.47$, $p_{V-P+} = 0.59$ and $p_{V-P+} = 0.39$ showing non significant changes between conditions.

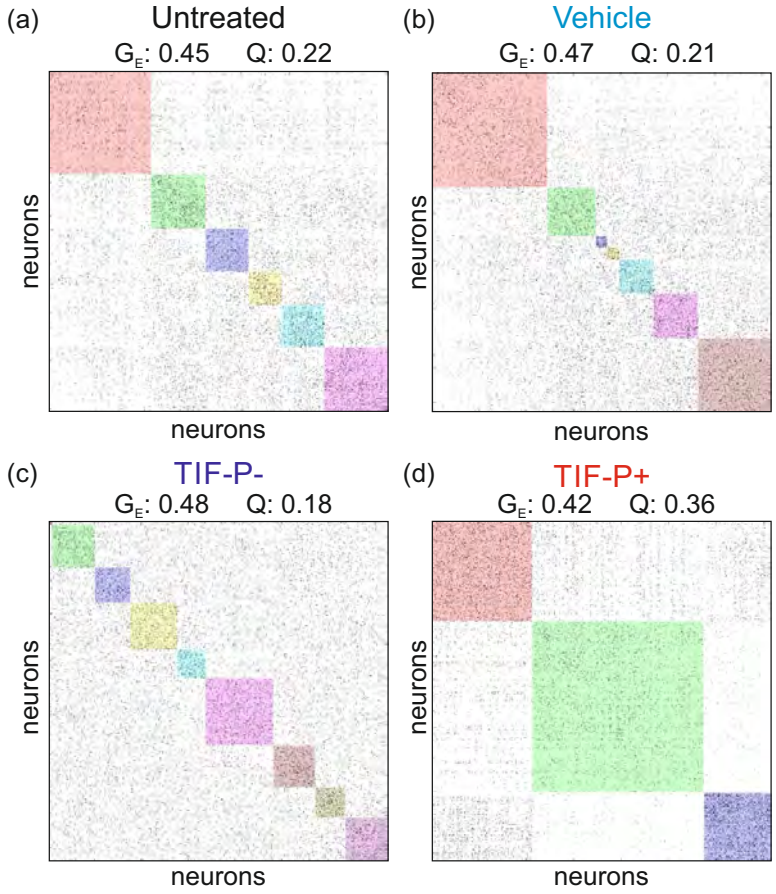

Figure 4.14. Connectivity analysis of cell derived tau treatment. The panels show representative connectivity matrices at DIV 16 together with their G_E and Q values for **(a)** untreated culture, **(b)** Vechicle condition, **(c)** TIF-P- (wild–type cell–derived tau) and **(d)** TIF-P+ (pathological cell–derived tau). Colour boxes indicate functional communities.

Presence of extracellular TIF-P+ tau did not alter functional connectivity *in vitro*

We extracted functional features from the activity data by applying GTE computations and complex networks analyses, as described in Chapter 3.

Figure 4.14 displays representative connectivity matrices obtained from each of the four scenarios at DIV 16. Connectivity matrices are computed as directed binarized networks, with each black representing an effective connection between neuronal pairs. Neuronal indexes are ordered to highlight neuronal communities along the diagonal of the matrix, and coloured for ease identification. Key magnitudes, namely Global Efficiency (G_E) and Modularity (Q) were computed from these matrices.

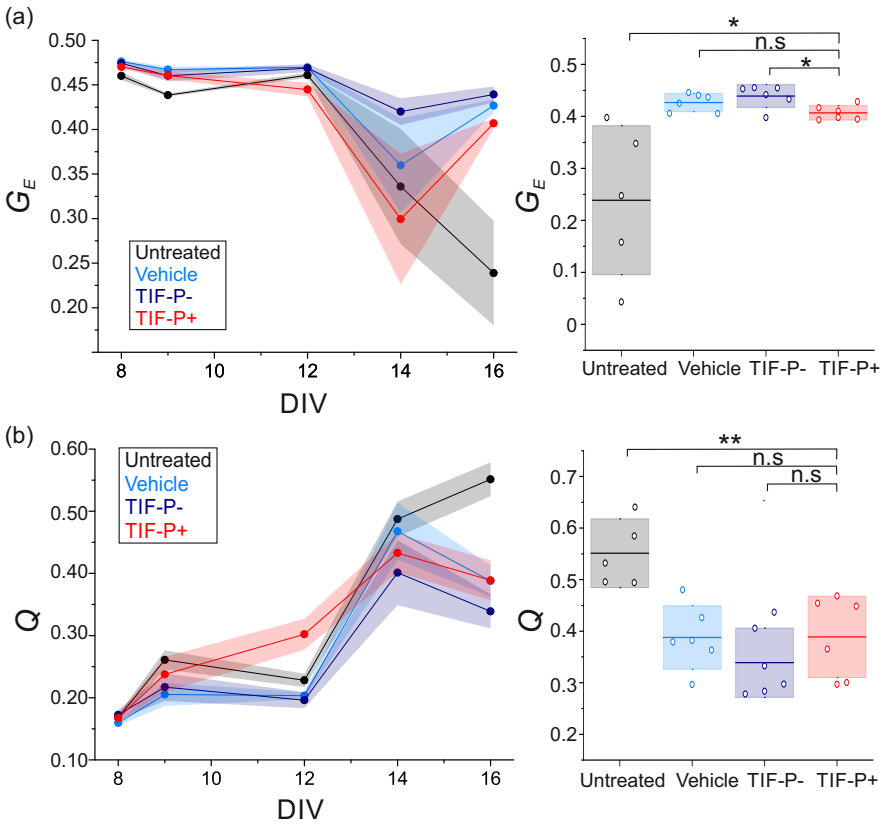

Figure 4.15. Cell derived tau treatment: Functional analysis. On the left, evolution of functional parameters with DIV for cultures treated with cell–derived tau. Shadings indicate standard error. Right, distribution of values at DIV 16. The colour boxes represents the standard deviation. **(a)** Evolution of G_E. **(b)** Evolution of Q. Each condition have a total of $N = 6$ (except untreated condition at DIV 16 for which $N = 4$). For these plots, * $p < 0.05$, ** $p < 0.01$, *** $p < 0.001$ (Student's t-test).

By visually inspecting the matrices of Figure 4.14, it is clear that all conditions except TIF-P+ (pathological tau) show a similar structure, with relatively small communities. However, the TIF-P+ network shows very large communities, indicating that neurons tend to communicate with one another more strongly than normal. Somehow,

the TIF-P+ network behaves as overexcited, for instance because there is a stronger excitatory drive or inhibition is absent.

To complete these results, we plotted the values of G_E and Q per culture and condition as a function of DIV along with its corresponding standard error. Results are shown in Figures 4.15a and b (left panels). Clear differences seems to appear at DIV 16, when the untreated–condition stands out from the others. In order to see if such a difference is significant, we plotted the distribution of values for G_E and Q at DIV 16 and calculated the p–value. Results are shown in Figures 4.15a and b (right). We found slightly significant changes between the pathological condition and the untreated one with $p_{U-P+} = 0.0179$ and $p_{U-P+} = 0.0054$ for G_E and Q respectively.

Remarkably, untreated cultures demonstrated significant differences when compared to the vehicle condition and to TIF-P-, with $p_{U-V} = 0.0105$ and $p_{U-P-} = 0.0077$ for G_E and $p_{U-V} = 0.0022$ and $p_{U-P-} = 5.37 \times 10^{-4}$ for Q. The differences between treated conditions (vehicle, TIF-P-, TIF-P+) and the untreated one suggest that the untreated cultures had some problem at this DIV for reasons we can not explain. Indeed, at DIV 16, we needed to discard two out of the six wells under study. Overall, despite our efforts, we conclude that the presence of pathological tau did not induce clear alterations in the functional organisation of neuronal cultures.

4.4.3 Modeling tauopathies by using sarkosyl fraction from P301S mice's brains

At this juncture, we were confounded to discover that there were no discernible dynamic or functional differences between the various conditions (untreated, vehicle, TIF-P-, and TIF-P+). This led us to contemplate whether extracellular tau, despite forming pathological species, might not possess the capacity to induce abnormalities in our cultures. Consequently, we made the decision to introduce the insoluble sarkosyl extract from homogenized P301S(+/-) mouse brains directly into the cultures, utilizing its P301S(-/-) counterpart as a control. Within these fractions, we included not only pTau but also other potential protein conformations, in addition to other insoluble substances that could potentially influence the propagation of pathology.

To do that, single–neurons were obtained by mechanical dissociation of cortical tissue from mice embryos, and placed in discrete 4 mm wells confined by a PDMS pattern. Spontaneous neuronal activity was recorded through calcium imaging in order to chart the evolution of dynamical patterns when cells were exposed to the treatment. As a reminder (see Figure 4.16), three different scenarios were considered: untreated condition, P301S (-/-) condition (extracellular wild–type protein tau) and P301S (+/-) condition (extracellular pathological protein tau).

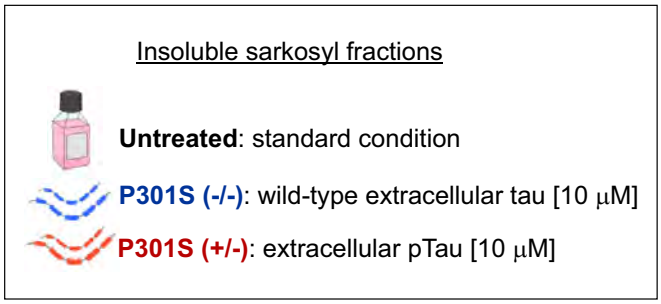

Figure 4.16. Illustrative scheme of conditions for modeling tauopathies by using sarkosyl–insoluble fraction from P301S mice brains.

The addition of P301S (+/-) sarkosyl-insoluble fraction did not significantly impact neuronal networks dynamics

Neuronal spontaneous activity was recorded every two days from DIV 7 to DIV 16. Calcium fluorescence recordings were analyzed and spike information were plotted in the form of raster plots. For the purpose of simplicity, in Figure 4.17 we showed a characteristic raster plot from one of the analyzed cultures at DIV 12 together with the population activity. This time point corresponded to one week after exposing the culture to the selected scenario. Results show that cells exposed to pathological pTau (Figure 4.17, right) exhibited a higher number of collective events that involved nearly the whole network, substantially different from the other conditions (Figure 4.17, left and centre). This increased synchronous activity in the P301S (+/-) condition suggested a hyperexcited state of neuronal activity at DIV 12.

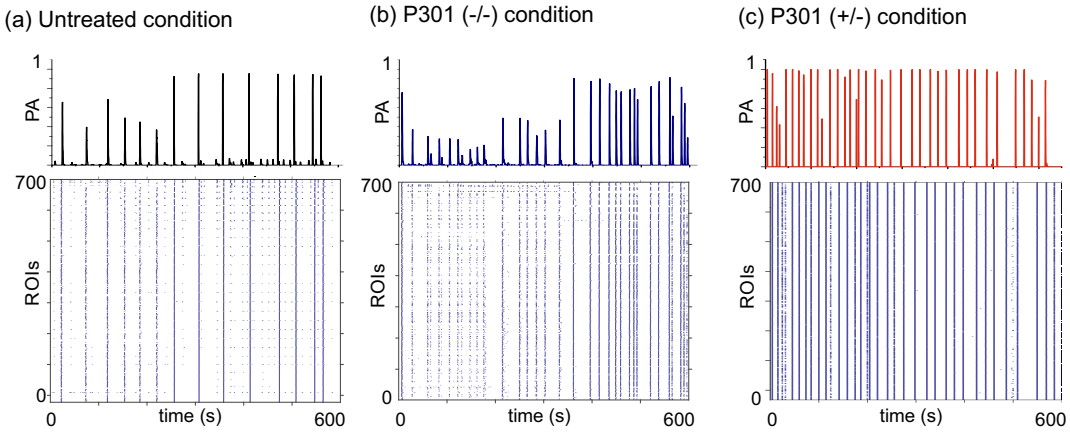

Figure 4.17. Sarkosyl tau treatment: representative raster plots and population activity for cultures at DIV 12, comparing **(a)** the untreated condition, **(b)** the wild–type P301S (-/-) condition, and **(c)** the pathological P301S (+/-) one.

To have a better picture of how this atypical state related to the global neuronal activity of the network, some dynamical parameters were extracted from the activity data. Front velocity, population activity and IBI were computed for each burst and combined to plot the mean value, together with its standard error. The evolution with time of the velocity of fronts is plotted in Figure 4.18a. Differences between scenarios were revealed at different time–points as extracellular tau (either wild–type or pTau) was affecting neurons in culture.

Figure 4.18b shows two propagating fronts for an untreated (top) and a pTau–treated culture (bottom) at DIV 12. It can be observed that the propagation pattern (represented by a black or white arrow) is similar i.e., a spiral–like front that propagates from the initial point (blue cross) to the edge of the culture. The untreated front exhibited a higher propagation velocity for this example. Figure 4.18c represents the distribution of mean velocities at DIV 12 for the three different conditions, with the statistical analysis evidencing that no significant differences were observed between the three conditions at this point of the development, with $p_{U-P-} = 0.46$, $p_{U-P+} = 0.45$ and $p_{P--P+} = 0.90$.

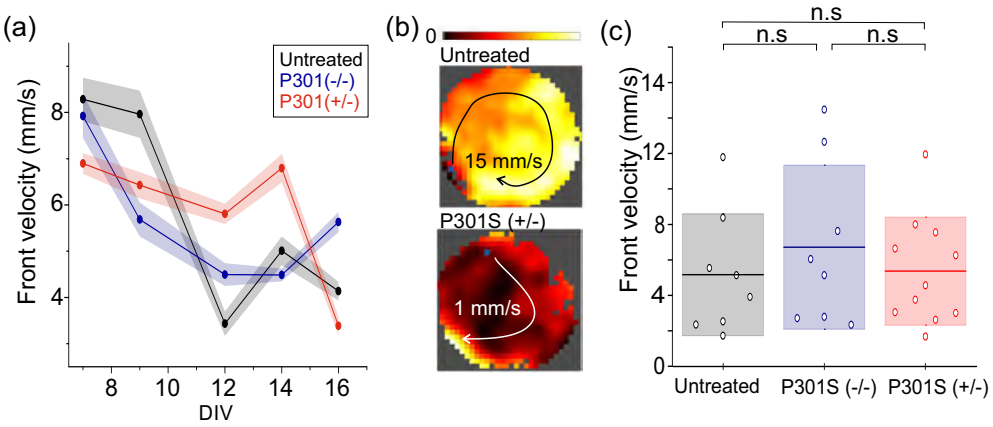

Figure 4.18. Propagation velocity comparison of cultures treated with insoluble sarkosyl fraction for either P301S (-/-) or P301S (+/-) mice brains. **(a)** Evolution of the mean front velocity with DIV together with the standard error. **(b)** Examples of spatiotemporal fronts of activity propagation for an untreated neuronal culture (top) and a culture treated with pTau (bottom). **(c)** Distribution of mean velocity values at DIV 12 for the three different scenarios. The horizontal lines represent the mean value and the colour boxes the standard deviation of the data. For this plot, N= 8 for untreated and P301S (-/-) and N= 14 for 'pathological´condition * $p < 0.05$, ** $p < 0.01$, *** $p < 0.001$ (Student's t-test).

Figure 4.19a (left) represents the evolution of the population activity with DIV. Interestingly, the presence of wild–type tau in the cultures considerably increased the population activity value at DIV 16, indicating enhanced synchrony of the neuronal culture. However, to compare the same developmental stage, we plotted the

distribution of population activity values at DIV 12 and computed the p–value (Figure 4.19a, right). At this time–point, statistically significant differences were not observed between conditions, either wild–type or seed–competent tau with $p_{U-P+} = 0.83$, $p_{P--P+} = 0.10$ and $p_{U-P-} = 0.21$.

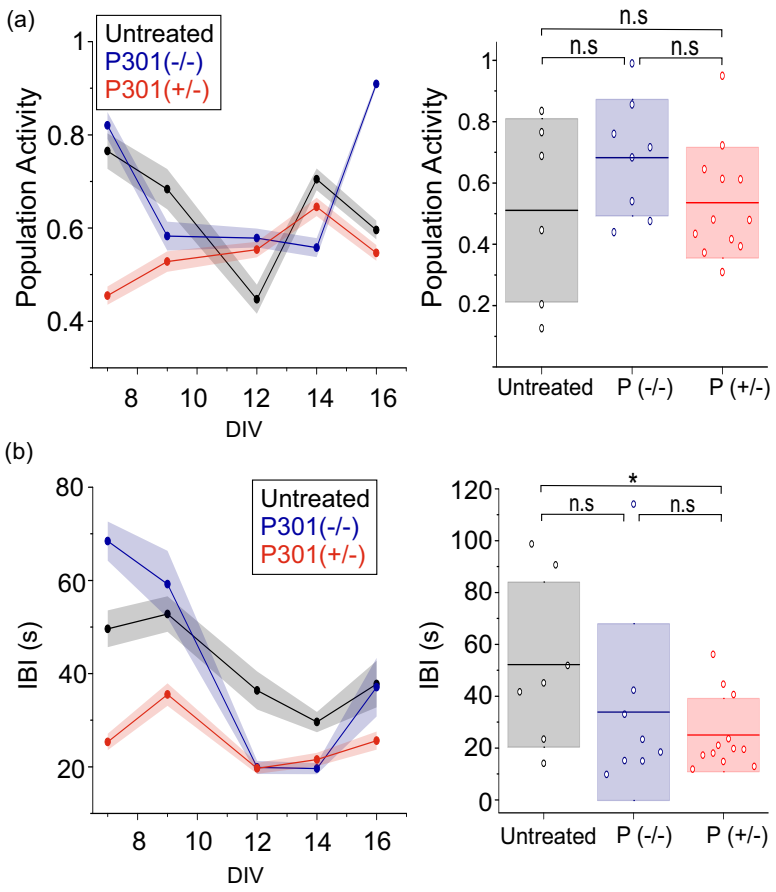

Figure 4.19. Population activity and IBI comparison for cultures treated with insoluble sarkosyl fraction, for either P301S (-/-) (P (-/-)) or P301S (+/-) (P (+/-)) mice brains. **(a)** Evolution of the mean population activity along DIV together with the standard error (left), and distribution of population activity values at DIV 12 for the three different scenarios (right). The horizontal lines represent the mean value and the colour boxes the standard deviation of the data. **(b)** Evolution of IBI with time together with the standard error (left) and box plot representing the distribution of IBI values at DIV 12. The horizontal lines represent the mean value and the colour boxes the standard deviation of the data. For these plots $N = 8$ for untreated and P301S (-/-), and $N = 14$ for 'pathological´condition. * $p < 0.05$, ** $p < 0.01$, *** $p < 0.001$ (Student's t-test).

Analysis of the IBI at different time–points exposed differences between untreated cultures and those seeded with pTau (Figure 4.19b, left). The fact that P301S (+/-) exhibited lower values of IBI is related to the hyperexcited state of neuronal activity previously noticed. The condition P301S (-/-) exhibited an aberrant behaviour, differing from the trend observed for the other two conditions. We hypothesize that these

changes in IBI might be caused by some anomalous behaviour in neuronal activity as a defense against the presence of an abnormal amount of extracellular tau in culture. Figure 4.19b (right) displays the distribution of IBI values at DIV 12 evidencing significant changes (though weak) between treated and untreated cultures with $p_{U-P+} = 0.02$. No changes between P301S (-/-) and P301S (+/-) were observed, with $p_{P--P+} = 0.43$ and $p_{U-P-} = 0.30$.

While significant changes were identified at specific developmental stages, a clear evolution of dynamical parameters with DIV was not apparent. Establishing whether these changes are attributable to the presence of tau or other, uncontrollable factors is exceptionally challenging without complementing these results with experiments at the physiological level, specifically focusing on synapses. Such experiments can provide insights into whether the connectivity is indeed being influenced by the presence of extracellular tau. Thus, given the weakness in the statistical significance of the data, we concluded that no overt alterations could be observed between pTau–treated cultures and other conditions.

Presence of extracellular pathological tau did not alter functional connectivity *in vitro*

The aim of this study was to determine how the presence of seeding–active tau affected healthy neurons in culture and their functional organisation *in vitro*. For that purpose, as discussed in Chapter 3, we applied tools from complex system to extract information from the spontaneous activity recordings of the neurons in culture. The results obtained for the functional analysis of the three conditions (untreated and treated with either P301S (-/-) or P301S (+/-) sarkosyl insoluble fractions) are depicted in Figure 4.20. For simplicity, only one characteristic connectivity matrix from one analyzed culture at DIV 12 is presented for each condition.

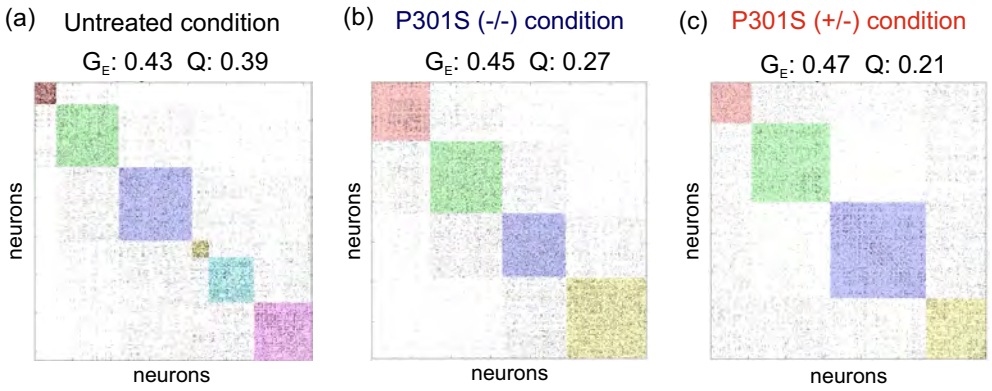

Figure 4.20. Connectivity matrices at DIV 12 for cultures treated with P301S sarkosyl insoluble fraction together with the G_E and Q values extracted from each matrix. **(a)** Untreated culture, **(b)** Culture treated with P301 (-/-) (wild–type tau), and **(c)** P301 (+/-) (pathological tau).

Figure 4.20a shows an example of the connectivity matrix for an untreated culture, with a global efficiency of G_E0.40 and a modularity of $Q \simeq 0.40$. These values indicate that the untreated culture built a globally well–connected network that included 6 characteristic communities that signaled local communication. Treated conditions, both P301S (-/-) and P301S (+/-) (Figures 4.20b and c), exhibited a similar global connectivity ($G_E \simeq 0.46$ on average) and a markedly much lower modularity ($Q \simeq 0.25$ on average), with only 4 communities and relatively big as compared to the untreated case. The low modularity and big communities indicate that the treated cultures tended to be, overall, more integrated.

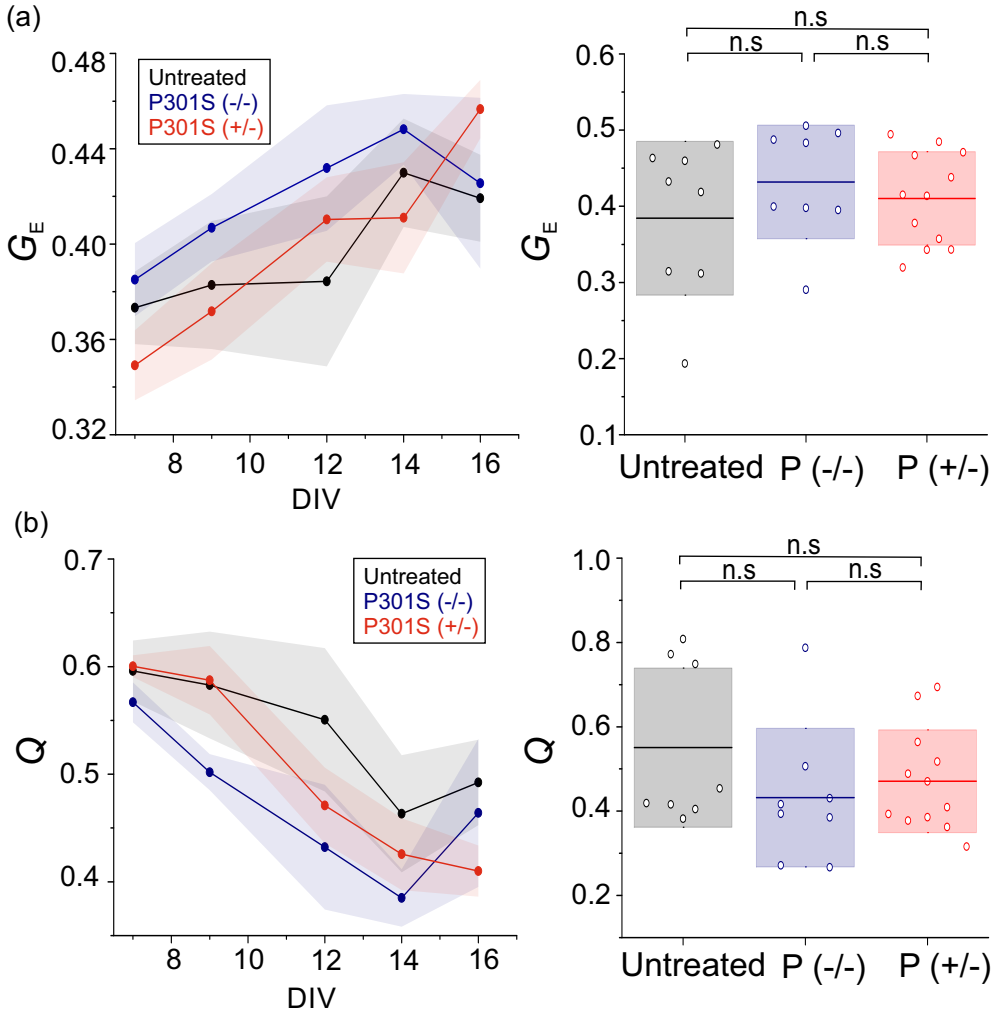

Figure 4.21. Evolution of functional features with DIV together with the standard error and box plot representing the distribution of values at DIV 12, in which the horizontal line represents the mean value and the colour boxes the standard deviation. **(a)** Evolution of G_E. **(b)** Evolution of Q. For this plot N= 8 for untreated and P301S (-/-) and N= 14 for P301S (+/-) condition * $p < 0.05$, ** $p < 0.01$, *** $p < 0.001$ (Student's t-test).

The behaviour of the cultures with all the data at hand was next considered. The mean value of G_E and Q, and their standard errors, were plotted as a function of DIV, as shown in Figures 4.21a and b (left). Overall, no evidence of changes in the functional connectivity of the neuronal networks could be appraised with or without any treatment. Both G_E and Q values had the same trend with DIV and no significant changes were found between any condition when computing the p–values for the data at DIV 12 (Figures 4.21a and b, right). Thus, despite some indices of possible damage in some pathological cultures that translated into a higher excitability (more bursting events and strongly integrated network functionality), no clear evidences for damage could be drawn when all data was taken into account.

4.4.4 Accelerating damage in culture: P301L mutation *in vitro*

We began to speculate whether the lack of observable functional changes could be attributed to the fact that the cultured neurons were young and wild–type, while it is well–documented that aging represents one of the foremost risk factors for sporadic forms of AD and other NDs (Braak and Braak, 1991; Frost, Götz, and Feany, 2015). Thus, the relative youthfulness of the cultured neurons might have contributed to the diminished manifestation of observed effects in our experimental setup.

In an attempt to accelerate damage in culture, we induced the over–expression of the mutant tau isoform P301L to predispose the primary neurons to a more pathological scenario prior treating them with extracellular tau. To this end, we transduced primary cortical cultures with AAV–P301L at DIV 1 and confirmed by biochemical analysis that they over–expressed P301L tau at DIV 6.

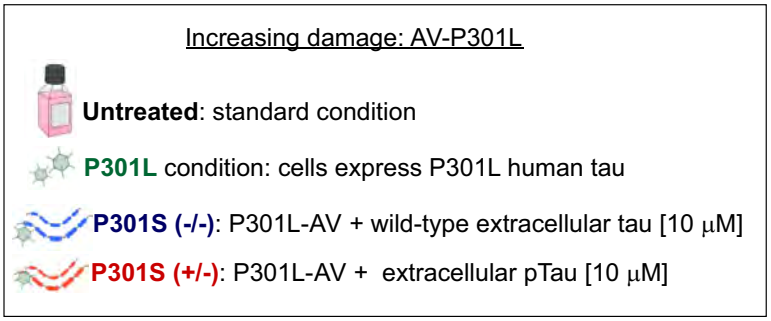

Figure 4.22. Illustrative scheme of conditions for modeling tauopathies by accelerating damage in culture: P301L mutation *in vitro*.

In these novel culture conditions, cells were not only exposed to extracellular pathological tau but they were also capable of generating P301L tau isoforms endogenously. With the aim of characterising potential dynamical and functional alterations in the resulting networks, spontaneous activity was recorded from DIV 7 to 16, and

spike event information was analyzed. Dynamical and functional properties were subsequently extracted from the raster plots. The results are described in the following sections. Figure 4.22 shows an illustrative scheme of the four applied conditions on this novel experimental setup.

Primary cortical cultures expressing P301L human tau show no significant dynamical changes in their spontaneous activity

Dynamical analysis of neuronal networks *in vitro* were performed. For clarity, in Figure 4.23 we displayed characteristic raster plots for analyzed data at DIV 12, which corresponds to 6 days after neurons were proved to express P301L mutation, and for each of the four conditions. By looking at the examples shown for the untreated condition (Figure 4.23a), P301L condition (Figure 4.23b), and for the treated conditions (wild-type tau, Figure 4.23c and pTau, Figure 4.23d) we concluded that the results reproduce what we observed in the previous section, i.e., that those cultures treated with P301S (+/-) insoluble sarkosyl fraction seemed to exhibit, at a first glance, a hyperexcited state of activity.

To obtain an in–depth understanding of the effects observed in cultured neurons exposed to P301L human tau, we conducted an analysis of the usual dynamic parameters derived from the spike data, i.e., the front velocity, the population activity, and IBI for each burst, and subsequently graphed the mean values, along with their corresponding standard errors. This graphical representation in Figure 4.24 effectively illustrates the temporal evolution of these characteristics.

The left panel of Figure 4.24a represents the evolution of the front velocity with DIV. We can observe that the four curves cross one another over time, giving no clear evidence of changes due to possible mechanisms of damage caused either by the expression of P301L tau ('PL') or the addition of extracellular tau (wild–type 'P-' or pTau 'P+'). Additionally, when comparing the distribution of values for the four conditions at DIV 12, as plotted in the right panel of Figure 4.24a, we spotted no significant differences between scenarios, with $p_{U-P+} = 0.07$, $p_{PL-P+} = 0.38$ and $p_{P--P+} = 0.28$.

The population activity (Figure 4.24b, left), presented notable changes in trend after 12 DIVs, when population activity for P301S (+/-) condition remained stable until DIV 16. Surprisingly, the presence of pathological tau together with the infected neurons increased the number of cells that took part in the collective events. Figure 4.24b (right) exhibits a box plot representing the distribution of population activity values at DIV 12. The analysis of p–value revealed no significant changes between conditions with $p_{U-P+} = 0.56$, $p_{PL-P+} = 0.34$ and $p_{P--P+} = 0.69$.

The increase in the number of bursting events can be noticed in the results for the IBI as a function of time (Figure 4.24c, left). A tendency was clearly observed for pTau–treated cultures that exhibited the lowest IBI value along the 9 days of tracking. At DIV 16 all conditions presented an analogous IBI value, following the trajectory

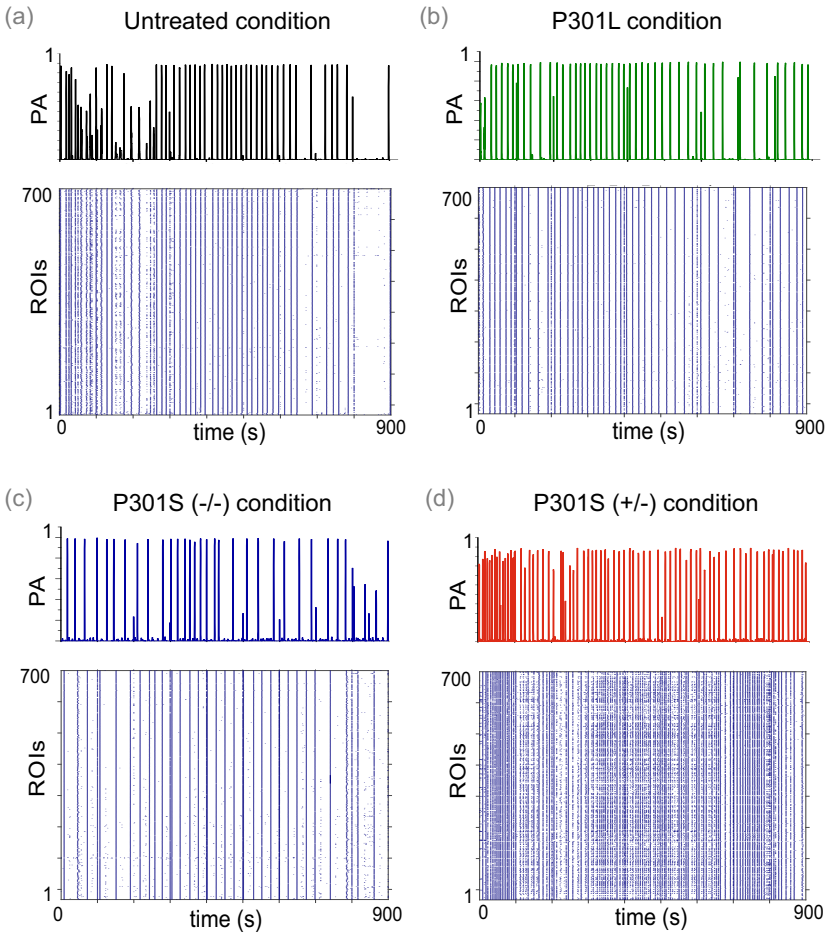

Figure 4.23. P301L scenario. Representative raster plots and population activity diagram at DIV 12. *(a)* untreated culture, *(b)* Culture infected with the P301L mutation at DIV 5, **(c)** Neurons expressing human P301L were incubated with P301S (-/-) **(d)** P301S (+/-) analogous.

drawn by P301S (+/-) cultures. As for the other two evaluated parameters, we illustrated the distribution of IBI values at DIV 12 in Figure 4.24c (right). P-values of $p_{U-P+} = 0.95$, $p_{PL-P+} = 0.02$, and $p_{P--P+} = 0.14$ indicate statistical significance for P301L and the pathological condition only. However, the low number of samples for cultures expressing human P301L tau diminishes the quality and interpretation of this comparison. Thus, giving these considerations, as well as the weak significance of the statistical comparison, we conclude that damage could be stated.

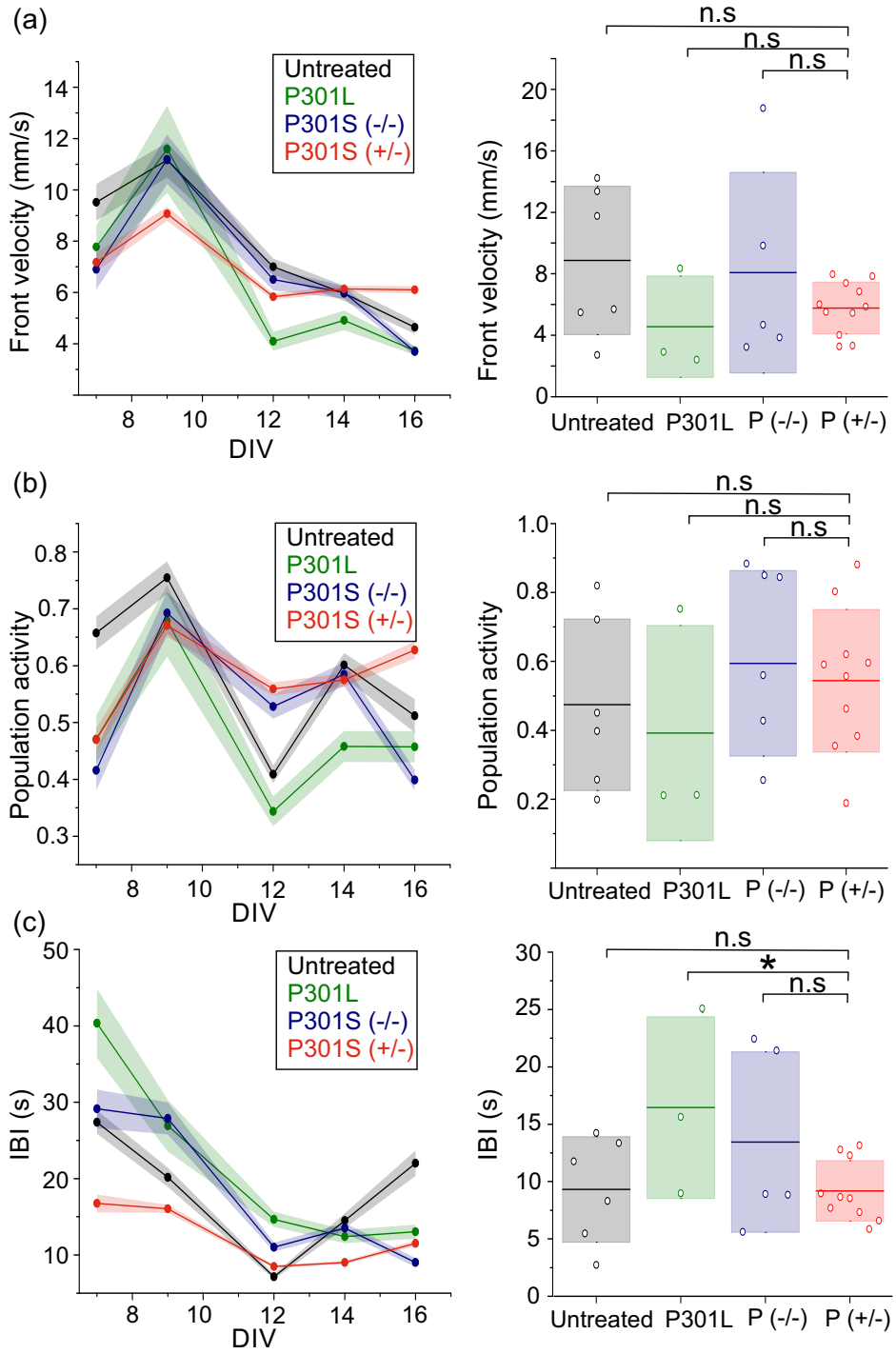

Figure 4.24. P301L scenario: Evolution of dynamical features from DIV 7 to 16, for untreated cultures and those that expressed P301L human tau, treated with either wild–type or pathological tau. **(a)** Evolution of the velocity of information flow. **(b)** Changes in the population activity. **(c)** Evolution of IBI. For these plots, $N = 6$ for untreated, $N = 4$ for P301L, $N = 5$ for P301S (-/-), and $N = 8$ for the P301S (+/-) condition. * $p < 0.05$, ** $p < 0.01$, *** $p < 0.001$ (Student's t-test).

Sarkosyl fractions from P301S (+/-) mice did not present an effect in functional organisation of primary cortical cultures expressing P301L human tau

To ascertain whether the expression of P301L human tau accelerated the damage scenario in treated cultures derived from P301S (-/-) and (+/-) mouse brains, we conducted effective connectivity analyses on the neuronal activity data of these cultures. In Figure 4.25, illustrative connectivity matrices are shown alongside the corresponding G_E and Q values for each of the four scenarios at DIV 12: untreated, expressing P301L human tau, and a combination of the latter condition with treatment using either P301S (-/-) or P301S (+/-) conditions. Connectivity matrices showed no clear trend, and even the untreated and pathological tau were very similar in behavior.

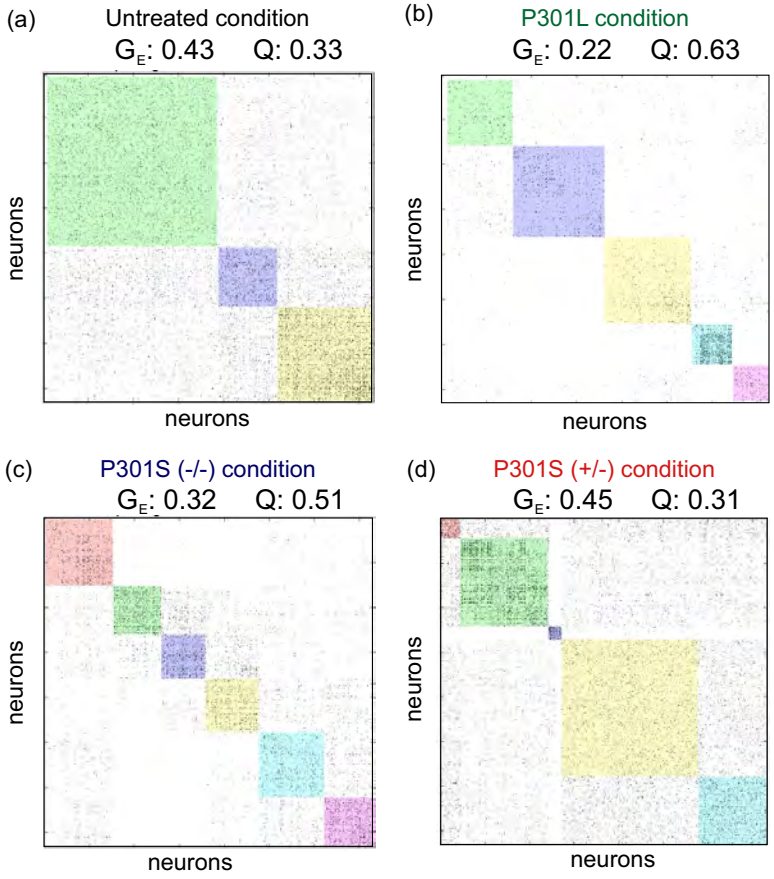

Figure 4.25. P301L scenario: Representative connectivity matrices at DIV 12 and functional analysis obtained for the different conditions applied to primary cortical neurons *in vitro* for the four different conditions: **(a)** Untreated culture. **(b)** AVV-P301L infected neurons. **(c)** Neurons expressing human P301L and incubated with P301S (-/-) or **(d)** P301S (+/-).

We next plotted the values of G_E and Q as a function of DIV, together with their standard errors, as shown in Figures 4.26a and b. Unfortunately, no significant changes were found in term of global efficiency or modularity in networks treated with any of

the possible conditions when considering all the performed experiments. Again, no indices of damage could be found.

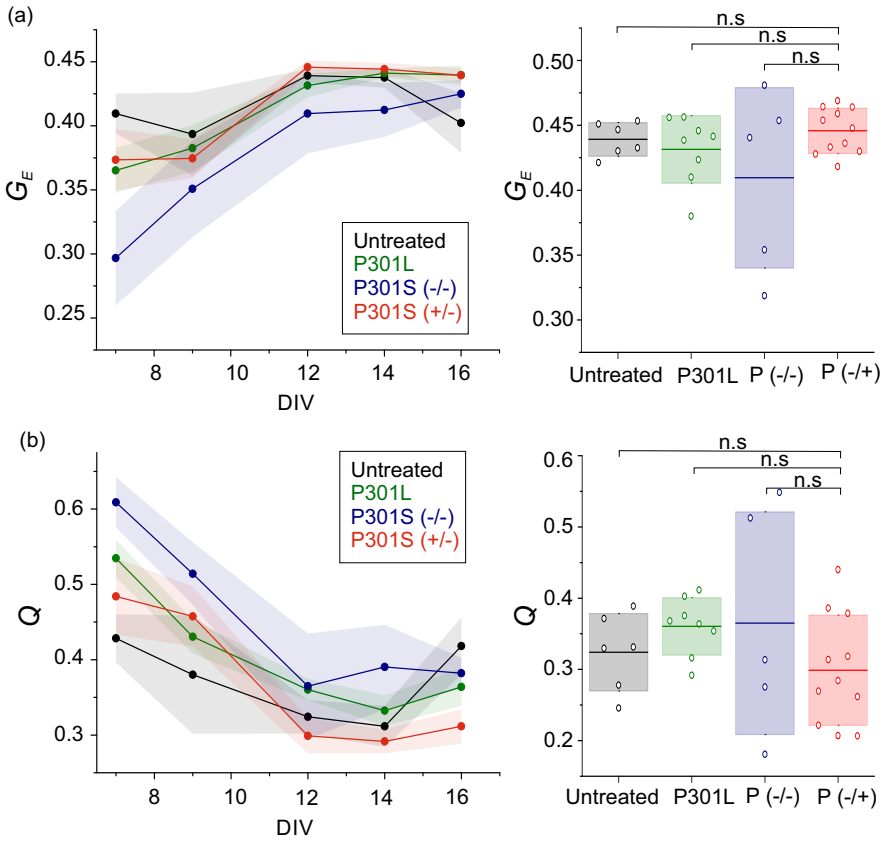

Figure 4.26. Functional analysis results of untreated cultures or cultures expressing P301L human tau, in addition some cultures were treated with P301S sarkosyl fraction. **(a)** Evolution of G_E with DIV. **(b)** Evolution of Q with DIV. or this plot N= 6 for untreated, N= 4 for P301L, N= 5 for P301S (-/-) and N= 8 for P301S (+/-) condition * $p < 0.05$, ** $p < 0.01$, *** $p < 0.001$ (Student's t-test).

4.4.5 pTau affects calcium fluorescence intensity

At this stage of the analysis, no discernible differences emerged between the untreated cultures, P301S (-/-) and P301S (+/-) conditions across the different aspects under investigation, including the dynamics of cultured network activity and functional organisation of the neuronal networks. However, it is worth highlighting an intriguing observation regarding the alteration in the nature of the calcium fluorescence traces obtained for each condition.

Fluorescence calcium traces provide valuable insights into the activity of neurons. For a neuron at rest, the fluorescence calcium trace appears relatively stable and at a baseline level. This baseline represents the resting calcium concentration within the

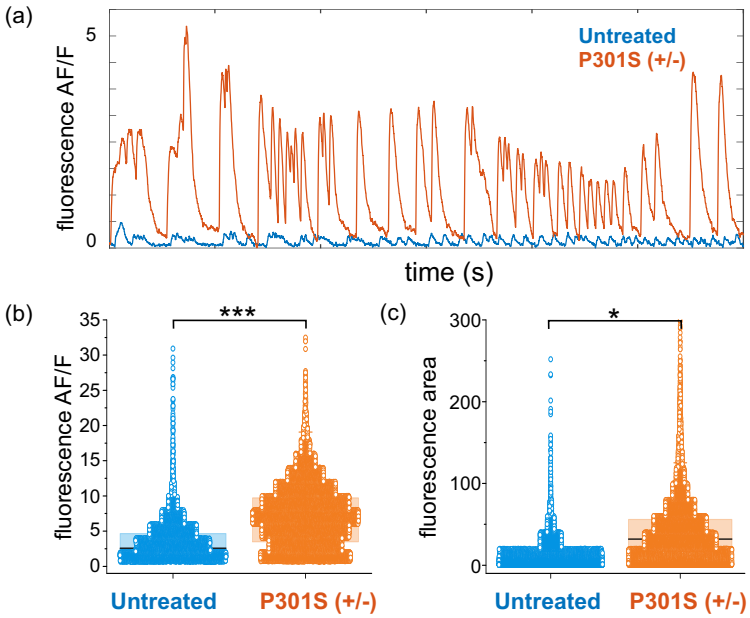

Figure 4.27. Analysis of fluorescence traces for untreated and 'pathological´ cultures. **(a)** Example of fluorescence traces for untreated (blue) and pTau-treated (orange) neurons at DIV 12. Fluorescence amplitude and shape change abruptly for treated neurons. **(b)** Distribution of maximum amplitudes for the traces in the example **(c)** Distribution of fluorescence areas for untreated and pTau traces evidencing that pTau traces last longer in time.

neuron. As the neuron receives excitatory signals or synaptic inputs, the calcium trace shows an upward shot, indicating an increase in intracellular calcium concentration. Neuron generates an action potential, triggering a characteristic spike in the calcium trace. Following the spike, there is a rapid decline in calcium levels and the calcium trace returns to the baseline level.

Interestingly, differences in calcium traces were observed at DIV 12, when the culture reached a sufficient state of maturation, for neurons treated with P301S (+/-) insoluble sarkosyl fraction at a concentration of 10 mg/mL. Examples of such traces are shown in Figure 4.27a. Results revealed that fluorescence traces for neurons treated with pTau presented a higher amplitude and lasted longer than those for untreated neurons in culture. It is also remarkable the fact that pathological traces showed a different shape of the calcium changes that described a spike: the calcium traces reached a maximum and, before returning to the baseline level (total depolarization of the cell membrane), the calcium level increased again or was maintained high, suggesting a maintained state of excitability for those neurons treated with pTau.

To have a better understanding of this anomaly we plotted the maximum fluorescence amplitude (Figure 4.27b) and the area of the fluorescence trace (Figure 4.27c) for traces obtained from untreated neurons and pTau–treated neurons. The pTau condition exhibited higher maximums of amplitude and wider traces, representing a steep

change in fluorescence from the basal state to the excited state that lasted longer in time. Student's test analysis showed significant differences with $p_{U-P+} = 1.09 \times 10^{-7}$ for the fluorescence amplitude and $p_{U-P+} = 0.046$ for the comparison of the fluorescence areas. We concluded that an alteration occurred and seemed strong, but we could not find arguments to understand it. Additionally, we could not replicate it consistently in all experiments.

4.4.6 Is pTau targeting inhibitory connections?– Bicuculline assay

Due to the aforementioned hyperactivity of pTau–treated cultures, we hypothesized that the accumulation of pTau in the extracellular medium could disrupt the balance between excitatory and inhibitory connections. To investigate this hypothesis, we conducted an experiment to determine whether pTau specifically targeted inhibitory connections in the culture, as previously demonstrated by Zheng and coworkers in hippocampal neurons in AD patients and mice *in vivo* (Zheng et al., 2020).

With the objective of proving such hypothesis, bicuculline, a selective antagonist of gamma-aminobutyric acid type A receptors ($GABA_A$) (the main inhibitory neurotransmitter receptors in the central nervous system) was employed in our study. Bicuculline functions by blocking the binding of GABA to its receptors, thereby inhibiting GABA's inhibitory function in the synapses (Bowery et al., 1981). In culture, bicuculline has been used to investigate the impact of inhibitory connections. For instance, in a culture with both excitation and inhibition active, network bursts are relatively mild in strength and IBI has a low value, but the blockade of inhibition shapes a highly excitable system in which bursting is very strong and the IBI increase. The reason is that neurons get exhausted from neurontransmitters after such a strong activation (Tibau, Valencia, and Soriano, 2013; Orlandi et al., 2013) and need longer time to recover and start again the recruitment process towards a new burst.

Our rationale for a possible scenario of damage in the inhibitory network, e.g., by the death of inhibitory neurons or the inactivity of their synapses, is that the presence of bicuculline would have no effect since in the overall dynamics of the network. Thus, we wanted to study whether pTau was targeting the inhibitory connection of the neuronal network *in vitro* by adding bicuculline to the extracellular medium and recording the resulting spontaneous activity. If inhibitory connections were already damaged by the presence of pTau, activity patterns and functional features should remain the same after bicuculline effects. We performed this experiment to both P301S (+/-) and untreated conditions, as shown in Figure 4.28a, and for those cultures previously treated with AVV-P301L, Figure 4.28b.

For untreated cultures, the results indicate a remarkable change in behaviour, indicating that inhibition is operating normally (Figure 4.28a). Results showed important, and expected, changes in network magnitudes due to inhibition blocking. For cultures

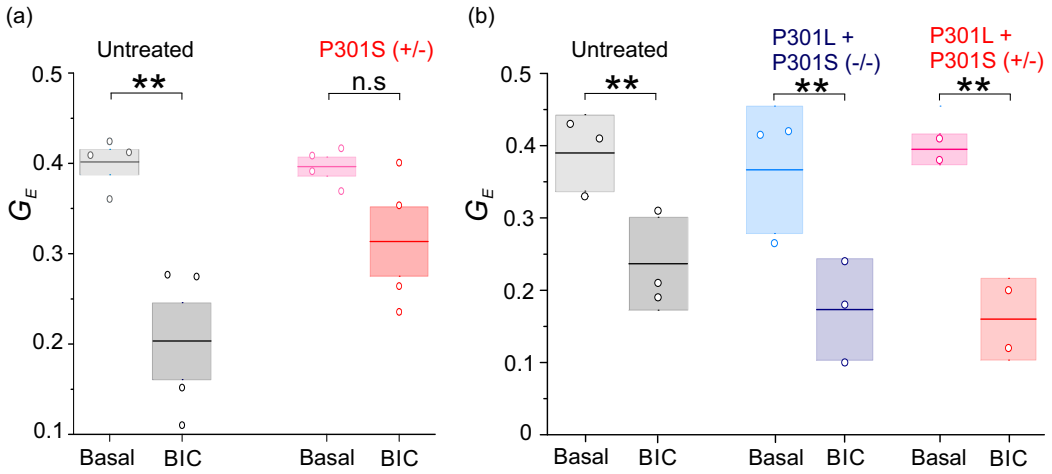

Figure 4.28. Bicuculline assay. Neurons in culture were tested with bicuculline to investigate whether pTau was targeting inhibitory connections in a tauopathies *in vitro* scenario. **(a)** Bicuculline test results for untreated and P301S (+/-) condition. **(b)** Results from untreated condition and cultures induced with the expression of P301L human tau and either P301S (-/-) or P301S (+/-) condition.

treated with pTau, variations in G_E value are not statistically significant, which means that inhibition is not acting correctly.

However, despite this initial positive outcome, the reproducibility of the results was not achieved when examining pathological cultures infected with AVV-P301L (Figure 4.28b). In contrast to the previous scenario, the analysis of pre– and post–bicuculline variations in this case indicated significant differences across all three conditions. This finding suggests that the inhibitory connections remain unaffected by the expression of human tau P301L, as well as the presence of extracellular tau, wild–type or pTau, within the culture medium.

4.5 Discussion

This Chapter meticulously documented and quantified the various endeavors undertaken to accomplish our mission within the 'La Caixa' Health Research 2019 project and the abundant scientific work carried out within this PhD Thesis. The primary aim was to recreate *in vitro* a methodology for assessing the harmful impact of extracellular pTau on neuronal network behaviour. This exploration delved into both the dynamics and the functional organisation at the neuronal network level. We used primary neuronal cultures from CD1 mice embryos (wild–type) as they are considered to be a proper disease–relevant model for studying sporadic tauopathies, in contrast to animal models over–expressing tau. These type of models differ from the insights into human conditions in which overexpression of tau does not occur but an accumulation of abnormal forms of insoluble tau. In this regard, the question of how extracellular

tau disturbs neuronal networks has received limited attention in the literature and it is where our study fits.

To conduct the neurotoxicity study on the IN–M4 inhibitors synthesized as part of the 'La Caixa' project, we compared the results of three distinct conditions: untreated primary cultures, cultures treated with DMSO (the preparation medium of the inhibitor solution) as a control, and the IN–M4 inhibitor itself at an elevated concentration of 50 μM. Neuronal activity was recorded for all cultures from DIV 7 to 16 by applying calcium imaging techniques. We employed previously described tools to perform a dynamic analysis of neuronal activity, examining parameters such as the velocity of the propagation front of population activity. Additionally, a functional study was conducted to gain information on the functional organisation of the resulting neuronal networks. Results showed that the designed tau–inhibitor did not have any effect on the propagation of the spontaneous neuronal activity along the neuronal culture, nor on the functional organisation of the network. Therefore, we could ascertain that the IN–M4 inhibitor did not affect neuronal development or behaviour *in vitro*.

The next challenge at hand involved establishing a robust *in vitro* tauopathy model. To achieve this, we introduced extracellular tau, obtained from various sources, into wild–type neuronal cultures. Our initial approach involved using 'cell–derived' tau from the Tau Biosensor cell line, enabling on–demand preparation and a greater quantity of samples. Cultures were incubated under four distinct scenarios: untreated, vehicle, TIF-P-, and TIF-P+. As demonstrated earlier, exposing neuronal cultures to these extracellular tau samples yielded no significant changes. However, a notable limitation of using TIF-P- and TIF-P+ fractions is that only synthesized and filtered tau is introduced into the culture, overlooking other potentially influential environmental elements.

At this stage, we were perplexed to find no observable dynamic or functional distinctions among the conditions discussed in the preceding section (untreated, vehicle, TIF-P-, and TIF-P+). This prompted us to question whether extracellular tau, despite forming pathological species, lacked the capacity to induce abnormalities in our cultures. Consequently, we opted to incorporate the insoluble sarkosyl extract from homogenized P301S(+/-) mouse brains directly into the cultures, employing its P301S(-/-) counterpart as a control. Within these fractions, we included not only pTau but also other potential protein conformations, along with other insoluble substances that could potentially impact the propagation of pathology.

We predicted changes in dynamical features of the neuronal network owning to the described effect of pTau in destabilizing microtubules and disrupting axons. The velocity of the propagating flow has been related in literature to the connectivity properties of the network (Golomb and Ermentrout, 1999; Bressloff, 2000; Feinerman, Segal, and Moses, 2005), with the velocity increasing with average network connectivity. Therefore, we hypnotized that extracellular pTau would decrease the velocity of the information flow in affected neuronal networks. Changes were expected in the

population activity as well, where we expected that the neuronal network would loss synchrony and would fail to generate collective events, e.g., due to the disruption of axons caused by pTau. Surprisingly, we were unable to identify significant differences between treated and untreated cells in culture, although a state of hyperexcited neuronal activity was observed in some of the cultures treated with extracellular pTau. Such a hyperexcitabilty could be ascribed to the loss of regulatory mechanisms such as inhibition, but we could not obtain an independent proof for such a strong assumption.

Following the same path, we expected changes in the functional organisation of the *in vitro* networks under the effects of seed–competent tau. In the described tauopathy scenario, the value of the global efficiency G_E should be lower compared to physiological conditions due to the (expectedly) reduced connectivity, which would hinder the exchange of information between neurons in the network. However, no significant differences were found when comparing G_E for treated and untreated cultures. Regarding the modularity Q, we presumed a higher number of neuronal communities, i.e., a higher value of Q, for treated cultures since extracellular tau is supposed to disrupt connections and therefore neurons would be more isolated. Remarkably, no clear differences were found in Q along the 16 days of monitoring for the three exposed conditions.

Our collaborators of the 'La Caixa' project demonstrated that sarkosyl–insoluble fractions from P301S (+/-) mice brains contained phospho–tau and insoluble filaments. In AD patients, the progress of the formation of pTau aggregates correlates with the progress of the disease (Delacourte et al., 1999). In this context, neurons containing insoluble filaments degenerate and liberate reactive forms of tau protein into the extracellular space, known as *ghost tangles*, that may accumulate and be toxic to the healthy neighbouring neurons (Goedert, 1999; Frost, Jacks, and Diamond, 2009). The addition of extracellular tau has been described to be toxic and promoted neuronal death for human neuroblastoma cells cultured *in vitro* (Gómez-Ramos et al., 2006). However, such toxicity was not obvious in our *in vitro* system, or it was masked by the capacity of standard 2D primary cultures to cope with damage and maintain strong levels of bursting activity.

In this direction, Stancu *et al.* treated primary neurons from P301S mice and their wild–type littermates with transgenic truncated human tau fragments either wild–type or P301L tau. After the treatment, the authors quantified the changes in calcium fluorescence by adding Fura-2 AM. Results showed changes in the amplitude of oscillations (rhythmic fluctuations in the electrical activity of the neuron) of those neurons derived from P301S mice treated with extracellular tau, while no changes were observed in wild–type neurons under treatment (Stancu et al., 2015). In our experiments, wild–type cortical neurons were treated with pathological tau, and no significant changes were observed attending to network parameters. This is consistent with the results obtained by Stancu *et al.* which brings us to question whether wild–type cells are resistant to the presence of extracellular tau. As of the time of writing this Thesis, and

to the best of our knowledge, no other study has explored the impact of extracellular tau *in vitro* using wild–type neuronal cultures, besides Stancu *et al.*, with the limitation that they only considered measures at DIV 1 for the analysis, i.e. only one time–point. It is important to note that their study was solely focused on measuring changes in network activity, and no further investigations were conducted regarding functional organisation. Based on the available information, no other studies have been carried out attending the evolution of functional connectivity in primary wild–type neuronal cultures under the effects of extracellular tau.

The progressive degeneration of neurons containing pTau can be a lengthy and gradual process, and aging has been identified as one of the primary risk factors for sporadic forms of AD and other NDs (Braak and Braak, 1991; Frost, Götz, and Feany, 2015). In our experimental approach, cells were not only wild–type but also embryonic, and experiments were carried out for 16 days, limited by the intrinsic degradation of the cultures in which they detached from the substrate where they grow. Thus, we considered that from DIV 16 onwards we would not be able to interpret whether the differences in activity were due to natural degradation of the neuronal network or to the action of the different treatment scenarios. For these reasons, and in an attempt to accelerate damage in culture, neurons were infected at DIV 1 with an AVV–P301L. In this new scenario, wild–type neurons were able to express P301L human tau in addition to being exposed to extracellular wild–type and pTau. Spontaneous activity recordings were performed every two days until DIV 16 and dynamical and functional parameters were extracted.

In this P301L scenario, no significant changes were found either in terms of dynamics or in the functional connectivity of the neuronal network for any of the four different conditions (untreated, P301L, P301S (-/-) and P301S (+/-)). Noteworthy, the treated cultures exhibited a notorious state of hyperactivity. It has been reported that the presence of extracellular tau increases the levels of intracellular calcium levels (Gómez-Ramos et al., 2008), in which authors described a different calcium fluorescence response in those neurons exposed to extracellular tau. These results are in agreement with our observations when monitoring the treated cultures with calcium imaging techniques (Figure 4.27a). Calcium traces for neurons treated with pTau had a greater amplitude and width than those for untreated neurons, describing a multi–peak fluorescence gradient, suggesting that neurons did not have time to complete their full depolarization when they were involved in a new activity event. Rocher et al., 2010 described that neurons from mice expressing P301L human tau exhibited a significantly depolarized resting membrane potential and increased action potential firing rates in response to depolarizing current steps, which resulted in a higher excitability.

Dysregulation of calcium homeostasis has been related to tau–induced pathology, aberrant excitatory activity, and imbalance in neuronal excitation–inhibition balance, with several studies linking such effects with AD pathology progression (Palop et al.,

2007; Maestú et al., 2021; Styr and Slutsky, 2018). It has been described that cortical activity regulates the release of endogenous tau in physiological conditions *in vivo* (Pooler et al., 2013), being excitatory neuronal activity strongly related with an increase of extracellular tau level. Yamada et al., 2014 linked presynaptic excitatory neuronal activity with the release of tau by neurons *in vivo*, suggesting that the propagation of tauopathies diseases might be an active process, associated with synapses, leaving behind the theory that extracellular tau comes only from neurons degenerated because of the disease (Kobayashi et al., 2019). In our experiments, the excited state may be a consequence of the presence of extracellular tau, suggesting that it could be a two–way road. In fact, literature exposed that early hyperactivation in AD patients could be a mechanism to compensate for the emerging cognitive decline (Dickerson et al., 2004; Targa Dias Anastacio, Matosin, and Ooi, 2022).

In this direction, some authors questioned the toxic role of pTau and assumed instead a protective role of insoluble tau filaments and NFTs. Lee et al., 2005 proposed an antioxidant role in the accumulation of phosphorylated tau as a response to oxidative damage, which has been reported as one of the main figures in AD progression alavi2015tau, cassidy2020oxidative. In contrast, Hanger, Anderton, and Noble, 2009 hypothesized that NFTs accumulation might be caused by an effort to restore physiological levels of protein tau available for microtubule binding in neurons when increasing the steady–state levels. These theories, coupled with the fact that the presence of extracellular tau does not appear to have significant effects in wild–type neurons, either in animal models or in culture, raise questions about the role of insoluble forms of tau in the development of tauopathies, leading to the fact, already postulated in the literature, that resulting NFTs might not be toxic but the toxicity of pTau relates to the presence of toxic tau intermediates Castellani et al., 2008; Cárdenas-Aguayo et al., 2014. Oligomeric forms are not available in our experimental setup. Moreover, conventional *in vitro* models pose limitations when studying neurodegenerative pathologies due to the dilution of cell–secreted neurotoxic factors in the culture medium, which are eventually eliminated during media changes. This contrasts with the *in vivo* seeding and spreading of these pathologies, where highly concentrated nucleation sites are formed in the extracellular space. In addition, pathologies like tauopathies are the results of complex fluctuations that might include signaling cascades, synaptic modifications, and network interaction that are extraordinarily difficult to replicate in a Petri dish (Palop, Chin, and Mucke, 2006).

Another important issue to address is the use of standard primary cultures as a suitable tool for investigating this type of diseases. Primary neuronal culture have been used in our lab to explore changes in functional connectivity caused by physical damage (Ayasreh et al., 2022) and focal lesion (Teller et al., 2020) as well as the characteristic time scales of the cultures to recover their pre–damage activity levels. Degradation in neuronal activity caused by the presence of amyloid–β and magnetite acting together (Teller et al., 2015) was also explored successfully. However, neuronal

cultures grown on a flat surface are locked in a extremely synchronous patterns of spontaneous activity that might mask changes in functional connectivity. Estévez–Priego *et al.* examined the response of embryonic cortical cultures to chemical perturbations and concluded that neuronal circuits possessed strong homeostatic plasticity mechanisms to cope with disturbances or damage. Their study demonstrated that embryonic primary cultures exhibit high plasticity and employ self–regulatory mechanisms when faced with external disruptions (Estévez-Priego et al., 2020)).

In this direction, primary wild–type neurons in our experimental model can be reacting to pathological perturbations by using compensation mechanisms, such as diverse forms of plasticity or hypersynchrony, in an attempt to maintain a homeostatic performance. Thus, neurons in culture might be in a state of continuous adaptation against the effect of extracellular tau. One possible adaptive mechanism is the one proposed by Desai *et al.*, who showed that neurons in culture increase their intrinsic excitability when their activity decreases (Desai, Rutherford, and Turrigiano, 1999). Synaptic plasticity acts by changing the synaptic weight in neuronal connectivity and is determined by the activity pattern of the network (Fauth, Wörgötter, and Tetzlaff, 2015). Such a mechanism can be hidden by the synchronous activity of standard primary neuronal cultures, resulting in higher excitability of the cultures with no detectable functional changes in the affected networks. Neuronal plasticity is widely recognized for its remarkable adaptability, playing a crucial role in maintaining neurological functions both in healthy states and in the presence of disease, but become by themselves a true nightmare when trying to isolate and model the specific mechanisms of neuronal damage.

4.6 Conclusions

This research has demanded extensive experimental endeavors and a comprehensive literature exploration. The initial goal outlined in the ‘La Caixa’ project was to assess the non–toxic nature of the molecules developed for inhibiting the aggregation of tau in its abnormal forms. To achieve this, we verified that the analysis of the dynamics of neuronal activity and the organisation of neuronal networks in culture remained unaffected by the presence of external agents such as the inhibitor. These experiments yielded successful results, confirming that the inhibitors did not disrupt the healthy development of our primary cultures.

It is disheartening that our efforts have yet to yield a clear and concise understanding of the damage induced by the presence of extracellular tau in wild–type primary neuronal cultures. Numerous experiments were conducted (see Figure 4.29), incorporating both authentic tauopathy models and models where damage was expedited through the induced expression of human P301L tau by the cultured neurons themselves. Regrettably, none of the described cases presented definitive evidence of tau damage.

This absence of damage might be attributed to the fact that the cultures consist of neurons from healthy embryos, making it challenging for symptoms to manifest. It is plausible that a more extended incubation time for the tau treatment is required for its effects to become apparent, or perhaps the cells activate some form of defense mechanism, enabling them to maintain normal levels of activity despite the presence of tau.

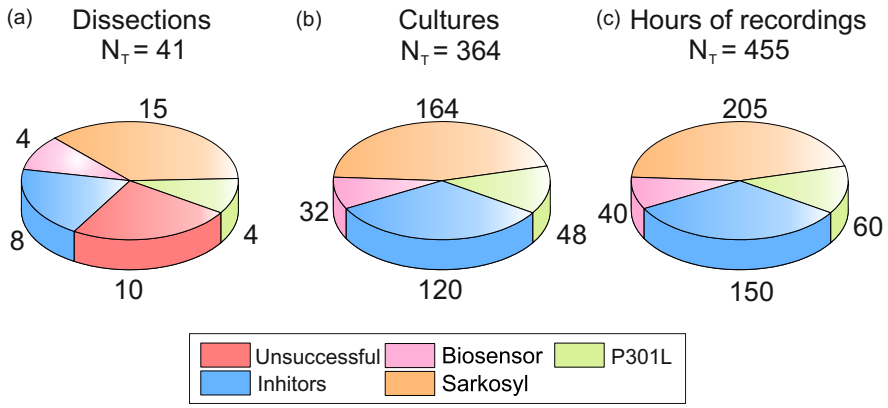

Figure 4.29. Illustrated summary of the experiments carried out within the framework of the 'La Caixa' Health Research project. **(a)** The chart illustrates the total number of CD1 mouse dissections conducted. **(b)** The 41 performed dissections encompass a total of 364 cultures, distributed across various phases of the project. **(a)** Each culture, segmented into two 4 mm cavities, underwent a 15–minute recording at DIVs 7, 9, 12, 14, and 16. This accumulates to a comprehensive 455 hours of recording split among different projects. It is worth noting that the subsequent hours dedicated to analyzing each culture are not reflected in these graphs. During the analysis phase, each culture underwent a duplicate examination, one for each of the 4 mm cavities.

5 Rheological characterisation of three-dimensional neuronal cultures embedded in PEGylated-fibrin hydrogels

5.1 Introduction

Standard neuronal cultures, in which neurons are seeded and grown on a flat surface, have been extensively used to study neuronal circuits in a controlled environment (Tetzlaff et al., 2010; Bang et al., 2021; Weir et al., 2023; Soriano, 2023). In fields such as physics or medicine, these cultures have helped to understand the complex functional organisation of living neuronal networks (Meunier, Lambiotte, and Bullmore, 2010), the emergence of activity patterns and their relation to electrophysiological activity in the brain (Raggenbass, 2001; Chiappalone et al., 2006), as well as the impact of physicochemical perturbations on neuronal networks' behaviour (Teller et al., 2015; Teller et al., 2020).

Despite these efforts, a central debate among the neuroscience community is whether these 2D neuronal cultures are adequate models to understand the complexity of naturally formed neuronal circuits such as the brain, which combines 2D and 3D organisation (Stiso and Bassett, 2018; Schwartz et al., 2023). Indeed, neuronal cultures grown in a 2D environment exhibit a much poorer repertoire of neuronal activity as compared to the brain (Wagenaar, Pine, and Potter, 2006; Orlandi et al., 2013; Cohen and D'Esposito, 2016) due to the fact that cell connectivity is restricted to one plane. Therefore, 3D neuronal cultures have been introduced in the last decade to develop better *in vitro* models. In typical 3D cultures, cells are embedded in rigid scaffolds, jelly matrices or a combination of both, facilitating brain–like neuronal development (Tang-Schomer et al., 2014; Chwalek et al., 2015; Bourke et al., 2018; Lam, Fischer, and Enright, 2021) and the emergence of organisational features such as modularity (Bourke et al., 2018; Dingle et al., 2020; Rabadan et al., 2022). Although different studies have shown that the 3D environment favors a richer neuronal morphology and network activity as compared to standard 2D preparations (Marder, 2011; Frega et al., 2014), reproducing the complexity of *in vivo* cell–cell as well as cell–matrix interactions remains a challenge.

The central problem when preparing 3D neuronal cultures is the selection of the bulk material in which the neurons will grow. This material needs to mimic the brain extracellular matrix (ECM), a fibrous network with a complex distribution of proteoglycans, such as hyaluronic acid, and elastic fibers embedded in a highly hydrated environment (Long and Huttner, 2019; Ozgun et al., 2022). The brain ECM is so unique that it allows for the efficient transport of molecules, nutrients and metabolic waste while providing structural support to the neurons and other cells. Thus, the chosen bulk material should be sufficiently permeable for molecular transport and exhibit adequate mechanical properties to support a stable neuronal network formation (Javier-Torrent, Zimmer-Bensch, and Nguyen, 2021). Mechanical properties such as stiffness as well as porosity are traits that may be central to regulate the capacity of the neurons to shape a rich arborization and project axons at long distances.

Among all possible ECM–mimicking materials, *hydrogels* have received special attention due to their highly hydrated structure, which is important since about $73-85\%$ of the human brain mass is water (Lau et al., 2013). Hydrogels are 3D elastic structures made from cross–linked polymer chains that are capable of holding a large amount of water, giving them a soft and flexible texture that resembles natural tissues. They can be engineered to have a wide range of physical and chemical characteristics, making them suitable for various applications. Hydrogels can be synthetic (e.g., polyacrylamide PAA, polyethylene glycol PEG, or polyvinyl alcohol PVA), natural biopolymers or a combination of both. Hydrogels with a natural origin include collagens (Dingle et al., 2020; Lam et al., 2020), hyaluronic acid–based hydrogels (Pan et al., 2009; Wu et al., 2017; Spearman et al., 2020), chitosan gels (Cao, Gilbert, and He, 2009; Tedesco et al., 2018) and fibrin hydrogels (Rowe, Lee, and Stegemann, 2007).

Although all these materials have emerged as attractive candidates for neuroscience applications, the semisynthetic PEGylated fibrin hydrogels have particularly caught the attention of researchers in neuroengineering and regenerative medicine (Galler et al., 2011; Dadashzadeh, Moghassemi, and Amorim, 2021). The reasons for such an interest include their excellent properties such as their biocompatibility and ease of manipulation (Rowe, Lee, and Stegemann, 2007), and their inherent synthetic nature enhances their resistance to degradation and overall favors long–term stability. PEGylated fibrin hydrogels are also transparent, enabling the study of the dynamic and functional characteristics of embedded neuronal networks through calcium–imaging techniques. Additionally, these hydrogels hold the potential for patient–specific applications, as fibrinogen and thrombin (main components of fibrin gel) can be directly sourced from patients, allowing for customization and personalized approaches in medical applications.

Despite these advantages, the physical characteristics of PEGylated fibrin hydrogels are still poorly understood, particularly in the context of developmental neuroscience, where neurons and connections continuously evolve within the hydrogel matrix and therefore may change their structural and mechanical properties. To shed

light on this quest, here we introduced a rheological protocol to investigate the appropriateness of PEGylated fibrin hydrogels for 3D neuronal cell culturing. Rheological analyses were performed with and without living neurons to evaluate whether neuronal development was altering the hydrogel structure. In either scenario, the hydrogels' behaviour was monitored for 20 days to evaluate possible degradation over time. This exploration was combined with immunostaining techniques to quantify the neuronal arrangement within the hydrogel structure (López-León, Soriano, and Planet, 2023).

5.2 Objectives

The aim of this investigation is to create a robust platform for conducting 3D neuronal cultures, in which neuron–matrix interactions do not change the mechanical conditions required for optimal neuronal growth and network functionality. For that, we chose a brain–ECM–like material, particularly PEGylated fibrin hydrogel, and performed rheological measures to investigate the effects of living neurons on the mechanical properties of the scaffold. The characterisation was performed along a 20–day period to follow the evolution with time and network development in the hydrogel structure. Briefly, the main objectives of this Chapter are:

- Build a suitable PEGylated fibrin platform for conducting 3D neuronal cultures.
- Design a protocol that allows to characterise the mechanical properties of the hydrogel scaffold.
- Track the evolution of the rheological properties of the scaffold along time, as well as with the presence of neurons and their development within the hydrogel.

5.3 Materials and methods

In this section we first summarize the 3D neuronal culture preparation protocol. Then we introduce the principles of rheology to have a better understanding of the techniques applied to characterise the rheological behaviour of the hydrogels. Finally, we describe the protocol followed to apply immunohistochemical techniques in order to visualize neurons within the hydrogel structure.

5.3.1 Hydrogels preparation

The realization of 3D neuronal cultures in PEGylated fibrin hydrogel was described in detail in the General Methods Chapter (Sec. 3.1.3). In a nutshell, PEGylated fibrin hydrogels were prepared by mixing a 25 mg/mL fibrinogen solution with 6 mg/mL PEG–NHS to obtain a 5 : 1 molar ratio. To promote crosslinking, the resulting mixture

was incubated at 37°C for 2 hours. PEGylated fibrinogen solution was then combined with cell suspension, previously prepared by dissociation of CD1 mouse embryo cortical tissue (Figure 5.1a). For further rheological characterisation of PEGylated fibrin scaffolds, the resulting solution was placed in an 8 mm PDMS mould (Figure 5.1b), so that the final hydrogel shaped an 8 mm cylinder that perfectly fit the rheometer geometry. The last step was the addition of a thrombin solution that cleaved specific bonds in the soluble fibrinogen, resulting in the production of insoluble fibrin monomers that polymerized, producing the final 3D structure. The resulting material was 100 μL in volume with a final concentration of 6.5 mg/mL fibrinogen and 0.25 U/mL thrombin.

The planned experiments included the study of the mechanical properties of hydrogel scaffolds with and without cells. For the hydrogels without cells, we applied the protocol described above but replaced the cell suspension with cell media without cells. Hydrogels were incubated at 37°C, 5% CO_2 and 95% humidity. Culture medium composition and refreshment was carried out similarly as in standard cultures (see Sec. 3.1.3). Hydrogels with and without cells were treated identically, i.e., they experienced the same manipulations and medium changes.

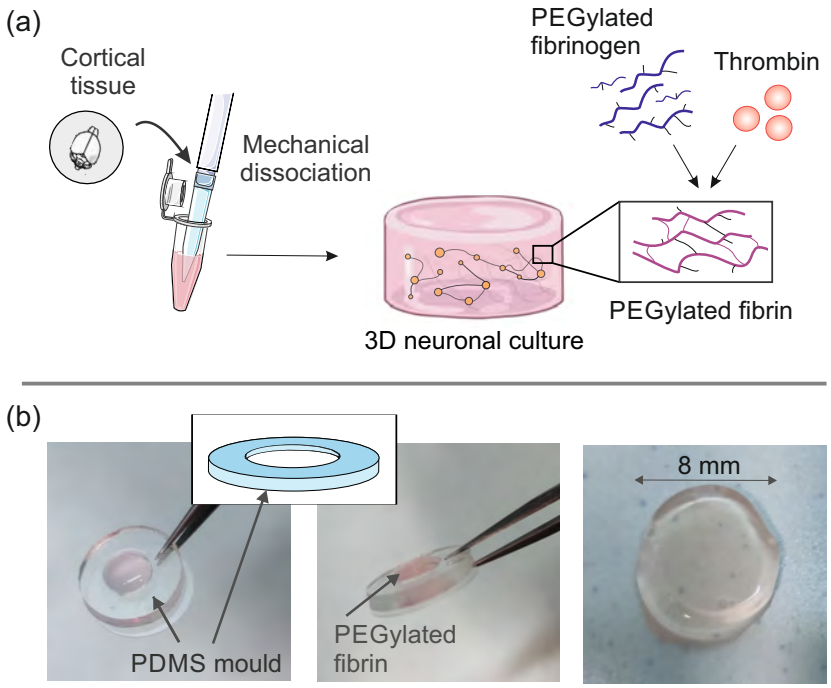

Figure 5.1. Hydrogels preparation. **(a)** Schematic representation of PEGylated fibrin hydrogel protocol. Cortical tissue is mechanically dissociated and mixed with cell medium. Single cells suspension is then combined with a mixture of PEGylated fibrinogen previously incubated for 2 h at 37°C. The final solution is placed in the center of an 8 mm PDMS well. At the same time, a thrombin solution is poured in. The soluble fibrinogen becomes then soluble fibrin and the hydrogel jellifies with the shape of an 8 mm cylinder. **(b)** Images of the PDMS mould containing the hydrogel. The right–most image shows the hydrogel without the PDMS ring.

To verify that cells were alive and developed healthily within the hydrogels, cultures with neurons were virally transduced with the calcium indicator GCaMP6s at the moment of preparation. A ratio of 1:1000 virus solution carrying the indicator was mixed with the cell suspension before adding the thrombin solution. Spontaneous activity was then verified from DIV 7 to 20 to detect clear signals of widespread spontaneous activity, a signature of healthy development and network–wide connectivity.

5.3.2 Hydrogels rheological characterisation

Rheology is the branch of physics and materials science that studies the flow and deformation of matter (Barnes, Hutton, and Walters, 1989; Malkin and Isayev, 2022), particularly liquids and soft materials like polymers, colloids, and suspensions. To do so, researchers use a rheometer, an instrument used to measure and control the flow and deformation of materials when they are subjected to applied forces, strains, and stresses. Rheometers, as the one shown in Figure 5.2, are equipped with a motor that applies a controlled shear stress (τ) or a controlled shear deformation (γ) in the material sample. The motor applies either rotational or oscillatory motion allowing researchers to perform two different kinds of tests, namely rotational and oscillatory. The former gives information about the material's flow curve and a direct measurement of its viscosity by applying a constant shear rate or stress to the sample; the latter involves applying small–amplitude deformations to the sample to study the viscoelastic response of the material.

Rheometers can be equipped with different geometries, including concentric cylinders, coaxial cylinders and parallel plates. The sample is hence placed between these geometries, where the shear forces or deformations are applied. The selection of one geometry or another depends on the nature of the material and the object of study. This kind of instruments are operated through a control software that allows users to set test parameters and acquire data in real–time thanks to highly sensitive sensors that measure the response of the material.

Most biological materials, including cells and tissues, exhibit viscoelastic behaviour, meaning that their reaction to mechanical stress (or strain) encompasses both elastic and viscous components. In turn, this behaviour is influenced by the timescales of the applied stress. The viscous or energy–dissipating attributes of tissues are typically assessed through dynamic tests such as oscillatory or stress–relaxation measurements. For that reason, we applied Small Amplitude Oscillatory Shearing (SAOS) for investigating the PEGylated fibrin rheological behaviour. This technique involves the application of an oscillatory test, subjecting the sample to periodic shear deformations of small amplitude. SAOS is particularly useful for characterising materials that exhibit non–linear, time–dependent, or frequency–dependent behaviour. Thus, SAOS can help researchers to understand the molecular interactions and structural changes within the material, providing insights into its behaviour and potential applications. Therefore, it

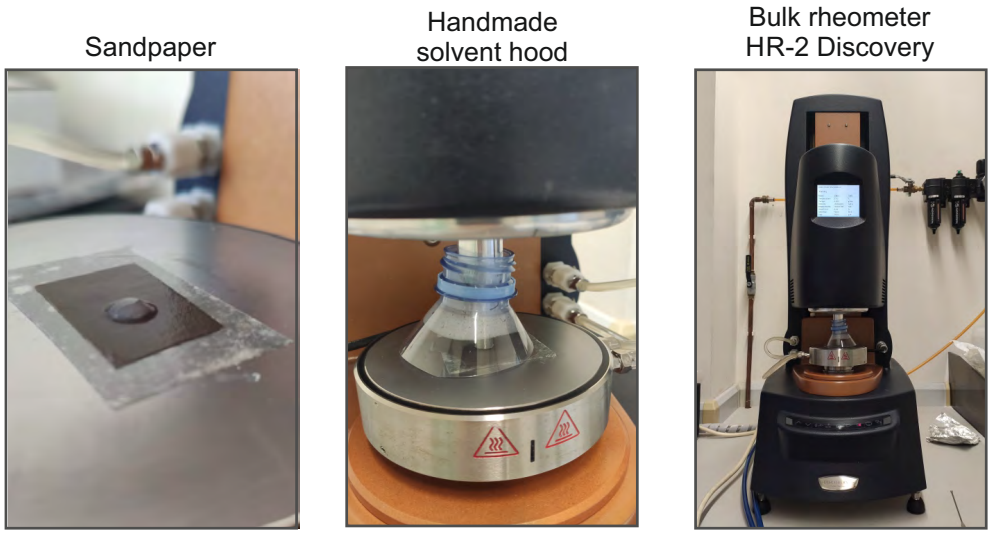

Figure 5.2. Images of the laboratory set-up used for performing the rheological characterisation of PEGylated fibrin hydrogels with and without cells. On the left, a detail image of the sand paper used to prevent the hydrogel sample from flowing during measurements. At the center, a zoom of the handmade solvent hood for avoiding evaporation of the liquid containing the hydrogel. On the right, an general image of the bulk rheometer HR-2 Discovery (TA instruments).

is widely used to study the viscoelastic properties of materials, particularly complex fluids like polymers, gels, and certain types of liquids to understand how materials behave under different conditions and forces.

For the experiments, we used a bulk rheometer HR-2 Discovery (TA instrument) installed in Dr. Jordi Ortin's Laboratory in the Faculty of Physics of the University of Barcelona. The instrument was equipped with an 8 mm plate–plate geometry together with a peltier that imposes a certain temperature to the sample during the measurements. All tests were performed at a constant temperature of 37°C, the physiological temperature of living neurons. Sandpaper (grit P600-BF08, Wurth, Künzelsau, Germany) was attached to both surfaces of the plate–plate geometry to prevent the hydrogel from slipping during measurements (Divoux, Barentin, and Manneville, 2011) (Figure 5.2, left). A handmade solvent hood was used to cover the sample, the environment was then saturated by placing a small amount of culture medium around the hydrogel, avoiding the evaporation of the liquid contained in the hydrogel during the test (Figure 5.2, center).

We applied SAOS to characterise the viscoelastic properties of the PEGylated fibrin hydrogel. The material was tested under a controlled shear deformation that oscillates sinusoidally as $\gamma(t) = \gamma_0 \sin(\omega t)$, where ω is the frequency of the oscillation. A schematic representation of these deformations is provided in Figure 5.3a. The general response of a viscoelastic material contains both in–phase and out–of–phase

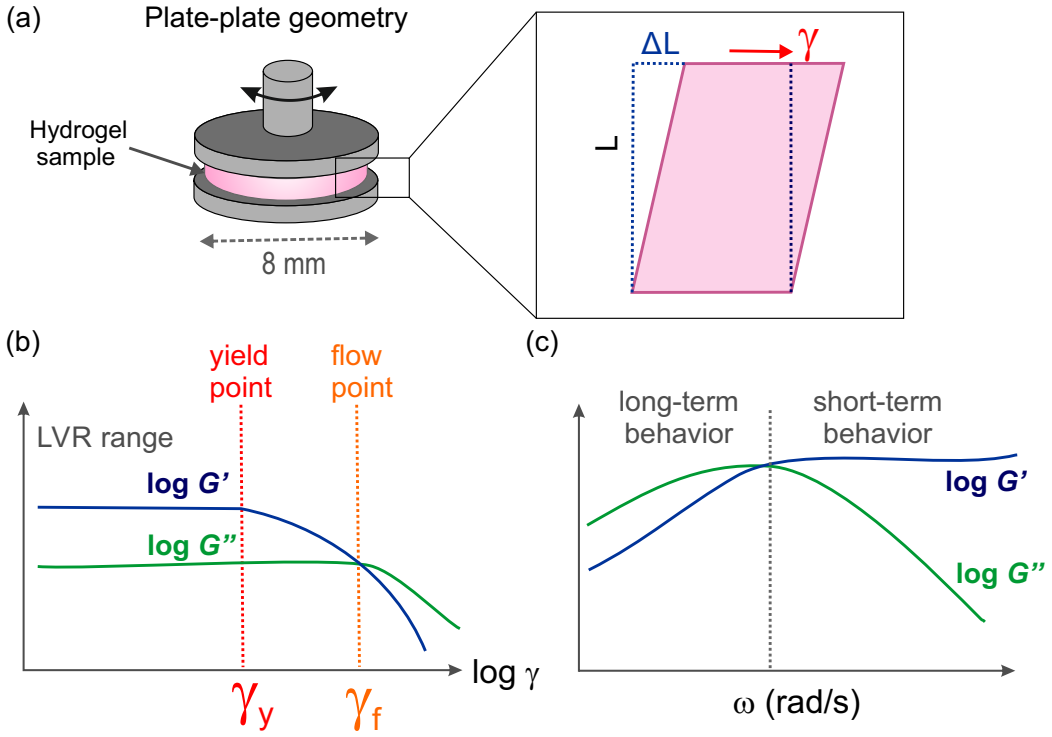

Figure 5.3. Rheological measurements. **(a)** Schematic representation of a hydrogel sample placed between the 8 mm plate–plate geometry of the rheometer set–up. The hydrogel is subjected to a controlled sample elongation of ΔL that results in a shear deformation strain ($\gamma = \Delta L/L$). **(b)** Example of the outputs obtained from a strain sweep test of a viscoelastic fluid. The sample shows an initial linear viscoelastic range (LVR) where $G' > G''$, indicative of solid–like behaviour. **(c)** Example of the outputs obtained from a frequency sweep test of the sample. Initially, this material exhibits characteristics of a liquid–like substance in the short–term ($G' < G''$). As time elapses, the elastic component predominates and the material behaves as a solid ($G' > G''$).

components, reflecting the elastic and viscous contributions, respectively. The *storage modulus* (G') represents the storage of elastic energy and accounts for solid–like behaviour of the material. On the other hand, the *loss modulus* (G'') represents the viscous dissipation of energy and gives information about the liquid–like behaviour of the material.

Both moduli are given as the outputs of the oscillatory tests, in which the stress response can be expressed as $\sigma(t) = \gamma_0 [G'(\omega)\sin(\omega t) + G''(\omega)\cos(\omega t)]$. The regime of small amplitude straining, in which the stress can be described in this form, is called the *linear viscoelastic regime* (LVR) (Oswald, 2009).

Figure 5.3b displays the behaviour of a viscoelastic material subjected to a constant oscillation frequency (ω_0) while changing the deformation strain (γ) of the test. This test is known as *strain sweep* and will be also described in detail in the following section. The material demonstrates an initial LVR in which G' and G'' do not depend on the applied deformation. For this sample material, $G' > G''$ at small deformations,

indicative of a predominantly solid–like behaviour. The material then reaches a point in which it begins to deform plastically and, thus, G' depends on the deformation applied. This point is known as yield point (γ_y) (Yip, 2007).

Beyond it, the sample no longer undergoes a purely elastic deformation. Under greater applied deformations, the material begins to flow (γ_f), signified by $G' < G''$. Subsequently, the material consistently exhibits properties akin to a liquid–like substance. This material embodies a non–Newtonian shear–thinning fluid, which displays a characteristic solid–like behaviour in a resting state or when subjected to minimal deformations. As the shear deformation increases, the polymer chains within the solution experience a stretching phenomenon, and the material transitions from solid–like behaviour to a more fluidic one. If the applied shear deformation becomes more significant, the polymer chains eventually undergo rupture or alignment in response to the high deformation forces. This juncture explains the material's ability to flow.

After the strain sweep test, the material is subjected to a *frequency sweep* test, in which the deformation strain (γ_0) remains constant while changing the oscillation frequency (ω) of the test. Figure 5.3c displays the outputs of this test, showing that the sample initially exhibits a behaviour typical of a liquid–like substance, as $G' < G''$, when subjected to high frequencies (short times). However, at long term the material transitions into an elastic one, with $G' > G''$, and it behaves as a solid–like material. These results can be representative of a sealant, a type of material that necessitates viscosity (liquid–like behaviour) for effective application. Following a drying period, the material is required to exhibit an elastic (solid–like) behaviour to fulfill its intended function.

Determination of rheological properties: data analysis

The measured G' and G'' moduli allowed for the definition of the *complex shear modulus*, $G^* = G' + iG''$, that accounts for the entire viscoelastic response of the material. Being a complex number, it is possible to extract its modulus $|G^*|$ and its phase δ since $G^* = |G^*|e^{i\delta}$. These two quantities provide useful insight in the material behaviour.

The *complex modulus*, expressed as:

$$|G^*| = \sqrt{(G')^2 + (G'')^2}\,, \tag{5.1}$$

gives information about the shear stiffness of the material (Patel, Smith, and Patrick Jr, 2005). By definition, the shear stiffness of a material accounts for the ratio of shear stress (force applied over the cross–sectional area of the material) to shear strain. Interestingly, $|G^*|$ can be related to the the Young's modulus, E, which quantifies the relationship between the tensile (or compressive) stress and the axial strain in the linear elastic region. Knowing $|G^*|$, E can be obtained as:

$$E = 2|G^*|(1+\nu)\,, \tag{5.2}$$

where ν is the Poisson's ratio (Oswald, 2009; Oyen, 2014). For the particular case of our work, in which we considered fibrin matrices, the Poisson's ratio was taken as $\nu \simeq 0.25$ (Duong, Wu, and Tawil, 2009).

Finally, the *phase shift*, δ, defined as (Janmey, Georges, and Hvidt, 2007; Oswald, 2009):

$$\tan\delta = \frac{G''}{G'}, \tag{5.3}$$

provides information about the tendency of the material to show an elastic or a viscous response. For $\delta = 0$ rad, the material response is the one of an ideally elastic material, while for $\delta = \pi/2 \simeq 1.57$ rad, the material response is the one of a perfect viscous liquid. Intermediate phase shifts reflect different degrees of viscoelastic behaviour.

Rheological Tests

We used a plate–plate rheometer under a controlled shear deformation rate to characterise the hydrogel samples. With this goal in mind, we applied SAOS oscillatory tests with a fixed gap of 500 μm. The gap space for these rheological tests was chosen to ensure the integrity of the samples. Preliminary tests were carried out in which the geometry of the rheometer was vertically displaced to squeeze the sample until the axial stress reached a value of $\simeq 0.2$ N, as shown in Figure 5.4. The applied force is adequate to hold the sample during the test without causing breakage, ensuring that we accurately measure the intact structure of the hydrogel.

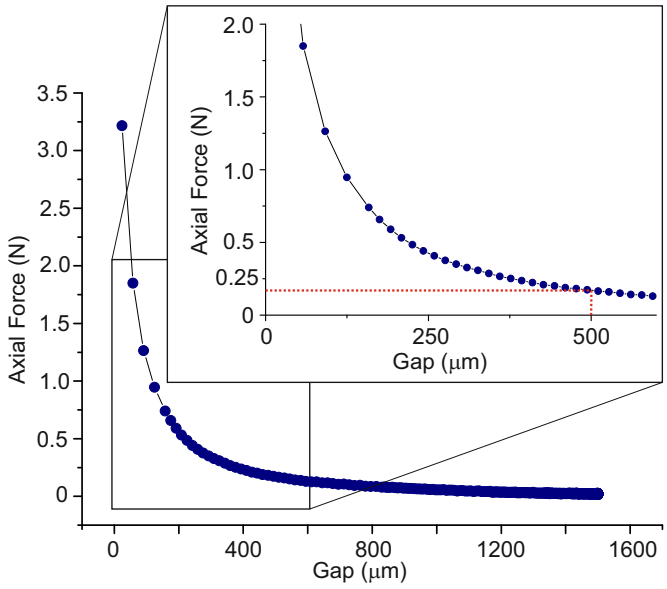

Figure 5.4. Test to determine the ideal gap in the plate–plate geometry. The gap was identified through a gap sweep, concurrently measuring the axial force applied to the samples. The objective was to choose a gap value at which the axial force was sufficient to compress the sample without causing breakage. The selected gap was fixed at 500 μm, corresponding to an approximate force of 0.25 N.

Table 5.1. Summary of the parameter values used to perform the three different oscillation tests. Hydrogels with and without cells are measured at different DIV along three weeks. All test were performed at 37°C with a 500 μm gap.

Parameters	Time Sweep	Strain Sweep	Frequency Sweep
Frequency ω (rad/s)	2π	2π	0.1-100
Strain γ (%)	5	0.1-100	5

Three different tests were performed on samples of PEGylated fibrin hydrogels with and without cells, with the aim of characterising their Young's modulus E. Changes in E might be caused by the presence of cells within the hydrogel structure, but also by the degradation of the hydrogel structure with time. For that reason, we performed a rheological characterisation of the samples at different DIVs along a three–week period. Each sample was used only for one test, and each test was repeated at least three times for statistical validation.

We started our measurements by performing, as a first step, a *time sweep test*, consisting in the application of a constant oscillation frequency, ω_0, and strain amplitude, γ_0, to provide information about the stability of the samples under shear deformations in time. This test was used to track the evolution of the hydrogel structure along time and to procure information such as solvent evaporation, degradation processes, or gelation mechanisms that might occur during the experiment duration.

As a second step, a *strain sweep test* was performed on the samples, in which the amplitude of the strain oscillation, γ, was changed periodically while the frequency, ω_0, remained constant (see Figure. 5.5a). This test was performed to determine the linear viscoelastic region (LVR). We note that, in the LVR regime, deformations are minimal and therefore the test can be safely carried out without damaging the microscopic structure of the sample, which is crucial to keep the scaffold and the inner neuronal network intact. For these experiments, ω was fixed to $\omega_0 = 2\pi$ rad/s (1 Hz) and γ was progressively increased from a 0.1 to 100% strain (see Table 5.1 for a summary).

As a final third step, a *frequency sweep test* was performed on the samples. Here, the oscillation frequency, ω, was progressively increased at a constant strain amplitude γ_0 (see Figure 5.5b). This test provided information about the rheological response of the hydrogels at different frequencies, and therefore at different timescales ($t \sim 1/\omega$), and revealed whether the sample softened or thickened at faster deformations. The tests were performed at a selected γ_0, ensuring that the sample remained in the LVR. For the present work, γ_0 was fixed at 5%, and ω increased from 0.1 to 100 rad/s.

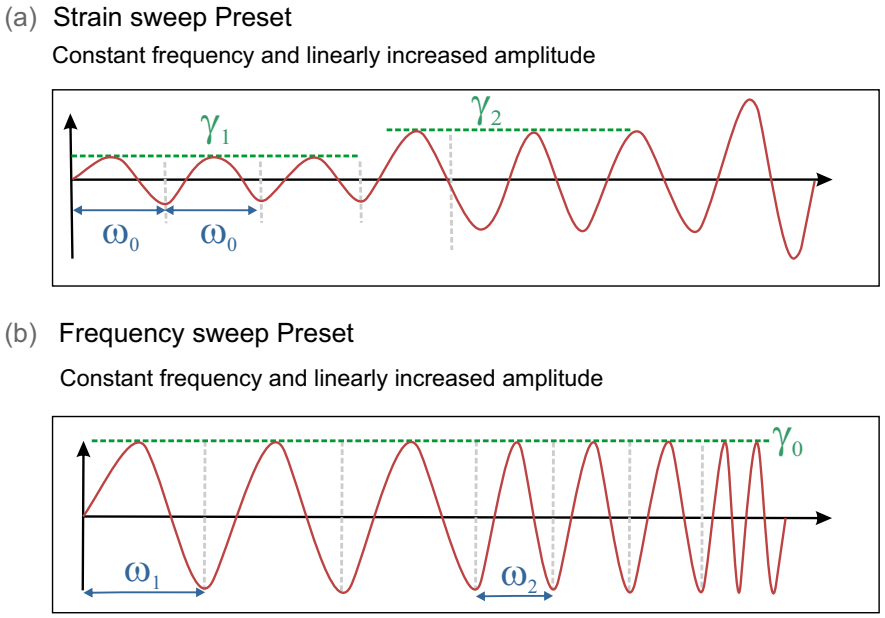

Figure 5.5. Established preset protocol for the mechanical characterisation of hydrogel samples. **(a)** Strain sweep test with constant ω_0 (blue) and varying γ (green). **(b)** Frequency sweep test with varying ω (blue) and constant γ_0 (green). Solid red lines represent the controlled shear deformation that oscillates sinusoidally.

5.3.3 Immunohistochemistry

The PEGylated fibrin hydrogels cultured with neurons were fixed with a 5% Paraformaldehyde solution (F8630-1G Sigma-Aldrich, St. Louis, MO, USA) in PBS for 30 minutes at room temperature, rinsed twice with PBS and incubated with a blocking solution containing 2% Triton (F8630-1G Sigma-Aldrich, St. Louis, MO, USA) and 5% Normal Goat Serum (Gibco, ThermoFisher Scientific, Waltham, MA, USA) in PBS for 2 h at room temperature and placed in a shaker (battery–powered Shaker KM 2, Carl Roth, Karlsruhe, Germany) at 75 RPM. A primary antibody against actinin (F8630-1G Sigma-Aldrich, St. Louis, MO, USA) was applied diluted in a blocking solution (1 : 300) and incubated overnight at 4°C while shaking. After rinsing 6 times with PBS, the Alexa568-conjugated secondary antibody against mice (Gibco, ThermoFisher Scientific, Waltham, MA, USA) was diluted in a blocking solution (1 : 400) and incubated for 2 hours at room temperature. The 3D cultures were then rinsed with PBS and mounted by using DAPI-fluoromount–G (1 : 500) (ShouternBiotech, Birmingham, AL, USA) and a CellMask Red Plasma Membrane Stain (Gibco, ThermoFisher Scientific, Waltham, MA, USA) for 1 hour at 75 RPM at room temperature. Immunocytochemical images were acquired on a confocal microscope (LSM800, Zeiss, Oberkochen, Germany; MicroFabSpace and Microscopy characterisation Facility, Unit 7 of ICTS "NANBIOSIS" from CIBER-BBN at IBEC).

5.4 Results

In this section we present the obtained results for the rheological characterisation of PEGylated fibrin hydrogels. Firstly, we measured the viscoelastic behaviour of the hydrogel scaffold, with and without cells, at DIV 1. This was useful in order to investigate whether the presence of neurons within the scaffold altered the characteristics of the bulk material. Secondly, we measured the hydrogels' response to the same tests along a three–week period to study the life span of the hydrogel structure and to assess whether the development of a neuronal network within the structure affected the mechanical properties of the final structure. Finally we show the results obtained from applying immunochemical techniques to the 3D cultures, demonstrating that there a healthy network of neurons was formed and that it extended across the entire 3D structure of the hydrogel.

5.4.1 Characterisation of hydrogels' viscoelastic behaviour

We characterised two different sets of samples of PEGylated fibrin hydrogels: a first set of pure PEGylated fibrin hydrogels, and a second set of PEGylated fibrin hydrogels loaded with neurons. For the latter, a calcium–imaging assay was carried out before any measurement to verify that the embedded neurons were healthy and spontaneously active.

As described before, three main rheological tests were performed, namely *time sweep* to evaluate the hydrogel's stability during a 15 min measurement at controlled shear deformation, with a constant ω_0 and γ_0, *strain sweep* to characterise the hydrogel's response to a varying amplitude strain γ with a fixed frequency ω_0, and *frequency sweep* to characterise the hydrogel's response to a varying frequency ω and fixed amplitude strain γ_0. In order to understand the experimental results, it must be noted that the accuracy of the equipment is an important constraint when designing the measurements since it bounds the range of exploration. For the HR-2 Discovery rheometer, the lower measurable limit corresponds to a 2 nN·m of oscillatory torque. According to this limit, some extracted values of G' and G'' from the strain sweep test were considered unreliable and therefore discarded.

Figure 5.6 shows the results obtained from the time sweep test for samples measured one day after preparation, i.e., at day *in vitro* (DIV) 1. The data points were obtained after averaging three different repetitions with the corresponding standard error.

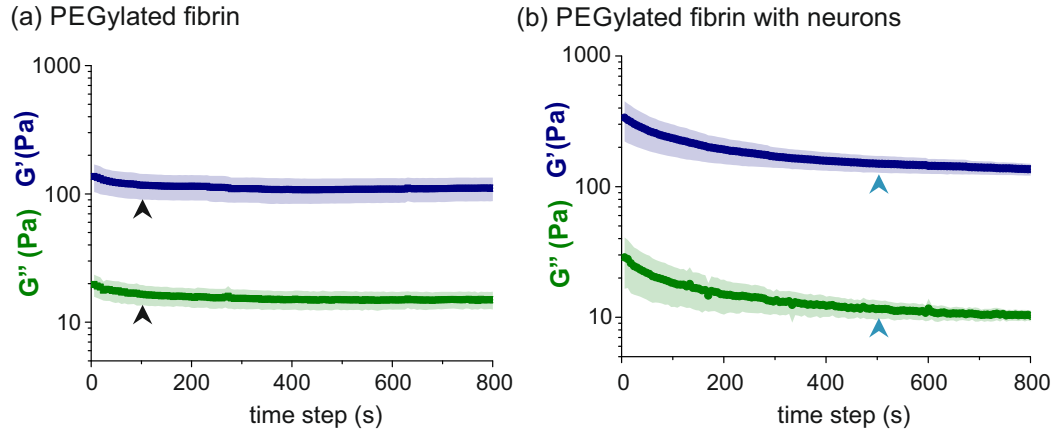

Figure 5.6. Time sweep results for **(a)** PEGylated fibrin hydrogels and **(b)** PEGylated fibrin hydrogels with neurons. Parameters ω_0 and γ_0 were fixed to 2π rad/s and 5%, respectively. Results show that samples reached equilibrium few minutes after the oscillatory effort was applied (arrowheads). Data are the average over 3 sample repetitions, and shadings are the corresponding standard errors.

When performing a time sweep test, a crossover between G' and G'' (leading to $G' > G''$) might be considered as a 'gelation point' of the sample. Figures 5.6a and 5.6b show the time sweep test for PEGylated fibrin with and without cells, revealing that the hydrogel's structure was already cured when the test was conducted and therefore no new structural links were formed within the hydrogel that could be ascribed to the longer relaxation time. As shown in Figure 5.6a, the hydrogel samples exhibited a stable response $\simeq$ 100 s after the deformation was applied (black arrowheads). The time taken to reach stability was about five times larger for the hydrogels with neurons (Figure 5.6b, blue arrowheads), meaning that the hydrogels with cells took longer to reach an equilibrium state after been subjected to an oscillatory deformation. We conjecture that the larger relaxation time is associated with the interwoven neuronal and hydrogel networks. The time sweep test results were reproducible across samples, with a consistent $G' > G''$ along the explored range, i.e., the curves never crossed. We typically measured a $G' \simeq 100$ Pa for the PEGylated fibrin scaffolds in the stable regime and $G' \simeq 200$ Pa for those samples containing neurons, indicating that the presence of the cells stiffened the scaffold. A G' value around 100 Pa was also reported in (Zuidema et al., 2014) for fibrin itself, which indicates that our protocol was properly adapted to measure the PEGylated fibrin hydrogel samples and that the results are consistent with the literature.

The strain sweep test was then performed to identify the LVR for the PEGylated fibrin hydrogels and to study in more detail whether the presence of the cells affected it. As shown in Figure 5.7a, the two types of samples (with and without cells) exhibited a small negative drift as the strain γ grew. Since the changes in G' and G'' were small enough in the region between the 1 and 10% strain, we considered them to be independent of γ.

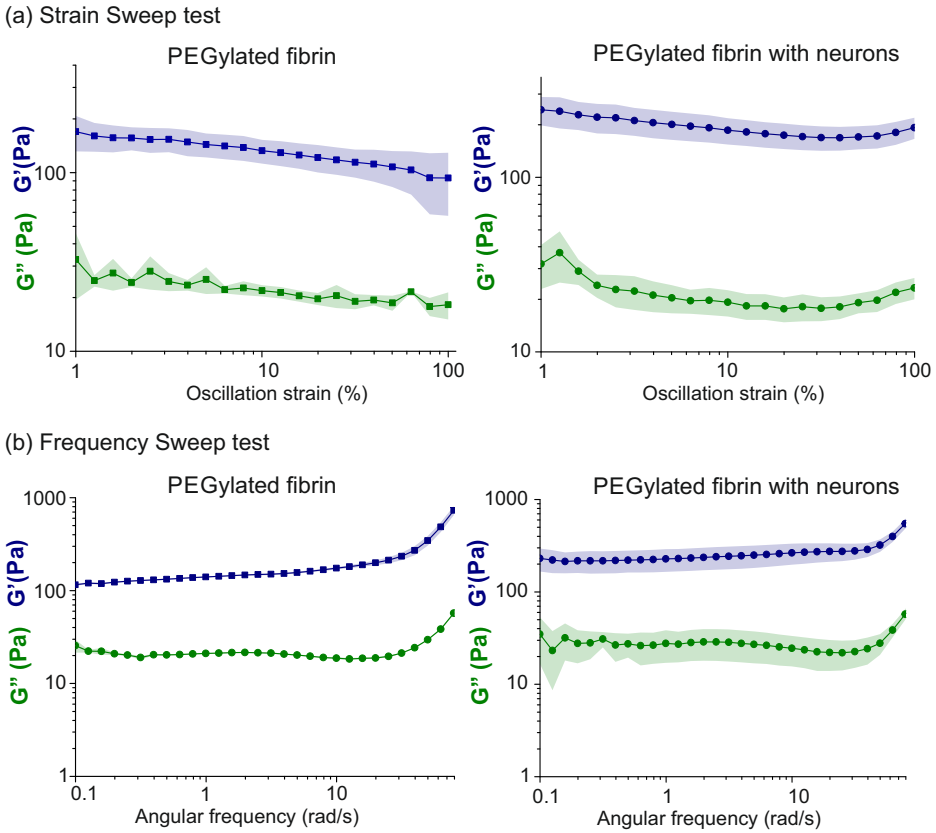

Figure 5.7. Characterisation of the viscoelastic behaviour of hydrogel samples with and without cells at DIV 1. The plots show the storage (G') and loss modules (G''), averaged over 3 repetitions with the corresponding standard errors. **(a)** Strain sweep test for PEGylated fibrin gels (left) and PEGylated fibrin gel with neurons (right), with $\omega_0 = 2\pi$ rad/s and γ in the range $[1, 100]\%$. **(b)** Frequency sweep test for PEGylated fibrin gels without neurons (left) and with neurons (right), with $\gamma_0 = 5\%$ and ω in the range $[0.1, 80]$ rad/s.

We then carried out a frequency sweep test for the samples with and without cells at $\gamma_0 = 5\%$, as shown in Figure 5.7b. This test is key to characterise the hydrogel structure since it informs us about the crosslinking grade of the internal structure of the hydrogel as well as whether the crosslinking reaction is reversible or not. As highlighted before, the absence of a crossing between the G' and G'' curves during the frequency sweep reveals a nonreversible chemically crosslinked structure (Stojkov et al., 2021), which comes together with the enzymatic reaction between thrombin and fibrinogen to form the fibrin hydrogel structure. The observed G' and G'' curves in Figure 5.7b are indeed typical for a hydrogel structure (Zhang et al., 2010), both exhibiting a plateau (despite small drifts or fluctuations) for low oscillation frequencies $\omega \lesssim 10$ rad/s that give evidence of a stable, crosslinked network whose values can be related to the stiffness of the hydrogel (Stojkov et al., 2021). The frequency tests also showed that $G' > G''$ for all frequencies, with $G' \simeq 100$ Pa for the PEGylated fibrin and $G' \simeq 200$ Pa for the

hydrogels seeded with neurons. Additionally, for all the hydrogels investigated, the mean value of δ, as derived from Equation (5.3) in the Materials and Methods section, was $\delta \simeq 0.1$ rad for both hydrogel preparations, a value that is consistent with an elastic response.

5.4.2 Time evolution of PEGylated fibrin hydrogels

To use PEGylated fibrin hydrogels as scaffolds for neuronal cultures, it is essential to understand the aging of the gels with time —as well as the impact of the embedded neuronal network— on their mechanical responses and overall stability. Indeed, knowledge of the stability of the scaffolds with time is crucial to prepare cultures with the appropriate lifespan and helps elucidating the impact of neuronal development and connectivity formation across the whole system. With this aim, we conducted a study on the temporal evolution of the mechanical properties of the hydrogel samples, with and without neurons. Since the values of G' are larger than those of G'' by a decade (see Figure 5.7), the elastic response dominates over the viscous behaviour. Thus, although both contributions exist, the hydrogels are predominantly elastic. We also note that, due to this elastic dominance, we do not show the plots of G'' in further analyses.

Time sweep tests were performed as the first step to verify the structural stability of the samples during the aging process when subjected to an oscillatory force. Next, strain sweep tests were performed on the samples with and without cells from DIV 1 to DIV 20 (Figure 5.8a). In both cases, the results showed a large sparsity across different DIVs, with the curves crossing one another within a range in G' values of $80 - 220$ Pa for the cell–free hydrogels and between $140 - 300$ Pa for the hydrogels laden with neurons. We note that, for the case of DIV 1, as exemplified in Figure 5.7a, the G' values exhibited as small negative drift with γ. This drift was also observed in the other DIVs along with a similar trend; i.e., the relative vertical position of the curves was maintained along γ. This stability in behaviour along the DIVs allowed us to take a fixed value of $\gamma_0 = 5\%$ for the frequency sweep test and for all the DIVs studied.

With this consideration in mind, Figure 5.8b shows the results obtained for the frequency sweep tests conducted at $\gamma_0 = 5\%$. Remarkably, the gel–characteristic low–frequency plateau (with a slight positive drift) was observed in all the samples at different DIVs for frequencies up to $\omega \simeq 30$ rad/s, indicating that neither the presence of cells nor the aging process induced substantial qualitative changes in the elastic behaviour of the hydrogel matrix. We note, however, that the drift along ω was more pronounced for the cell–free hydrogels, suggesting that the network matrix stabilized the hydrogel's response.

We also observed, as shown in Figure 5.8b, a strong thickening of the hydrogels at large frequencies ($\omega > 50$ rad/s) and for all the studied DIVs. This thickening at high-frequency oscillations could be related to the failure of the gel's network to rearrange

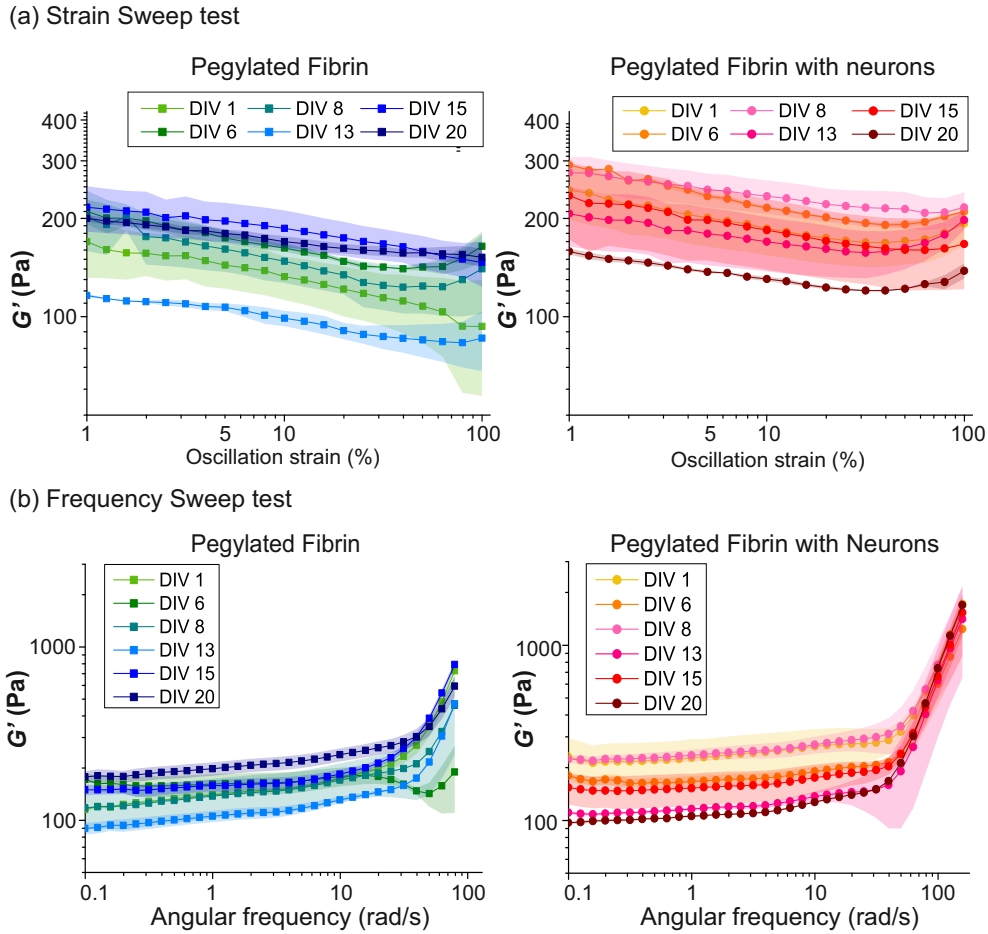

Figure 5.8. Evolution of PEGylated fibrin hydrogels with and without cells from DIV 1 to DIV 20. **(a)** Strain sweep test, with $\omega_0 = 2\pi$ rad/s and γ in the range $[1, 100]\%$. **(b)** Frequency sweep test, with $\gamma_0 = 5\%$ and ω in the range $[0.1, 100]$ rad/s. In all panels, G' values were averaged over 3 repetitions with the corresponding standard error shown as colored shadings. Data corresponding to PEGylated fibrin hydrogels without cells are shown on the left, and data with the inclusion of cells on the right.

when subjected to fast oscillations, i.e., short time–scale perturbations (Ghosh et al., 2005). We note, however, that high–frequency perturbations may induce inertia effects in the response of the hydrogel, and thus the observed thickening could reflect both the network's difficulty at rearranging itself and the inertial forces from the experimental system (Krieger, 1990; Ewoldt, Johnston, and Caretta, 2015).

To gain a deeper understanding of the evolution of the hydrogels' elasticity, we used the frequency test results (G' and G'') to calculate the Young's modulus E of the PEGylated fibrin hydrogels by using Equations (5.1) and (5.2) in the Materials and Methods section of this Chapter. The outcomes are shown as boxplots in Figure 5.9, which displays the distribution of E values divided into three evolutionary stages (early 'e', young 'y' and mature 'm') for the hydrogels with and without cells. The mean

value of the Young's modulus for each stage is indicated by a black horizontal line.

The distributions shown in the boxplot reveal that the presence of cells exert an effect on the internal structure of the hydrogels, altering the stiffness of the matrix. In the hydrogels without neurons, the Young's modulus remained approximately constant in terms of the experimental variability during development, with $E = 420 \pm 130$ Pa (mean $\pm$ standard deviation of the mean) ($p_{e-y} = 0.23, p_{y-m} = 0.97, p_{e-m} = 0.19$), demonstrating that the PEGylated fibrin hydrogels generate highly stable scaffolds. By contrast, for the hydrogels with neurons, the mean value of E within each evolutionary stage gradually decayed, from $E = 590 \pm 210$ Pa at the early developmental stages to $E = 340 \pm 100$ Pa at the mature ones, a decrease of practically a factor of two that was statistically significant ($p_{e-y} = 0.28, p_{y-m} = 0.011, p_{e-m} = 0.0055$). This substantial decrease in E is puzzling. Intuitively, one would expect that the formation of a neuronal network within the hydrogel strengthens its internal cohesion and makes it less deformable (higher E), but we observed the opposite. Thus, we hypothesize that the neurons altered the hydrogel microscopic organisation during network formation, either through physical damage from growing axons and dendrites or from enzymatic action from neurons.

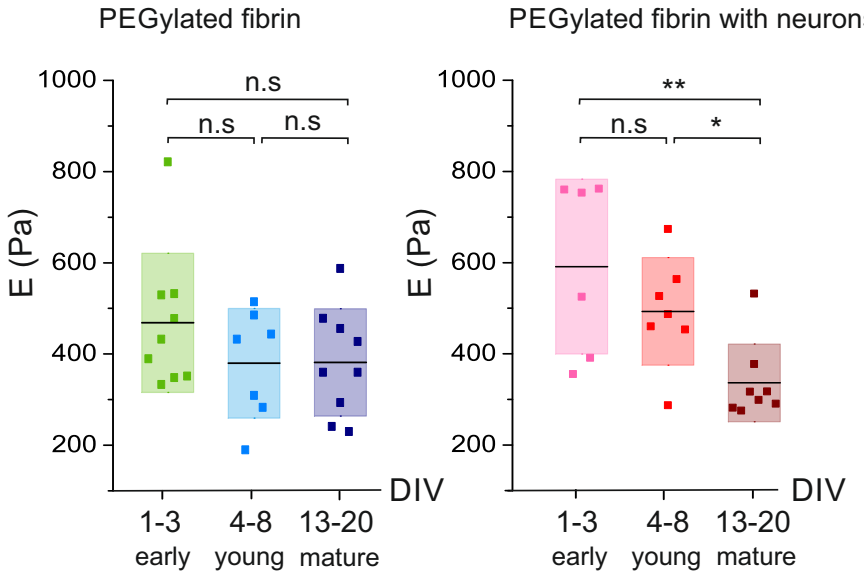

Figure 5.9. Evolution of the Young's modulus E with time for PEGylated fibrin hydrogels with and without neurons. Data are plotted as boxplot distributions of E values in representative stages of evolution, namely early (DIV $1-3$), young (DIV $4-8$) and mature (DIV $13-20$). Each dot in the boxplots is an experimental repetition. The black lines mark the mean of the distribution and the colour boxes mark the standard deviation. * $p < 0.05$, ** $p < 0.01$ (Student's t-test).

5.4.3 Immunostaining Results

The neuronal cultures grown within the PEGylated fibrin hydrogel were immunostained to examine the formation of the neuronal connections across the volume, providing evidence of healthy neuronal development as well as the neurons' capacity to extend processes and navigate beyond a single plane within the hydrogel (Figure 5.10). Actin was marked in red by using Alexa568 conjugated as a secondary antibody, together with a CellMask Red Plasma Membrane Stain that identified every cell body (the cytoskeleton and soma). The cell's nucleus was marked in blue with DAPI. These markers revealed that the neurons were extensively distributed throughout the entire volume of the hydrogel, forming connections along all three axes.

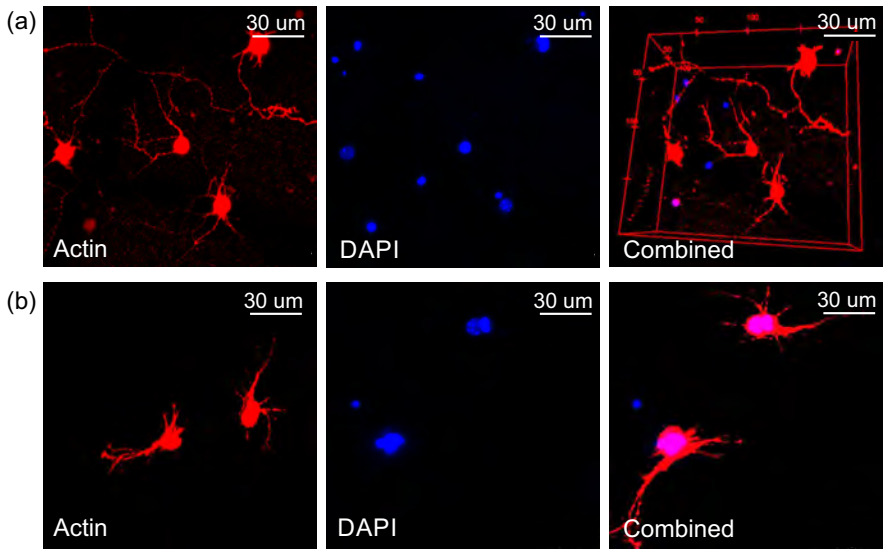

Figure 5.10. Immunostaining images of neurons within the 3D PEGylated fibrin hydrogel scaffolds showing actin in red (left) and nucleus in blue (center); the panels on the right are the merged images of both channels, showing concurrently the actin filaments and cell nuclei in the 3D culture. In the merged image, pink represents the overlapping of red (actin) and blue (nucleus). **(a)** Sample 1 of PEGylated fibrin hydrogel with neurons at DIV 7, **(b)** Sample 2 of PEGylated fibrin hydrogel with neurons at DIV 7.

Due to the difficulty of implementing immunostaining techniques in volumes, it was not possible to obtain results for the evolution of the neuronal network during development. Nevertheless, we concluded that the neurons established connections across different layers of the hydrogel matrix, as shown in Figure 5.10, which depicts two different samples of the PEGylated fibrin seeded with neurons at DIV 7. From these images, we measured that the axons had a typical diameter of 1 μm that could easily extend beyond 50 μm. These observations are compatible with the pore size of our hydrogels, in the range $2-8$ μm in diameter according to the data provided by Zhang et al., 2010, who investigated the structural properties of PEGylated fibrin hydrogels similar to ours by using scanning electron microscopy. Additionally,

neurons' morphology corresponds to healthy cells, a result that, together with the observation of spontaneous activity through calcium imaging, indicates that the neurons developed healthily and established a well–connected network.

5.5 Discussion

Building a 3D microenvironment for cell culturing is crucial to design *in vitro* models that better emulate the physiology and connectivity of *in vivo* circuits such as the brain (Frega et al., 2014). However, reproducing the complexity of *in vivo* cell–cell as well as cell–matrix interactions remains a challenge, particularly due to the difficulty of choosing adequate ECM–like materials that support cell development.

To advance in this quest, here we investigated the mechanical properties of hydrogels, a family of synthetic materials widely used in neuroscience given their versatility in tailoring both chemical and mechanical properties to fit particular requirements. We focused our attention on PEGylated fibrin, a semisynthetic hydrogel made of PEG and a fibrin gel. On the one hand, PEG is one of the most used polymers in biomedical applications due to its biocompatibility, its nontoxicity and its good biodegradability. However, it shows a low cellular adhesion, which makes it, in principle, not suitable for cell culturing (Pasut and Veronese, 2006). On the other, fibrin gels are composed of a mixture of two blood coagulation components, fibrinogen and thrombin (Mosesson, 2005; Ozgun et al., 2022). Fibrinogen is a blood plasma protein involved in blood clotting during the coagulation process. Thrombin acts as a serine protease and initiates the polymerization reaction in which the soluble fibrinogen is converted into insoluble strands of fibrin that polymerize into a 3D organised clot (Blombäck and Bark, 2004). The main drawback of fibrin gels is that they are extremely susceptible to protease–mediated degradation, so they cannot be used for long–term cell culturing. Thus, to overcome the limitations presented by these two materials separately, an innovative strategy consists of combining them together through a reaction named *PEGylation*. This reaction involves the terminal hydroxyl group of the PEG molecules and the amino groups of the fibrinogen protein to generate a molecular crosslinking that enhances the stability of the bonds and reduces the degradation of the material (Liu, Collins, and Suggs, 2006; Damodaran and Fee, 2010). However, the PEGylation of fibrin hydrogels reduces cell attachment as PEG molecules chemically modify fibrin binding sides (Mosesson, 2005; Liu, Collins, and Suggs, 2006). Despite this fact, PEGylated fibrin has been successfully used in cellular cultures (Zhang et al., 2010), showing that the reduction in binding sites does not interfere with the viability of the hydrogel. Therefore, the resulting semisynthetic hydrogel demonstrates an overall excellent biocompatibility, adequate cellular adhesion and sufficient stability with time to support extended cell culturing.

Despite the growing importance of PEGylated fibrin hydrogels, little is known about their mechanical properties, and even less about their evolution with time in

realistic experimental conditions. Indeed, the mechanical properties of the matrix can affect axon stability and development, which can result in different neuronal networks depending on the final stiffness of the material (Long and Huttner, 2019; Lam et al., 2019; Si, Gong, and Yang, 2023). The relative composition of thrombin and fibrinogen in the fibrin hydrogel significantly influences its bulk properties (Rowe, Lee, and Stegemann, 2007). Therefore, it becomes imperative to characterise the precise mechanical properties of the resulting hydrogels and compare them to the mechanical behaviour of the human brain. This evaluation is vital in determining whether the hydrogel adequately mimics the mechanical environment required for optimal neuronal growth and functionality.

Indeed, neurons in their natural *in vivo* environment experience mechanical forces from the brain ECM as well as interactions with neighbouring cells. These mechanical cues play crucial roles in various neuronal processes, including migration, the regulation of synapse formation and the plasticity of the existing synapses. These effects are achieved through mechanotransduction, where neurons sense and respond to the biomechanical properties of their surrounding environment (Javier-Torrent, Zimmer-Bensch, and Nguyen, 2021). Considering the significant impact of mechanical forces on neuronal development and functionality, the material chosen to construct the scaffold should meet specific criteria to facilitate the healthy growth of the neuronal culture. In our study, we investigated the behaviour of PEGylated fibrin scaffolds and showed that they exhibited the properties of elastic gels. These hydrogel matrices provide the necessary stiffness for neurons to attach and proliferate effectively. In turn, they create a suitable porous and hydrated environment that facilitates the dynamic flow of nutrients and waste products.

Several studies have analyzed human brain tissue to understand its viscoelastic behaviour and to establish a relationship between its mechanical properties and neuronal development. Budday *et al.* combined compression and tension shear stress to conclude that the human brain is a nonlinear elastic tissue that dissipates stress over time and presents a compression–tension asymmetry (Budday et al., 2017; Kim and Choi, 2019). Related to this, recent studies have shown that the brain Young's modulus E^{Brain} depends on the analyzed region (Barnes, Przybyla, and Weaver, 2017) and the stage of development (Samanipour et al., 2022), with values ranging from $E^{\text{Brain}}_{\text{early}} \simeq 110$ Pa after birth to $E^{\text{Brain}}_{\text{mature}} \simeq 1$ kPa in adulthood, an increase of a factor of 10 that can be ascribed to the formation and refinement of the connections within the ECM matrix. These values fall within the range of our measurements, with $E^{\text{PEG-Fib}}_{\text{neurons, early}} \simeq 590$ Pa and $E^{\text{PEG-Fib}}_{\text{neurons, mature}} \simeq 340$ Pa (Figure 5.9), although we observed the opposite trend, with the Young's modulus decreasing with development. Since in our experiments we had measurements without neurons as a reference, with $E^{\text{PEG-Fib}}_{\text{no cells}} \simeq 420$ Pa, we hypothesize the following scenario: Firstly, the presence of neurons makes the hydrogel stiffer, possibly due to the attachment of cells to the microscopic fabric of the scaffold in combination with the swift development of connections (axons and dendrites),

effectively increasing the hydrogel Young's modulus to about 590 Pa. We note that network formation in early developmental stages is highly dependent on the neuronal spatial arrangement and density, as observed in 2D cultures (Tibau et al., 2020), which may explain the strong variability in the DIV $1-3$ stage of Figure 5.9. And, secondly, as neurons within the hydrogel start to exhibit strong collective activity, by DIV $4-8$ (Tibau et al., 2020; Montalà-Flaquer et al., 2022; Estévez-Priego et al., 2023), they undergo a readjustment of connectivity that leads to the pruning of axons, which translates into a weakening of the scaffold's cohesion and a reduction in its Young's modulus down to about 340 Pa.

Our hypothesis is consistent with the development of neurons in their natural, brain-like environment. Spedden *et al.*, for instance, observed that the stabilization of neurons' microtubule cytoskeleton affects the stiffness of the brain (Spedden et al., 2012). Additionally, during the maturation of the nervous system, the mechanism known as pruning has been extensively reported, in which structural connections between neurons are removed by retracting previously formed axons. Pruning allows the neuronal network to re–evaluate its own efficiency and to selectively eliminate connections between neurons that do not exhibit a strong functional association (Low and Cheng, 2006). Pruning plays a crucial role in shaping the neural circuitry, refining connectivity and optimizing the overall functionality of the nervous system as it develops. In the aforementioned study by Spedden et al., 2012, they applied fluorescence and atomic force microscopy to analyze the elasticity maps of living neurons and observed that an initial increase in neuronal stiffness was followed by a subsequent decrease as a result of pruning events. This decrease in stiffness was related to the depolymerization of the microtubule structures in the connections that were removed. Overall, these observations suggest a direct correlation between the mechanical properties of neurons and the structural modifications that occur during the development of neuronal networks. Thus, for our hydrogels with neurons, we attribute the sharp increase in the Young's modulus and subsequent decrease to intrinsic formation–pruning processes in network connectivity that are fundamental to shape a healthy and richly active neuronal culture.

PEGylated fibrin hydrogels are extremely easy to prepare and manipulate, but they are highly sensitive to the details of the preparation process. We indeed observed important differences in the rheological behaviour of the hydrogel batches that slightly differed in their preparation protocols, most notably their temperature and neuronal density. For this reason, the standard error was remarkably high at some developmental timepoints (see, e.g., the strain sweep tests at DIV 1 in Figure 5.7). Due to this variability across repetitions, some extracted values of G' and G'' from the strain sweep test were considered unreliable and therefore discarded. It is noticeable that most of the variability occurred at DIV 1, which indicates that the neuronal density, and possibly the neuronal distribution across the 3D matrix, strongly dictated the initial spread of the neural connections and thus the elastic behaviour of the material.

As a final remark, we note that our experiments were carried out with mouse primary neuronal cultures, but they could be extended to hiPSCs given their relevance in medical applications, particularly in the context of neurological disorders. However, hiPSCs require longer protocols as compared to primary cultures (Estévez-Priego et al., 2023) and are more difficult to maintain *in vitro*. We preferred to use primary cultures to be sure that a healthy neuronal network was formed and that it remained functional for the three–week period of analysis. Nevertheless, there are already studies that explored the behaviour of hiPSCs in 3D environments, such as the work of Samanta et al., 2022 who considered induced cortical neurons in hyaluronic acid–based scaffolds, or the work of Adil *et al.*, who built hiPSC–derived dopaminergic neurons in a Mebiol thermoresponsive hydrogel (Adil et al., 2017).

5.6 Conclusions

We introduced PEGylated fibrin hydrogels as competitive candidates for culturing primary neurons in a 3D matrix and rheologically characterised them in order to prove their viability to host living cells for as long as three weeks. We observed that the 3D matrix itself, without neurons, exhibited an elastic response with a Young's modulus $E^{\text{PEG-Fib}}_{\text{no cells}} \simeq 420$ Pa that remained remarkably stable throughout the investigated time frame. Such a stability indicates the suitability of PEGylated fibrin hydrogels by themselves for long–term biomedical applications. The observed elastic behaviour of the bulk material persisted when the neurons were grown inside the hydrogel, but the Young's modulus boosted at early stages to $E^{\text{PEG-Fib}}_{\text{neurons}} \simeq 590$ Pa and then gradually decayed with time up to about 340 Pa. Based on the intrinsic processes related to the formation of a neuronal network, most notably the fast growth of axons followed by intensive pruning, we conclude that the decay in the Young's modulus is associated with natural processes within the network that are difficult to control or act on. Thus, our results show that PEGylated fibrin hydrogels are by themselves excellent materials, but one has to be prudent when growing neurons within them since the intrinsic functional development of the embedded neuronal network may alter the mechanical properties of the material with time. This aspect may be important when deciding timepoints of interest to monitor activity in such networks or when designing tailored 3D *in vitro* models for medical applications.

6 Impact of hydrogel's thrombin concentration on the behaviour of 3D neuronal cultures

6.1 Introduction

In vitro systems have played a crucial role in understanding the physiological mechanisms and pathological conditions of the nervous system, while also serving as platforms for assessing the safety and effectiveness of potential therapeutic agents. Nevertheless, most of these experiments are conducted on flat, unnaturally rigid substrates like silicone elastomers or glass. These rigid substrates fail to replicate the intricacies of the *in vivo* environment, leading to altered cellular behaviour and response. Hence, 3D cell culture systems were introduced to leverage their advantages over 2D platforms. Central to this transition is the careful selection of the bulk materials in which cultures are realized, as well as the strategic tuning of their mechanical properties.

Due to the structural resemblance of hydrogels to native tissue, they have proven useful across diverse cell culture applications, being able of regulating cell behaviour in ways not possible with conventional culture substrates (Petersen et al., 1992; Musah et al., 2012). When selecting a suitable hydrogel, researchers might consider factors such as the adhesivity of cells, the stability of the formed culture, as well as biophysical properties such as the hydrogel Young's modulus, which needs to be similar to the one reported for human brain tissue (Barnes, Przybyla, and Weaver, 2017; Samanipour et al., 2022). Fibrin hydrogels are widely used for biomedical applications due to their rich bioactivity and the convenience that they offer in tailoring material attributes through the manipulation of fibrin polymerization dynamics.

Fibrin is a product of the coagulation cascade, its polymerization starts when the serine protease thrombin converts the soluble precursor molecule fibrinogen to fibrin (Weisel, Nagaswami, and Makowski, 1987). In addition to polymerising, fibrin fibers are able to branch out, forming a 3D network that gives fibrin its gel–like characteristics. The distances between branching points, as well as their total number, may vary depending on the original structure of the fibrinogen molecule and the conditions of polymerization (Ryan et al., 1999). Therefore, the polymerization process directly affects the porosity, fiber thickness and degree of branching of the gel, setting the mechanical properties of the final structure. By changing the amount of fibrinogen,

thrombin or even the concentration of salts present in the clot, researchers are able to modulate the final microstructure of the fibrin gel.

It has been reported that the thrombin concentration present at the time of gelation profoundly influences the fibrin hydrogel structure (Wolberg, 2007; Weisel and Litvinov, 2013). Low concentrations of thrombin lead to the formation of fibrin gels formed by thick fibers, few branching points and large pores (Figure 6.1a). On the other hand, high concentrations results in gels consisting of tightly packed thin fibers. An increase in thrombin concentration generates the cleavage of more fibrinogen molecules, leading to the release of protofibrils and the subsequent polymerization of fibrin. This results in the formation of a dense fibrin network, giving on to the strengthening and stabilization of the blood clot (Brown and Barker, 2014) (Figure 6.1b). Taking these factors into consideration, the stiffness of the final hydrogel correlates well with thrombin concentration and, thus, optimization of rheological properties for culturing can be achieved by tuning the final amount of thrombin.

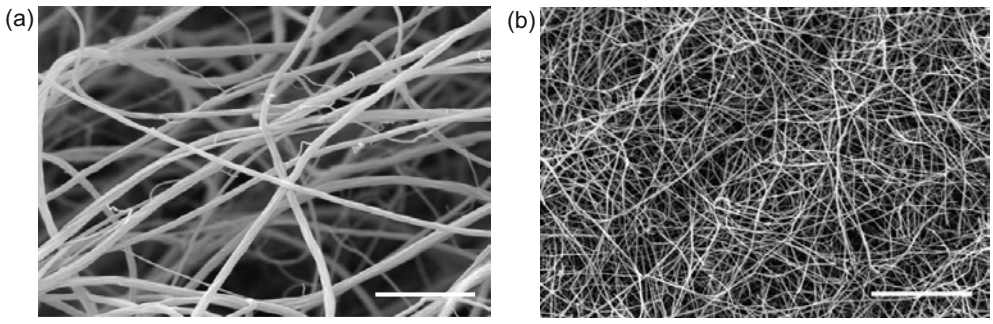

Figure 6.1. Example of SEM micrographs for fibrin clots with different concentrations of thrombin (exctrated from Weisel, 2004). **(a)** Recalcified plasma with low thrombin concentration presents thick fibers and few branching points. **(b)** Recalcified plasma at high thrombin concentration has thin fibers and many branching points. Scale bars correspond to 5 μm.

Fibrin's structure can be also tailored by a polymeric modification, particularly by introducing PEG polymer chains in the hydrogel's recipe. PEG can be crosslinked with fibrin's natural fibers by a reaction known as *PEGylation* (Liu, Collins, and Suggs, 2006; Damodaran and Fee, 2010). The synthetic polymer within the system establishes a network of interconnections with regulated mechanical attributes and degradation, whereas the natural part provides the distinct ECM for controlling neuronal cell morphogenesis (Berkovitch and Seliktar, 2017). The resultant hydrogel, named *PEGylated fibrin*, presents enhanced degradation kinetics and mechanical properties of the structure (Temenoff et al., 2002). PEGylation of fibrin is pivotal to expand the life–span of the fibrin hydrogels (Liu, Collins, and Suggs, 2006) as PEG coating prevents the recognition of fibrin fibers by proteolytic enzymes that can lead to a degradation processes. This is crucial for applications in which the matrix needs to provide mechanical support during a long period of time. Thus, the described semisynthetic hydrogel demonstrates

an overall excellent biocompatibility, adequate cellular adhesion and sufficient stability with time to support extended cell culturing.

Several studies have revealed that neuronal growth *in vitro*, development patterns, neurite extension and branching patterns change with substrate stiffness (Balgude et al., 2001; Flanagan et al., 2002; Jiang et al., 2010). In Koser et al., 2016, two substrates with different stiffness were used to culture retinal ganglion cell to prove axon mechanosensitivity. They concluded that axons grow faster on stiffer substrates, straighter and more parallel. On the other hand, a lower stiffness promotes slowed exploratory growth and splaying of axons. In addition, it has been reported that substrate flexibility had also a significant effect on neurite branching. Neurons grown on softer substrates formed more than three times as many branches as those grown on stiffer gels (Flanagan et al., 2002). However, an increased gel stiffness has been reported to decrease the rate of neurite extension (Balgude et al., 2001). In this sense, a balance needs to be reach in order to optimize mechanical properties and maximize neurite number and extension. In this regard, considering not only the substrate stiffness but also its pore size is crucial. Larger pores in matrices facilitate easier axon spreading, while too small pore sizes can hinder the exploration of the entire matrix volume. Thus, the internal microstructure and the mechanical properties of the matrix can affect axon stability and development, which can result in different neuronal networks depending on the final stiffness of the material (see Figure 6.2).

With all this background in mind, and considering that the mechanical traits of PEGylated fibrin hydrogels rely, among other factors, on thrombin concentration, and acknowledging the correlation between axon growth, network development, and matrix rigidity, a question arises: Can we fine–tune the functional connectivity of the resultant network through hydrogel stiffness manipulation?

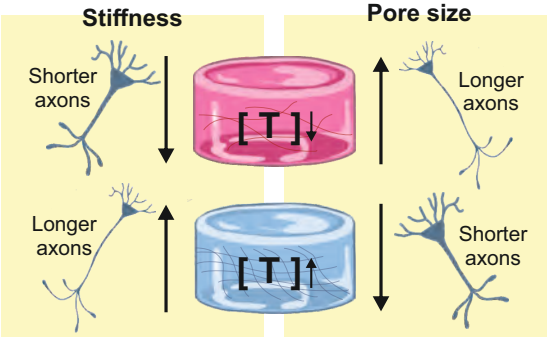

Figure 6.2. Competition between stiffness and porosity in determining axon length. In hydrogels with lower thrombin concentrations (pink hydrogel), the reduced stiffness leads to shorter axons, yet the larger pores facilitate longer axons. Conversely, higher thrombin concentrations (blue hydrogel) yield increased stiffness, resulting in longer axons; however, the smaller pore size hinders axonal growth, leading to shorter axons.

To answer this question, and to bridge the gap between scaffold mechanical attributes and the nature of emerging functional connectivity, we fabricated three distinct variants of PEGylated fibrin hydrogels, each employing a different thrombin concentration. These hydrogels were then utilized to investigate the functional arrangement of the resultant networks, which were extracted from GTE analysis of spontaneous activity recordings. Considering all the factors mentioned earlier, our hypothesis postulates that hydrogels with higher concentrations of thrombin will exhibit an increased stiffness. This trait will, in turn, influence the neural network formed within the scaffold. We conjecture that, as the hydrogel's stiffness increase, the resulting network becomes more intricately compartmentalized due to the competition between the stiffness and the porosity of the resultant matrix. Consequently, we expect the following direct correlation to emerge: higher thrombin levels lead to an increase in network segregation since axons may find difficult to extend long distances and would therefore connect to more local neighbourhoods. Such a correlation is illustrated in Figure 6.3.

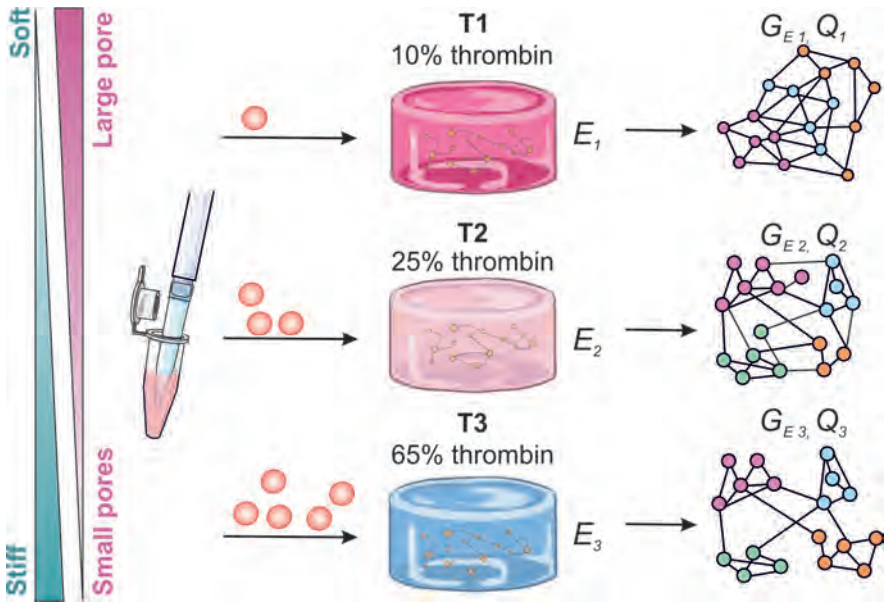

Figure 6.3. Schematic representation of the experimental procedure followed for assessing the relationship between the mechanical properties of the hydrogel scaffold and the functional organisation of the neuronal network. Three different types of PEGylated fibrin hydrogels, named T1, T2 and T3 were prepared by changing the amount of thrombin in the hydrogels preparation. We measured the hydrogels' Young's modulus in order to determine the stiffness of the hydrogel. Finally we recorded the spontaneous activity of neurons in culture to extract the main features of the functional neuronal network developed within the scaffolds, namely the global efficiency G_E and the modularity Q.

6.2 Objectives

The aim of this study is to establish a relationship between the mechanical characteristics of the hydrogel scaffold and the presence of specific functional connectivity features in the resultant neuronal network. By modifying thrombin concentration in PEGylated fibrin, we prepared three different hydrogel scaffolds. These samples were subsequently evaluated in terms of their stiffness and elasticity by using rheological techniques. Then, they were used for culturing primary cortical neurons extracted from mouse embryos. By applying calcium imaging techniques, we recorded spontaneous neuronal activity over a time span of 20 days. The ensuing functional organisation of these networks was then investigated by applying tools based on complex networks and, when possible, functional traits were compared to the progression of the matrix's mechanical characteristics.

To summarize, the main objectives of this Chapter are:

- To prepare neuronal cultures embedded in different types of PEGylated fibrin hydrogels by changing the concentration of thrombin.
- To characterise the rheological behaviour of the different hydrogels and its evolution with time by applying the protocol designed in Chapter 5.
- To track the evolution of functional features of neuronal networks built in the different types of hydrogels.
- To establish a relationship between the stiffness of the hydrogel and the emergence of distinct functional organisational traits in neurons grown within the scaffold.

6.3 Materials and methods

To achieve this, We prepared PEGylated fibrin hydrogels characterised by three varying concentrations of thrombin. We measure their Young's modulus through the rheological measurements introduced in Chapter 5. Finally, we computed key functional features of the neuronal networks by analysing data extracted from spontaneous activity recordings of neurons in culture within the 3D hydrogel scaffolds. A schematic representation of the followed experimental procedure is shown in Figures 6.3 and 6.4.

6.3.1 PEGylated fibrin hydrogels preparation with different thrombin concentrations

For these experiments we prepared three different types of PEGylated fibrin hydrogels with concentrations of 10%, 25% and 65% in volume of thrombin. We will refer to

them as T1, T2 and T3 PEGylated fibrin, respectively. We note that the T2 configuration corresponds to the hydrogels employed in Chapter 5.

PEGylated fibrin hydrogels were prepared as explained in Chapter 3. As a reference, we initially considered a hydrogel volume of 100 μL (Figure 6.4), as used in Chapter 5, and whose composition for T1, T2, and T3 is summarized in Table 6.1. However, these volumes procured very small networks that, possibly, contained an insufficient population of neurons for a reliable functional analysis. Thus, to ensure that the networks in the present study were sufficiently large, we also considered 800 μL hydrogels prepared in 4–well plates with a well's size of 13 mm in diameter and 10 mm in height (Figure 6.4). Such networks could easily house about 1,000 neurons. Table 6.2 summarizes the exact quantities used to prepare 800 μL PEGylated fibrin hydrogels.

It is important to note that we kept a constant concentration of fibrinogen throughout the experiments, so that the differences observed across hydrogels were only caused by changes in the thrombin levels. Additionally, the cell concentration was adjusted to be the same across all scenarios, with a uniform distribution of neurons upon plating. Once prepared, hydrogels were incubated at 37°C, 5% CO_2, and 95% humidity. At DIV 5 Plating medium was replaced to Changing Medium to limit glial growth, and thereafter at DIV 7 to Final Medium (see Table 3.1 for details). From here onwards, Final Medium was refreshed every two days.

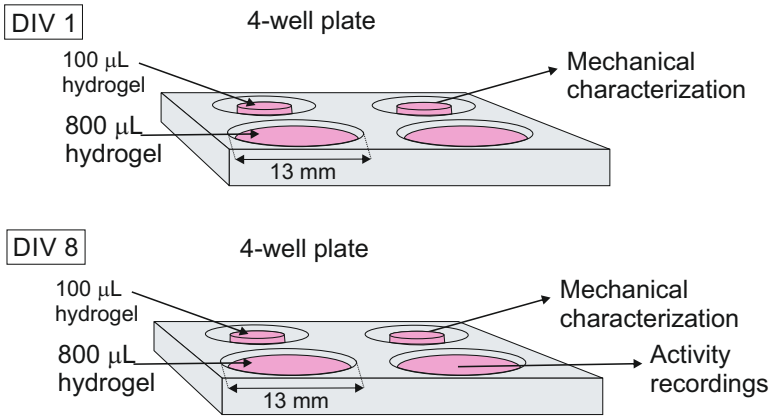

Figure 6.4. Protocol for rheological and neuronal activity measurements. At DIV 1, 100μL hydrogels were used for mechanical characterisation of the samples; 800μL hydrogels were not ready to record activity since the neurons start expressing the fluorescence probe at DIV 7. Sample used in the rheometer were discarded after the measurements. AT DIV 8, 100μL hydrogels were used to characterise the evolution of the mechanical properties of the samples, and discarded afterwards. Neuronal activity was recorded in parallel from 800μL hydrogels. These hydrogels were kept in the incubator until DIV 20.

Table 6.1. Volumes for preparing 100 μL hydrogels for the different concentration of thrombin (T1, T2 and T3). Note that the amount of PEGylated fibrinogen solution is kept constant for the three samples.

Hydrogel	Cell medium (μL)	PEGylated fibrinogen (μL)	Thrombin (μL)
T1 (10%)	65	25	10
T2 (25%)	50	25	25
T3 (65%)	10	25	65

Table 6.2. Volumes for preparing 800 μL hydrogels for the different concentration of thrombin (T1, T2 and T3). Note that the among of PEGylated fibrinogen solution is kept constant for the three samples. In all the mixtures, GCaMP6s calcium sensor was included in a 1 : 1000 ratio.

Hydrogel	Cell medium (μL)	PEGylated fibrinogen (μL)	Thrombin (μL)
T1 (10%)	520	200	80
T2 (25%)	400	200	200
T3 (65%)	80	200	520

6.3.2 Rheological characterisation

The rheological protocol described in Chapter 5 was also used here to characterise T1, T2 and T3 PEGylated fibrin hydrogels. As a reminder, a bulk rheometer HR-2 Discovery was used with an 8 mm plate–plate geometry and a fixed gap of 500 μm. Sandpaper was attached to both surfaces of the plate–plate geometry to prevent the hydrogel from slipping during the measurements (Divoux, Barentin, and Manneville, 2011). A solvent trap was used to avoid the evaporation of the liquid contained in the hydrogel during the test. All tests were performed at a constant temperature of 37°C, the physiological temperature of living neurons. Each sample was used only for one test, and each test was repeated at least three times for statistical validation.

We performed the three different tests described in Chapter 5 on the PEGylated fibrin hydrogels: time sweep, strain sweep and frequency sweep tests. We always used the parameters described in Table 5.1. Experiments were carried out along a three–week period to investigate the evolution of the Young's modulus E along time for T1, T2 and T3 hydrogels seeded with neurons.

6.3.3 Functional analysis

We assessed the functional connectivity of cells in cultures embedded in 800 μL PEGylated fibrin hydrogels. To do so, spontaneous neuronal activity was recorded for

15 min at 33 fps from DIV 7, when cells started to express the fluorescence marker, until DIV 20 to track the cell culture viability for the same period than for the rheological characterisation. We note that our microscopy equipment allows us to record a single plane at a time of the entire 3D structure (marked in red in Figure 6.5), and therefore our 2D recording is a proxy of the 3D behaviour.

Activity recordings were analysed by using our custom–made Matlab software NETCAL (Orlandi et al., 2017). A typical raster plot from a 3D culture at DIV 15 is plotted in Figure 6.5. Functional connectivity was then computed by applying GTE together with the *Brain Connectivity Toolbox* run in Matlab, as explained in detail in Chapter 3. The functional analysis was performed for networks developed within the hydrogels in order to compare the values of global efficiency G_E and modularity Q. By relating them with E, obtained from the rheological characterisation, we established a relationship between the scaffold stiffness and the functional organisation of the resulting network along a three–week period.

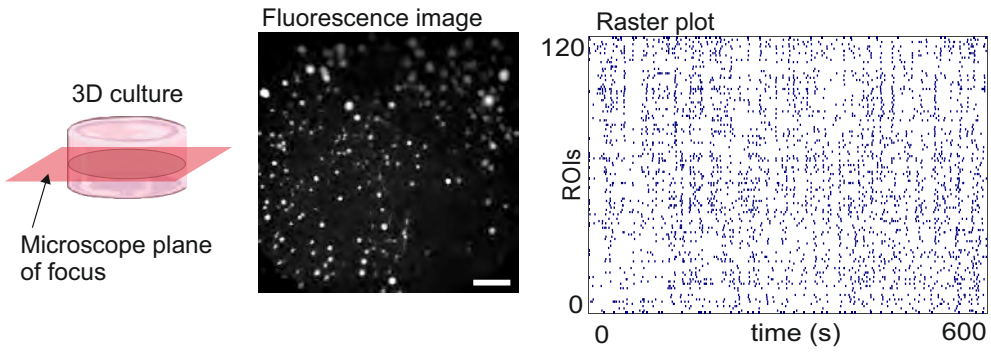

Figure 6.5. Activity recording in 800μL hydrogels. We captured a single plane of the entire 3D volume of the hydrogel (left), and a representative fluorescence image of such plane (center) depicts the neurons within the hydrogel as bright objects. A raster plot (right) illustrates the obtained data. Scale bar is 1 mm.

6.4 Results

In this section, we present, firstly, the outcomes of the rheological characterisation conducted on the PEGylated fibrin hydrogels samples, T1, T2, and T3 seeded with neurons. The primary objective is to comprehend the alterations in the mechanical response resulting from variations in thrombin. Following our approach from Chapter 5, we initiated the investigation by evaluating the rheological attributes of the samples at DIV 1. Subsequently, we inspected potential modifications over a span of three weeks due to the presence of neurons within the scaffold.

Secondly, we describe the findings related to the functional analysis of the neuronal networks developed within each hydrogel variant. This allows us to discern whether

the mechanical characteristics of the scaffold exert any influence on the functional arrangement of the living neuronal networks.

6.4.1 Rheological characterisation of T1, T2 and T3 PEGylated fibrin hydrogels

Hydrogels (loaded with cells) were studied as scaffolds for neuronal networks by using SAOS rheology, as it provides direct information about the bulk mechanical properties of the material (Yan and Pochan, 2010; Stojkov et al., 2021). Since we recorded activity for the study of functional connectivity, viability test were already conducted. These test were successful for T1 and T2 samples, in which we were able to capture spontaneous neuronal activity from DIV 7 to DIV 20. Unfortunately, no evidence of neuronal activity was found for T3 hydrogels. We hypothesised that the high amount of thrombin impaired the ability of neurons to distribute themselves throughout the 3D structure and to develop healthy connections.

Characterisation of hydrogels' viscoelastic behaviour

Figure 6.6 shows the results for the time sweep tests applied to the T1, T2 and T3 samples at DIV 1. Data points were obtained after averaging three different repetitions with the corresponding standard error.

Time sweep test showed a stable response of the hydrogels samples after a stabilization period, being $\simeq 150$ s for T1 and T3 samples and $\simeq 300$ s for T2 hydrogels (black arrows). This clearly indicated that T2 hydrogels took longer times to reach an equilibrium state after been subjected to an oscillatory deformation. For all samples of PEGylated fibrin, results were reproducible with $G' > G''$ during the studied range of time, meaning that the elastic component of the hydrogels is more important than the viscous one. This fact evidenced that the hydrogels were cured and presented a 'solid–like' behaviour.

Strain sweep tests were then performed at DIV 1 to investigate whether changes in thrombin concentration affected the range of the linear viscoelastic region (LVR). The left panels of Figure 6.7 reveal that all sample types (T1, T2 and T3) displayed a slight negative trend as the strain γ increased. Given the marginal fluctuations in G' and G'' within the range of 1 to 10% strain, we considered them to be uncorrelated with γ. We fixed $\gamma_0 = 5\%$ to perform the frequency sweep test for the three different samples. This frequency test is used to characterise the changes in the hydrogel's structure caused by the concentration of thrombin, since it tells us about the crosslinking grade of the internal structure of the hydrogel. Results are depicted in the right panels of Figure 6.7. As noticed in Chapter 5, the observed G' and G'' curves are typical for a hydrogel structure (Zhang et al., 2010), both displaying a plateau at low oscillation frequencies $\omega \lesssim 10$ rad/s, providing evidences for a stable, crosslinked network whose values

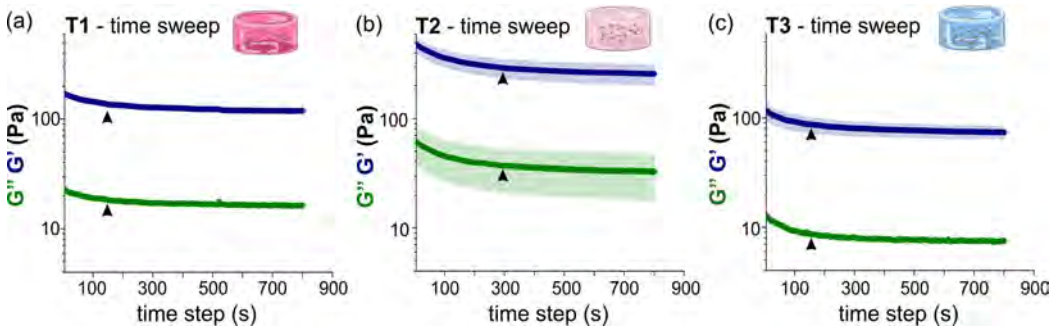

Figure 6.6. Time sweep results for **(a)** T1 (10% thrombin), **(b)** T2 (25% thrombin) and **(c)** T3 (65% thrombin) samples. Parameters ω_0 and γ_0 were fixed to 2π rad/s and 5%, respectively. Results show that $G' > G''$ for the three different types of hydrogels. Arrowheads mark the time needed to reach equilibrium after the oscillatory stress was applied, being this one $\sim$ 150s for T1 and T3 and 300s for T2 samples. The plotted data correspond to the average over 3 sample repetitions, and shadings corresponds to standard error.

can be related to the stiffness of the hydrogel (Stojkov et al., 2021). The results also revealed that $G' > G''$ for all frequencies, with $G' \simeq 100$ Pa for T1 and T3 hydrogels and $G' \simeq 200$ Pa for the T2 ones. Therefore, $G'_{T2} > G'_{T1}$, indicating that a larger amount of thrombin stiffened the scaffold. However this relationship was not fulfilled for T2 and T3 with $G'_{T3} < G'_{T2}$.

In the context of these results, Weisel, 2007 reported that maximal stiffness are found for fibrin gels that display fiber lengths, diameters, densities and branch point densities that are intermediate in magnitude, which provides a justification for the observed $G'_{T2} > G'_{T3}$ although in the work of Weisel a lower concentration of thrombin was used.

Evolution of T1, T2 and T3 hydrogels during development

Here we studied the evolution of the mechanical properties of the hydrogel samples during development, from DIV 1 to 20. Since G' exceeded G'' by a decade (see Figure 6.7), we did not show the plots of G'' in these and further analyses.

As a first set of measurements, time sweep tests were performed to verify the structural stability of the samples during the aging process when subjected to an oscillatory strain. As a second step, a strain sweep test was carried out to verify that the development of a neuronal network within the scaffold did not affect the range of the LVR, previously established for DIV 1 (see Figure 6.7). Results for the strain sweep test for T1, T2 and T3 samples from DIV 1 to DIV 20 are shown in the left panels of Figure 6.8. T1 hydrogels showed a larger variability in G' values across different DIVs. G' values oscillated between $80 - 290$ Pa with trends that crossed between each other and exhibiting an evident drift as the strain γ grew. Despite the drift and fluctuations, we considered that the LVR spans up to 5% for T1 hydrogels. For T2 hydrogels, G'

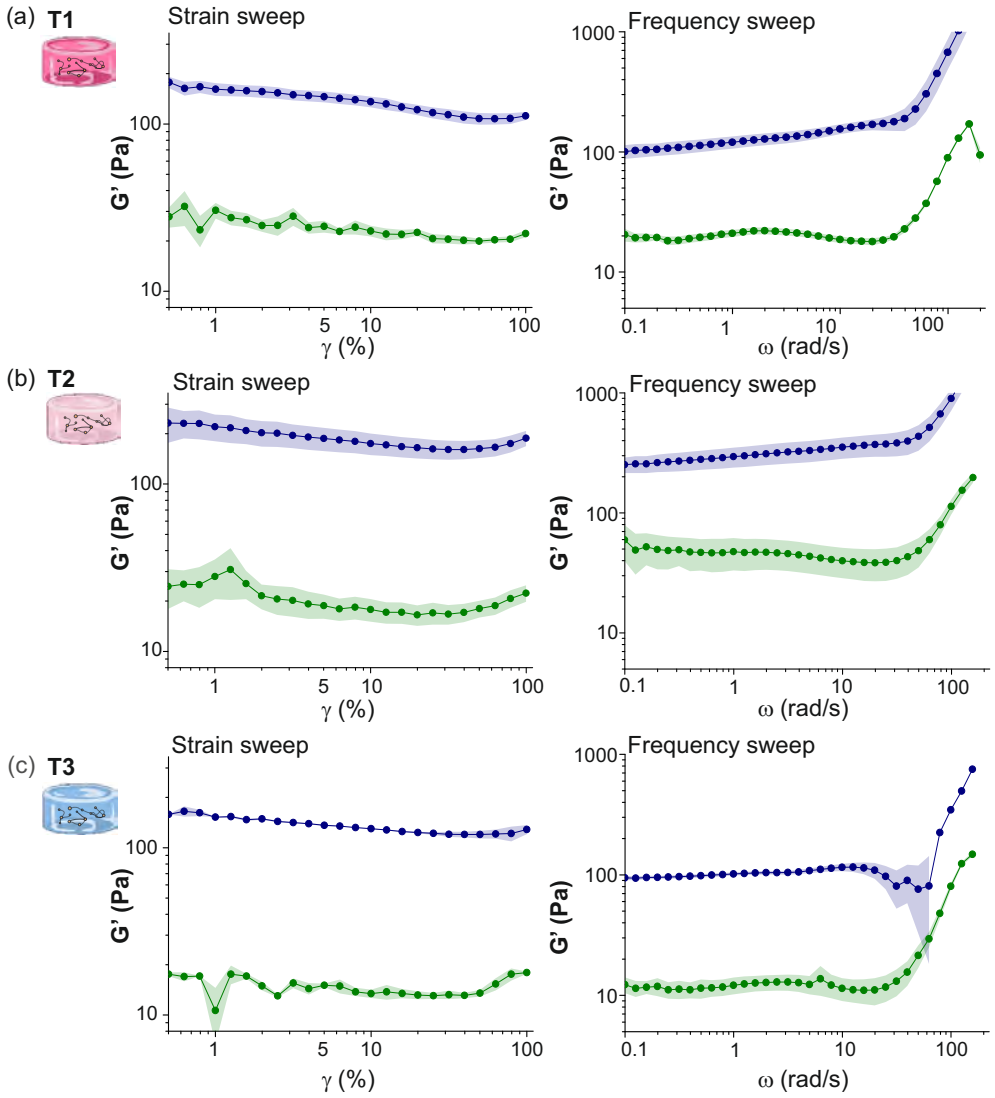

Figure 6.7. Evolution of PEGylated fibrin hydrogels with different concentrations of thrombin at DIV 1. For the strain sweep test, $\omega_0 = 2\pi$ rad/s and $\gamma \in [1, 100]\%$. Frequency sweep test imposed a $\gamma_0 = 5\%$ and $\omega \in [0.1, 100]$ rad/s. **(a)** T1, Strain sweep test (left) and frequency sweep test (right) **(b)** T2, Strain sweep test (left) and frequency sweep test (right) (c) T3, Strain sweep test (left) and frequency sweep test (right). In all panels, G' values were averaged over 3 repetitions with the corresponding standard error shown as coloured shadings.

was within a range of $140 - 300$ Pa, presenting less sparsity across different DIVs. T3 exhibited a reproducible behaviour with a G' value within a range of $150 - 200$ Pa for all tested DIVs. There is a noticeable deviation in the results at DIV 8, which could be attributed to a calibration error, a mismatch during the measurement of the base sandpaper, or even an error in the sample preparation. The cause of this result remains unclear. The minimal dispersion observed in the T3 results could be attributed

to a more compact matrix, which experiences less deformation, the absence of altering neural networks within the scaffold, or a combination of both.

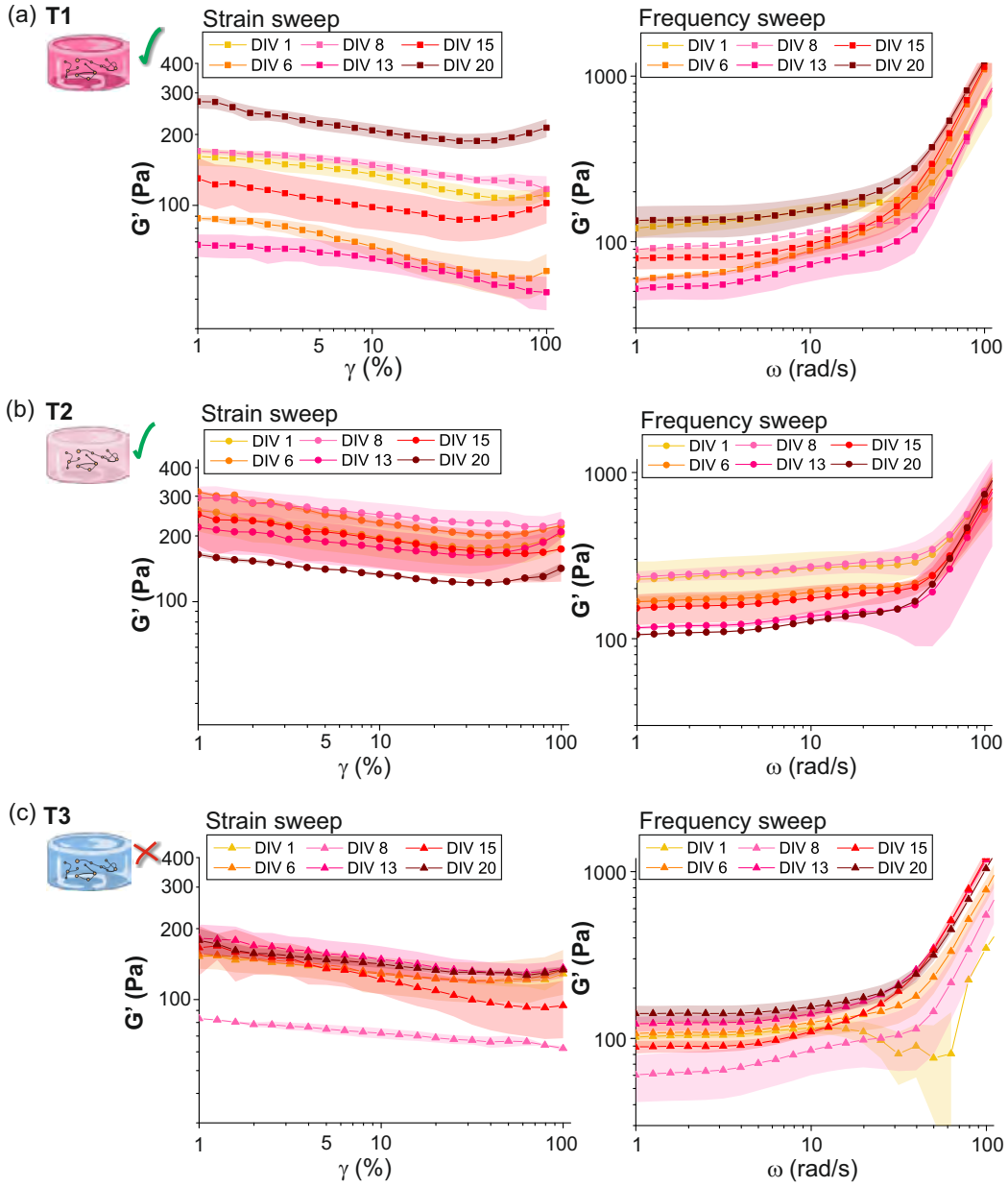

Figure 6.8. Evolution of PEGylated fibrin hydrogels with different concentrations of thrombin from DIV 1 to DIV 20. For the strain sweep test, $\omega_0 = 2\pi$ rad/s and $\gamma \in [1, 100]\%$. Frequency sweep test imposed a $\gamma_0 = 5\%$ and $\omega \in [0.1, 100]$ rad/s. **(a)** T1, Strain sweep test (left) and frequency sweep test (right), **(b)** T2, Strain sweep test (left) and frequency sweep test (right), **(c)** T3, Strain sweep test (left) and frequency sweep test (right). In all panels, G' values were averaged over 3 repetitions with the corresponding standard error shown as coloured shadings. The green tick indicates that the gel is viable for culturing, while the red cross indicates that cells did not survive.

The right panels of Figure 6.8 display the results obtained for the frequency sweep tests conducted at $\gamma_0 = 5\%$. It is worth to note that the gel–characteristic low–frequency plateau was presented in all the samples at different DIVs. However, we observed distinctions in the drift patterns exhibited by the samples, with the plateau regime ending at frequencies reaching up to $\omega \simeq 10$ rad/s for T1 and T3 hydrogels, and extending to approximately $\omega \simeq 30$ rad/s for the T2 ones. This observation suggests that an intermediate concentration of thrombin contributed to enhancing the stability of the hydrogel's behaviour. In addition, the strong thickening of the hydrogels at large frequencies ($\omega > 50$ rad/s) described in Chapter 5 was more pronounced for T1 and T3 hydrogels as compared to T2 samples. As explained before, this thickening at high–frequency oscillations could be related to the failure of the gel's network to rearrange when subjected to fast oscillations, i.e., short–time-scale perturbations (Ghosh et al., 2005). However, this effect might be also caused by high–frequency perturbations that may induce inertia effects in the response of the hydrogel (Krieger, 1990; Ewoldt, Johnston, and Caretta, 2015).

Thickening of T1 and T3 hydrogels might be caused by the difficulty found by the gel's network to rearrange. Intermediate thrombin concentration results in higher stiffness and resilience within the fibrin network, attributed to greater crosslinking density (Weisel, Nagaswami, and Makowski, 1987; Lai et al., 2012). It is plausible that the polymeric network of T1 and T3 exhibited diminished resistance, leading to an earlier decline in its capability of its polymer chains to rearrange subjected to fast oscillations (short time–scale perturbations), compared to T2. Another plausible scenario is that, due to the comparatively lower stiffness of the T1 and T3 structures, inertia effects triggered at high frequencies could exert a more pronounced impact on the resulting curves.

The Young's modulus E for the three variants of PEGylated fibrin, was calculated by using Eqs. (5.1)–(5.2), as described in Chapter 5. Results are shown in Figure 6.9, which displays the distribution of E values for three evolutionary stages (early 'e', young 'y' and mature 'm') for T1, T2 and T3 hydrogels. The mean value of E for each stage is indicated by a black horizontal line. Colour boxes indicate the standard deviation of the samples. The evolution of E for T1 hydrogels (Figure 6.9a) shows a significant evolution from the early stage of development ($E_e = 300 \pm 50$ Pa) to the young one, but there are no significant differences between the young and mature stages, in which $E = 200 \pm 50$ Pa. For these values p was $p_{e-y} = 0.041, p_{y-m} = 0.912, p_{e-m} = 0.017$. The E invariance observed in T1–type gels may result from numerous factors beyond the scope of our study. For instance, the well–established neuronal network from early stages may contribute, where the absence of growth or pruning phenomena leads to no discernible change in the microstructure of the hydrogels. However, without advanced microscopy techniques, we are unable to support this assumption.

Results for T2 (Figure 6.9b) were already commented in the previous Chapter. Briefly, the mean value of E within each evolutionary stage gradually decayed, from

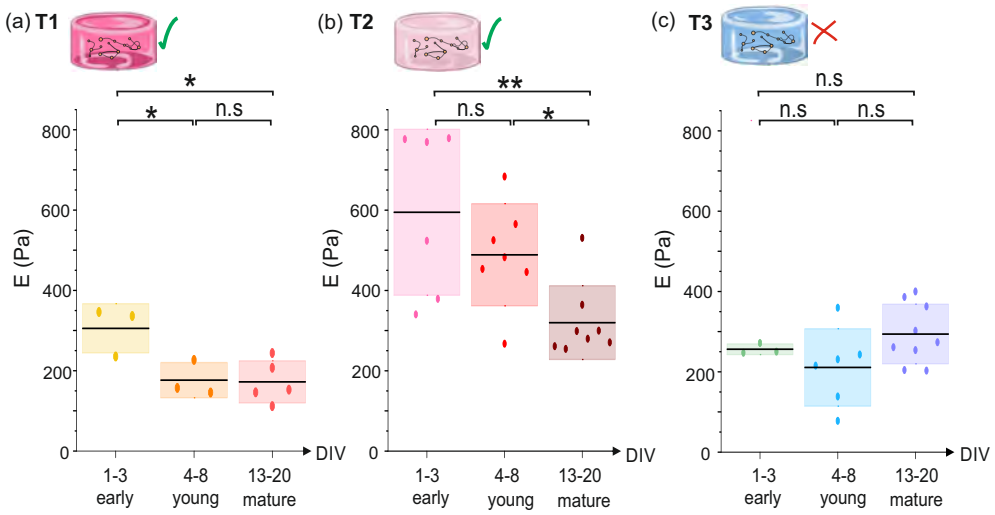

Figure 6.9. Evolution of PEGylated fibrin hydrogels with different concentrations of thrombin from DIV 1 to DIV 20. Boxplot represents the distribution of E values for early (DIV $1-3$), young (DIV $4-8$) and mature (DIV $13-20$) stages for **(a)** T1, **(b)** T2 and **(c)** T3 hydrogels. Each dot in the boxplots is an experimental repetition. The black lines mark the mean of the distribution and the colour boxes mark the standard deviation. * $p < 0.05$, ** $p < 0.01$ (Student's t-test). The green tick indicates that the gel was viable for culturing, while the red cross indicates that cells did not survive.

$E = 590 \pm 210$ Pa at the early developmental stages to $E = 340 \pm 100$ Pa at the mature ones, a decrease of practically a factor of two that was statistically significant ($p_{e-y} = 0.28, p_{y-m} = 0.011, p_{e-m} = 0.0055$). We postulated that these alterations could potentially be caused by the presence of neurons within the structure. Neurons might have an impact on the hydrogel's microscopic arrangement during the process of network formation, possibly through mechanisms such as physical disruption resulting from the growth of axons and dendrites, or enzymatic actions originating from the neurons themselves. On the other hand, E for T3 hydrogels (Figure 6.9c) did not show an evolution with time. The mean value of E for each evolutionary stage were $E = 250 \pm 50$ Pa for all developmental stages with no significant changes ($p_{e-y} = 0.707, p_{y-m} = 0.206, p_{e-m} = 0.415$). This could be attributed to its cell–free nature, as we lack data on the survival of cells within it, which could potentially influence the degradation processes of the hydrogel.

Overall, for all the developmental stages, T2 presented the highest stiffness, showing that intermediate levels of thrombin already favor highly stiff structures. When comparing T1 and T3 we found that $E_{T1} < E_{T3}$ (with the exception of the early stage) meaning that T3 is stiffer than T1.

6.4.2 Functional analysis of the 3D neuronal networks

As previously stated, there was a lack of observable neuronal activity in the case of T3 hydrogels, indicating that neurons did not survive the preparation of these 3D hydrogels. We hypothesize that elevated levels of thrombin hindered neurons' capacity to evenly disperse within the 3D structure. Due to this lack of viability, it was not possible to extract activity data and, consequently, functional connectivity information. However, we did record neuronal activity from T1 and T2 hydrogels, but the results described next should be considered as very preliminary, as the number of samples studied is $n = 3$ for T1 and only $n = 1$ for T2, due to the difficulty in running more experiments in the time frame of this Thesis. It is crucial to note that activity recorded from 3D volumes is conducted in a single plane. Consequently, our functional analysis serves as a 2D approximation for a 3D system, where the neurons observed in the plane are interconnected throughout the entire volume

Neuronal activity in T1 and T2 hydrogels

Figure 6.10 shows representative raster plots for spontaneous neuronal activity recorded at DIV 15 for T1 (a) and T2 (b) PEGylated fibrin hydrogels. The obtained results unveiled raster plots that were characteristic of 3D cultures, wherein activity events encompass a substantial population of cultured neurons. Discerning the spaciotemporal propagation of collective activity events is challenging due to the elevated levels of background activity. Notably, it is important to highlight that the automated identification of ROIs from the high–contrast fluorescence image (see Figure 6.10 top) detected 120 ROIs for T1 hydrogel, in contrast to 80 ROIs for T2. This underscores the intricacies involved in generating reproducible data, a necessity for a meaningful comparison between the two networks.

Functional analysis for T1 and T2 networks

GTE was applied to the spontaneous activity data to extract functional information about the neuronal networks grown in T1 and T2 hydrogels. Figure 6.11a shows an example of a connectivity matrix developed within a T1 hydrogel at DIV 15. It exhibited a global efficiency —a measure of whole network communication— of $G_E \simeq 0.40$, which indicates a relatively strong global exchange of information among neurons within the network. Alongside this, a weak modularity of $Q \simeq 0.34$ was observed. Despite the presence of functional communities in the connectivity matrix (color boxes along the diagonal), the low value of Q indicates that these communities were strongly interconnected. Such a feature is also clear by just looking at the connectivity matrix itself, where the density of black dots (connections among neurons) is similar within the boxes and between boxes. Overall, communities exist but they are strongly integrated, effectually shaping a globally connected system. The representation of the

spatial distribution of the detected functional communities is plotted in Figure 6.11a, right. These spatial maps were drawn with the software Gephi (Bastian, Heymann, and Jacomy, 2009). Neurons with the same colour belong to the same community.

Some communities tended to be nearby, indicating that neurons easily communicated at short distances, although combined with long range communication given the strong overall integration of the network. Thus, altogether, we hypothesize that the soft hydrogel promoted a balanced system with both short– and long–range axons. Obviously, since effective connectivity is not structural one, such a hypothesis should be verified by independent methods such as immunostaining.

Figure 6.11b displays the connectivity matrix and spatial map obtained for a neuronal network built in a T2 hydrogel at DIV 15. The G_E and Q values were similar to those discovered for T1 network, although with subtle differences. First, G_E was slightly lower and Q slightly larger than in T1, overall picturing a more segregated system. Although more data and independent validations are needed, the results suggest that the T2 hydrogel, stiffer than T1, procured a network that accentuated local connectivity, with an overall lower capacity to communicate at large scales.

The mean values of G_E and Q, and their standard error, were plotted as a function of DIV for networks developed within T1 and T2 hydrogels. Results are shown in Figures 6.12a and b. Error bars are absent for T2 data since there is only one observation ($n = 1$), so the plotted data corresponds to the single experiment available. Preliminary results evidenced changes in the functional connectivity of the neuronal network for both scenarios. For networks built in T1 hydrogels, G_E (Figure 6.12a)

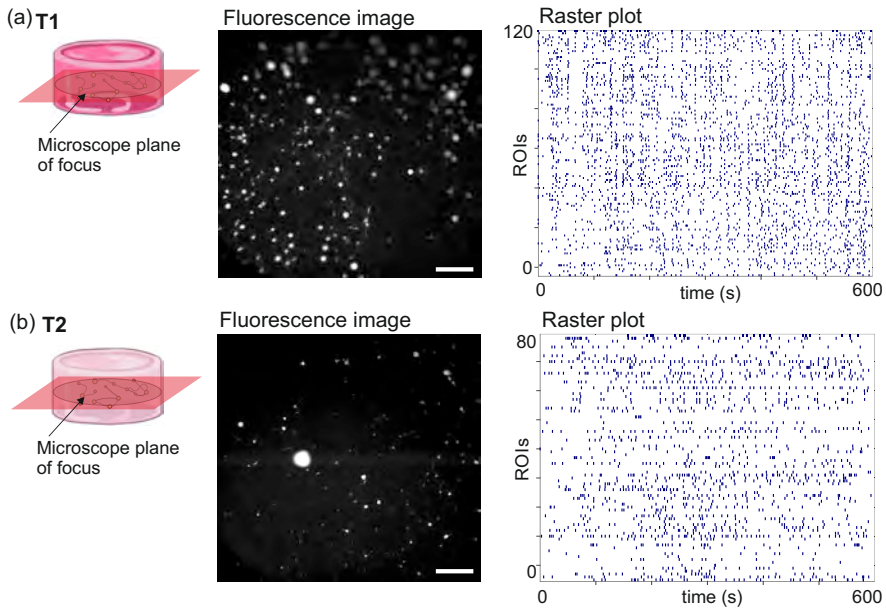

Figure 6.10. Representative fluorescence image of neurons in culture and the extracted raster plots for **(a)** T1 and **(b)** T2 3D neuronal cultures in PEGylated fibrin hydrogels at DIV 15. Scale bar is 1 mm.

gradually increased with time, meaning that the network became more globally efficient as it progressed toward maturer developmental stages. T1 network evolved from a segregated stage at DIV 7 with G_E values of $G_E \simeq 0.15$ and $Q \simeq 0.70$ to a integrative stage in which G_E was close to 0.40 and $Q \simeq 0.20$. On the other hand, T2 networks exhibited a developmental stage in which G_E and Q remained stable along DIV $7-12$ with $G_E \simeq 0.15$ and $Q \simeq 0.70$, which can be understood as the presence of functional communities that exchange information locally. At DIV 15, the network underwent an abrupt change in its functional organisation to a more integrated state with $G_E \simeq 0.35$ and $Q \simeq 0.40$, values similar to those of the T1 network. The sudden change in the stiffer network may be attributed to abnormal activity observed in early–day raster plots (see Figure 6.12c, left), where the culture did not exhibit continuous activity throughout the entire recording time

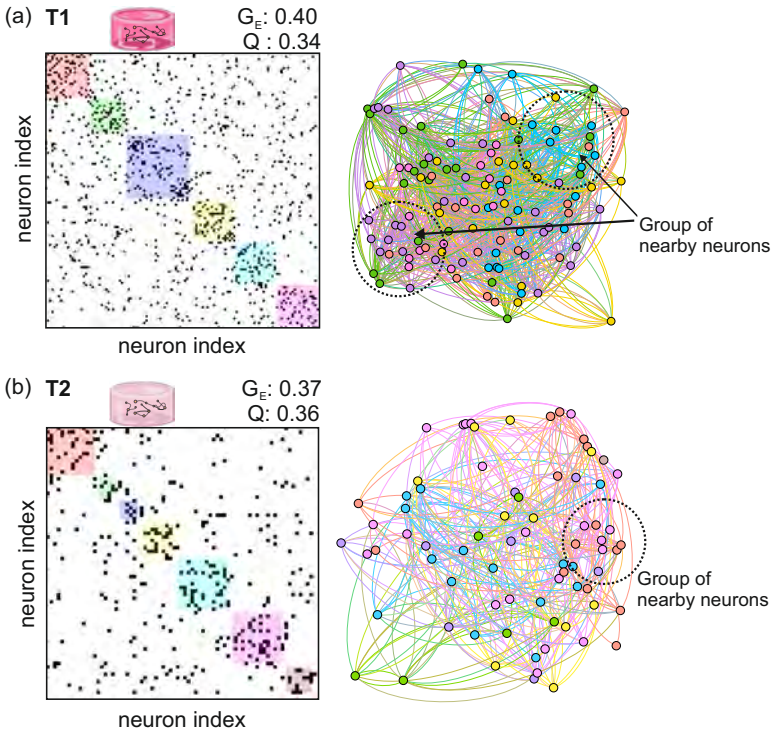

Figure 6.11. Representative connectivity matrices and Gephi graphs for neuronal networks at DIV 15 grown within **(a)** T1 PEGylated fibrin and **(b)** T2 PEGylated fibrin. Results showed a remarkably similar functional connectivity in both scenarios, albeit with a slightly less efficient information exchange observed in the T2 network.

6.5 Discussion

In this Chapter we generated three different hydrogels scaffolds by modifying the thrombin concentration in PEGylated fibrin. The three variants were named T1, T2 and T3 with 10%, 25% and 65% volume of thrombin respectively. To have a better control over the mechanical properties of the final structure, the concentration of fibrinogen remained constant for the three preparations, as well as the cell–density within the structure.

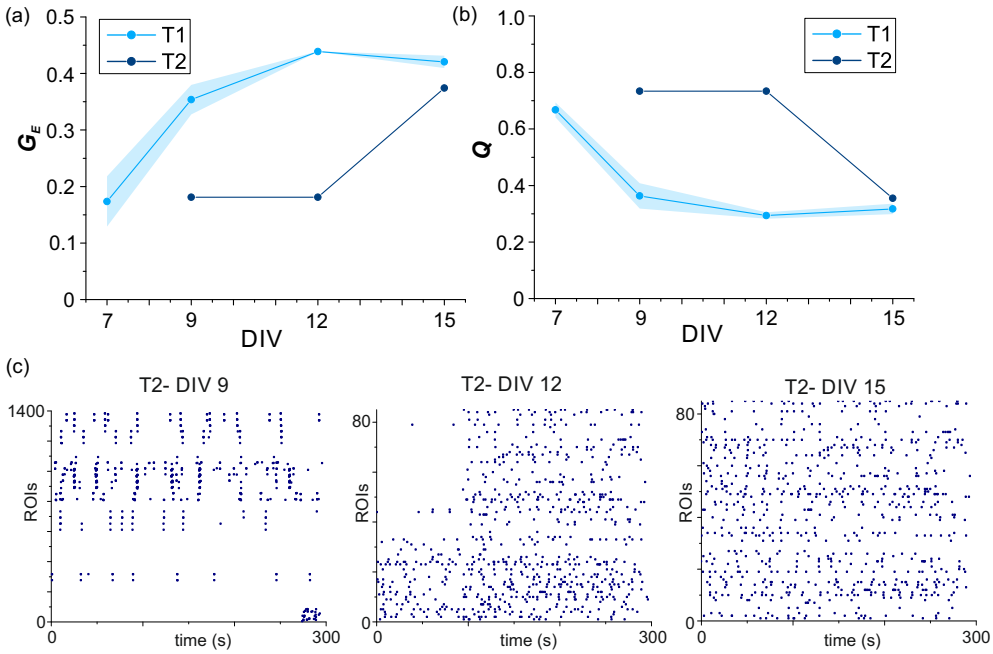

Figure 6.12. Evolution with time of functional features for neuronal networks developed in T1 (light blue) and T2 (dark blue) PEGylated fibrin 3D scaffolds. **(a)** Evolution of the global efficiency G_E, **(b)** Evolution of modularity Q. **(c)** Raster plots for T2 networks at DIV 9, 12 and 14.

By applying the protocol designed in Chapter 5 to measure the rheological behaviour of PEGylated fibrin hydrogels, we aimed at linking the concentration of thrombin (and the final stiffness of the hydrogel) with neuronal activity traits. We monitored the evolution of the Young's modulus (E) over a three–week period and, when possible, combined this information with activity analyses.

The final objective of this investigation was to optimize the mechanical properties of the hydrogels for culturing primary neurons. With that purpose, viability tests were performed to proof that healthy cells were growing within the hydrogel scaffolds. For doing that, we transduced neurons in culture with the calcium marker GCaMP6s and recorded spontaneous neuronal activity from DIV 7, when neurons start expressing the fluorescence protein, to DIV 20. Activity recordings allowed to have data for the same period of time as for the rheological measurements. These tests were successful for

T1 and T2 samples but, unfortunately, no evidence of neuronal activity was found for T3 hydrogels. For T3 hydrogels, with the highest concentration of thrombin, neurons did not survive the gelation process of the scaffold. We conjecture that there is a thrombin limit concentration above which neurons are not able to survive, maybe due to the highly compacted environment of fibrin fibers, in which the porous size is not big enough to host healthy neurons.

Free thrombin concentration at the time of gelation has been reported to influence fibrin hydrogel structure (Wolberg, 2007; Weisel and Litvinov, 2013). As mentioned before, low concentrations of thrombin lead to the formation of fibrin gels formed by thick fibers, few branching points and large pores, while higher concentrations lead to the formation of gels consisting of tightly packed thin fibers. Taking these factors into consideration, the stiffness of the final hydrogel correlates with thrombin concentration since a network of coarse, less compact fibres will have less stiffness than a network of fine–compact fibres, which will better resist the application of an external force or deformation strain. With the intention of proving if this statements are correct for our prepared hydrogels, we characterised the viscoelastic behaviour of T1, T2 and T3 PEGylated fibrin samples along a three–week period. Figure 6.9 shows the measured evolution of E with time (and neuronal development) for the three hydrogels samples. Indeed, we found that $E_{T1} < E_{T2}$, for every developmental stage, meaning that those hydrogels with greater amount of thrombin exhibited a higher stiffness. Nevertheless, $E_{T3} < E_{T2}$, this interesting effect was described by Weisel, 2007 that reported that maximal stiffness is found for fibrin gels that display fiber lengths, diameters, densities and branch point densities that are intermediate in magnitude. These elevated stiffness values seem to stem from a equilibrium between an increased level of branching and thicker fibers, attributes that enhance network rigidity. However, these characteristics are contradictory, as greater branching is associated with thinner fibers, while thicker fibers correspond to reduced branching. It thus seems that there is a limit for the fiber thickness above which a high degree of inelasticity during deformation appears for thicker fibers.

The brain Young's modulus has been reported to be $\simeq 110$ Pa after birth. As neurons develop over time, the value of E reaches around 1kPa in adulthood. Both measurements, E_{T1}, E_{T2} and E_{T3}, at every developmental stage, align with the known range of brain elasticity. However, our observations reveal a contrasting pattern where E decreases with development. This suggests a potential link between the reduction in E and the degradation of PEGylated fibrin, since existing literature described that stiffness of cortical neurons increases with maturation as a result of the stabilization of neuron's microtubule cytoskeleton (Spedden et al., 2012). In line with this, Berkovitch and Seliktar, 2017, conducted a study comparing the mechanical properties of semi–synthetic hydrogels made from PEG and various natural protein combinations, including fibrinogen. They assessed hydrogel density during incubation with culture

medium, calculated in relation to the corresponding dry weight of samples. The results exhibited a decline in hydrogel density over time for all materials. This process, in the absence of cells, arises from enzymes such as proteases present in the culture medium, leading to enzymatic and hydrolytic degradation of the hydrogels.

Hydrogel's mechanical properties and degradation kinetics play a crucial role in reflecting the level of stiffness that cells need to overcome when invading the scaffold, as well as the resistance of that matrix to proteolytic degradation by the invading cells. In physiological conditions, *fibrinolysis* i.e the degradation of fibrin's clot, is mainly governed by the serine–protease *plasmin*, which is derived from its inactive precursor, plasminogen. This conversion is usually triggered by substances like tissue plasminogen activator (tPA) or urokinase plasminogen activator (uPA) (Brown and Barker, 2014). Fibrinolysis is tightly regulated to prevent excessive bleeding as well as the absence of thrombi in the bloodstream. The architecture of fibrin gel has an impact on the rates of fibrinolysis (Gabriel, Muga, and Boothroyd, 1992), although the relationships involved are not straightforward. Studies have revealed that a fibrin matrix formed in the presence of low thrombin concentrations, comprising thicker fibers tends to undergo faster lysis compared to structures with thinner fibrin fibers (high thrombin concentrations) (Carr Jr and Alving, 1995; Weisel, 2007; Wolberg, 2007; Lord, 2011). However, it's worth noting that in contrast, at the level of individual fibers, thin fibers are actually lysed more rapidly than thick ones (Collet et al., 2000). Therefore, this phenomenon is related to the more rapid diffusion of tPA through a loose fibrin network compared to a dense fibrin network. Attending to the exposed facts, the results shown in Figure 6.9 can be explained in terms of degradation of fibrin structure.

Interestingly, neurons and other cells in the CNS has been reported to express tPA to promote events associated with synaptic plasticity and seizures (Qian et al., 1993; Seeds, Williams, and Bickford, 1995; Yepes et al., 2002), which can accelerate the degradation of fibrin gels *in vitro*. Regarding this information, T2 hydrogels should have a structure made of thinner and compact fibers, experiencing a slower degradation process than T1 structures, where tPA generated by neurons can travel along the volume faster. However, results (Figure 6.9) showed a slower degradation process for T1 hydrogels, in which E_{T1} did not change significantly during the first 4 days of monitoring. Without conducting additional investigation or employing imaging techniques like SEM, we are unable to furnish a more comprehensive understanding of the internal dynamics within the structure and the possible mechanisms that are governing the degradation of the system.

We note that thrombin concentration not only regulates the stiffness and architecture of the fibrin structure, but also the stability of the gel when used for culturing cells. Tissue stiffness regulates the length of neuronal axons and their degree of spreading (Long and Huttner, 2019; Lam et al., 2019; Si, Gong, and Yang, 2023). Therefore, knowing the precise mechanical properties of the resulting T1 and T2 hydrogels, it

becomes crucial to characterise the functional connectivity of the hosted neuronal networks. This evaluation is vital to establish a relationship between mechanical properties of the matrix and the optimal neuronal growth and functionality. Koser et al., 2016 reported than in 2D cultures, a matrix with higher stiffness caused persistent growth in axons, facilitating fasciculation (axons running in parallel), whereas a matrix with lower stiffness promoted slowed exploratory growth resulting in splaying of axons (cross–linked network).

When considering T1 and T2 3D structures, two antagonistic factors come into consideration. From one perspective, the scaffold's porosity plays a crucial role. It stands to reason that higher porosity would provide an advantageous environment for the neural network's development, enabling axons to extend and mature throughout the matrix's entire volume. Conversely, a smaller pore size might impose constraints on the structural expansion of the neuronal network. On the other hand, as indicated by the findings of Koser et al., 2016, the stiffness of the matrix holds its own importance. A stiffer scaffold appears to promote the growth of longer and more directed axons, whereas lower stiffness tends to result in shorter and more branched axons. Indeed it is not obvious to predict the resultant functional connectivity of networks grown in T1 and T2 scaffolds, as a balance between porosity and stiffness might be considered. It is also crucial to note that, within the brain, genetic mechanisms are at play, orchestrating axonal growth and facilitating the formation of connections essential for the organism's optimal functioning. In contrast, *in vitro* settings do not present these mechanisms, resulting in neurons growing without predefined guidance and, thus, forming connections in a random way.

T1 hydrogels had a lower stiffness but a higher pore size. We hypothesized that neurons would develop a great number of axons that would connect with their closer neighbours, as the low stiffness of the matrix would allow axons to only recognise areas in the vicinity of the source neuron. However, a smaller number of axons would be able to explore longer distances through the porous structure of the matrix. These aspects would result in a integrative network with an efficient functional connectivity in terms of information exchange. Attending to the results shown in Figure 6.12, for young developmental stages (DIV 7), G_E has a low initial value $G_{E-T1} \simeq 0.15$ for DIV 7 together with a high Q value, of almost $Q_{T1} \simeq 0.75$ referring to a segregated neuronal network with very low levels of communication at a network level. During development, as axons grew, neurons in culture established long–distance connection resulting in a more efficient functional connectivity in which G_E increased while Q decreased with time. In the case of T2 structures, we predicted a neuronal growing that involve straight and directed axons that would find problems for growing across the intricate mesh of fibrin fibers. That would result in a lower level of connectivity and, therefore, lower levels of efficient exchange of information (lower G_E and, consequently, higher Q). Results showed a young developmental stage with $G_{E-T2} \simeq 0.15$ and $Q_{T2} \simeq 0.75$ for DIV 9 and 12, evolving in a final stage similar to that found for

T1, with growing G_E that result in a more efficient state of communication.

To summarize, it appears that the matrix–stiffness relationship primarily impacts the initial stages of the neuronal network. As neurons mature, they navigate to establish efficient connections to facilitate energy and information exchange. Consequently, the manipulation of mechanical properties in PEGylated fibrin gels allows for a degree of control over the initial development of functional connectivity within the hosted neuronal network. However, this control seems to decrease as the network progresses toward its final stages of development.

6.6 Conclusions and future directions

In conclusion, we have introduced a viable platform to conduct primary neuronal cultures grown in different types of PEGylated fibrin hydrogels. Our findings serve as a *proof of concept*, affirming the feasibility of extracting valuable insights regarding the functional organisation of neural networks cultivated in hydrogels with varying stiffness levels. This achievement paves the way for future investigations that researchers in the laboratories of Dr. Jordi Soriano and Dr. Ramon Planet may undertake. It is essential to highlight the limitations inherent in the preliminary findings exposed here. The mechanical characterisation of T1, T2, and T3 PEGylated fibrin hydrogels is subject to the significant influence of the preparation protocol, particularly with regards to temperature and neuronal density. Another crucial consideration is the inherent accuracy of the rheometer, notably the TA Instrument Discovery HR-2 model, which has a lower measurable limit of 2 nN·m for oscillation torque. This limitation resulted in the exclusion of certain extracted values of G' and G'' from the strain sweep test, potentially concealing slight differences between hydrogels. For prospective investigations, the application of immunostaining or SEM techniques could be highly insightful for investigating structural differences among T1, T2, and T3 hydrogels, alongside tracking the developmental progress of neuronal networks. Additionally, delving into the threshold concentration of thrombin that allows for neuronal growing within the fibrin structure holds promise for comprehensively exploring the potential of PEGylated fibrin gels. In the realm of functional characterisation of neuronal networks grown within hydrogel scaffolds, the pursuit of a more extensive sample size is imperative to yield precise outcomes that effectively establish connections between the matrix mechanical properties and network functional organization.

Throughout our research, we unraveled the intricate role of the mechanical properties of scaffolds in 3D neural cultures and their impact on the development of neural networks with distinct characteristics. We laid the groundwork for modeling the mechanical properties of PEGylated fibrin gels by manipulating the concentration of thrombin in their structure. Across the three variants created for our study, we identified a maximum thrombin concentration that hinders the survival of neurons, rendering it unsuitable for our research purposes.

Functional analyses conducted on neuronal networks cultivated in these diverse matrices provided insights into the nuanced relationship between the matrix and neuronal development. Factors like porosity and stiffness, we discovered, can counteract each other in complex ways. While our results are preliminary, they serve as a foundation for future investigations that may involve advanced microscopy techniques and a more extensive array of assays, essential for drawing clear and conclusive findings.

7 Contribution to other projects

In this chapter, I will outline my contributions to other projects, whose work has been already published, and that also form part of my PhD Thesis. Indeed, over the course of four years in Soriano's laboratory, I dedicated myself to delving into my scientific interests and gaining expertise on a diverse range of experimental techniques. This interest led to scientific publications and projects that were beyond the scope of my own research.

■ Neuronal cultures on PDMS patterns

A first project was the characterisation of neuronal cultures grown on substrates with spatial constraints, published in Montalà-Flaquer et al., 2022, in which we explored the functional richness of rat cortical networks grown on PDMS topographical patterns, as shown in Figure 7.1. By using fluorescence calcium imaging we tracked the evolution of spontaneous activity in these cultures along 20 DIVs. The networks in culture exhibited intricate spatiotemporal activity patterns covering from small regions of the culture to its whole extent, and an overall dynamic repertoire that was much richer than the one observed in standard cultures grown on flat surfaces, where a persistent whole–network bursting behaviour predominates.

Through effective connectivity analysis, we observed the formation of spatially compact functional modules. These modules were intricately linked to the underlying topographical features and the prevailing spatiotemporal activity fronts. The results of this investigation highlighted the ability of spatial constraints to shape both activity and functional organisation, presenting novel avenues for understanding the interplay between structure and function in living neuronal circuits. This investigation also showed that neuronal cultures with a patterned substrate exhibit brain–like dynamical traits, which make them much more interesting as model system than standard cultures. In this context, I contributed by running experiments and helped to review the final version of the published paper.

■ Damage in neuronal cultures

A second project was related to my tenure as a scientist in the laboratory, where I have had the privilege of mentoring undergraduate students in their final degree projects. Notably, a project led by the bachelor's in physics students Sàlem Ayasreh and Imanol Jurado, under my guidance and that of Dr. Jordi Soriano, was successfully published in

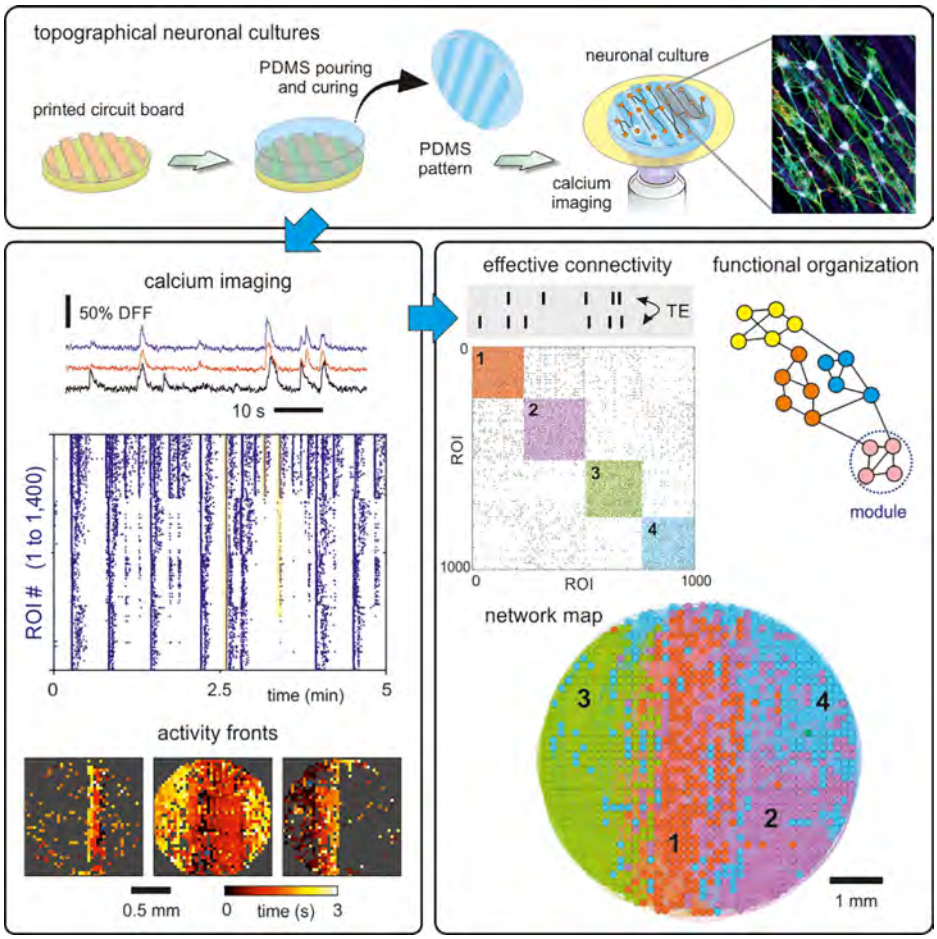

Figure 7.1. Visual abstract of 'Rich dynamics and functional organisation on topographically designed neuronal networks *in vitro´* (Montalà-Flaquer et al., 2022). Primary neuronal cultures were established atop topographical PDMS patterns. Neuronal activity was recorded and analyzed to ascertain whether the structural connectivity dictated by the patterns influenced the actual connectivity of the resulting networks.

Micromachines in November 2022 (Ayasreh et al., 2022). In this study, we explored the resilience of primary neuronal cultures to damage (Figure 7.2). Rat embryonic cultures were prepared in two variants: as homogeneous on flat PDMS surfaces and as aggregated on glass. For the homogeneous cultures, the spontaneous activity in neuronal networks was investigated before and after cutting it in half with an scalpel, to assess the network ability to reconnect and recover the same levels of spontaneous activity. In the aggregated cultures, we locally damaged the neuronal network by removing those aggregates of neurons that were central for information flow, investigating the culture's capacity to maintain activity and recover after the loss of one or multiple hubs.

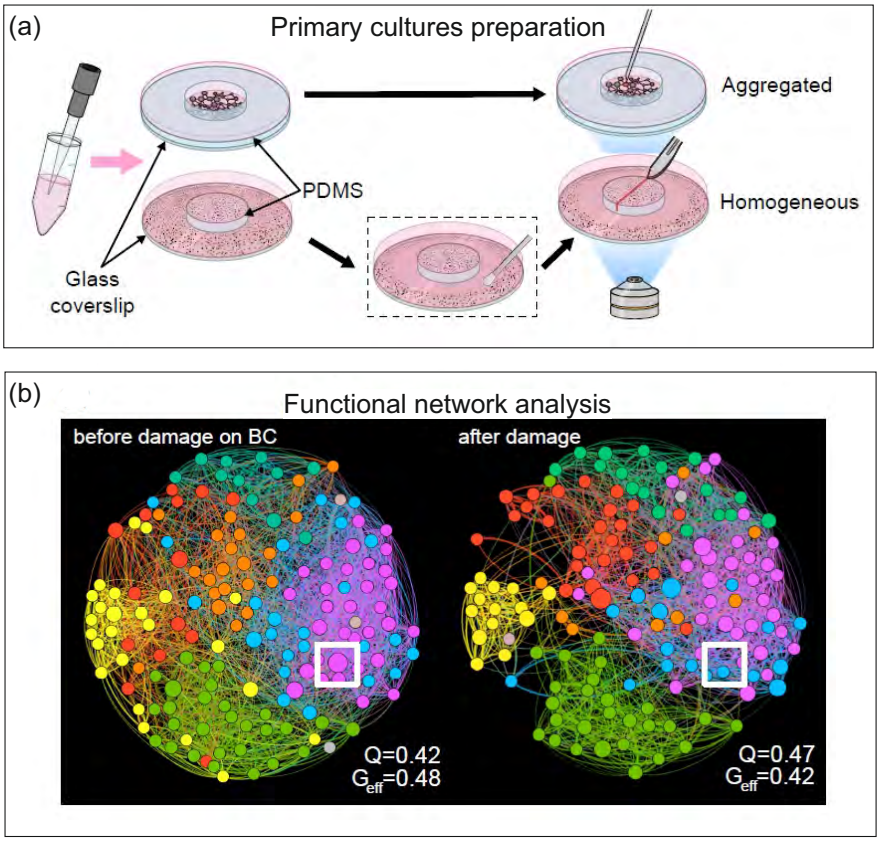

Figure 7.2. Visual abstract of 'Dynamic and functional alterations of neuronal networks *in vitro* upon physical damage: a proof of concept´ (Ayasreh et al., 2022). **(a)** The outline of the primary steps in culture preparation and damage initiation is as follows: Aggregated cultures were formed by cultivating neurons directly on bare glass, and subsequent damage was induced using a needle. In contrast, homogeneous cultures were established on PLL–coated PDMS discs and subjected to damage through a controlled cut down the middle using a scalpel. Notably, the PDMS disc was encircled by a population of neurons that grew on glass, presenting the option for removal if needed (indicated by a black dashed contour). **(b)** Functional connectivity maps from a representative experiment are presented both before and after a targeted attack on a hub. The removed node is identified by a white square. Following the targeted attack, the network exhibits an overall increase in segregation, characterised by elevated Q and reduced G. Nodes in the maps are colour–coded based on their functional community affiliation.

In this work, dynamical and functional alterations in neuronal connectivity were characterised using by calcium imaging techniques and subsequent analysis. In both scenarios, we observed impressive resilience within the neuronal cultures, allowing them to maintain high activity levels and restore lost communication pathways. Particularly for the homogeneous cultures subjected to physical division, it was observed that a reservoir of healthy neurons surrounding the damaged area played a crucial role in enhancing resilience and fostering recovery. This reservoir provided stimulation and

acted as a communication bridge across disconnected regions. These findings underscored the remarkable ability of neuronal cultures to endure and recover from damage, serving as inspirational concepts for the development of future hybrid biological–electronic systems.

■ Other contributions

Throughout my pre–doctoral training, I had the privilege of attending numerous national and international conferences, including the SENC meeting in 2021, the FENS Forum in 2022, and the Annual European Rheology Conference in 2022. One notable experience was my involvement in a conference on 'Nonlinear Dynamics in Biological Systems', organised by Carlos III University in Madrid in June 2022. During this congress, we seized the opportunity to contribute to a book, co–authoring a chapter that not only summarizes the results presented during the congress but also provided an overview of the research conducted in our laboratory. This chapter is scheduled for publication in the book *Nonlinear Dynamics in Biological Systems*, a collaborative effort between the American Institute of Physics and Springer, expected for early 2024.

8 General Discussion

In this Thesis, the convergence of neuronal cultures, physics of complex systems, and material engineering has opened up a fascinating field of interdisciplinary exploration. The neuronal cultures serve as the dynamic protagonists, dancing to the intricate rhythm of interconnected networks. As we delve deeper into the physics of complex systems, the threads of nonlinear behaviour and self–organisation intertwine, revealing the elegant choreography that underlies seemingly chaotic neuronal activities. Materials engineering acts as a stage, providing a platform to host such a truly complex network. Together, these disciplines transcend their individual realms, offering a profound understanding of the symbiotic relationship between neurons, the biophysics that govern their interactions, and the materials that shape their environment. This synthesis not only advances our scientific understanding but also opens new frontiers for innovative applications, laying the groundwork for future breakthroughs at the intersection of neuroscience, physics, and material science.

On tau experiments

Throughout the last 100 years, neuronal cultures have evolved into a fundamental tool for understanding the brain and its dysfunctions. Their appeal lies in the capacity to manipulate the structure and environment of their biological building blocks, neurons and glia, a feature that has prompted numerous studies to replicate the scenarios of neurological and psychiatric disorders (Stam, 2014; Medaglia and Bassett, 2017). The framework provided by physics of complex systems has been instrumental in developing experimental and analytical resources, allowing for the effective comparison of structural and functional networks in both healthy and diseased states. Within the framework of the 'La Caixa Health Research Program 2019' project, our focus was on investigating a model of *in vitro* tauopathies —a group of diseases that form the basis for conditions as significant as Alzheimer's disease. Our objective was to establish a relation between structural alterations resulting from the disease and subsequent functional deficits, observing their evolution over time.

In recent times, mounting evidence has supported the hypothesis that tau pathology spreads along neuronal networks, contributing to the progression of human tauopathies. These theories have centered around the prion–like hypothesis, suggesting shared pathogenic mechanisms between tauopathies and other disorders with prion disease (PrD) traits (Clavaguera et al., 2009; Kfoury et al., 2012; Guo and Lee, 2014; Sanders et al.,

2016). An essential component of the mechanisms supporting this hypothesis is the progression of extracellular seed–competent tau from an affected neuron to an adjacent healthy one during cell–to–cell transmission. The confirmation of the presence of extracellular pathological tau in the cerebrospinal fluid and interstitial fluid of human patients with AD (Kurz et al., 1998; Takeda et al., 2016), as well as in murine and cellular models (Yamada et al., 2011; Barten et al., 2011; Takeda et al., 2015), has made extracellular tau species an attractive target for tau–directed therapies. This includes inhibitors of tau aggregation (Seidler et al., 2019; Crowe et al., 2020). In Chapter 4, toxicity tests were conducted on a peptide structure designed as an inhibitor to pTau aggregation. IN–M4 has exhibited successful inhibitory behaviours (Seidler et al., 2019). However, prior to its application in *in vivo* studies, it was imperative to establish its non–toxic nature. To address this issue, neuronal primary cultures were prepared from CD1 (wild–type) mouse embryo cortical tissue and inoculated with the aforementioned inhibitor at an extreme concentration of 50 μM. The results of the spontaneous activity analysis of these cultures revealed similarities among untreated, control (50 μM of DMSO), and inhibitor–treated cultures. This indicates that the presence of IN–M4 did not adversely impact the developmental processes of neurons in culture.

While many tau–directed therapies have demonstrated success in preclinical studies, both *in vitro* and *in vivo*, their benefits have persistently failed to replicate in human clinical trials. This challenge is partly attributed to the limited translational value of the experimental models employed (Zahs and Ashe, 2010; Boxer et al., 2013). The gold standard for creating tauopathy models involves the overexpression of aggregation–prone tau isoforms. However, the majority of human tauopathies are sporadic, meaning they are not linked to genetic mutations or alterations in tau expression levels. Furthermore, some experimental approaches have utilized preformed fibril to induce tau pathology, with their biological activities significantly deviating from the actual tau aggregates present in the human brain. As a result, the biological relevance of these models remains uncertain.

Thus, the primary objective of our investigation was to explore the impact of extracellular seed–competent tau species in an adequate *in vitro* model. In Chapter 4, we analyzed alterations in neuronal spontaneous activity attributed to the presence of extracellular tau in primary cortical cultures. Following the prion–like hypothesis, tau pathology originates in a restricted number of neurons in the brain, then propagates trans–cellularly to synaptically connected healthy neurons. In consideration of this, we chose to employ primary neuronal cell cultures derived from wild–type mice. To investigate the effects of extracellular tau, we conducted time–course experiments, monitoring neuronal activity over a two–week period.

Results showed that, independently of the amount of tau or its biological origin, neuronal cultures displayed a highly synchronous activity patterns as they matured. Despite this rigidity in behaviour, we examined dynamical parameters of collective

neuronal activity, such as the velocity of the information flow, the population activity and the IBI, hopping to find changes induced by pathological tau. Extrapolating to neurons in the human brain, we expected synaptic dysfunction and, eventually, synapse loss that could affect connectivity patterns (Decker et al., 2015). By the same token, we expected to find differences in functional organisation parameters such as G_E, Q, and average connectivity, which would reveal alterations in the exchange of information between neurons in the network. However, despite gigantic efforts, we could not demonstrate that the presence of extracellular seed–competent tau affected neuronal network activity and functional organisation. Indeed, no differences were observed between tau–treated and untreated cultures, neither in experiments where tau was present in the TIF-P+ fraction, nor in those using the sarkosyl fraction from P301 (+/-) mouse brain. In a less relevant model we studied neurons that overexpressed P301L human tau, but the same negative results were found in this new scenario, finding that cells inoculated with P301 (+/-) sarkosyl fraction exhibited a statistically similar behaviour as the rest of conditions.

It is essential to acknowledge that the unexpected negative results reported in Chapter 4 are noteworthy, particularly in light of the numerous published studies documenting tau–associated alterations or damage in various cellular models (Tian et al., 2013; Stancu et al., 2015; Pickhardt et al., 2017). However, as discussed earlier, many of these studies did not employ healthy primary neurons. Instead, a majority utilized mammalian immortalized cell lines overexpressing mutated tau isoforms, primary neuronal cultures derived from tau transgenic animals, or cultures virally induced to overexpress mutated tau isoforms. We attribute the lack of success in replicating positive results from these models in our experimental design to our preference for disease–relevant approaches, i.e. wild type healthy neurons that did not express tau isoforms but that became affected due to the presence of tau in the environment.

Moreover, our use of embryonic primary cell cultures poses an additional consideration. Given that aging is the main risk factor for most sporadic NDs, it is likely that primary cell cultures do not accurately replicate the complex structure of an aged brain (Estévez-Priego et al., 2020). Another consideration when using embryonic cells is that the ratio between 3R– and 4R–tau isoforms is developmentally determined. Embryonic mice primarily express 3R–tau, while adult rodents predominantly express 4R–tau isoforms (Guo, Noble, and Hanger, 2017). Consequently, most of the used exogenous tau seeds (extracted from adults rodents) did not include the predominant isoforms endogenously produced by the primary neurons in culture (embryonic cells). This mismatch could introduce incompatibilities or even prevent tau–mediated cytotoxicity, as demonstrated by Ferrer et al., 2022 who observed differences between newborn and adult wild–type mice upon inoculation of tau derived from AD patients.

Looking ahead, future experiments should focus on enhancing the survival of primary neurons. This will allow us to investigate whether prolonged incubation times

after tau treatment yield detectable changes in neuronal activity. Additionally, incorporating brain–derived materials from patients with AD in the experimental design would be valuable, as they encompass disease–relevant tau isoforms. Lastly, replicating the tauopathy disease scenario in a 3D environment could be of interest, as the absence of 3D organisation in traditional culture plates might alter the susceptibility of primary neurons to be affected by extracellular seed–competent tau.

On 3D cultures

Expanding on the aforementioned, a central debate within the neuroscience community revolves around whether standard 2D neuronal cultures suffice as models to comprehend the intricacies of naturally formed neuronal circuits, such as those found in the brain, which exhibit a combination of 2D and 3D organisation (Stiso and Bassett, 2018; Schwartz et al., 2023). In response to this, 3D neuronal cultures have been introduced in the last decade to establish improved *in vitro* models. The structure chosen to house the neuronal culture must fulfill specific requirements to support the healthy development of the neuronal network. The selected material must mimic the brain ECM, facilitating efficient molecule transport while offering structural support to the neurons. Additionally, it should be biocompatible, non–toxic, and promote robust cellular adhesion. Given that our focus is on studying neuronal activity, optical transparency is also essential to permit the passage of light through its structure.

In Chapter 5, we employed a semi–synthetic hydrogel to create 3D neuronal cultures. PEGylated fibrin is composed by a synthetic part, PEG, and a natural part, a fibrin gel formed from the enzymatic reaction of the binding of thrombin and fibrinogen, molecules present in the blood clotting reaction. While PEGylated fibrin has been successfully utilized in cellular cultures (Zhang et al., 2010), there is limited knowledge about its mechanical properties, especially their evolution over time under realistic experimental conditions. Assessing this is crucial for determining whether the hydrogel effectively replicates the mechanical environment necessary for optimal neuronal growth and functionality. To conduct this investigation, we prepared hydrogels both with and without cortical neurons derived from CD1 mouse embryos and characterised their mechanical properties over a three–week period using a plate–plate rheometer.

The results revealed a material with the mechanical properties akin to that of an elastic gel, possessing sufficient stiffness for neurons to attach and proliferate effectively. As a reference, the Young's modulus (E) of the brain varies depending on the analyzed region and developmental stage, ranging from 110 Pa after birth to 1 kPa in adulthood (Barnes, Przybyla, and Weaver, 2017; Samanipour et al., 2022). These variations are attributed to the formation and refinement of connections within the extracellular matrix (ECM). Our tested hydrogels with cells exhibited an E value within this range, making them conducive for neuronal development. However, the E for these neuron–laden hydrogels exhibited a decrease along development. This phenomenon

may be attributed to the presence of the living, developing cells themselves, rendering the scaffold stiffer as new connections form. In physiological conditions, it has been observed that the stabilization of the neuronal microtubule cytoskeleton affects the stiffness of the brain (Spedden et al., 2012). Since neurons in culture, as observed in our laboratory, begin to exhibit strong collective activity around days *in vitro* (DIV) $4-8$ (Tibau et al., 2020; Estévez-Priego et al., 2020; Montalà-Flaquer et al., 2022), they undergo a complex connectivity adjustment that combines formation of connections and their pruning. Axonal pruning in particular leads to a weakening of the scaffold's cohesion and a reduction of its E. Despite these alterations, PEGylated fibrin hydrogels proved to be suitable candidates for 3D neuronal cultures, as the exhibited E remained stable throughout the culture lifespan and fell within the range for mimicking the brain ECM. As a final note, it is worth mentioning that while our experiments were conducted with mouse primary neuronal cultures, they could be extended to hiPSCs, given their relevance in medical applications, especially within the context of neurological disorders and implants.

In line with these experiments, and in a broader context, it is clear that any scientist dreams of playing with a complex system, e.g., for moulding their interactions, influencing behaviours, or dissecting the mechanisms that make them unique. In Chapter 6, we harnessed material science to access the intricate task of modeling the functional behaviour of a neuronal network by tuning the mechanical properties of the hydrogel scaffold. The mechanical properties of PEGylated fibrin can be fine–tuned by altering the composition of the fibrin gel, a vital component of the hydrogel. Fibrin gel is composed by thrombin and fibrinogen and its polymerization process directly affects the porosity, fiber thickness and degree of branching of the gel, affecting the mechanical properties of the final structure. Studies have highlighted that the concentration of thrombin during gelation significantly shapes the structure of fibrin hydrogels (Wolberg, 2007; Weisel and Litvinov, 2013). Indeed, low thrombin concentrations result in fibrin gels characterised by thick fibers, few branch points, and large pores. Conversely, high concentrations yield gels with tightly packed, thin fibers which makes the final structure stiffer, i.e the stiffness of the final hydrogel correlates with thrombin concentration. Considering these factors, we created three distinct variants of PEGylated fibrin scaffolds by adjusting the thrombin concentration in PEGylated fibrin and seeded them with cortical neurons. These variants, named T1, T2, and T3, corresponded to 10%, 25% and 65% volume of thrombin respectively.

We implemented the protocol outlined in Chapter 5 to characterise the mechanical behaviour of these hydrogel variants over a three–week period. The goal was to establish a stiffness profile for comparison with the functional analysis of the resulting neuronal networks. Before conducting measurements, we assessed the convenience of the three structures to support neuronal cultures by performing viability tests, recording spontaneous neuronal activity from the hydrogel samples. Unfortunately, these tests failed for the T3 hydrogels, in which the thrombin concentration was the highest.

we hypothesised that the elevated thrombin concentration in T3 made it impossible for neurons to survive the gelation process of the scaffold. We then established a threshold for thrombin concentration beyond which neurons are unable to survive, possibly due to the highly compact environment of fibrin fibers, where the pore size is insufficient to accommodate healthy neurons.

Our results provide a proof of concept, affirming the feasibility of extracting valuable insights into the functional organisation of neuronal networks cultivated in hydrogels with varying stiffness levels. However, establishing a proper relationship between PEGylated fibrin, levels of thrombin, stiffness, and the functional organisation of hosted neuronal networks requires the consideration of numerous factors. As mentioned before, thrombin concentration regulates the stiffness and architecture of the fibrin structure. Yet, within the internal structure, other parameters come into play, such as pore size, to explain specific effects like the speed of the fibrinolysis process (fibrin degradation) or axonal growth. Regarding the development of the neuronal network within the structure, opposing effects influencing the length and branching of axons embedded in a matrix converge. High tissue stiffness increases the length of neuronal axons and their degree of spreading (Long and Huttner, 2019; Lam et al., 2019), whereas high scaffold's porosity facilitates the elongation and exploration of growing axons. It is remarkable that, for instance, in T2 hydrogels, the matrix's stiffness is higher but pores are smaller, which makes difficult to assess which of these magnitudes ultimately governs the development of the neuronal network. Additionally, it is crucial to note that within the brain, genetic mechanisms orchestrate axonal growth and facilitate the formation of connections essential for optimal organism functioning. In contrast, *in vitro* settings lack these mechanisms, resulting in neurons growing without predefined guidance and forming connections randomly.

The results from this investigation pave the way for future studies, where sophisticated optical tools, like SEM or 3D imaging, will be essential to characterise various scaffold variables, establishing a robust relationship between thrombin concentrations of PEGylated fibrin and final biological structures. With such tools, and a greater number of trials to study the dynamic behaviour of 3D networks, it will be possible to determine which environmental factors truly affect the development and functional organisation of a neuronal network.

9 General Conclusions

This thesis is the result of three years of research and the convergence of three distinct disciplines: neuronal cultures, physics of complex systems, and material engineering. It unfolds a captivating narrative in which neuronal cultures occupy the center of the stage, with complex system physics serving as a tool to unravel the intricate network of communication pathways that neurons form. The stage itself, designed through materials engineering, becomes a dynamic platform for this multidimensional performance. As the curtain falls on this exploration, it leaves us not just with answers but with a myriad of questions, propelling us toward further discovery in the fascinating landscape where the brain, physics, and materials converge. In closing this doctoral thesis, I aim to outline the key conclusions drawn from the diverse research lines.

In Chapter 4 we assessed some aspects of tauopathies, a ND disease characterised by the abnormal aggregation of tau proteins. After multiple experiments, the concluding points are the following:

- IN–M4 inhibitors did not disrupt the healthy development of primary neuronal cultures.
- Despite our efforts, we were unable to determine the damage caused by pTau in primary wild–type neuronal cultures.
- Modeling tauopathies' scenario *in vitro* is a complex endeavor due to the numerous factors that play an important role in this intriguing group of diseases.
- The relative simplicity of primary neuronal cultures, in which high levels of synchrony dominate activity, might mask dynamic and functional alterations, rendering our results inconclusive.
- For future experiments we suggest to extend the incubation time for the tau treatment, to move to 3D platforms or to use ihPSCs.

Along Chapters 5 and 6, we delved into the mechanical properties of 3D scaffolds composed of PEGylated fibrin hydrogels —semisynthetic materials selected for their biocompatibility and suitability for hosting neuronal cultures. The mechanical characterisation of PEGylated fibrin hydrogels, along with the manipulation of their mechanical properties through thrombin concentration adjustments, has yielded the following conclusions:

- We introduced PEGylated fibrin hydrogels as competitive candidates for culturing primary neurons in a 3D matrix.
- PEGylated fibrin hydrogels displayed a stiffness comparable to that of the human brain, and this value remained stable over a three–week period. This stability renders it suitable for long–term biomedical applications.
- The decay in the Young's modulus for PEGylated fibrin hydrogels seeded with neurons is associated with natural processes within the neuronal network, such as the development of axons or pruning mechanisms, that are difficult to control or act on.
- We successfully tailored the mechanical properties of PEGylated fibrin hydrogels by modifying the concentration of thrombin in the final structure.
- Viability test of neuronal networks grown within the different PEGylated fibrin variants (T1, T2 and T3) demonstrated an upper limit of thrombin concentration that did not allow the survival of neurons within the scaffold.
- Functional analysis of the neuronal networks grown in T1 and T2 hydrogels revealed that factors like porosity and stiffness, could counterbalance each other in complex ways, thus making difficult to understand the mechanisms responsible for the development of neuronal networks within the matrix.
- Future investigations might explore the utilization of advanced microscopy techniques, such as SEM, to obtain detailed information about the microstructure of the hydrogels and the growing neurons within them.

10 List of publications

■ Publications directly related to this Thesis:

- C. F. López-León *et al.* 'Rheological Characterization of Three-Dimensional Neuronal Cultures Embedded in PEGylated Fibrin Hydrogels'. Published in *Gels* in August 2023 (López-León, Soriano, and Planet, 2023).
- C. F. López-León *et al.* 'Emergent complex dynamics in neuronal cultures and its relation to neuroengineering and medicine' book chapter in *Nonlinear Dynamics in Biological Systems*, American Institute of Physics & Springer. To be published in early 2024.
- C. F. López-León *et al.*. 'Preparation and mechano–functional characterization of PEGylated fibrin hydrogels: impact of thrombin concentration'. Submitted to *Gels*.
- C. F. López-León *et al.*. 'Are primary neuronal cultures a good model to study networks functional alterations in tauopathies?'. In preparation, to be submitted to *Biomedicines*.

■ Contribution to other works:

- M. Montalà-Flaquer *et al.* 'Rich dynamics and functional organization on topographically designed neuronal networks *in vitro*'. Published in *iScience* in December 2022 (Montalà-Flaquer et al., 2022).
- S. Ayasreh *et al.* 'Dynamic and functional alterations of neuronal networks *in vitro* upon physical damage: a proof of concept'. Published in *Micromachines* in November 2022 (Ayasreh et al., 2022).

Bibliography

Achard, Sophie et al. (2006). "A resilient, low-frequency, small-world human brain functional network with highly connected association cortical hubs". In: *Journal of Neuroscience* 26.1, pp. 63–72.

Adil, Maroof M et al. (2017). "Efficient generation of hPSC-derived midbrain dopaminergic neurons in a fully defined, scalable, 3D biomaterial platform". In: *Scientific reports* 7.1, p. 40573.

Ahtiainen, Annika et al. (2021). "Astrocytes exhibit a protective role in neuronal firing patterns under chemically induced seizures in neuron–astrocyte co-cultures". In: *International Journal of Molecular Sciences* 22.23, p. 12770.

Albers, Jonas and Andreas Offenhäusser (2016). "Signal propagation between neuronal populations controlled by micropatterning". In: *Frontiers in bioengineering and biotechnology* 4, p. 46.

Allen, Bridget et al. (2002). "Abundant tau filaments and nonapoptotic neurodegeneration in transgenic mice expressing human P301S tau protein". In: *Journal of Neuroscience* 22.21, pp. 9340–9351.

Amorim Da Costa, Nuno Miguel M and Kevan Martin (2010). "Whose cortical column would that be?" In: *Frontiers in neuroanatomy* 4, p. 1265.

Andreadis, Athena (2006). "Misregulation of tau alternative splicing in neurodegeneration and dementia". In: *Alternative splicing and disease*, pp. 89–107.

Ardhanareeswaran, Karthikeyan et al. (2017). "Human induced pluripotent stem cells for modelling neurodevelopmental disorders". In: *Nature Reviews Neurology* 13.5, pp. 265–278.

Arenas, Alex et al. (2007). "Size reduction of complex networks preserving modularity". In: *New Journal of Physics* 9.6, p. 176.

Audouard, Emilie et al. (2016). "High–molecular-weight paired helical filaments from Alzheimer brain induces seeding of wild-type mouse tau into an Argyrophilic 4R tau pathology in vivo". In: *The American journal of pathology* 186.10, pp. 2709–2722.

Ayasreh, Sàlem et al. (2022). "Dynamic and Functional Alterations of Neuronal Networks In Vitro upon Physical Damage: A Proof of Concept". In: *Micromachines* 13.12, p. 2259.

Bacci, Alberto et al. (1999). "Synaptic and intrinsic mechanisms shape synchronous oscillations in hippocampal neurons in culture". In: *European Journal of Neuroscience* 11.2, pp. 389–397.

Balgude, AP et al. (2001). "Agarose gel stiffness determines rate of DRG neurite extension in 3D cultures". In: *Biomaterials* 22.10, pp. 1077–1084.

Ballatore, Carlo, Virginia M-Y Lee, and John Q Trojanowski (2007). "Tau-mediated neurodegeneration in Alzheimer's disease and related disorders". In: *Nature reviews neuroscience* 8.9, pp. 663–672.

Bang, Seokyoung et al. (2021). "Engineered neural circuits for modeling brain physiology and neuropathology". In: *Acta Biomaterialia* 132, pp. 379–400.

Banker, Gary A and W Maxwell Cowan (1977). "Rat hippocampal neurons in dispersed cell culture". In: *Brain research* 126.3, pp. 397–425.

Barabási, Albert-László (2009). "Scale-free networks: a decade and beyond". In: *science* 325.5939, pp. 412–413.

Barnes, Howard A, John Fletcher Hutton, and Kenneth Walters (1989). *An introduction to rheology*. Vol. 3. Elsevier.

Barnes, J Matthew, Laralynne Przybyla, and Valerie M Weaver (2017). "Tissue mechanics regulate brain development, homeostasis and disease". In: *Journal of cell science* 130.1, pp. 71–82.

Barten, Donna M et al. (2011). "Tau transgenic mice as models for cerebrospinal fluid tau biomarkers". In: *Journal of Alzheimer's Disease* 24.s2, pp. 127–141.

Bassett, Danielle S and Olaf Sporns (2017). "Network neuroscience". In: *Nature neuroscience* 20.3, pp. 353–364.

Bassett, Danielle Smith and ED Bullmore (2006). "Small-world brain networks". In: *The neuroscientist* 12.6, pp. 512–523.

Bastian, Mathieu, Sebastien Heymann, and Mathieu Jacomy (2009). "Gephi: an open source software for exploring and manipulating networks". In: *Proceedings of the international AAAI conference on web and social media*. Vol. 3. 1, pp. 361–362.

Bayer, Shirley Ann and Joseph Altman (1991). "Neocortical development". In: *(No Title)*.

Beggs, John M and Dietmar Plenz (2003). "Neuronal avalanches in neocortical circuits". In: *Journal of neuroscience* 23.35, pp. 11167–11177.

Berkovitch, Yulia and Dror Seliktar (2017). "Semi-synthetic hydrogel composition and stiffness regulate neuronal morphogenesis". In: *International Journal of Pharmaceutics* 523.2, pp. 545–555.

Bessadok, Alaa, Mohamed Ali Mahjoub, and Islem Rekik (2022). "Graph neural networks in network neuroscience". In: *IEEE Transactions on Pattern Analysis and Machine Intelligence* 45.5, pp. 5833–5848.

Betzel, Richard F et al. (2014). "Changes in structural and functional connectivity among resting-state networks across the human lifespan". In: *Neuroimage* 102, pp. 345–357.

Biernat, J et al. (1993). "Phosphorylation of Ser262 strongly reduces binding of tau to microtubules: distinction between PHF-like immunoreactivity and microtubule binding". In: *Neuron* 11.1, pp. 153–163.

Bijsterbosch, Janine et al. (2020). "Challenges and future directions for representations of functional brain organization". In: *Nature neuroscience* 23.12, pp. 1484–1495.

Bisio, Marta et al. (2014). "Emergence of bursting activity in connected neuronal subpopulations". In: *PloS one* 9.9, e107400.

Blankenship, Aaron G and Marla B Feller (2010). "Mechanisms underlying spontaneous patterned activity in developing neural circuits". In: *Nature Reviews Neuroscience* 11.1, pp. 18–29.

Blombäck, Birger and Niklas Bark (2004). "Fibrinopeptides and fibrin gel structure". In: *Biophysical chemistry* 112.2-3, pp. 147–151.

Blondel, Vincent D et al. (2008). "Fast unfolding of communities in large networks". In: *Journal of statistical mechanics: theory and experiment* 2008.10, P10008.

Bologna, Luca Leonardo et al. (2010). "Investigating neuronal activity by SPYCODE multi-channel data analyzer". In: *Neural Networks* 23.6, pp. 685–697.

Bouillet, Thomas et al. (2022). "Revisiting the involvement of tau in complex neural network remodeling: analysis of the extracellular neuronal activity in organotypic brain slice co-cultures". In: *Journal of Neural Engineering* 19.6, p. 066026.

Bourke, Justin L et al. (2018). "Three-dimensional neural cultures produce networks that mimic native brain activity". In: *Journal of Tissue Engineering and Regenerative Medicine* 12.2, pp. 490–493.

Bowery, Norman G et al. (1981). "Bicuculline-insensitive GABA receptors on peripheral autonomic nerve terminals". In: *European journal of pharmacology* 71.1, pp. 53–70.

Boxer, Adam L et al. (2013). "Frontotemporal degeneration, the next therapeutic frontier: molecules and animal models for frontotemporal degeneration drug development". In: *Alzheimer's & Dementia* 9.2, pp. 176–188.

Braak, Heiko and Eva Braak (1991). "Neuropathological stageing of Alzheimer-related changes". In: *Acta neuropathologica* 82.4, pp. 239–259.

Bressloff, Paul C (2000). "Traveling waves and pulses in a one-dimensional network of excitable integrate-and-fire neurons". In: *Journal of Mathematical Biology* 40, pp. 169–198.

Brewer, GJ (1995). "Serum-free B27/neurobasal medium supports differentiated growth of neurons from the striatum, substantia nigra, septum, cerebral cortex, cerebellum, and dentate gyrus". In: *Journal of neuroscience research* 42.5, pp. 674–683.

Brewer, Gregory J et al. (1993). "Optimized survival of hippocampal neurons in B27-supplemented neurobasal™, a new serum-free medium combination". In: *Journal of neuroscience research* 35.5, pp. 567–576.

Brofiga, Martina et al. (2020). "Three-dimensionality shapes the dynamics of cortical interconnected to hippocampal networks". In: *Journal of Neural Engineering* 17.5, p. 056044.

Brofiga, Martina et al. (2021). "On the road to the brain-on-a-chip: a review on strategies, methods, and applications". In: *Journal of Neural Engineering* 18.4, p. 041005.

Brown, Ashley C and Thomas H Barker (2014). "Fibrin-based biomaterials: modulation of macroscopic properties through rational design at the molecular level". In: *Acta biomaterialia* 10.4, pp. 1502–1514.

Brown, Rebecca C, Alan H Lockwood, and Babasaheb R Sonawane (2005). "Neurodegenerative diseases: an overview of environmental risk factors". In: *Environmental health perspectives* 113.9, pp. 1250–1256.

Budday, Silvia et al. (2017). "Mechanical characterization of human brain tissue". In: *Acta biomaterialia* 48, pp. 319–340.

Buitenweg, Jan Reinoud, Wim LC Rutten, and Enrico Marani (2002). "Modeled channel distributions explain extracellular recordings from cultured neurons sealed to microelectrodes". In: *IEEE transactions on biomedical engineering* 49.12, pp. 1580–1590.

Bullmore, Ed and Olaf Sporns (2009). "Complex brain networks: graph theoretical analysis of structural and functional systems". In: *Nature reviews neuroscience* 10.3, pp. 186–198.

— (2012). "The economy of brain network organization". In: *Nature reviews neuroscience* 13.5, pp. 336–349.

Bullmore, Edward T and Danielle S Bassett (2011). "Brain graphs: graphical models of the human brain connectome". In: *Annual review of clinical psychology* 7, pp. 113–140.

Cajal, Santiago Ramón y (1954). *Neuron theory or reticular theory?* Editorial CSIC-CSIC Press.

Calafate, Sara et al. (2015). "Synaptic contacts enhance cell-to-cell tau pathology propagation". In: *Cell reports* 11.8, pp. 1176–1183.

Calatayud, Carles et al. (2019). "CRISPR/Cas9-mediated generation of a tyrosine hydroxylase reporter iPSC line for live imaging and isolation of dopaminergic neurons". In: *Scientific Reports* 9.1, p. 6811.

Campenot, Robert B (1977). "Local control of neurite development by nerve growth factor". In: *Proceedings of the National Academy of Sciences* 74.10, pp. 4516–4519.

Cao, Zheng, Ryan J Gilbert, and Wei He (2009). "Simple Agarose- Chitosan gel composite system for enhanced neuronal growth in three dimensions". In: *Biomacromolecules* 10.10, pp. 2954–2959.

Cárdenas-Aguayo, María del Carmen et al. (2014). "The role of tau oligomers in the onset of Alzheimer's disease neuropathology". In: *ACS chemical neuroscience* 5.12, pp. 1178–1191.

Carola, Giulia et al. (2021). "Parkinson's disease patient-specific neuronal networks carrying the LRRK2 G2019S mutation unveil early functional alterations that predate neurodegeneration". In: *npj Parkinson's Disease* 7.1, p. 55.

Carr Jr, ME and BM Alving (1995). "Effect of fibrin structure on plasmin-mediated dissolution of plasma clots." In: *Blood coagulation & fibrinolysis: an international journal in haemostasis and thrombosis* 6.6, pp. 567–573.

Castellani, Rudy J et al. (2008). "Phosphorylated tau: toxic, protective, or none of the above". In: *Journal of Alzheimer's Disease* 14.4, pp. 377–383.

Chen, J et al. (1992). "Projection domains of MAP2 and tau determine spacings between microtubules in dendrites and axons". In: *Nature* 360.6405, pp. 674–677.

Chen, Qian et al. (2012). "Tau protein is involved in morphological plasticity in hippocampal neurons in response to BDNF". In: *Neurochemistry international* 60.3, pp. 233–242.

Chen, Tsai-Wen et al. (2013). "Ultrasensitive fluorescent proteins for imaging neuronal activity". In: *Nature* 499.7458, pp. 295–300.

Chiappalone, Michela, Valentina Pasquale, and Monica Frega (2019). *In vitro neuronal networks: From culturing methods to neuro-technological applications*. Vol. 22. Springer.

Chiappalone, Michela et al. (2006). "Dissociated cortical networks show spontaneously correlated activity patterns during in vitro development". In: *Brain research* 1093.1, pp. 41–53.

Chiappalone, Michela et al. (2007). "Network dynamics and synchronous activity in cultured cortical neurons". In: *International journal of neural systems* 17.02, pp. 87–103.

Chklovskii, Dmitri B (2004). "Exact solution for the optimal neuronal layout problem". In: *Neural computation* 16.10, pp. 2067–2078.

Chow, Siu Yu A et al. (2022). "Advances in construction and modeling of functional neural circuits in vitro". In: *Neurochemical Research* 47.9, pp. 2529–2544.

Churchland, Patricia Smith and Terrence Joseph Sejnowski (1992). *The computational brain*. MIT press.

Chwalek, Karolina et al. (2015). "Engineered 3D silk-collagen-based model of polarized neural tissue". In: *JoVE (Journal of Visualized Experiments)* 104, e52970.

Clavaguera, Florence et al. (2009). "Transmission and spreading of tauopathy in transgenic mouse brain". In: *Nature cell biology* 11.7, pp. 909–913.

Clavaguera, Florence et al. (2015). "Invited review: Prion-like transmission and spreading of tau pathology". In: *Neuropathology and applied neurobiology* 41.1, pp. 47–58.

Cleveland, Don W, Shu-Ying Hwo, and Marc W Kirschner (1977). "Purification of tau, a microtubule-associated protein that induces assembly of microtubules from purified tubulin". In: *Journal of molecular biology* 116.2, pp. 207–225.

Cohen, Eyal et al. (2008). "Determinants of spontaneous activity in networks of cultured hippocampus". In: *Brain research* 1235, pp. 21–30.

Cohen, Jessica R (2018). "The behavioral and cognitive relevance of time-varying, dynamic changes in functional connectivity". In: *NeuroImage* 180, pp. 515–525.

Cohen, Jessica R and Mark D'Esposito (2016). "The segregation and integration of distinct brain networks and their relationship to cognition". In: *Journal of Neuroscience* 36.48, pp. 12083–12094.

Collet, JP et al. (2000). "Influence of fibrin network conformation and fibrin fiber diameter on fibrinolysis speed: dynamic and structural approaches by confocal microscopy". In: *Arteriosclerosis, thrombosis, and vascular biology* 20.5, pp. 1354–1361.

Crowe, Alex et al. (2020). "Compound screening in cell-based models of tau inclusion formation: Comparison of primary neuron and HEK293 cell assays". In: *Journal of Biological Chemistry* 295.12, pp. 4001–4013.

Dadashzadeh, Arezoo, Saeid Moghassemi, and CA Amorim (2021). "Evaluation of PEGylated fibrin as a three-dimensional biodegradable scaffold for ovarian tissue engineering". In: *Materials Today Chemistry* 22, p. 100626.

Damodaran, Vinod Babu and Conan Fee (2010). "Protein PEGylation: An overview of chemistry and process considerations". In: *European Pharmaceutical Review* 15.1, pp. 18–26.

Damoiseaux, Jessica S and Michael D Greicius (2009). "Greater than the sum of its parts: a review of studies combining structural connectivity and resting-state functional connectivity". In: *Brain structure and function* 213, pp. 525–533.

David, Della C et al. (2005). "Proteomic and functional analyses reveal a mitochondrial dysfunction in P301L tau transgenic mice". In: *Journal of Biological Chemistry* 280.25, pp. 23802–23814.

Dawson, Ted M, Todd E Golde, and Clotilde Lagier-Tourenne (2018). "Animal models of neurodegenerative diseases". In: *Nature neuroscience* 21.10, pp. 1370–1379.

De Calignon, Alix et al. (2012). "Propagation of tau pathology in a model of early Alzheimer's disease". In: *Neuron* 73.4, pp. 685–697.

Decker, Jochen Martin et al. (2015). "Pro-aggregant Tau impairs mossy fiber plasticity due to structural changes and Ca++ dysregulation". In: *Acta neuropathologica communications* 3.1, pp. 1–18.

Deco, Gustavo and Viktor K Jirsa (2012). "Ongoing cortical activity at rest: criticality, multistability, and ghost attractors". In: *Journal of Neuroscience* 32.10, pp. 3366–3375.

Deco, Gustavo, Viktor K Jirsa, and Anthony R McIntosh (2011). "Emerging concepts for the dynamical organization of resting-state activity in the brain". In: *Nature reviews neuroscience* 12.1, pp. 43–56.

Deco, Gustavo et al. (2008). "The dynamic brain: from spiking neurons to neural masses and cortical fields". In: *PLoS computational biology* 4.8, e1000092.

Deco, Gustavo et al. (2015). "Rethinking segregation and integration: contributions of whole-brain modelling". In: *Nature Reviews Neuroscience* 16.7, pp. 430–439.

DeFelipe, Javier (2011). "The evolution of the brain, the human nature of cortical circuits, and intellectual creativity". In: *Frontiers in neuroanatomy* 5, p. 29.

Deitcher, Yair et al. (2017). "Comprehensive morpho-electrotonic analysis shows 2 distinct classes of L2 and L3 pyramidal neurons in human temporal cortex". In: *Cerebral Cortex* 27.11, pp. 5398–5414.

Delacourte, André et al. (1999). "The biochemical pathway of neurofibrillary degeneration in aging and Alzheimer's disease". In: *Neurology* 52.6, pp. 1158–1158.

Desai, Niraj S, Lana C Rutherford, and Gina G Turrigiano (1999). "Plasticity in the intrinsic excitability of cortical pyramidal neurons". In: *Nature neuroscience* 2.6, pp. 515–520.

Dickerson, BC et al. (2005). "Increased hippocampal activation in mild cognitive impairment compared to normal aging and AD". In: *Neurology* 65.3, pp. 404–411.

Dickerson, Bradford C et al. (2004). "Medial temporal lobe function and structure in mild cognitive impairment". In: *Annals of neurology* 56.1, pp. 27–35.

Dingle, Yu-Ting L et al. (2020). "Functional characterization of three-dimensional cortical cultures for in vitro modeling of brain networks". In: *IScience* 23.8.

Divoux, Thibaut, Catherine Barentin, and Sébastien Manneville (2011). "From stress-induced fluidization processes to Herschel-Bulkley behaviour in simple yield stress fluids". In: *Soft Matter* 7 (18), pp. 8409–8418.

Dixit, Ram et al. (2008). "Differential regulation of dynein and kinesin motor proteins by tau". In: *Science* 319.5866, pp. 1086–1089.

D'Souza, Gary X et al. (2021). "The application of in vitro-derived human neurons in neurodegenerative disease modeling". In: *Journal of neuroscience research* 99.1, pp. 124–140.

Dugger, Brittany N and Dennis W Dickson (2017). "Pathology of neurodegenerative diseases". In: *Cold Spring Harbor perspectives in biology* 9.7, a028035.

Duong, Haison, Benjamin Wu, and Bill Tawil (2009). "Modulation of 3D fibrin matrix stiffness by intrinsic fibrinogen–thrombin compositions and by extrinsic cellular activity". In: *Tissue Engineering Part A* 15.7, pp. 1865–1876.

Eidenmüller, Jochen et al. (2001). "Phosphorylation-mimicking glutamate clusters in the proline-rich region are sufficient to simulate the functional deficiencies of hyperphosphorylated tau protein". In: *Biochemical Journal* 357.3, pp. 759–767.

Eiraku, Mototsugu et al. (2008). "Self-organized formation of polarized cortical tissues from ESCs and its active manipulation by extrinsic signals". In: *Cell stem cell* 3.5, pp. 519–532.

Engle, Sandra J, Laura Blaha, and Robin J Kleiman (2018). "Best practices for translational disease modeling using human iPSC-derived neurons". In: *Neuron* 100.4, pp. 783–797.

Espuny-Camacho, Ira et al. (2013). "Pyramidal neurons derived from human pluripotent stem cells integrate efficiently into mouse brain circuits in vivo". In: *Neuron* 77.3, pp. 440–456.

Essen, David C van (1997). "A tension-based theory of morphogenesis and compact wiring in the central nervous system". In: *Nature* 385.6614, pp. 313–318.

Esteras, Noemi and Andrey Y Abramov (2020). "Mitochondrial calcium deregulation in the mechanism of beta-amyloid and tau pathology". In: *Cells* 9.9, p. 2135.

Estévez-Priego, Estefanía et al. (2020). "Functional strengthening through synaptic scaling upon connectivity disruption in neuronal cultures". In: *Network Neuroscience* 4.4, pp. 1160–1180.

Estévez-Priego, Estefanía et al. (2023). "Long-term calcium imaging reveals functional development in hiPSC-derived cultures comparable to human but not rat primary cultures". In: *Stem Cell Reports* 18, pp. 1–15. ISSN: 22136711.

Ewoldt, R.H., M.T. Johnston, and L.M. Caretta (2015). "Experimental challenges of shear rheology: how to avoid bad data". In: *Complex Fluids in Biological Systems*. Ed. by S. Spagnolie. Springer.

Eyal, Guy et al. (2016). "Unique membrane properties and enhanced signal processing in human neocortical neurons". In: *Elife* 5, e16553.

Farahani, Farzad V, Waldemar Karwowski, and Nichole R Lighthall (2019). "Application of graph theory for identifying connectivity patterns in human brain networks: a systematic review". In: *frontiers in Neuroscience* 13, p. 585.

Fauth, Michael, Florentin Wörgötter, and Christian Tetzlaff (2015). "The formation of multi-synaptic connections by the interaction of synaptic and structural plasticity and their functional consequences". In: *PLoS computational biology* 11.1, e1004031.

Feinerman, Ofer, Menahem Segal, and Elisha Moses (2005). "Signal propagation along unidimensional neuronal networks". In: *Journal of neurophysiology* 94.5, pp. 3406–3416.

Feinstein, Stuart C and Leslie Wilson (2005). "Inability of tau to properly regulate neuronal microtubule dynamics: a loss-of-function mechanism by which tau might mediate neuronal cell death". In: *Biochimica et Biophysica Acta (BBA)-Molecular Basis of Disease* 1739.2-3, pp. 268–279.

Felleman, Daniel J and David C Van Essen (1991). "Distributed hierarchical processing in the primate cerebral cortex." In: *Cerebral cortex (New York, NY: 1991)* 1.1, pp. 1–47.

Fernández-García, Sara et al. (2020). "Deficits in coordinated neuronal activity and network topology are striatal hallmarks in Huntington's disease". In: *BMC biology* 18.1, pp. 1–16.

Fernández-Santiago, Rubén et al. (2015). "Aberrant epigenome in iPSC-derived dopaminergic neurons from Parkinson's disease patients". In: *EMBO molecular medicine* 7.12, pp. 1529–1546.

Ferrer, Isidro et al. (2022). "Differences in Tau Seeding in Newborn and Adult Wild-Type Mice". In: *International Journal of Molecular Sciences* 23.9, p. 4789.

Finc, Karolina et al. (2020). "Dynamic reconfiguration of functional brain networks during working memory training". In: *Nature communications* 11.1, p. 2435.

Flanagan, Lisa A et al. (2002). "Neurite branching on deformable substrates". In: *Neuroreport* 13.18, p. 2411.

Fornito, Alex, Andrew Zalesky, and Michael Breakspear (2015). "The connectomics of brain disorders". In: *Nature Reviews Neuroscience* 16.3, pp. 159–172.

Forró, Csaba et al. (2018). "Modular microstructure design to build neuronal networks of defined functional connectivity". In: *Biosensors and Bioelectronics* 122, pp. 75–87.

Fox, Michael D and Michael Greicius (2010). "Clinical applications of resting state functional connectivity". In: *Frontiers in systems neuroscience* 4, p. 1443.

Frandemiche, Marie Lise et al. (2014). "Activity-dependent tau protein translocation to excitatory synapse is disrupted by exposure to amyloid-beta oligomers". In: *Journal of Neuroscience* 34.17, pp. 6084–6097.

Frega, Monica et al. (2014). "Network dynamics of 3D engineered neuronal cultures: a new experimental model for in-vitro electrophysiology". In: *Scientific reports* 4.1, pp. 1–14.

Frega, Monica et al. (2019). "Neuronal network dysfunction in a model for Kleefstra syndrome mediated by enhanced NMDAR signaling". In: *Nature communications* 10.1, p. 4928.

Friedrich, Johannes, Pengcheng Zhou, and Liam Paninski (2017). "Fast online deconvolution of calcium imaging data". In: *PLoS computational biology* 13.3, e1005423.

Friston, Karl J (2011). "Functional and effective connectivity: a review". In: *Brain connectivity* 1.1, pp. 13–36.

Fromherz, Peter et al. (1991). "A neuron-silicon junction: a Retzius cell of the leech on an insulated-gate field-effect transistor". In: *Science* 252.5010, pp. 1290–1293.

Frost, Bess and Marc I Diamond (2010). "Prion-like mechanisms in neurodegenerative diseases". In: *Nature Reviews Neuroscience* 11.3, pp. 155–159.

Frost, Bess, Jürgen Götz, and Mel B Feany (2015). "Connecting the dots between tau dysfunction and neurodegeneration". In: *Trends in cell biology* 25.1, pp. 46–53.

Frost, Bess, Rachel L Jacks, and Marc I Diamond (2009). "Propagation of tau misfolding from the outside to the inside of a cell". In: *Journal of biological chemistry* 284.19, pp. 12845–12852.

Gabriel, Don A, Kathleen Muga, and Emily M Boothroyd (1992). "The effect of fibrin structure on fibrinolysis." In: *Journal of Biological Chemistry* 267.34, pp. 24259–24263.

Galler, Kerstin M et al. (2011). "Bioengineering of dental stem cells in a PEGylated fibrin gel". In: *Regenerative medicine* 6.2, pp. 191–200.

Gan, Li et al. (2018). "Converging pathways in neurodegeneration, from genetics to mechanisms". In: *Nature neuroscience* 21.10, pp. 1300–1309.

Ghosh, Kaustabh et al. (2005). "Rheological Characterization of in Situ Cross-Linkable Hyaluronan Hydrogels". In: *Biomacromolecules* 6.5, pp. 2857–2865.

Goedert, MGSM et al. (1989). "Multiple isoforms of human microtubule-associated protein tau: sequences and localization in neurofibrillary tangles of Alzheimer's disease". In: *Neuron* 3.4, pp. 519–526.

Goedert, Michel (1999). "Filamentous nerve cell inclusions in neurodegenerative diseases: tauopathies and alpha-synucleinopathies". In: *Philosophical transactions of the royal society of london. Series B: biological sciences* 354.1386, pp. 1101–1118.

Golomb, David and G Bard Ermentrout (1999). "Continuous and lurching traveling pulses in neuronal networks with delay and spatially decaying connectivity". In: *Proceedings of the National Academy of Sciences* 96.23, pp. 13480–13485.

Gómez-Ramos, Alberto et al. (2006). "Extracellular tau is toxic to neuronal cells". In: *FEBS letters* 580.20, pp. 4842–4850.

Gómez-Ramos, Alberto et al. (2008). "Extracellular tau promotes intracellular calcium increase through M1 and M3 muscarinic receptors in neuronal cells". In: *Molecular and Cellular Neuroscience* 37.4, pp. 673–681.

Gong, C-X et al. (2005). "Post-translational modifications of tau protein in Alzheimer's disease". In: *Journal of neural transmission* 112, pp. 813–838.

Gonzalez-Islas, Carlos and Peter Wenner (2006). "Spontaneous network activity in the embryonic spinal cord regulates AMPAergic and GABAergic synaptic strength". In: *Neuron* 49.4, pp. 563–575.

Götz, Jürgen, Glenda Halliday, and Rebecca M Nisbet (2019). "Molecular pathogenesis of the tauopathies". In: *Annual Review of Pathology: Mechanisms of Disease* 14, pp. 239–261.

Greig, Luciano Custo et al. (2013). "Molecular logic of neocortical projection neuron specification, development and diversity". In: *Nature Reviews Neuroscience* 14.11, pp. 755–769.

Grewe, Benjamin F et al. (2010). "High-speed in vivo calcium imaging reveals neuronal network activity with near-millisecond precision". In: *Nature methods* 7.5, pp. 399–405.

Grienberger, Christine and Arthur Konnerth (2012). "Imaging calcium in neurons". In: *Neuron* 73.5, pp. 862–885.

Gross, Guenter W (1979). "Simultaneous single unit recording in vitro with a photoetched laser deinsulated gold multimicroelectrode surface". In: *IEEE Transactions on Biomedical Engineering* 5, pp. 273–279.

Grundke-Iqbal, Inge et al. (1986). "Microtubule-associated protein tau. A component of Alzheimer paired helical filaments." In: *Journal of Biological Chemistry* 261.13, pp. 6084–6089.

Guillery, Rainer W (2005). "Observations of synaptic structures: origins of the neuron doctrine and its current status". In: *Philosophical Transactions of the Royal Society B: Biological Sciences* 360.1458, pp. 1281–1307.

Guo, Jing L and Virginia MY Lee (2014). "Cell-to-cell transmission of pathogenic proteins in neurodegenerative diseases". In: *Nature medicine* 20.2, pp. 130–138.

Guo, Jing L et al. (2016). "Unique pathological tau conformers from Alzheimer's brains transmit tau pathology in nontransgenic mice". In: *Journal of Experimental Medicine* 213.12, pp. 2635–2654.

Guo, Tong, Wendy Noble, and Diane P Hanger (2017). "Roles of tau protein in health and disease". In: *Acta neuropathologica* 133, pp. 665–704.

Hagmann, Patric et al. (2008). "Mapping the structural core of human cerebral cortex". In: *PLoS biology* 6.7, e159.

Hanger, Diane P, Brian H Anderton, and Wendy Noble (2009). "Tau phosphorylation: the therapeutic challenge for neurodegenerative disease". In: *Trends in molecular medicine* 15.3, pp. 112–119.

Harrison, Ross Granville (1910). "The outgrowth of the nerve fiber as a mode of protoplasmic movement". In: *Journal of Experimental Zoology* 9.4, pp. 787–846.

Hernández-Navarro, Lluís et al. (2021). "Noise-driven amplification mechanisms governing the emergence of coherent extreme events in excitable systems". In: *Physical Review Research* 3.2, p. 023133.

Hillman, Elizabeth MC et al. (2019). "Light-sheet microscopy in neuroscience". In: *Annual review of neuroscience* 42, pp. 295–313.

Holmes, Brandon B et al. (2014). "Proteopathic tau seeding predicts tauopathy in vivo". In: *Proceedings of the National Academy of sciences* 111.41, E4376–E4385.

Homma, Ryota et al. (2009). "Wide-field and two-photon imaging of brain activity with voltage and calcium-sensitive dyes". In: *Dynamic Brain Imaging: Multi-Modal Methods and In Vivo Applications*, pp. 43–79.

Horwitz, Barry (2003). "The elusive concept of brain connectivity". In: *Neuroimage* 19.2, pp. 466–470.

Hou, Yujun et al. (2019). "Ageing as a risk factor for neurodegenerative disease". In: *Nature Reviews Neurology* 15.10, pp. 565–581.

Huh, Dongeun et al. (2010). "Reconstituting organ-level lung functions on a chip". In: *Science* 328.5986, pp. 1662–1668.

International, Alzheimer's Disease (2023). *Dementia facts figures*. URL: `https://www.alzint.org/about/dementia-facts-figures/` (visited on 10/23/2023).

Ittner, Lars M et al. (2010). "Dendritic function of tau mediates amyloid-β toxicity in Alzheimer's disease mouse models". In: *Cell* 142.3, pp. 387–397.

Jacobi, Shimshon and Elisha Moses (2007). "Variability and corresponding amplitude–velocity relation of activity propagating in one-dimensional neural cultures". In: *Journal of neurophysiology* 97.5, pp. 3597–3606.

Jacobi, Shimshon, Jordi Soriano, and Elisha Moses (2010). "BDNF and NT-3 increase velocity of activity front propagation in unidimensional hippocampal cultures". In: *Journal of neurophysiology* 104.6, pp. 2932–2939.

Janmey, Paul A, Penelope C Georges, and Søren Hvidt (2007). "Basic rheology for biologists". In: *Methods in cell biology* 83, pp. 1–27.

Javier-Torrent, Míriam, Geraldine Zimmer-Bensch, and Laurent Nguyen (2021). "Mechanical forces orchestrate brain development". In: *Trends in Neurosciences* 44.2, pp. 110–121.

Jeganathan, Sadasivam et al. (2008). "The natively unfolded character of tau and its aggregation to Alzheimer-like paired helical filaments". In: *Biochemistry* 47.40, pp. 10526–10539.

Jiang, Frank Xue et al. (2010). "Effect of dynamic stiffness of the substrates on neurite outgrowth by using a DNA-crosslinked hydrogel". In: *Tissue Engineering Part A* 16.6, pp. 1873–1889.

Jun, Sang Beom et al. (2007). "Low-density neuronal networks cultured using patterned poly-l-lysine on microelectrode arrays". In: *Journal of neuroscience methods* 160.2, pp. 317–326.

Kfoury, Najla et al. (2012). "Trans-cellular propagation of Tau aggregation by fibrillar species". In: *Journal of Biological Chemistry* 287.23, pp. 19440–19451.

Khazipov, Rustem and Heiko J Luhmann (2006). "Early patterns of electrical activity in the developing cerebral cortex of humans and rodents". In: *Trends in neurosciences* 29.7, pp. 414–418.

Kim, Hong Nam and Nakwon Choi (2019). "Consideration of the Mechanical Properties of Hydrogels for Brain Tissue Engineering and Brain-on-a-chip". In: *BioChip Journal* 13.1, pp. 8–19.

Kim, M Justin et al. (2011). "The structural and functional connectivity of the amygdala: from normal emotion to pathological anxiety". In: *Behavioural brain research* 223.2, pp. 403–410.

Kim, Raeyoung et al. (2014). "Recent trends in microelectrode array technology for in vitro neural interface platform". In: *Biomedical Engineering Letters* 4, pp. 129–141.

Kimura, Tetsuya et al. (2014). "Microtubule-associated protein tau is essential for long-term depression in the hippocampus". In: *Philosophical Transactions of the Royal Society B: Biological Sciences* 369.1633, p. 20130144.

Klein Gunnewiek, TM et al. (2019). "Mitochondrial dysfunction impairs human neuronal development and reduces neuronal network activity and synchronicity". In: *bioRxiv*, p. 720227.

Kobayashi, Shunsuke et al. (2019). "Enhanced tau protein translation by hyper-excitation". In: *Frontiers in Aging Neuroscience* 11, p. 322.

Koester, Helmut J and Bert Sakmann (2000). "Calcium dynamics associated with action potentials in single nerve terminals of pyramidal cells in layer 2/3 of the young rat neocortex". In: *The Journal of physiology* 529.3, pp. 625–646.

Koroleva, Anastasia et al. (2021). "In vitro development of human iPSC-derived functional neuronal networks on laser-fabricated 3D scaffolds". In: *ACS Applied Materials & Interfaces* 13.7, pp. 7839–7853.

Koser, David E et al. (2016). "Mechanosensing is critical for axon growth in the developing brain". In: *Nature neuroscience* 19.12, pp. 1592–1598.

Krieger, Irvin M. (May 1990). "Bingham Award Lecture—1989: The role of instrument inertia in controlled-stress rheometers". In: *Journal of Rheology* 34.4, pp. 471–483. ISSN: 0148-6055.

Ksiezak-Reding, Hanna et al. (2003). "Akt/PKB kinase phosphorylates separately Thr212 and Ser214 of tau protein in vitro". In: *Biochimica et Biophysica Acta (BBA)-Molecular Basis of Disease* 1639.3, pp. 159–168.

Kullback, Solomon and Richard A Leibler (1951). "On information and sufficiency". In: *The annals of mathematical statistics* 22.1, pp. 79–86.

Kurz, Alexander et al. (1998). "Tau protein in cerebrospinal fluid is significantly increased at the earliest clinical stage of Alzheimer disease". In: *Alzheimer Disease & Associated Disorders* 12.4, pp. 372–377.

Lai, Victor K et al. (2012). "Mechanical behavior of collagen-fibrin co-gels reflects transition from series to parallel interactions with increasing collagen content". In.

Lam, Doris, Nicholas O Fischer, and Heather A Enright (2021). "Probing function in 3D neuronal cultures: A survey of 3D multielectrode array advances". In: *Current Opinion in Pharmacology* 60, pp. 255–260.

Lam, Doris et al. (2019). "Tissue-specific extracellular matrix accelerates the formation of neural networks and communities in a neuron-glia co-culture on a multielectrode array". In: *Scientific Reports* 9.1, pp. 1–15.

Lam, Doris et al. (2020). "Optimizing cell encapsulation condition in ECM-Collagen I hydrogels to support 3D neuronal cultures". In: *Journal of neuroscience methods* 329, p. 108460.

Lancaster, Madeline A et al. (2013). "Cerebral organoids model human brain development and microcephaly". In: *Nature* 501.7467, pp. 373–379.

Lasagna-Reeves, Cristian A et al. (2012). "Alzheimer brain-derived tau oligomers propagate pathology from endogenous tau". In: *Scientific reports* 2.1, p. 700.

Latora, Vito and Massimo Marchiori (2001). "Efficient behavior of small-world networks". In: *Physical review letters* 87.19, p. 198701.

— (2003). "Economic small-world behavior in weighted networks". In: *The European Physical Journal B-Condensed Matter and Complex Systems* 32, pp. 249–263.

Lau, Lorraine W et al. (2013). "Pathophysiology of the brain extracellular matrix: a new target for remyelination". In: *Nature Reviews Neuroscience* 14.10, pp. 722–729.

Laughlin, Simon B and Terrence J Sejnowski (2003). "Communication in neuronal networks". In: *Science* 301.5641, pp. 1870–1874.

Lee, Hyoung-gon et al. (2005). "Tau phosphorylation in Alzheimer's disease: pathogen or protector?" In: *Trends in molecular medicine* 11.4, pp. 164–169.

Lee, Virginia MY, Michel Goedert, and John Q Trojanowski (2001). "Neurodegenerative tauopathies". In: *Annual review of neuroscience* 24.1, pp. 1121–1159.

Lennie, Peter (2003). "The cost of cortical computation". In: *Current biology* 13.6, pp. 493–497.

Li, Zheng and Morgan Sheng (2003). "Some assembly required: the development of neuronal synapses". In: *Nature reviews Molecular cell biology* 4.11, pp. 833–841.

Liu, Hui, Scott F Collins, and Laura J Suggs (2006). "Three-dimensional culture for expansion and differentiation of mouse embryonic stem cells". In: *Biomaterials* 27.36, pp. 6004–6014.

Liu, Li et al. (2012). "Trans-synaptic spread of tau pathology in vivo". In: *PloS one* 7.2, e31302.

Lodato, Simona and Paola Arlotta (2015). "Generating neuronal diversity in the mammalian cerebral cortex". In: *Annual review of cell and developmental biology* 31, pp. 699–720.

Logothetis, Nikos K (2008). "What we can do and what we cannot do with fMRI". In: *Nature* 453.7197, pp. 869–878.

Long, Katherine R and Wieland B Huttner (2019). "How the extracellular matrix shapes neural development". In: *Royal Society Open Biology* 9.1, p. 180216.

Looger, Loren L and Oliver Griesbeck (2012). "Genetically encoded neural activity indicators". In: *Current opinion in neurobiology* 22.1, pp. 18–23.

López-León, Clara F, Jordi Soriano, and Ramon Planet (2023). "Rheological Characterization of Three-Dimensional Neuronal Cultures Embedded in PEGylated Fibrin Hydrogels". In: *Gels* 9.8, p. 642.

LoPresti, Patrizia et al. (1995). "Functional implications for the microtubule-associated protein tau: localization in oligodendrocytes." In: *Proceedings of the National Academy of Sciences* 92.22, pp. 10369–10373.

Lord, Susan T (2011). "Molecular mechanisms affecting fibrin structure and stability". In: *Arteriosclerosis, thrombosis, and vascular biology* 31.3, pp. 494–499.

Low, Lawrence K and Hwai-Jong Cheng (2006). "Axon pruning: an essential step underlying the developmental plasticity of neuronal connections". In: *Philosophical Transactions of the Royal Society B: Biological Sciences* 361.1473, pp. 1531–1544.

Ludl, Adriaan-Alexander and Jordi Soriano (2020). "Impact of physical obstacles on the structural and effective connectivity of in silico neuronal circuits". In: *Frontiers in computational neuroscience* 14, p. 77.

Luhmann, Heiko J et al. (2016). "Spontaneous neuronal activity in developing neocortical networks: from single cells to large-scale interactions". In: *Frontiers in neural circuits* 10, p. 40.

Maestú, Fernando et al. (2021). "Neuronal excitation/inhibition imbalance: core element of a translational perspective on Alzheimer pathophysiology". In: *Ageing Research Reviews* 69, p. 101372.

Malkin, Alexander Y and Avraam I Isayev (2022). *Rheology: concepts, methods, and applications*. Elsevier.

Mandelkow, Eva-Maria and Eckhard Mandelkow (2012). "Biochemistry and cell biology of tau protein in neurofibrillary degeneration". In: *Cold Spring Harbor perspectives in medicine* 2.7.

Marder, Eve (2011). "Variability, compensation, and modulation in neurons and circuits". In: *Proceedings of the National Academy of Sciences* 108, pp. 15542–15548.

Martens, Marijn Bart et al. (2016). "Euchromatin histone methyltransferase 1 regulates cortical neuronal network development". In: *Scientific reports* 6.1, p. 35756.

Martin, Ludovic, Xenia Latypova, and Faraj Terro (2011). "Post-translational modifications of tau protein: implications for Alzheimer's disease". In: *Neurochemistry international* 58.4, pp. 458–471.

Martin, Ludovic et al. (2013). "Tau protein phosphatases in Alzheimer's disease: the leading role of PP2A". In: *Ageing research reviews* 12.1, pp. 39–49.

Martinoia, Sergio et al. (2004). "Cultured neurons coupled to microelectrode arrays: circuit models, simulations and experimental data". In: *IEEE transactions on biomedical engineering* 51.5, pp. 859–863.

Mazzoni, Alberto et al. (2007). "On the dynamics of the spontaneous activity in neuronal networks". In: *PloS one* 2.5, e439.

Medaglia, John D and Danielle S Bassett (2017). "Network analyses and nervous system disorders". In: *arXiv preprint arXiv:1701.01101*.

Messé, Arnaud et al. (2014). "Relating structure and function in the human brain: relative contributions of anatomy, stationary dynamics, and non-stationarities". In: *PLoS computational biology* 10.3, e1003530.

Meunier, David, Renaud Lambiotte, and Edward T Bullmore (2010). "Modular and hierarchically modular organization of brain networks". In: *Frontiers in neuroscience* 4, p. 200.

Meyer, Helmut E et al. (1995). "Microtubule-associated protein/microtubule affinity-regulating kinase (p110mark): a novel protein kinase that regulates tau-microtubule interactions and dynamic instability by phosphorylation at the Alzheimer-specific site serine 262". In: *Journal of Biological Chemistry* 270.13, pp. 7679–7688.

Millet, Larry J and Martha U Gillette (2012). "Over a century of neuron culture: from the hanging drop to microfluidic devices". In: *The Yale journal of biology and medicine* 85.4, p. 501.

Miyawaki, Atsushi et al. (1997). "Fluorescent indicators for Ca2+ based on green fluorescent proteins and calmodulin". In: *Nature* 388.6645, pp. 882–887.

Mondadori, Christian RA et al. (2006). "Enhanced brain activity may precede the diagnosis of Alzheimer's disease by 30 years". In: *Brain* 129.11, pp. 2908–2922.

Montalà-Flaquer, Marc et al. (2022). "Rich dynamics and functional organization on topographically designed neuronal networks in vitro". In: *Iscience* 25.12, p. 105680.

Mosesson, Michael W (2005). "Fibrinogen and fibrin structure and functions". In: *Journal of thrombosis and haemostasis* 3.8, pp. 1894–1904.

Mountcastle, Vernon B (1997). "The columnar organization of the neocortex." In: *Brain: a journal of neurology* 120.4, pp. 701–722.

Mukrasch, Marco D et al. (2009). "Structural polymorphism of 441-residue tau at single residue resolution". In: *PLoS biology* 7.2, e1000034.

Müller, Reinhold et al. (1997). "Expression of microtubule-associated proteins MAP2 and tau in cultured rat brain oligodendrocytes". In: *Cell and tissue research* 288, pp. 239–249.

Musah, Samira et al. (2012). "Glycosaminoglycan-binding hydrogels enable mechanical control of human pluripotent stem cell self-renewal". In: *ACS nano* 6.11, pp. 10168–10177.

Muzzi, Lorenzo et al. (2023). "Human-derived cortical neurospheroids coupled to passive, high-density and 3D MEAs: a valid platform for functional tests". In: *Bioengineering* 10.4, p. 449.

Nakai, Junichi, Masamichi Ohkura, and Keiji Imoto (2001). "A high signal-to-noise Ca2+ probe composed of a single green fluorescent protein". In: *Nature biotechnology* 19.2, pp. 137–141.

Nam, Yoonkey, Darren W Branch, and Bruce C Wheeler (2006). "Epoxy-silane linking of biomolecules is simple and effective for patterning neuronal cultures". In: *Biosensors and bioelectronics* 22.5, pp. 589–597.

Neher, Erwin and Takeshi Sakaba (2008). "Multiple roles of calcium ions in the regulation of neurotransmitter release". In: *Neuron* 59.6, pp. 861–872.

Nishikawa, Shin-ichi, Robert A Goldstein, and Concepcion R Nierras (2008). "The promise of human induced pluripotent stem cells for research and therapy". In: *Nature reviews Molecular cell biology* 9.9, pp. 725–729.

Ohmiya, Yoshihiro and Takashi Hirano (1996). "Shining the light: the mechanism of the bioluminescence reaction of calcium-binding photoproteins". In: *Chemistry & biology* 3.5, pp. 337–347.

Öngür, Dost et al. (2010). "Default mode network abnormalities in bipolar disorder and schizophrenia". In: *Psychiatry Research: Neuroimaging* 183.1, pp. 59–68.

Opitz, Thoralf, Ana D De Lima, and Thomas Voigt (2002). "Spontaneous development of synchronous oscillatory activity during maturation of cortical networks in vitro". In: *Journal of neurophysiology* 88.5, pp. 2196–2206.

Orlandi, Javier G et al. (2013). "Noise focusing and the emergence of coherent activity in neuronal cultures". In: *Nature Physics* 9.9, pp. 582–590.

Orlandi, Javier G et al. (2014). "Transfer entropy reconstruction and labeling of neuronal connections from simulated calcium imaging". In: *PloS one* 9.6, e98842.

Orlandi, Javier G et al. (2017). "NETCAL: an interactive platform for large-scale, NETwork and population dynamics analysis of CALcium imaging recordings". In: *Neuroscience*.

Osaki, Tatsuya et al. (2018). "In vitro microfluidic models for neurodegenerative disorders". In: *Advanced healthcare materials* 7.2, p. 1700489.

Oswald, Patrick (2009). *Rheophysics: The Deformation and Flow of Matter*. Cambridge University Press.

Oyen, ML (2014). "Mechanical characterisation of hydrogel materials". In: *International Materials Reviews* 59.1, pp. 44–59.

Ozgun, Alp et al. (2022). "Biomaterials-based strategies for in vitro neural models". In: *Biomaterials Science* 10.5, pp. 1134–1165.

Palop, Jorge J, Jeannie Chin, and Lennart Mucke (2006). "A network dysfunction perspective on neurodegenerative diseases". In: *Nature* 443.7113, pp. 768–773.

Palop, Jorge J and Lennart Mucke (2010). "Synaptic depression and aberrant excitatory network activity in Alzheimer's disease: two faces of the same coin?" In: *Neuromolecular medicine* 12, pp. 48–55.

Palop, Jorge J et al. (2007). "Aberrant excitatory neuronal activity and compensatory remodeling of inhibitory hippocampal circuits in mouse models of Alzheimer's disease". In: *Neuron* 55.5, pp. 697–711.

Pan, Liangbin et al. (2015). "An in vitro method to manipulate the direction and functional strength between neural populations". In: *Frontiers in neural circuits* 9, p. 32.

Pan, Linjie et al. (2009). "Viability and differentiation of neural precursors on hyaluronic acid hydrogel scaffold". In: *Journal of Neuroscience Research* 87.14, pp. 3207–3220.

Pannese, Ennio (1999). "The Golgi stain: invention, diffusion and impact on neurosciences". In: *Journal of the History of the Neurosciences* 8.2, pp. 132–140.

Park, Jae Woo et al. (2013). "Advances in microfluidics-based experimental methods for neuroscience research". In: *Lab on a Chip* 13.4, pp. 509–521.

Park, Myung Uk et al. (2021). "Collective dynamics of neuronal activities in various modular networks". In: *Lab on a Chip* 21.5, pp. 951–961.

Paşca, Anca M et al. (2015). "Functional cortical neurons and astrocytes from human pluripotent stem cells in 3D culture". In: *Nature methods* 12.7, pp. 671–678.

Pasquale, V et al. (2008). "Self-organization and neuronal avalanches in networks of dissociated cortical neurons". In: *Neuroscience* 153.4, pp. 1354–1369.

Pasut, Gianfranco and Francesco M Veronese (2006). "PEGylation of proteins as tailored chemistry for optimized bioconjugates". In: *Polymer Therapeutics I*, pp. 95–134.

Patel, Parul Natvar, Connie Kathleen Smith, and Charles W Patrick Jr (2005). "Rheological and recovery properties of poly (ethylene glycol) diacrylate hydrogels and human adipose tissue". In: *Journal of Biomedical Materials Research Part A: An Official Journal of The Society for Biomaterials, The Japanese Society for Biomaterials, and The Australian Society for Biomaterials and the Korean Society for Biomaterials* 73.3, pp. 313–319.

Petersen, Ole William et al. (1992). "Interaction with basement membrane serves to rapidly distinguish growth and differentiation pattern of normal and malignant human breast epithelial cells." In: *Proceedings of the National Academy of Sciences* 89.19, pp. 9064–9068.

Pickhardt, Marcus et al. (2017). "Time course of Tau toxicity and pharmacologic prevention in a cell model of Tauopathy". In: *Neurobiology of aging* 57, pp. 47–63.

Pine, Jerome (1980). "Recording action potentials from cultured neurons with extracellular microcircuit electrodes". In: *Journal of neuroscience methods* 2.1, pp. 19–31.

Pooler, Amy M et al. (2013). "Physiological release of endogenous tau is stimulated by neuronal activity". In: *EMBO reports* 14.4, pp. 389–394.

Qi, Haoling et al. (2015). "Nuclear magnetic resonance spectroscopy characterization of interaction of Tau with DNA and its regulation by phosphorylation". In: *Biochemistry* 54.7, pp. 1525–1533.

Qian, Zhuo et al. (1993). "Tissue-plasminogen activator is induced as an immediate–early gene during seizure, kindling and long-term potentiation". In: *Nature* 361.6411, pp. 453–457.

Quadrato, Giorgia et al. (2017). "Cell diversity and network dynamics in photosensitive human brain organoids". In: *Nature* 545.7652, pp. 48–53.

Rabadan, M Angeles et al. (2022). "An in vitro model of neuronal ensembles". In: *Nature Communications* 13.1, p. 3340.

Raggenbass, Mario (2001). "Vasopressin-and oxytocin-induced activity in the central nervous system: electrophysiological studies using in-vitro systems". In: *Progress in neurobiology* 64.3, pp. 307–326.

Rash, Brian G and Elizabeth A Grove (2006). "Area and layer patterning in the developing cerebral cortex". In: *Current opinion in neurobiology* 16.1, pp. 25–34.

Riccomagno, Martin M and Alex L Kolodkin (2015). "Sculpting neural circuits by axon and dendrite pruning". In: *Annual review of cell and developmental biology* 31, pp. 779–805.

Rocher, AB et al. (2010). "Structural and functional changes in tau mutant mice neurons are not linked to the presence of NFTs". In: *Experimental neurology* 223.2, pp. 385–393.

Rolston, John D, Daniel A Wagenaar, and Steve M Potter (2007). "Precisely timed spatiotemporal patterns of neural activity in dissociated cortical cultures". In: *Neuroscience* 148.1, pp. 294–303.

Rowe, Shaneen L, SungYun Lee, and Jan P Stegemann (2007). "Influence of thrombin concentration on the mechanical and morphological properties of cell-seeded fibrin hydrogels". In: *Acta biomaterialia* 3.1, pp. 59–67.

Rubinov, Mikail and Olaf Sporns (2010). "Complex network measures of brain connectivity: uses and interpretations". In: *Neuroimage* 52.3, pp. 1059–1069.

Ryan, Esther A et al. (1999). "Structural origins of fibrin clot rheology". In: *Biophysical journal* 77.5, pp. 2813–2826.

Saberi-Moghadam, Sohrab et al. (2018). "In vitro cortical network firing is homeostatically regulated: a model for sleep regulation". In: *Scientific reports* 8.1, p. 6297.

Sala-Jarque, Julia et al. (2020). "Neuromuscular activity induces paracrine signaling and triggers axonal regrowth after injury in microfluidic lab-on-chip devices". In: *Cells* 9.2, p. 302.

Sala-Jarque, Julia et al. (2022). "Towards a mechanistic model of tau-mediated pathology in tauopathies: what can we learn from cell-based in vitro assays?" In: *International Journal of Molecular Sciences* 23.19, p. 11527.

Samanipour, Roya et al. (2022). "A review on 3D printing functional brain model". In: *Biomicrofluidics* 16.1, p. 011501.

Samanta, Sumanta et al. (2022). "Bidirectional cell-matrix interaction dictates neuronal network formation in a brain-mimetic 3D scaffold". In: *Acta Biomaterialia* 140, pp. 314–323.

Sanders, David W et al. (2014). "Distinct tau prion strains propagate in cells and mice and define different tauopathies". In: *Neuron* 82.6, pp. 1271–1288.

Sanders, David W et al. (2016). "Prions and protein assemblies that convey biological information in health and disease". In: *Neuron* 89.3, pp. 433–448.

Santos-Sierra, Daniel de et al. (2014). "Emergence of small-world anatomical networks in self-organizing clustered neuronal cultures". In: *PloS one* 9.1, e85828.

Scannell, JW et al. (1999). "The connectional organization of the cortico-thalamic system of the cat". In: *Cerebral Cortex* 9.3, pp. 277–299.

Schlachetzki, Johannes, Soraya Wilke Saliba, and Antonio Carlos Pinheiro de Oliveira (2013). "Studying neurodegenerative diseases in culture models". In: *Brazilian Journal of Psychiatry* 35, S92–S100.

Schöll, Michael et al. (2016). "PET imaging of tau deposition in the aging human brain". In: *Neuron* 89.5, pp. 971–982.

Schreiber, Thomas (2000). "Measuring information transfer". In: *Physical review letters* 85.2, p. 461.

Schwartz, Ernst et al. (2023). "Evolution of cortical geometry and its link to function, behaviour and ecology". In: *Nature communications* 14.1, p. 2252.

Seeds, Nicholas W, Brian L Williams, and Paula C Bickford (1995). "Tissue plasminogen activator induction in Purkinje neurons after cerebellar motor learning". In: *Science* 270.5244, pp. 1992–1994.

Seeley, William W et al. (2009). "Neurodegenerative diseases target large-scale human brain networks". In: *Neuron* 62.1, pp. 42–52.

Seidler, Paul Matthew et al. (2019). "Structure-based inhibitors halt prion-like seeding by Alzheimer's disease–and tauopathy–derived brain tissue samples". In: *Journal of Biological Chemistry* 294.44, pp. 16451–16464.

Semple, Bridgette D et al. (2013). "Brain development in rodents and humans: Identifying benchmarks of maturation and vulnerability to injury across species". In: *Progress in neurobiology* 106, pp. 1–16.

Shannon, Claude Elwood (1948). "A mathematical theory of communication". In: *The Bell system technical journal* 27.3, pp. 379–423.

Shein-Idelson, Mark, Eshel Ben-Jacob, and Yael Hanein (2011). "Engineered neuronal circuits: a new platform for studying the role of modular topology". In: *Frontiers in neuroengineering* 4, p. 10.

Shi, Yanhong et al. (2017). "Induced pluripotent stem cell technology: a decade of progress". In: *Nature reviews Drug discovery* 16.2, pp. 115–130.

Shimomura, Osamu, Frank H Johnson, and Yo Saiga (1962). "Extraction, purification and properties of aequorin, a bioluminescent protein from the luminous hydromedusan, Aequorea". In: *Journal of cellular and comparative physiology* 59.3, pp. 223–239.

Shin, Hyogeun et al. (2021). "3D high-density microelectrode array with optical stimulation and drug delivery for investigating neural circuit dynamics". In: *Nature communications* 12.1, p. 492.

Shipp, Stewart (2007). "Structure and function of the cerebral cortex". In: *Current Biology* 17.12, R443–R449.

Shovon, Md Hedayetul Islam et al. (2017). "Directed connectivity analysis of functional brain networks during cognitive activity using transfer entropy". In: *Neural Processing Letters* 45, pp. 807–824.

Si, Weijin, Jihong Gong, and Xiaofei Yang (2023). "Substrate stiffness in nerve cells". In: *Brain Science Advances* 9.1, pp. 24–34.

Silva, Teresa P et al. (2019). "Design principles for pluripotent stem cell-derived organoid engineering". In: *Stem Cells International* 2019.

Smetters, Diana, Ania Majewska, and Rafael Yuste (1999). "Detecting action potentials in neuronal populations with calcium imaging". In: *Methods* 18.2, pp. 215–221.

Soriano, Jordi (2023). "Neuronal Cultures: Exploring Biophysics, Complex Systems, and Medicine in a Dish". In: *Biophysica* 3.1, pp. 181–202.

Soriano, Jordi et al. (2008). "Development of input connections in neural cultures". In: *Proceedings of the National Academy of Sciences* 105.37, pp. 13758–13763.

Souza, Natalie de (2017). "Organoid variability examined". In: *Nature Methods* 14.7, pp. 655–655.

Spearman, Benjamin S et al. (2020). "Tunable methacrylated hyaluronic acid-based hydrogels as scaffolds for soft tissue engineering applications". In: *Journal of Biomedical Materials Research Part A* 108.2, pp. 279–291.

Spedden, Elise et al. (2012). "Elasticity maps of living neurons measured by combined fluorescence and atomic force microscopy". In: *Biophysical journal* 103.5, pp. 868–877.

Spitzer, Nicholas C (2006). "Electrical activity in early neuronal development". In: *Nature* 444.7120, pp. 707–712.

Sporns, Olaf (2011). "The non-random brain: efficiency, economy, and complex dynamics". In: *Frontiers in computational neuroscience* 5, p. 5.

— (2013a). "Network attributes for segregation and integration in the human brain". In: *Current opinion in neurobiology* 23.2, pp. 162–171.

— (2013b). "The human connectome: origins and challenges". In: *Neuroimage* 80, pp. 53–61.

Sporns, Olaf, Giulio Tononi, and Rolf Kötter (2005). "The human connectome: a structural description of the human brain". In: *PLoS computational biology* 1.4, e42.

Stam, Cornelis J (2014). "Modern network science of neurological disorders". In: *Nature Reviews Neuroscience* 15.10, pp. 683–695.

Stamer, K et al. (2002). "Tau blocks traffic of organelles, neurofilaments, and APP vesicles in neurons and enhances oxidative stress". In: *The Journal of cell biology* 156.6, pp. 1051–1063.

Stancu, Ilie-Cosmin et al. (2015). "Templated misfolding of Tau by prion-like seeding along neuronal connections impairs neuronal network function and associated behavioral outcomes in Tau transgenic mice". In: *Acta neuropathologica* 129, pp. 875–894.

Stetter, Olav et al. (2012). "Model-free reconstruction of excitatory neuronal connectivity from calcium imaging signals". In.

Steward, Anna et al. (2022). "Functional network segregation is associated with attenuated tau spreading in Alzheimer's disease". In: *Alzheimer's & Dementia*.

Stiso, Jennifer and Danielle S Bassett (2018). "Spatial Embedding Imposes Constraints on Neuronal Network Architectures". In: *Trends in cognitive sciences* 22.12, pp. 1127–1142.

Stojkov, Gorjan et al. (2021). "Relationship between structure and rheology of hydrogels for various applications". In: *Gels* 7.4, p. 255.

Styr, Boaz and Inna Slutsky (2018). "Imbalance between firing homeostasis and synaptic plasticity drives early-phase Alzheimer's disease". In: *Nature neuroscience* 21.4, pp. 463–473.

Sultan, Audrey et al. (2011). "Nuclear tau, a key player in neuronal DNA protection". In: *Journal of Biological Chemistry* 286.6, pp. 4566–4575.

Sun, Jyh-Jang, Werner Kilb, and Heiko J Luhmann (2010). "Self-organization of repetitive spike patterns in developing neuronal networks in vitro". In: *European Journal of Neuroscience* 32.8, pp. 1289–1299.

Takahashi, Kazutoshi and Shinya Yamanaka (2006). "Induction of pluripotent stem cells from mouse embryonic and adult fibroblast cultures by defined factors". In: *cell* 126.4, pp. 663–676.

Takahashi, Kazutoshi et al. (2007). "Induction of pluripotent stem cells from adult human fibroblasts by defined factors". In: *cell* 131.5, pp. 861–872.

Takeda, Shuko et al. (2015). "Neuronal uptake and propagation of a rare phosphorylated high-molecular-weight tau derived from Alzheimer's disease brain". In: *Nature communications* 6.1, p. 8490.

Takeda, Shuko et al. (2016). "Seed-competent high-molecular-weight tau species accumulates in the cerebrospinal fluid of Alzheimer's disease mouse model and human patients". In: *Annals of neurology* 80.3, pp. 355–367.

Tang-Schomer, Min D et al. (2014). "Bioengineered functional brain-like cortical tissue". In: *Proceedings of the National Academy of Sciences* 111.38, pp. 13811–13816.

Targa Dias Anastacio, Helena, Natalie Matosin, and Lezanne Ooi (2022). "Neuronal hyperexcitability in Alzheimer's disease: what are the drivers behind this aberrant phenotype?" In: *Translational Psychiatry* 12.1, p. 257.

Tedesco, Maria Teresa et al. (2018). "Soft chitosan microbeads scaffold for 3D functional neuronal networks". In: *Biomaterials* 156, pp. 159–171.

Tedesco, Mariateresa et al. (2017). "Structurally and functionally interconnected 3D in vitro neuronal assemblies coupled to Micro-Electrode Arrays". In: *2017 8th International IEEE/EMBS Conference on Neural Engineering (NER)*. IEEE, pp. 235–238.

Teller, Sara et al. (2014). "Emergence of assortative mixing between clusters of cultured neurons". In: *PLoS computational biology* 10.9, e1003796.

Teller, Sara et al. (2015). "Magnetite-Amyloid-β deteriorates activity and functional organization in an in vitro model for Alzheimer's disease". In: *Scientific Reports* 5.1, p. 17261.

Teller, Sara et al. (2020). "Spontaneous functional recovery after focal damage in neuronal cultures". In: *Eneuro* 7.1.

Temenoff, Johnna S et al. (2002). "Effect of poly (ethylene glycol) molecular weight on tensile and swelling properties of oligo (poly (ethylene glycol) fumarate) hydrogels for cartilage tissue engineering". In: *Journal of Biomedical Materials Research: An Official Journal of The Society for Biomaterials, The Japanese Society for Biomaterials, and The Australian Society for Biomaterials and the Korean Society for Biomaterials* 59.3, pp. 429–437.

Tetzlaff, Christian et al. (2010). "Self-organized criticality in developing neuronal networks". In: *PLoS computational biology* 6.12, e1001013.

Thomas Jr, CA et al. (1972). "A miniature microelectrode array to monitor the bioelectric activity of cultured cells". In: *Experimental cell research* 74.1, pp. 61–66.

Tian, Huilai et al. (2013). "Trimeric tau is toxic to human neuronal cells at low nanomolar concentrations". In: *International journal of cell biology* 2013.

Tibau, Elisenda, Miguel Valencia, and Jordi Soriano (2013). "Identification of neuronal network properties from the spectral analysis of calcium imaging signals in neuronal cultures". In: *Frontiers in neural circuits* 7, p. 199.

Tibau, Elisenda et al. (2018). "Neuronal spatial arrangement shapes effective connectivity traits of in vitro cortical networks". In: *IEEE Transactions on Network Science and Engineering* 7.1, pp. 435–448.

Tibau, Elisenda et al. (2020). "Neuronal Spatial Arrangement Shapes Effective Connectivity Traits of in vitro Cortical Networks". In: *IEEE Transactions on Network Science and Engineering* 7 (1), pp. 435–448. ISSN: 23274697.

Ulloa Severino, Francesco Paolo et al. (2016). "The role of dimensionality in neuronal network dynamics". In: *Scientific reports* 6.1, p. 29640.

Van Der Meer, Andries D and Albert Van Den Berg (2012). "Organs-on-chips: breaking the in vitro impasse". In: *Integrative Biology* 4.5, pp. 461–470.

Vassallo, Andrea et al. (2017). "A multi-laboratory evaluation of microelectrode array-based measurements of neural network activity for acute neurotoxicity testing". In: *Neurotoxicology* 60, pp. 280–292.

Vershinin, Michael et al. (2007). "Multiple-motor based transport and its regulation by Tau". In: *Proceedings of the National Academy of Sciences* 104.1, pp. 87–92.

Vicente, Raul et al. (2011). "Transfer entropy—a model-free measure of effective connectivity for the neurosciences". In: *Journal of computational neuroscience* 30.1, pp. 45–67.

Violet, Marie et al. (2014). "A major role for Tau in neuronal DNA and RNA protection in vivo under physiological and hyperthermic conditions". In: *Frontiers in cellular neuroscience* 8, p. 84.

Vogel, Jacob W et al. (2020). "Spread of pathological tau proteins through communicating neurons in human Alzheimer's disease". In: *Nature communications* 11.1, p. 2612.

Von Bartheld, Christopher S, Jami Bahney, and Suzana Herculano-Houzel (2016). "The search for true numbers of neurons and glial cells in the human brain: A review of 150 years of cell counting". In: *Journal of Comparative Neurology* 524.18, pp. 3865–3895.

Wagenaar, Daniel A, Jerome Pine, and Steve M Potter (2006). "An extremely rich repertoire of bursting patterns during the development of cortical cultures". In: *BMC neuroscience* 7.1, pp. 1–18.

Wang, Yipeng and Eckhard Mandelkow (2016). "Tau in physiology and pathology". In: *Nature reviews neuroscience* 17.1, pp. 22–35.

Wang, Zhaohe et al. (2023). "Microfluidic Brain-on-a-Chip: From Key Technology to System Integration and Application". In: *Small*, p. 2304427.

Ward, Sarah M et al. (2012). "Tau oligomers and tau toxicity in neurodegenerative disease". In: *Biochemical Society Transactions* 40.4, pp. 667–671.

Weingarten, Murray D et al. (1975). "A protein factor essential for microtubule assembly." In: *Proceedings of the National Academy of Sciences* 72.5, pp. 1858–1862.

Weir, Janelle Shari et al. (2023). "Selective inhibition of excitatory synaptic transmission alters the emergent bursting dynamics of in vitro neural networks". In: *Frontiers in Neural Circuits* 17, p. 9.

Weisel, John W (2004). "The mechanical properties of fibrin for basic scientists and clinicians". In: *Biophysical chemistry* 112.2-3, pp. 267–276.

— (2007). "Structure of fibrin: impact on clot stability". In: *Journal of Thrombosis and Haemostasis* 5, pp. 116–124.

Weisel, John W and Rustem I Litvinov (2013). "Mechanisms of fibrin polymerization and clinical implications". In: *Blood, The Journal of the American Society of Hematology* 121.10, pp. 1712–1719.

Weisel, John W, Chandrasekar Nagaswami, and Lee Makowski (1987). "Twisting of fibrin fibers limits their radial growth." In: *Proceedings of the National Academy of Sciences* 84.24, pp. 8991–8995.

Weiss, Paul (1941). "Nerve patterns: the mechanisms of nerve growth". In: *Growth* 5, pp. 163–203.

Wheeler, Bruce C (2008). "Building a brain on a chip". In: *2008 30th Annual International Conference of the IEEE Engineering in Medicine and Biology Society*. IEEE, pp. 1604–1606.

Wheeler, Bruce C and Gregory J Brewer (2010). "Designing neural networks in culture". In: *Proceedings of the IEEE* 98.3, pp. 398–406.

Wibral, Michael et al. (2011). "Transfer entropy in magnetoencephalographic data: quantifying information flow in cortical and cerebellar networks". In: *Progress in biophysics and molecular biology* 105.1-2, pp. 80–97.

Wolberg, Alisa S (2007). "Thrombin generation and fibrin clot structure". In: *Blood reviews* 21.3, pp. 131–142.

Wu, Jessica W et al. (2013). "Small misfolded Tau species are internalized via bulk endocytosis and anterogradely and retrogradely transported in neurons". In: *Journal of Biological Chemistry* 288.3, pp. 1856–1870.

Wu, Jian-Young, Xiaoying Huang, and Chuan Zhang (2008). "Propagating waves of activity in the neocortex: what they are, what they do". In: *The Neuroscientist* 14.5, pp. 487–502.

Wu, Shaohua et al. (2017). "Three-dimensional hyaluronic acid hydrogel-based models for in vitro human iPSC-derived NPC culture and differentiation". In: *Journal of Materials Chemistry B* 5.21, pp. 3870–3878.

Xu, Longqian et al. (2021). "Trends and recent development of the microelectrode arrays (MEAs)". In: *Biosensors and Bioelectronics* 175, p. 112854.

Yamada, Kaoru et al. (2011). "In vivo microdialysis reveals age-dependent decrease of brain interstitial fluid tau levels in P301S human tau transgenic mice". In: *Journal of Neuroscience* 31.37, pp. 13110–13117.

Yamada, Kaoru et al. (2014). "Neuronal activity regulates extracellular tau in vivo". In: *Journal of Experimental Medicine* 211.3, pp. 387–393.

Yamamoto, Hideaki et al. (2018). "Impact of modular organization on dynamical richness in cortical networks". In: *Science advances* 4.11, eaau4914.

Yan, Congqi and Darrin J Pochan (2010). "Rheological properties of peptide-based hydrogels for biomedical and other applications". In: *Chemical Society Reviews* 39.9, pp. 3528–3540.

Yang, Yaxiong et al. (2018). "Improved calcium sensor GCaMP-X overcomes the calcium channel perturbations induced by the calmodulin in GCaMP". In: *Nature communications* 9.1, p. 1504.

Yao, Zhijun et al. (2010). "Abnormal cortical networks in mild cognitive impairment and Alzheimer's disease". In: *PLoS computational biology* 6.11, e1001006.

Yepes, Manuel et al. (2002). "Regulation of seizure spreading by neuroserpin and tissue-type plasminogen activator is plasminogen-independent". In: *The Journal of clinical investigation* 109.12, pp. 1571–1578.

Yi, YoonYoung et al. (2015). "Central nervous system and its disease models on a chip". In: *Trends in biotechnology* 33.12, pp. 762–776.

Yip, Sidney (2007). *Handbook of materials modeling*. Springer Science & Business Media.

Yuste, Rafael (2015). "From the neuron doctrine to neural networks". In: *Nature reviews neuroscience* 16.8, pp. 487–497.

Zahs, Kathleen R and Karen H Ashe (2010). "'Too much good news'–are Alzheimer mouse models trying to tell us how to prevent, not cure, Alzheimer's disease?" In: *Trends in neurosciences* 33.8, pp. 381–389.

Zhang, Ge et al. (2010). "Vascular differentiation of bone marrow stem cells is directed by a tunable three-dimensional matrix". In: *Acta biomaterialia* 6.9, pp. 3395–3403.

Zhang, Jiangang et al. (2022). "Recent progresses in novel in vitro models of primary neurons: A biomaterial perspective". In: *Frontiers in Bioengineering and Biotechnology* 10, p. 953031.

Zheng, Jie et al. (2020). "Interneuron accumulation of phosphorylated tau impairs adult hippocampal neurogenesis by suppressing GABAergic transmission". In: *Cell Stem Cell* 26.3, pp. 331–345.

Zuidema, Jonathan M et al. (2014). "A protocol for rheological characterization of hydrogels for tissue engineering strategies". In: *Journal of Biomedical Materials Research Part B: Applied Biomaterials* 102.5, pp. 1063–1073.